



HAL
open science

Geomorphic impacts of the 1257 CE eruption of Samalas along the Alas strait, West Nusa Tenggara, Indonesia

Bachtiar Wahyu Mutaqin

► To cite this version:

Bachtiar Wahyu Mutaqin. Geomorphic impacts of the 1257 CE eruption of Samalas along the Alas strait, West Nusa Tenggara, Indonesia. *Geography*. Université Panthéon-Sorbonne - Paris I; Universitas Gadjah Mada (Yogyakarta, Indonésie), 2018. English. NNT : 2018PA01H071 . tel-02413719v1

HAL Id: tel-02413719

<https://theses.hal.science/tel-02413719v1>

Submitted on 16 Dec 2019 (v1), last revised 16 Dec 2019 (v2)

HAL is a multi-disciplinary open access archive for the deposit and dissemination of scientific research documents, whether they are published or not. The documents may come from teaching and research institutions in France or abroad, or from public or private research centers.

L'archive ouverte pluridisciplinaire **HAL**, est destinée au dépôt et à la diffusion de documents scientifiques de niveau recherche, publiés ou non, émanant des établissements d'enseignement et de recherche français ou étrangers, des laboratoires publics ou privés.



ECOLE DOCTORALE DE GÉOGRAPHIE DE PARIS (ED 434)

Laboratoire de Géographie Physique - UMR 8591

Doctoral Thesis in Geography

Bachtiar Wahyu MUTAQIN

**IMPACTS GÉOMORPHIQUES DE L'ÉRUPTION DU SAMALAS EN 1257
LE LONG DU DÉTROIT D'ALAS, NUSA TENGGARA OUEST, INDONÉSIE**



Defense on: 11 December 2018

Supervised by: Prof. Franck LAVIGNE (Université Paris 1 – Panthéon Sorbonne)
Prof. HARTONO (Universitas Gadjah Mada)
Rapporteurs : Prof. Hervé REGNAULD (Université de Rennes 2)
Prof. SUWARDJI (Universitas Mataram)
Examiners : Prof. Nathalie CARCAUD (AgroCampus Ouest)
Dr. Danang Sri HADMOKO (Universitas Gadjah Mada)

Abstract

As the most powerful event in Lombok's recent eruptive history, volcanic materials that were expelled by the Samalas volcano in 1257 CE covered the entire of Lombok Island and are widespread in its eastern part. Almost 800 years after the eruption, the geomorphological impact of this eruption on the island of Lombok remains unknown, whereas its overall climatic and societal consequences are now better understood. A combination of stratigraphic information, present-day topography, geophysical measurement with two-dimensional resistivity profiling technique, local written sources, as well as laboratory and computational analysis, were used to obtain detailed information concerning geomorphic impacts of the 1257 CE eruption of Samalas volcano on the coastal area along the Alas Strait in West Nusa Tenggara Province, Indonesia. This study provides new information related to the geomorphic impact of a major eruption volcanic in coastal areas, in this case, on the eastern part of Lombok and the western coast of Sumbawa. In the first place, the study result shows that since the 1257 CE eruption, the landscape on the eastern part of Lombok is still evolved until the present time. The volume of the 1257 CE volcanic material remains about 14% from the initial volume. Secondly, the discovery of Babad Suwung provides additional explanation of Samalas eruption and may become the oldest visual observation of pyroclastic surges and volcanic fallout, following those by Pliny the Younger in 79 CE. Finally, the 1257 CE eruption of Samalas volcano has proven triggered a minor tsunami that hit Belang Island, on the west coast of Sumbawa.

Keywords: landscape evolution, coastal, written source, paleo tsunami, Samalas.

Sommaire

| | |
|--|-----|
| Abstract..... | 2 |
| Sommaire | 4 |
| Executive Summary in French..... | 6 |
| Acknowledgments..... | 12 |
| Introduction..... | 16 |
| Part 1: State of the art, field presentation, and research methodology..... | 22 |
| Chapter 1: Coastal evolution related to volcanic eruptions..... | 24 |
| Chapter 2: Lombok Island, Sumbawa Island, and Samalas volcano..... | 54 |
| Chapter 3: Research methodology | 68 |
| Part 2: Geomorphic impacts of the 1257 CE eruption of Samalas volcano along the Alas Strait | 88 |
| Chapter 4: Local impacts of the 1257 CE eruption in East Lombok | 90 |
| Chapter 5: Regional impacts of the 1257 CE eruption in West Sumbawa..... | 116 |
| Chapter 6: Did the 1257 CE eruption of Samalas trigger a tsunami? | 134 |
| Conclusion | 156 |
| References | 160 |
| Table of Contents | 194 |
| List of Figures | 198 |
| List of Tables | 204 |
| Appendices..... | 206 |

Executive Summary in French

L'une des éruptions les plus importantes et les plus puissantes au monde au cours des 7 000 dernières années a eu lieu à Lombok, en Indonésie, en 1257 et a impliqué le volcan Samalas dans le complexe volcanique de Rinjani (Lavigne et al., 2013; Vidal et al., 2015; Vidal et al., 2016). Avec un indice d'explosivité volcanique (VEI) de 7, cette éruption a engendré un volume de plus de 40 km³ d'équivalent de roches denses (DRE) de dépôts volcaniques (Lavigne et al., 2013; Vidal et al., 2015).

Ces dépôts se composaient de:

- (i) 7–9 km³ DRE de produits de retombées pliniennes,
- (ii) 16 km³ DRE de dépôts de courant de densité pyroclastique (PDC), et
- (iii) 8–9 km³ DRE de cendres de co-PDC, produites par des explosions lors de l'entrée en mer des PDC.

Les matériaux volcaniques expulsés par le volcan en 1257 couvraient l'ensemble des îles de Lombok et de Bali, ainsi que certaines parties des îles de Sumbawa et de Java. Près de 800 ans après l'éruption de 1257, les dépôts volcaniques du Samalas ont contribué à l'excellente préservation de la paléo-surface pré-éruptive à Lombok. Cependant, l'impact géomorphologique de cette éruption sur l'île reste inconnu, alors que ses conséquences climatiques et sociétales globales sont désormais mieux comprises (Stothers, 2000; Kim and Kim, 2012; Guillet et al., 2017).

En tant qu'événement parmi les plus puissants de l'histoire éruptive récente de Lombok avec plus de 40 km³ DRE de dépôts volcaniques, les matériaux volcaniques expulsés par le volcan Samalas en 1257 couvrent toute l'île de Lombok et sont largement répandus dans sa partie est. L'objectif principal de cette étude est d'explorer

et de comprendre les impacts géomorphologiques de l'éruption du volcan Samalas, en 1257, le long du détroit d'Alas, entre les îles Lombok et Sumbawa. Cette recherche se concentre sur la partie est de l'île de Lombok, étant donné que cette zone avait été durement touchée par les PDC, qu'elle présentait un environnement très dynamique comportant plusieurs processus physiques et une utilisation complexe des terres. De plus, il y a un manque de données et d'informations provenant de recherches antérieures sur l'impact de l'éruption des Samalas en 1257 sur cette région. Des études antérieures de Lavigne et al. (2013) et Vidal et al. (2015) se sont concentrés principalement sur les zones situées au nord-ouest et au sud-ouest du volcan en raison de la quantité limitée de données disponibles sur le terrain. Néanmoins, les habitants de la province de Nusa Tenggara Ouest vivent pour la plupart à l'est de Lombok depuis 1995. Un autre facteur qui rend la partie est de Lombok intéressante sur le plan scientifique est le fait que la matière volcanique de cet endroit est entrée dans la mer (Vidal et al. 2015) et pourrait avoir engendré un tsunami déclenché par la PDC (Choi et al. 2003; Freundt, 2003; Lander et al. 2003; Pelinovsky et al. 2004; Pararas-Carayannis, 2006; Mattioli et al. 2007) dans d'autres îles entourant, par exemple, la côte ouest de Sumbawa.

Il existe trois problématiques scientifiques liées aux objectifs:

1. Peut-on reconstituer précisément l'évolution du paysage depuis le début du XIII^e siècle, c'est-à-dire avant, pendant et après l'éruption du volcan Samalas en 1257?
2. Y a-t-il des sources écrites locales sur l'éruption des Samalas et de ses impacts sur l'île de Lombok et les îles environnantes?
3. L'éruption du volcan Samalas en 1257 a-t-elle déclenché un tsunami le long des rivages du détroit d'Alas?

Pour répondre à ces questions, nous avons mené une approche multidisciplinaire comprenant des relevés géomorphologiques sur des affleurements naturels et artificiels, des mesures géophysiques à l'intérieur des terres et près des côtes avec une technique de profilage de résistivité bidimensionnelle (réseau dipolaire-dipolaire), des techniques de système d'information géographique (SIG), des entretiens approfondis, des analyses de sources écrites locales, analyse de laboratoire et informatique.

Le premier objectif de cette étude était de reconstituer précisément l'évolution du paysage depuis le début du XIII^e siècle, c'est-à-dire avant, pendant et après l'éruption du volcan Samalas en 1257. Nous avons été en mesure d'obtenir un modèle valide de topographies pré et post-1257 grâce à la reconstruction de plus de 1 300 points paléotopographiques. L'évolution du paysage à l'est de Lombok comporte quatre phases, à savoir:

- (i) avant l'éruption de 1257; le matériel pré 1257 dans la partie est de Lombok est constitué de couches alternées de brèches calcaires et de lave datant de la fin du Pliocène jusqu'au mi- Pléistocène; avec deux paysages vallonnés bordent cette zone dans la partie nord et sud.
- (ii) au lendemain de l'éruption de 1257; des PDC riches en pierre ponce ont recouvert la partie est de Lombok après l'éruption du volcan Samalas en 1257. Les vallées pré-éruptives ont été remplies du matériau volcanique nouvellement déposé en suivant les contours de la topographie pré-éruptive.
- (iii) après l'érosion des dépôts de PDC riches en pierre ponce; un nouveau réseau hydrographique est apparu assez rapidement, les grandes vallées principales étant principalement situées là où se trouvaient les vallées antérieures à 1257, et de nouveaux affluents plus courts, où se trouvaient des dépôts de PDC riches en pierre ponce. La matière volcanique déposée a été progressivement érodée à la

suite d'intenses pluies provoquées par des ruisseaux de montagne transportant des sables, des cailloux et des ponces.

(iv) aujourd'hui; l'extraction de la pierre ponce, très répandue dans toute l'île de Lombok, a accéléré l'évolution du paysage naturel, comme l'extension des zones cultivées des terres sous-exploitées aux grandes rizières, la pollution des cours d'eau et les dégâts des récifs coralliens.

Les résultats de l'étude montrent que le paysage de la partie est de Lombok est encore évolué jusqu'à présent. On peut le montrer par le volume de matière volcanique de l'éruption des Samalas en 1257 qui reste à environ 14% (soit $625 \times 10^6 \pm 5,5 \text{ m}^3$) du volume initial (soit $4\,435 \times 10^6 \pm 5,5 \text{ m}^3$), même si de nombreux processus d'érosion se sont produits entre 1257 et 2018.

Le deuxième objectif était de trouver et d'analyser des sources écrites locales liées à l'éruption du volcan Samalas en 1257, ainsi que ses impacts sur Lombok et les îles environnantes. Les sources écrites locales en Indonésie ont prouvé qu'elles peuvent fournir des informations détaillées sur les événements historiques comme les processus volcaniques du volcan Samalas en 1257 décrits dans la Babad Lombok (Lavigne et al., 2013). Dans cette thèse, la découverte et la traduction d'une autre source locale oubliée, appelée Babad Suwung, fournissent une description supplémentaire de l'éruption des Samalas sur l'île de Sumbawa. Ainsi, nous pensons que les processus volcaniques décrivant l'éruption du volcan Samalas dans la Babad Suwung pourraient être la plus ancienne observation visuelle de déferlantes pyroclastiques après celle de Pline le Jeune en 79 pour la Vésuve.

Le troisième objectif était recherché si un tsunami avait été déclenché par l'éruption du volcan Samalas en 1257. En général, les tsunamis provoqués par les éruptions volcaniques en Indonésie sont encore peu étudiés, que ce soient leurs

causes ou leurs conséquences. Néanmoins, nous avons pu trouver deux dépôts de tsunami le long de la côte ouest de Sumbawa, à savoir sur l'île de Belang et des bassins à poissons (*tambak*) abandonnés dans le village de Kiantar. Sur la base des résultats des datations au radiocarbone sur des échantillons de corail et de coquillage, l'éruption du volcan Samalas en 1257 dont les dépôts déclenché un tsunami mineur qui frappé l'île de Belang. Deux autres tsunamis se situent dans des bassins à poissons abandonnés datent du 4ème et du 9ème siècle de notre ère. Nous concluons que ces tsunamis ont été déclenchés par des activités tectoniques, car aucune éruption volcanique n'a eu lieu près du détroit d'Alas à ce moment-là, qui pourrait déclencher un tsunami.

Cette étude fournit de nouvelles informations relatives à l'impact géomorphologique d'une éruption volcanique majeure dans des zones côtières, dans ce cas-ci, dans la partie est de Lombok, ainsi que sur la côte ouest de Sumbawa. Cet apport est très important puisque l'Indonésie est connue comme un pays riche en volcans, avec plus de 130 volcans actifs. En outre, presque toutes les grandes villes d'Indonésie sont situées dans la zone côtière. Le manque d'informations liées à l'impact géomorphologique des éruptions volcaniques dans les zones côtières accroîtra le risque d'une future éruption volcanique majeure.

Acknowledgments

I would like to express my gratitude to all the people who have given me their trust, their help, and their time during my study for four years in France and Indonesia. This study was carried out at the Laboratory of Physical Geography - CNRS UMR 8591 Meudon with full support from:

- Indonesia Endowment Fund for Education (Indonesian Ministry of Finance – LPDP; S-320/LPDP.3/2014);
- Universitas Gadjah Mada, Indonesia (UGM/GE/3463/KP/09/13 and 4239/UNI.P.IV/SDM/DA/2018);
- University Paris 1 Panthéon Sorbonne (AAP Politique Scientifique Project: “*SAMALAS 1257 AD – Impacts environnementaux et sociétaux de l'une des plus grosses éruptions de l'Histoire*”);
- Indonesian Institute of Sciences - Research Center for Geotechnology (LIPI Geoteknologi);
- Universitas Mataram, Indonesia;
- Centre national de la recherche scientifique de la France (CNRS – PICS n°260868);
- Australian Research Council (Linkage Project LP150100649; “Hazards, Tipping Points, Adaptation and Collapse in the Indo-Pacific World”) led by Murdoch University;
- Ecole Doctorale de Géographie de Paris through its prize in the Scientific Poster Competition 2015 in Paris;
- Franco-Indonesian Association for the Development of Science (AFIDES) through its prize "Mahar Schützenberger 2017" in Paris;

- International Association of Geomorphologists (IAG/AIG) through its grants for young geomorphologist 2017 in New Delhi; and
- France Embassy and Institut Français in Indonesia through its prize in the *Ma Thèse en 180s Indonésie* 2018 in Poitiers, France.

I would like to thank Professor Franck Lavigne and Professor Hartono, my thesis directors, for directing and supporting me throughout this thesis, not only for their academic support but also for moral and financial support. Many appreciations are also given to members of the jury, Prof. Hervé Regnaud, Prof. Suwardji, Prof. Nathalie Carcaud, and Dr. Danang Sri Hadmoko, for their contributions to the thesis improvement.

I thank the Rector of Universitas Gadjah Mada in Yogyakarta, the Dean of the Faculty of Geography, and the Head of the Department of Geography and Environmental Science who allowed and supported me during my study in France. My gratitude also goes to Mrs. Emmy Indjatmiati SDM UGM and the members of SDM UGM who took care of my administrative files and the rescue fund at the end of my study.

Special thanks to Lalu Syafi'i, Bagus Septiangga, Syamsuddin, Hiden, Zet Mashadi, Arfian Ari, and all local peoples in Lombok and Sumbawa who were participated and helped me during the fieldwork. I would say many thanks to R.A. Zimmerman, M. Gims, P. Van Haver, D. Guetta, A. Van Buuren, M.B. Mathers III, I. Fals, Via Vallen, Nella Kharisma, NDX aka Familia, E.G. Ade, Pendhoza, and O.M. Monata for their support and encouragement during the writing process.

I would say many thanks to Kim, Sandy, Anne-Kyria, Louis, Marc, Marion, Anaëlle, Valentina, Annaig, Ludovic, Sarah, David, Yohan, Melody, Hippolyte, and all members of the Laboratory of Physical Geography for their help and sharing during my study.

My thanks and my deepest thoughts are addressed to my family in Yogyakarta and Purwokerto, as well as Didier and Véronique Obejero, who have always encouraged and accompanied me in happiness and difficulties.

Finally, this thesis is dedicated to my wife, Arum Puspitorukmi, and my children, Hanum and Hayu Mutaqin, for their understanding, sacrifice, and supports during my study in France.

Matur nuwun...

Terima kasih...

Merci beaucoup...

Introduction

Coastal area form at the interface between three major natural systems at the earth's surface, namely atmosphere, ocean, and land surface, which continually changes in response to human and natural forces, in the form of both physical and non-physical processes, such as storms, currents, erosion, and sedimentation (Kay and Alder, 1999; Beatley et al., 2002; Davidson-Arnott, 2010). One example of the natural forces that could change coastal outlines very rapidly and dramatically is volcanism. As the foremost agent of inland growth, volcanism contributes to expanding shorelines and can simultaneously build and destroy coastal landscapes, as well as contribute significantly to sediment production (Peterson, 1976; Ramalho et al., 2013).

A large volcanic eruption can trigger a caldera collapse (Lavigne et al., 2013; Torrecillas et al., 2013) and add huge quantities of sediment to rivers. Major et al. (2000) note that volcanic activity often leads to high rates of erosion and sedimentation, since eruptions, (especially explosive eruptions), destroy vegetation and deposit tephra over wide areas. Such conditions lead to increased rates of surface runoff during rainstorms and dramatically increase the amount of loose debris that can be eroded and transported into river valleys. This may cause widespread damage and sedimentation in downstream areas, including shore and nearshore areas (Smith and Lowe, 1991; Segschneider et al., 2002; Schneider et al., 2004; Kataoka et al., 2009; Németh et al., 2009; Kataoka et al., 2016), which can result in the land being extended (Cole et al., 2001; Németh and Cronin, 2007) or even a new island being created (Jakobsson and Gudmundsson, 2003).

One of the world's greatest and most powerful eruptions of the last 7,000 years took place on Lombok, Indonesia in 1257 CE, and involved the Samalas volcano in the Rinjani Volcanic Complex (Lavigne et al., 2013; Vidal et al., 2015; Vidal et al., 2016). Volcanic material expelled by the volcano in 1257 CE covered the islands of Lombok and Bali in their entirety, as well as parts of the islands of Sumbawa and Java. Four eruptive phases have been identified, referred to as P1–P4. Volcanic deposits in phase P1 are characterized by pumice fallout material with a reversely graded base. Normally graded pumice fallout deposits, accretionary lapilli, ash fallout, and pyroclastic surge deposits were produced during phase P2. The most widespread pumice fallout unit of the eruption was produced during phase P3. P4 volcanic deposits are characterized by pumice-rich PDC and co-PDC ash fall deposits (Vidal et al., 2015).

With a Volcanic Explosivity Index (VEI) of 7, this eruption generated more than 40 km³ dense rock equivalent (DRE) of volcanic deposits (Lavigne et al., 2013; Vidal et al., 2015). These deposits consisted of: (i) 7–9 km³ DRE of pumiceous Plinian fall products, (ii) 16 km³ DRE of pyroclastic density current (PDC) deposits, and (iii) 8–9 km³ DRE of co-PDC ash that settled over the surrounding islands. The material from P4 was identified as far as 660 km from its source, on the flanks of the Merapi volcano on Java Island (Figure 1; Vidal et al., 2015).

Almost 800 years after the 1257 CE eruption, Samalas volcanic deposits have contributed towards the excellent preservation of the paleo-surface, making it suitable for further investigation, such as the reconstruction of the 1257 CE topography, calculation of the volume of volcanic material from the 1257 CE eruptions, and analysis of its geomorphological impact. However, the geomorphological impact of this eruption on the island of Lombok remains unknown, whereas its overall climatic and societal

consequences are now better understood (Stothers, 2000; Kim and Kim, 2012; Guillet et al., 2017).

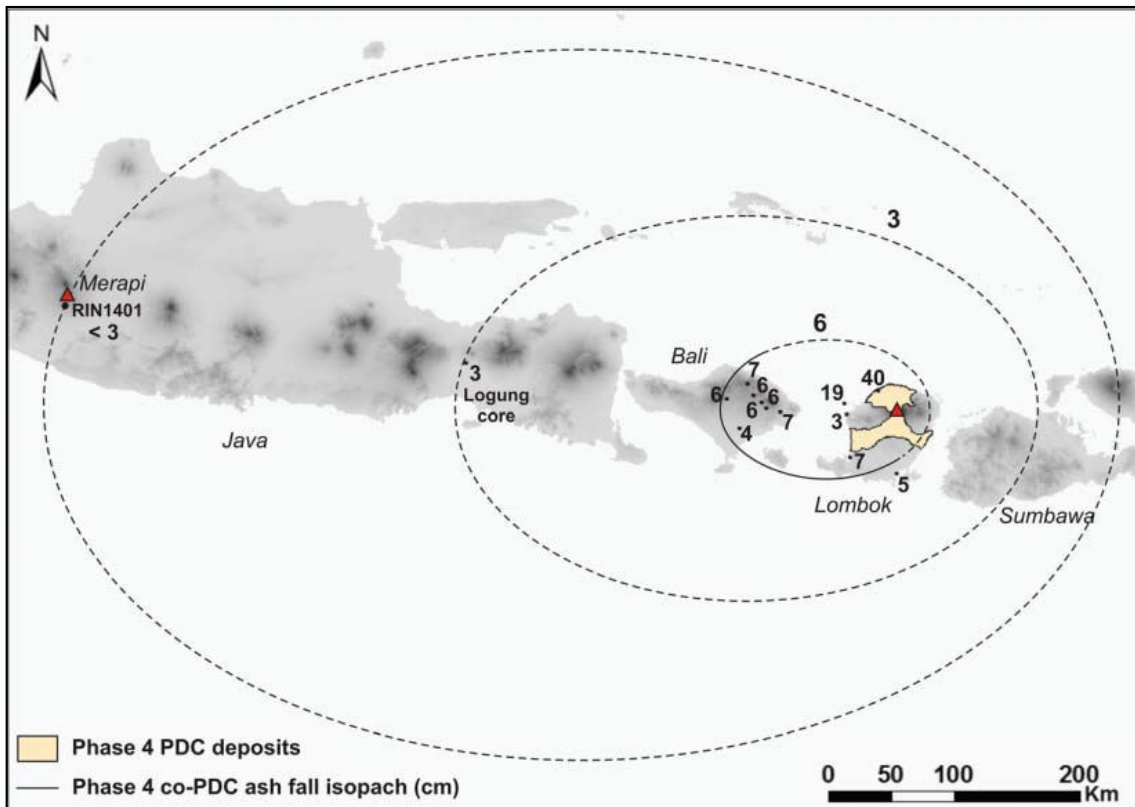


Figure 1. Onshore distribution of PDC deposits emplaced during phase P4, and isopach contours of associated P4 co-PDC ash fallout (in cm) (Source: Vidal et al., 2015).

The main objective of this study is to explore and to understand geomorphic impacts of the 1257 CE eruption of Samalas volcano along the Alas Strait between Lombok and Sumbawa Islands in Indonesia. There are three scientific questions related to the objectives such as follows:

1. Can we precisely reconstruct the landscape evolution since the early 13th century, i.e., before, during, and after the 1257 CE eruption of Samalas volcano?

2. Are there any local written sources about the Samalas eruption and its impacts on Lombok Island and or another surrounding island?
3. Did the 1257 CE eruption of Samalas volcano trigger a tsunami along the shore of the Alas Strait?

To answer these challenging questions, we carried out a multidisciplinary approach that included geomorphological surveys on natural and human-made outcrops, inland and near-shore geophysical measurement, remote sensing and geographic information system (GIS) techniques, in-depth interview, as well as an analysis of local written sources.

This Ph.D. thesis consists of 6 chapters (Figure 2) such as follows:

Part 1: State of the art, field presentation, and research methodology

- Chapter 1: Coastal evolution related to volcanic eruptions

This chapter describes the coastal dynamics especially in the tropical area, its definition and influencing factors, type of volcanic materials reaching the sea and its impacts on the sea.

- Chapter 2: Lombok Island, Sumbawa Island, and Samalas volcano

It describes the study area including geographic information, its geomorphological features; geological setting, as well as its relation with the Samalas volcano.

- Chapter 3: Research methodology

This chapter displays in detail about the methods in this study, which includes data collection, field investigations, and data analysis.

Part 2: Geomorphic impacts of the 1257 CE eruption of Samalas volcano along the Alas Strait

- Chapter 4: Local impacts of the 1257 CE eruption in East Lombok

This chapter presents the reconstruction of the pre-1257 CE topography on the eastern part of Lombok, which had been severely affected by the PDCs, including calculation of the actual volume of the 1257 CE PDC deposits in this area. This chapter has been published in *Geomorphology* (2018). It is entitled “Landscape Evolution on the Eastern Part of Lombok Island (Indonesia) related to the 1257 CE Eruption of Samalas Volcano”. Some data in Chapter 4 were presented at two international conferences: first, at the 9th IAG – International Conference on Geomorphology, on November 6 – 11, 2017, New Delhi, India; and second, at the 15th Annual Meeting of Asia Oceania Geosciences Society (AOGS), on June 3 – 8, 2018, Honolulu, the United States of America.

- Chapter 5: Regional impacts of the 1257 CE eruption in West Sumbawa

This chapter presents the regional impacts of the 1257 CE eruption of Samalas volcano in West Sumbawa. The relation between local written sources with the 1257 CE eruption processes, such as volcanic ash and PDCs are also discussed in this chapter, as well as the anthropogenic impacts of the 1257 CE eruption up to now.

- Chapter 6: Did the 1257 CE eruption of Samalas trigger a tsunami?

In this chapter, we tried to answer the third issue from our three scientific questions as mentioned above, i.e., did a tsunami occur following the 1257 CE eruption of Samalas volcano? Furthermore, this chapter also presents the results of our fieldwork on the west coast of Sumbawa related to the 1257 CE PDC-triggered tsunami. Some data in Chapter 6 were presented at the 2nd International

Conference on Environmental Resources Management in Global Region (ICERM), on October 22 – 23, 2018, Yogyakarta, Indonesia.

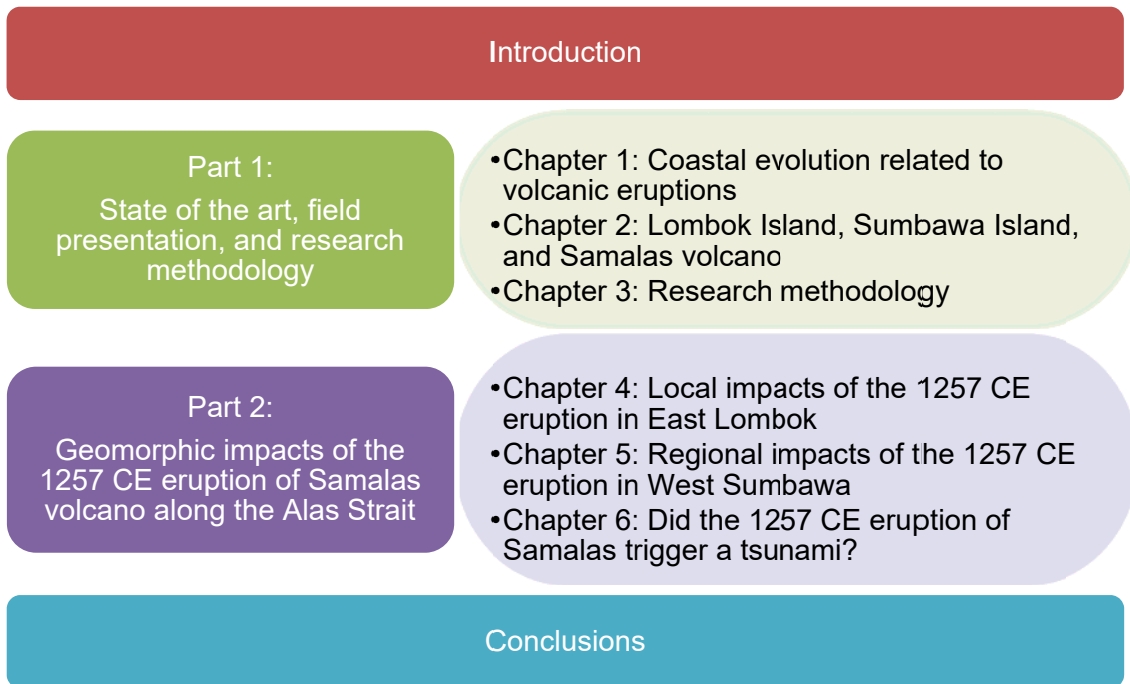


Figure 2. Ph.D. thesis outline.

Indonesia Endowment Fund for Education (Indonesian Ministry of Finance - LPDP) fully supports this study, and as part of a collaboration project between Universitas Gadjah Mada, University Paris 1 Panthéon Sorbonne, Indonesian Institute of Sciences - Research Center for Geotechnology, and Universitas Mataram. Field works were funded by the University of Paris 1 Panthéon Sorbonne (AAP Politique Scientifique), the Centre national de la recherche scientifique (CNRS – PICS n°260868), and the Australian Research Council (Linkage Project LP150100649) led by Murdoch University.

PART 1
State of the art, field presentation,
and research methodology

Chapter 1: Coastal evolution related to volcanic eruptions

The first chapter provides an overview of the related literature used to support the discussion in this research. It discusses the coastal dynamics in the tropical area, its definition and influencing factors, type of volcanic materials arriving at sea and its impacts on the sea.

1.1. Coastal dynamics in the tropical area

1.1.1. Conceptual framework and terminology

Coastal areas in its most general terms consist of the interface between land and sea, with the landward boundary encompassing the mainland, either dry or submerged in water which is still influenced by the sea breeze, tide, seawater intrusion, and characterized by typical vegetation. The landward boundary in the coastal area can genetically derive from marine processes, fluvio-marine processes, or aeolian processes. Seaward boundary is the outer limit of the continental shelf, which has unique characteristics and still influenced by the natural processes occurring on the land, such as sedimentation and freshwater flows, and processes caused by human activities on land such as deforestation and pollution (French, 1997; Beatley et al., 2002).

According to Kay and Alder (1999), coastal areas include terrestrial and marine components. They encompass the land and sea borders, which are determined by the level of influence of the land to the sea and vice versa. Furthermore, they do not have a similarity of width, depth, and height. Coastal areas have significant economic benefits,

which are obtained from the richness and diversity of ecosystems. Currently, coastal areas are the most densely populated and most complex landuse compared to other areas. More than 60% of the population lives in coastal areas (Figure 3) that carry the consequence of high natural resource exploitation, e.g., fisheries, mining, and forestry (Kay and Alder, 1999). The high intensity of human activities in coastal areas such as industrial, urban, residential, conservation, mining, gives rise to some conflicts from one to another.

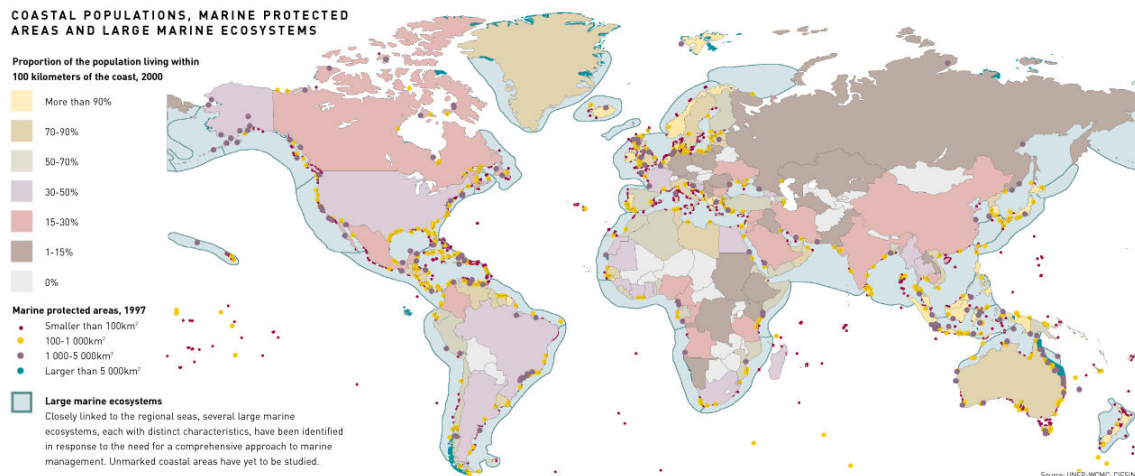


Figure 3. Coastal populations, marine protected areas, and large marine ecosystems around the world. The number of coastal population is a proportion of the population living within 100 km of the coast in 2000 (Source: Harrison and Pearce, 2000).

Coastal areas are divided into different parts, such as shore, coastline, foreshore, backshore, nearshore, and offshore (Figure 4). The shore is the area between the low tide line and the upper limit of normal wave action, usually extending to the cliff base or the vegetation line (Duxbury et al., 2002; Schwartz, 2005; Bird, 2008; Davidson-Arnott, 2010).

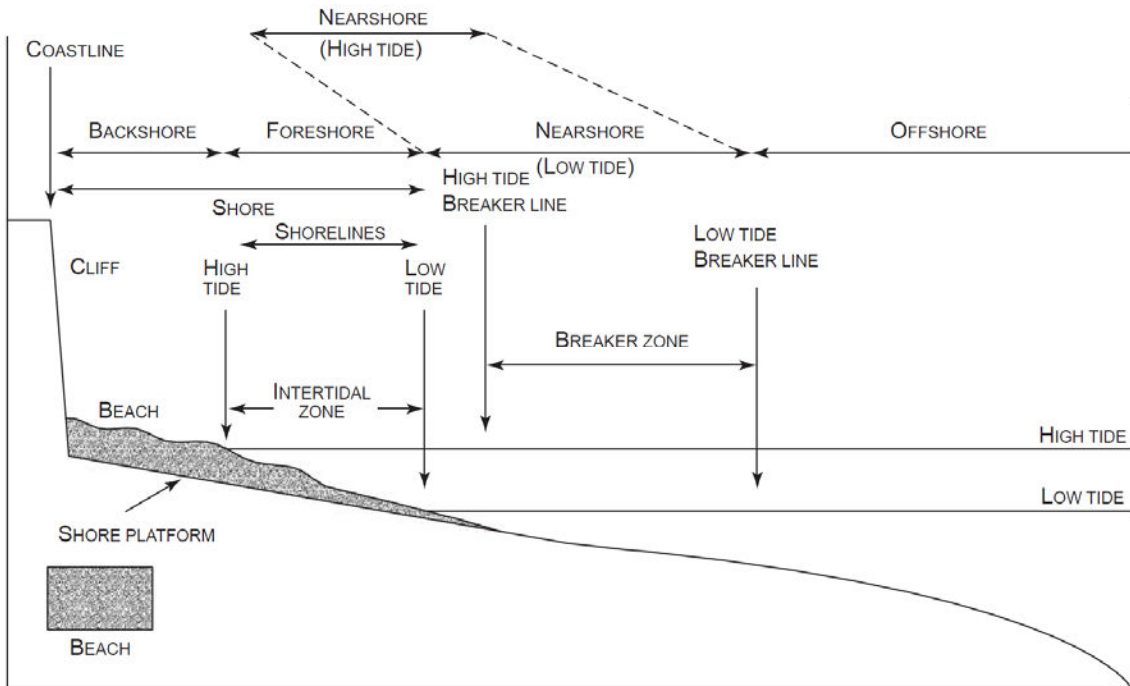


Figure 4. Coastal terminology (Source: Bird, 2008).

The shoreline is defined as the area that is delimited by high tide and low tide line which is highly dynamic due to vertical movements of the continent and variations of sea level. The existence of shoreline in the tropics can be in the form of a sandy beach, rocky beach, a cliff, a mangrove or an artificial boundary, e.g., a dock and a retaining wall (Vieux et al., 2008).

In the American literature, the term of shoreline is often used as a synonym of coastline while the coast is elaborating to the coastal area (Bird, 2008). The main difference between these terms is that the shoreline moves back and forth as the tide rises and falls, whereas the coastline is submerged only in exceptional circumstances, such as during storm surges or tsunamis. The coastline is defined as a line that forms the boundary between the land and the ocean, usually marked by the vegetation line or the cliff base during high tide.

The nearshore is defined as an area that extends from the line where waves begin to break to the low tide line further inland, while the beach is an area where loose sediments, such as sand and shingle, are accumulated. Due to its location in the area where three major natural systems at the earth's surface meet and interact, a series of processes occur in the coastal area. These processes include effects of tides, waves, and currents in the sea, tectonic movements, sea level change, sedimentation, tsunami, as well as global warming (Figure 5).

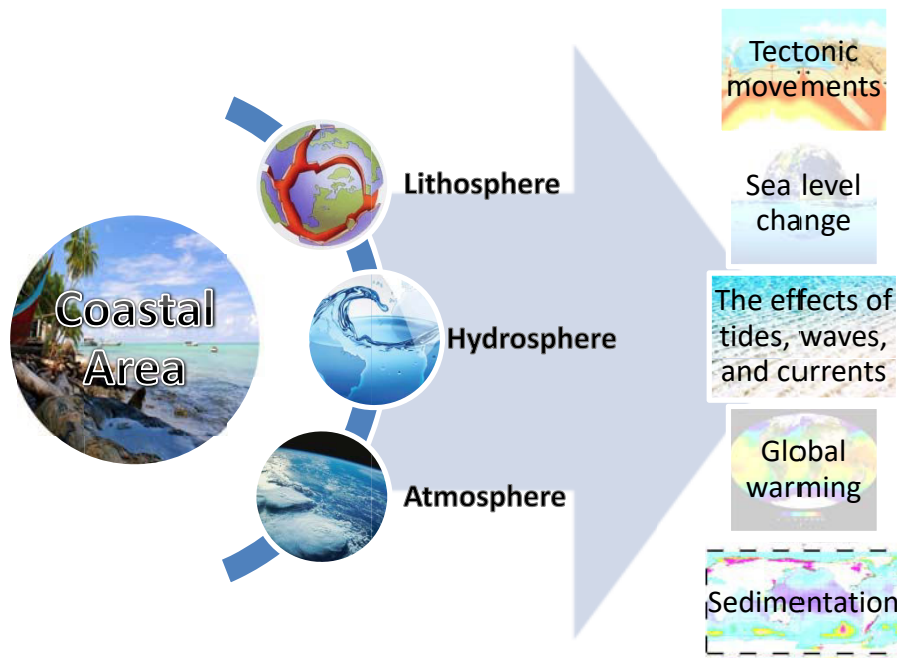


Figure 5. The processes series in the coastal area.

1.1.2. Typology of the coastal area

An understanding of the classification system of the coast is needed to study the typology of the coastal area. There are several classification systems for the coastal area, for example, Davis (1996) classified the coast in 2 categories, 1) formed by erosion and 2) formed by deposition, while other researchers have their categories

based on 1) the type of sediment, i.e., coarse clastic (shingle and sand) or muddy (King, 1959), 2) emerged or submerged (Johnson, 1919; Valentin, 1952), and 3) according to tectonics (Inman and Nordström, 1971).

The classification of coastal systems by Shepard (1973); and revised in following years, is the most considerably used in the coastal studies in Anglo-Saxon countries (Figure 6). This classification system refers to the most dominant processes in the coast. Shepard (1973) classified the coast into two classes: first, the primary coast is mainly formed and controlled by land processes, such as erosion, sedimentation, volcanic, and diastrophism. The primary coasts include land erosion coasts such as drowned river valleys (Ria coasts) and karst coasts. Other primary coasts include subaerial deposition coast, e.g., deltaic coast; volcanic coast, e.g., lava-flow and tephra coast; and structurally shaped coast such as faults and fold coast.

Second, the secondary coast is shaped primarily by the sea or by marine organisms. The secondary coast includes marine deposition coast, which is formed by the deposition of marine sediment material due to waves and currents actions. Other secondary coasts include wave erosion coasts and coast builds by organisms. Wave erosion coast is a coast where the coastline is formed by wave action and may result in the straightened or irregular cliff. While a coast built by organisms is the result of construction by either fauna or flora, e.g., coral reef coast, atolls, and mangrove coast, which is very common in the tropics.

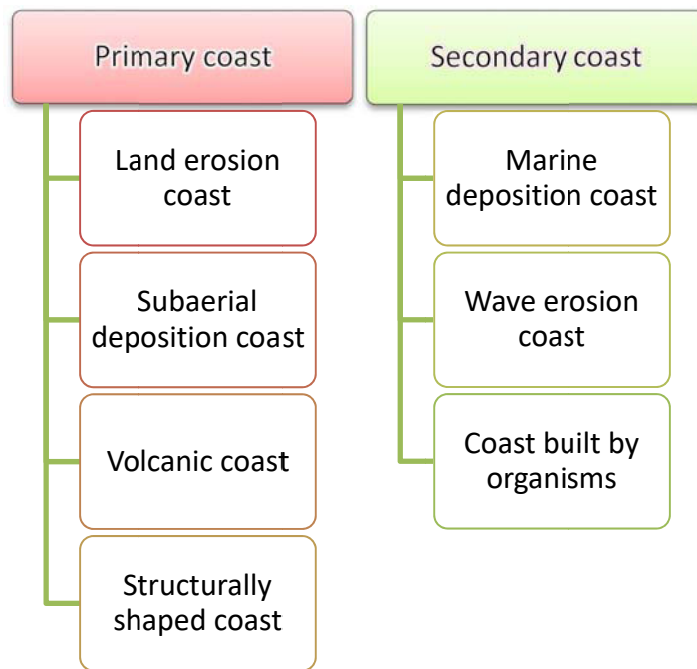


Figure 6. The classification of coastal systems by Shepard (1973).

1.1.3. Factors influencing coastal dynamics

Coastal dynamics is the change of space and time in coastal areas caused by astrodynamics, aerodynamics, hydrodynamics, morphodynamics, geodynamics, ecodynamics, and anthropodynamics factor (Figure 7; Sunarto, 2000). Astrodynamics factor occurs due to the influence of the celestial object position, such as the Moon and the Sun. These factors affect sea tides, seasonal changes, wind movement, humidity, and temperature. Extreme weather, for example during the seasonal changes or the peak of East Monsoon, can result in the increasing of wind and wave energy which led to destructive waves in the coastal area (Shore Protection Manual, 1984; Davidson-Arnott, 2010; Mutaqin et al., 2014; Mutaqin, 2017).

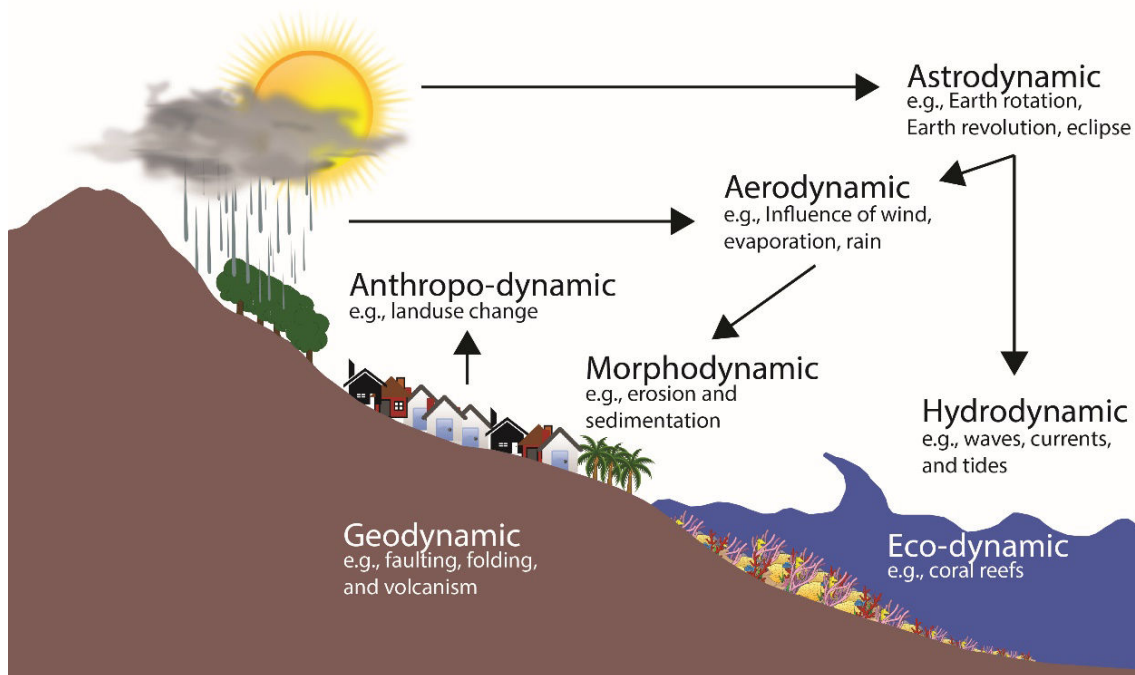


Figure 7. Factors influencing coastal dynamics.

Aerodynamic factors occur due to the influence of air or wind movement, e.g., coastal upwelling. Coastal upwelling is the result of wind-driven currents; it transports cold and nutrient-rich water to the surface. This phenomenon inhibits the increase in the number of sweltering days as well as the formation of tropical cyclones, e.g., El Nino, which may destruct the coastal environment, for example in the Atlantic Iberian sector, Moroccan subregion, and Colombia (de Castro et al., 2014; Santos et al., 2016).

The hydrodynamic factor is the result of seawater movements such as waves, currents, and tides. An example of a hydrodynamic factor is longshore current, which generated within the surf zone and moves parallel to the shoreline. A longshore current could transport the sediment along the shore, which can cause erosion or accretion in

the beach and coastline (Komar and Inman, 1970; Kobayashi et al., 2007; Gomes and Silva, 2014; Jackson et al., 2017).

Geodynamic factors from endogenic processes such as faulting, folding, and volcanism also can lead to the coastal evolution. Coastal uplift due to tectonic movements is a common phenomenon in active tectonic areas, especially following to a megathrust earthquake, as mentioned by Searle (2006), Kitamura and Kobayashi (2014), Mouslopoulou et al. (2016), and von Huene et al. (2016).

The existence of primary ecosystems in the coastal area, i.e., coral reefs, mangroves, and seagrass (Mutaqin and Rohmah, 2013; Guannel et al. 2016) which is an eco-dynamics factor, may affect the coastal landscape. Coral reefs as the first barrier can reduce the energy of waves that strike the shore (Ferrario et al., 2014; Costa et al., 2016; Hongo et al., 2018; Harris et al., 2018). Furthermore, coral reefs as coastal protection may minimize the coastal erosion (Silva et al., 2016; Reguero et al., 2018) and significantly reduce the risk from coastal hazard for about 200 million people in the world (Ferrario et al., 2014).

Human activities, either inland or in the sea, which causes landscape evolution in the coastal area categorizes into anthropo-dynamic factor. Since the Holocene era, human activities are mentioned as one of the factors that can affect the coastal dynamics (Alizadeh et al., 2015). Thenceforth, human pressures in the coastal area (e.g., land reclamation, landuse change) had increased due to their needs related to economic factors (Aretano et al., 2017; Mutaqin, 2017). Furthermore, another negative impact of an anthropo-dynamic factor in the coastal area is morphological changes such as erosion, accretion, and an evolution of the delta (Carrasco et al., 2012; Wang et al., 2015; Ogorodov et al., 2016; Zhu et al., 2016; Du et al., 2016).

A morphodynamic factor may cause erosion and sedimentation in the coastal area (Paskoff, 1981, 1998), for example, is the delta formation and changes in the direction of river flow in the estuary. Delta, in general, is a vulnerable geomorphic landscape in the coastal area that can evolve rapidly due to several elements, e.g., hydrodynamic factors (Anthony, 2015; Deng et al., 2016; Su et al., 2017).

There is an inter-relation between upstream and downstream areas in one system which is called a watershed. Indonesian Act Number 7 of 2004 stated that a watershed is a landscape, a bounded hydrological system, which is receiving, storing, and flowed water through the rivers and has a single outlet in the lake or the ocean. It means that upstream activities will have impacts on downstream. Watershed system continually changes in response to natural and human forces.

Coastal sedimentation occurs when the eroded material has deposited downstream by runoff into surface waters such as estuaries. The sedimentation rate is the most informative quantitative indicator of the sedimentary process. Naturally, sedimentation rates in the coastal area are high and will get worse when the people did lousy conservation practices and by altering circulation patterns (Schubel, 1977). In past years, sediment input has dramatically increased in coastal areas due to material from the volcanic eruption (Vogel and Märker, 2010; Ramalho et al., 2013), rising of upstream erosion, bedload, and suspended load.

Annual sediment yields in worldwide rivers based on Garrels and Mackenzie (1971) suggest that 20.2 billion tons of suspended sediment enter the ocean each year (Figure 8), while in Indonesia, 44,197 tons/km² enter the ocean each year (FAO, 2000). The NOAA National Geophysical Data Center (NGDC) has compiled a digital total sediment thickness database for the world's oceans and marginal seas with five arc-

minutes (10 km) spatial resolution (Figure 9) from three principal sources (Divins, 2003): first, from previously published isopach maps from Ludwig and Houtz (1979), Matthias et al. (1988), Divins and Rabinowitz (1990), Hayes and LaBrecque (1991), and Divins (2003); second, from ocean drilling results, either from the Ocean Drilling Program (ODP) or the Deep Sea Drilling Project (DSDP); and third, from the NGDC seismic profiles combined with seismic data and isopach maps from Intergovernmental Oceanographic Commission (Udinstev, 2003).

| SEDIMENT TRANSPORTATION PROCESS | AMOUNT OF SEDIMENT TRANSPORTED (BILLIONS OF TONS PER YEAR) |
|--|---|
| Suspended sediment in rivers | + 20.2 |
| Dissolved chemicals in rivers | + 4.6 |
| Ice | + 2.2 |
| Ground water | + 0.47 |
| Marine erosion | + 0.28 |
| Wind-blown dust | + 0.06 |
| Salt spray | - 0.29 |
| TOTAL SEDIMENT TO OCEAN | + 27.5 Billion tons per year |

Figure 8. Amount of sediment transported to the ocean (Source: Garrels and Mackenzie, 1971).

High sedimentation rates in Indonesia for example in Segara Anakan Lagoon, and in the Porong River in Java Island. Sedimentation over the years in these areas has resulted in silting and narrowing of the lagoon area. Upstream erosion occurs intensively and contributes up to 1,000,000 m³ sediment per year (Sukardi, 2010). Since huge amounts of mud materials from the Lumpur Sidoarjo Volcano in northeastern Java have been sent to the sea through Porong River, and then it causes high rates of sedimentation in the mangrove forests in Porong Delta. Sidik et al. (2016) mention that rates of sedimentation in the mangrove forests in Porong Delta are up to

20 cm/year and dry season rates of about 5 cm/year. Consequently, there is a reduced growth of mangrove trees (i.e., *Avicennia sp.*), as well as provided increase to high soil surface elevation gains.

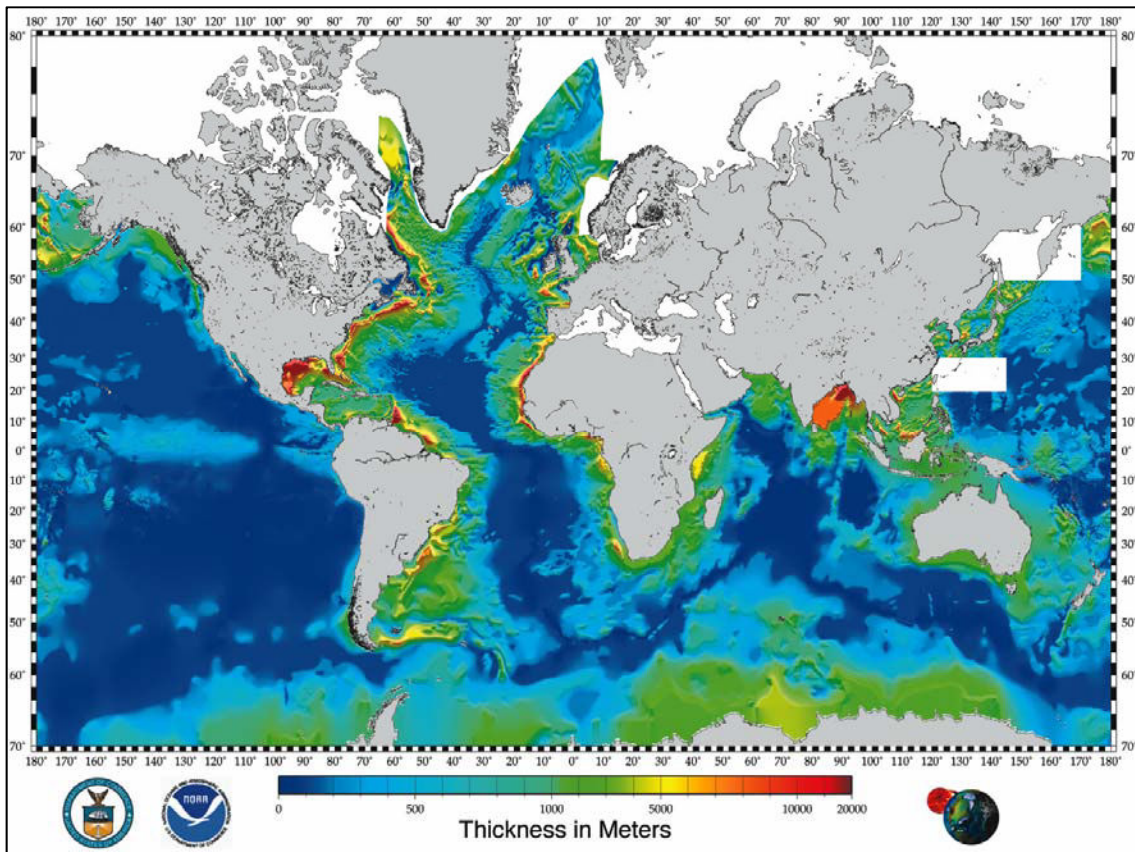


Figure 9. Total sediment thickness database for the world's oceans and marginal seas (Source: Divins, 2003).

Human is a geological agent, and human activity can cause a profound impact on coastal landforms and sedimentation (Mei-e, 1992). High soil erodibility, deforestation, lousy cultivation, and landuse change can accelerate the processes of erosion, transport, and sedimentation. High erosion in the upstream area can cause local scour problems along with severe sedimentation downstream (Julien, 2010). Annammala et al. (2013) also mentioned that sedimentation is downstream consequences in large

tropical catchments affected by upstream logging and landuse change and recent increases in rainstorm magnitude-frequency.

1.2. Coastal sedimentation caused by volcanism

The material of volcanic origin may be transported and deposited in a considerable distance from the source; started from near the crater or caldera, and can reach the sea in several ways: fallout, PDC, and lahars (Fisher and Smith, 1991; McPhie et al., 1993; Manville et al., 2009).

1.2.1. Fallout

Volcanic eruptions can eject a wide variety of materials in the air, defined as tephra. An explosive eruption ejects large amounts of bombs or blocks, lapilli, volcanic ash, pumice, and gas into the atmosphere with dangerous consequences for the environment and climate. According to grain size, bombs or blocks are larger than 64 mm in diameter, while lapilli are fragment with 2 mm to 64 mm in diameter (Fisher et al. 2006). Volcanic ash is an example of the fine material, which in classical sedimentology refers to pyroclasts less than 2 mm in diameter (Fisher et al., 2006; Rose and Durant, 2009; Duggen et al., 2010) and typically has a high dust content (Walker, 1981). Volcanic ash normally consists of three primary elements, i.e., particles of minerals, glass shards with pumice fragments (occasionally); and accidental lithic particles (Stix and Gaonac'h, 2000). As an output of explosive eruptions, volcanic ash reaches the troposphere and stay above for days to weeks (Duggen et al., 2010), before travel a significant distance along with the wind and then deposited on the earth's surface (Karstens et al., 2013) (Figure 10). In the case of a large explosive

eruption (VEI > 3), the volcanic ash may reach the stratosphere and travel thousands of kilometers away from their source.

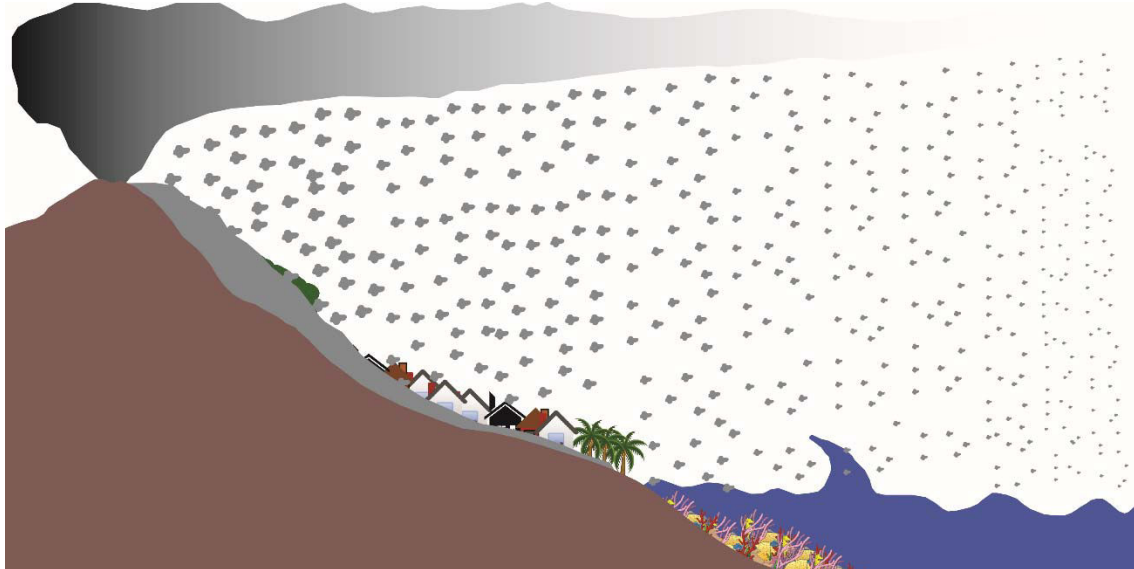


Figure 10. Volcanic ash deposits are thick and coarse in particle size near the volcano.

However, at a distance, the deposit gets thinner and finer.

Volcanic ash from explosive eruptions may fall immediately from eruption columns or co-ignimbrite clouds generated by pyroclastic flows (e.g., Montserrat, 1996 - 1998) (Baxter, 2000). There are four types of volcanic eruptions which produce fine ash and dust in vast quantities, i.e., ignimbrite-forming, Plinian, Vulcanian, and phreatomagmatic eruption (Walker, 1981; Sigurdsson and Carey, 1989).

In addition to volcanic ash, pumice is also a fragmentary material that is ejected during most explosive volcanic eruptions and can potentially enter the ocean at the same time with volcanic ash during the tephra fallout. Pumice is a porous volcanic material with low density ($0.5 - 1.5 \text{ g/cm}^3$), has light gray or brown color, and typically has $0.2 - 10 \text{ cm}$ in diameter (Dehn and McNutt, 2000). Fiske et al. (2001) explain that

pumice clasts cooling in the atmosphere would have ingested air as magmatic steam condensed which generates a light-weight material. The fallout of pumice over the ocean in enormous quantities may cause pumice raft formation (McKee et al., 1985). The pumice raft (Figure 11) is very transportable along with the currents and also played an essential role in tephra spreading (Coombs and Landis, 1966; Tani et al., 2008), as well as plant migration in a long distance from its source through the sea (Bryan et al., 2004; Kusky, 2008).

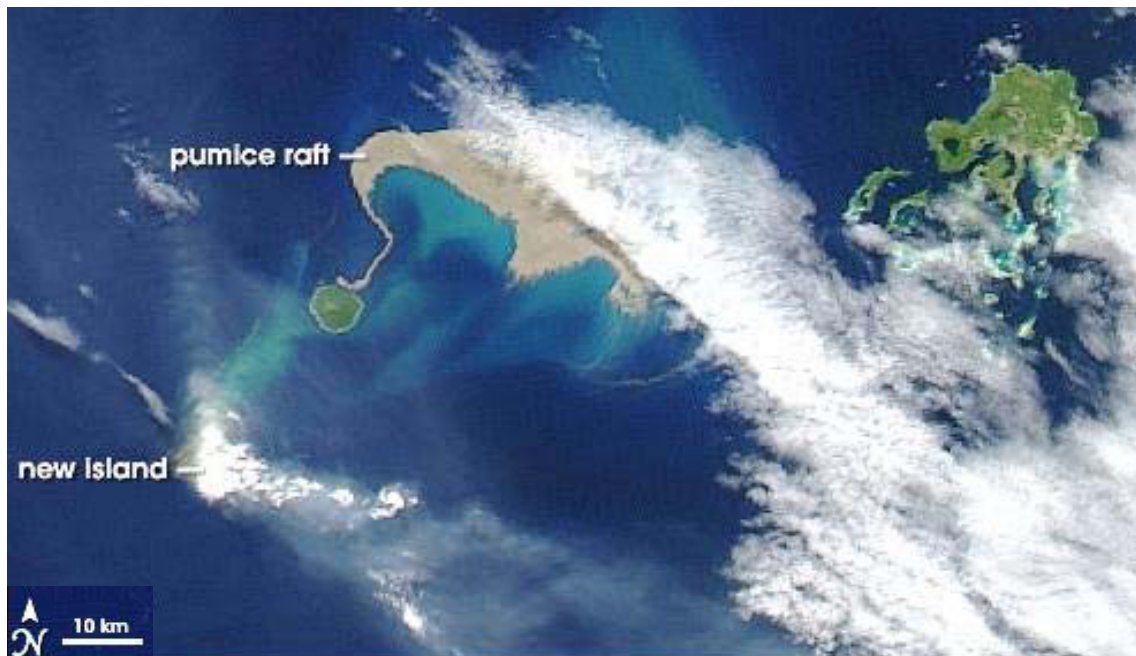


Figure 11. Pumice raft in Tonga Islands, South Pacific from Aqua MODIS satellite on 10 August 2006 (Courtesy: NASA Earth Observatory, 2006).

1.2.2. Pyroclastic density currents (PDCs)

Near-shore volcanoes that trigger explosive eruptions can produce pyroclastic density currents (PDCs), which can penetrate the sea and produce volcanoclastic submarine sediments (Le Friant et al., 2009, 2010; Karstens et al., 2013). Explosive

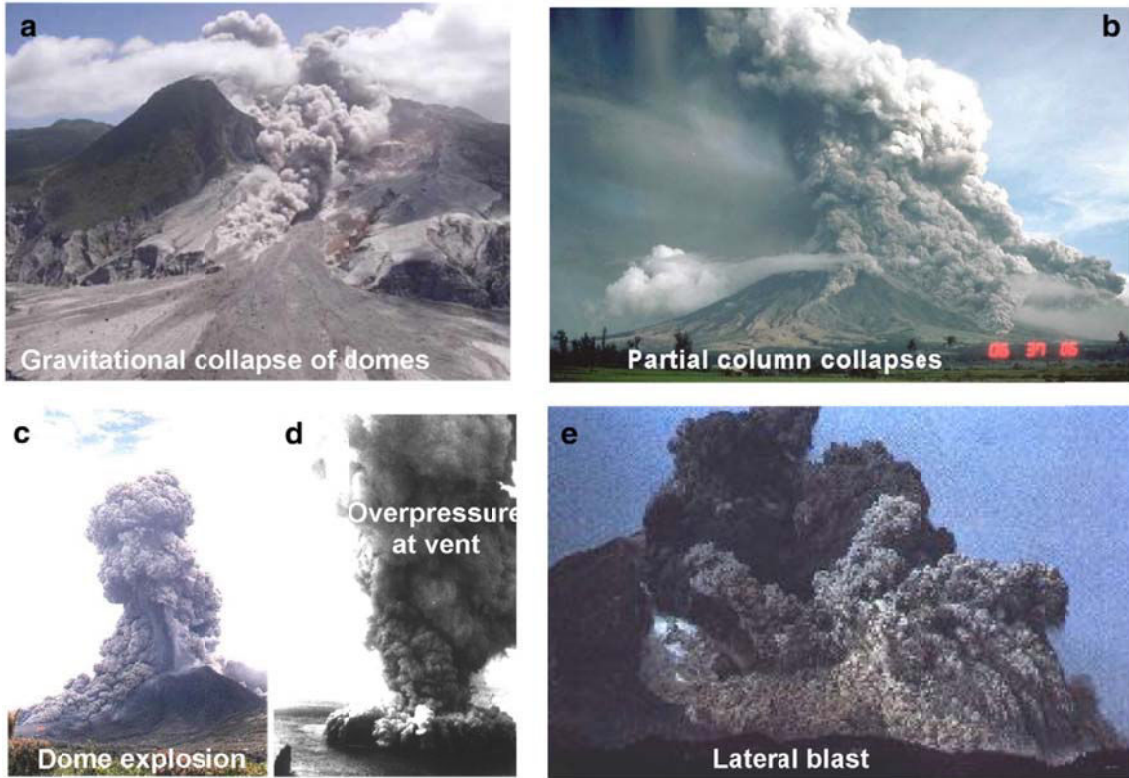
volcanic eruptions generate multiphase flows composed of solid and gas-particle, which descend from the volcano due to gravity and topographic differences (Doronzo and Dellino, 2014; Sulpizio et al., 2014). PDC deposits frequently have cross-bedded layers with fallout deposits following Plinian and Subplinian eruptions. They result from pyroclastic flows formed by the collapse, either total or partial, of the eruptive column (Cioni et al., 2000).

There are two types of pyroclastic density currents, i.e., dilute end-member and concentrated end-member. Dilute end-member also known as pyroclastic surges that are low particle concentration and strongly turbulent PDCs. While concentrated end-members refer to a pyroclastic flow which is a high particle concentration with a poorly sorted material and composed of hot-dry rock fragments mixed with hot gases (Cas and Wright, 1988; Wilson and Houghton, 2000).

Sulpizio et al. (2014) mention that based on the duration of the current, PDC is classified into two categories namely short-lived (e.g., dome collapse, partial column collapse, dome explosion, lateral blast) and long-lived (e.g., continuous column collapse and boiling over of pyroclastic mixture) phenomena. Both can be induced either by magmatic or phreatomagmatic magma fragmentation (Figure 12).

There are three possibilities or scenarios when a PDC reaches the ocean (Freundt et al., 2000; Freundt, 2003) (Figure 13): first, happening of coastal steam blasts due to mixing between PDCs and seawater. In addition to that, PDCs which mix with seawater may result in high-concentration turbidity currents or debris flows. Second, PDCs travel across the seawater, and then at some distance, drop the sediment into the ocean. Third, PDCs which remain intact force out the shallow water in the nearshore until they convert into debris flows.

Short-lived (transient) phenomena



Long-lived (continuous) phenomena

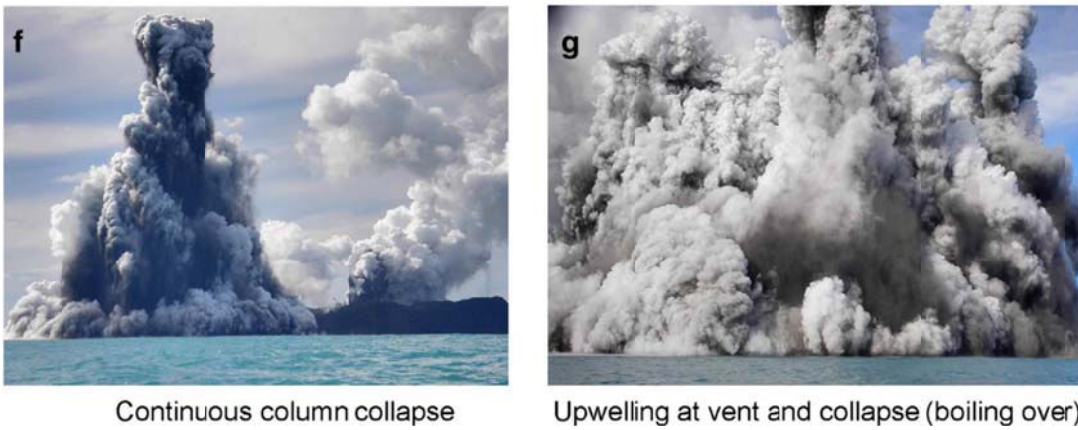


Figure 12. Examples of PDCs generation from various eruptive processes (Source: Sulpizio et al., 2014).

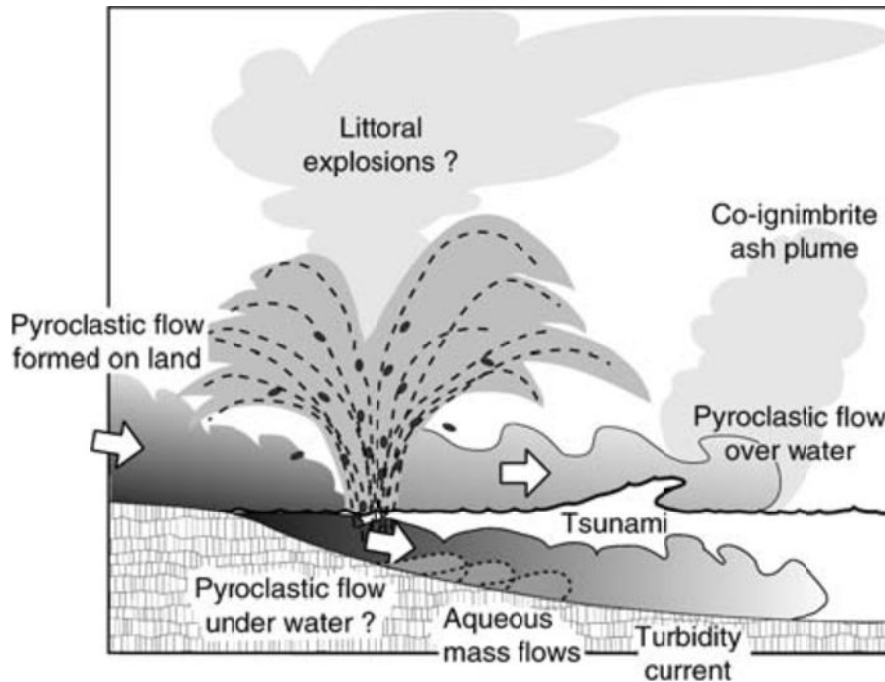


Figure 13. Illustration of several scenarios where pyroclastic flows formed on land enters the sea (Source: Freundt, 2003).

1.2.3.Lahars

"Lahar" is an Indonesian term that most frequently refers to flow from a volcano which characterizes by poorly sorted sediment-laden composed of rock debris and water with more quantity than regular streams (Lavigne and Thouret, 2003; Lavigne et al., 2007). Lahar describes a process of volcanic erosion, it brings the volcanic materials that mixed with water, and it is characterized by a rapid flow from upstream to downstream (van Bemmelen, 1949; Smith and Fritz, 1989; Neall, 2004; Vallance, 2005).

Lahars have an extensive variation in magnitude and a high frequency of occurrence as they can occur during an eruption, after an eruption, or without eruption (syn-, post-, and non-eruptive lahars) (Crandell, 1971; Vallance and Iverson, 2000;

Lavigne and Thouret, 2000; Lavigne and Thouret, 2003). The rock materials carried by lahars make them particularly destructive; the abundant liquid in lahars allows them to float on gentle gradients and inundating the areas far from their sources. Unlike any other volcanic hazard, lahars do not require an eruption. Vallance (2000) explained that the occurrence of lahar needs several requirements, i.e., 1) a sufficient water source; 2) affluent unconsolidated debris (e.g., pyroclastic flow and pyroclastic fall material); 3) steep slopes and significant relief at the source; and 4) a triggering event. Severe weather, e.g., heavy rain or rainfall runoff, is an example of a triggering event which may trigger a lahar (Rodolfo, 2000). Due to their characteristics as mentioned above, lahars can flood and reach coastal areas, tens of kilometers away from the volcano crater, then affect the landscape dynamics in the area (McCoy and Heiken, 2000; Encinas et al., 2006; Bartolini et al., 2014).

Lahars deposits result from reworked pyroclastic deposits by water. These deposits are generally characterized by a thickness of metric order per event and can reach up to several meters. The size of the materials transported by lahars is varied from several meters (e.g., blocks) to a few microns (e.g., clay fraction). The stratification of a volcanoclastic deposit can categorize as 1) normal, 2) reverse, 3) inverse to normal symmetric, 4) normal to inverse symmetric, 5) multi-normal, and 6) multi-reverse (Figure 14).

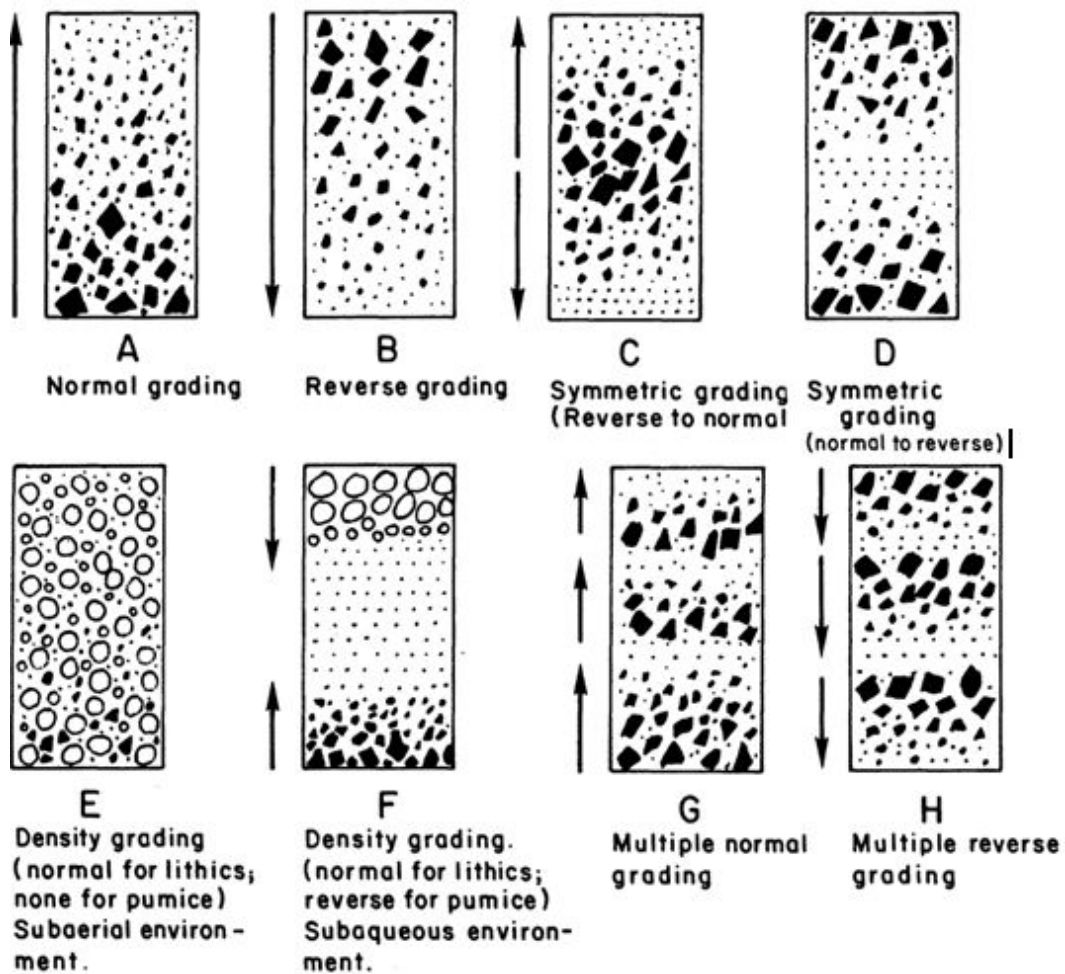


Figure 14. The stratification of a volcaniclastic deposit (lahars) (Source: Fisher et Schmincke, 1984).

For lahars that contain pumice after a large eruption ($VEI \geq 4$), there is a mixture between a normal granulation for lithic and a lack of granulation for pumice vesicles, evenly distributed within the deposit (Fisher et Schmincke, 1984). Figure 15 illustrates the sources, transport, and processes of volcanic materials (e.g., fallout, PDC, and lahar) in the coastal area.

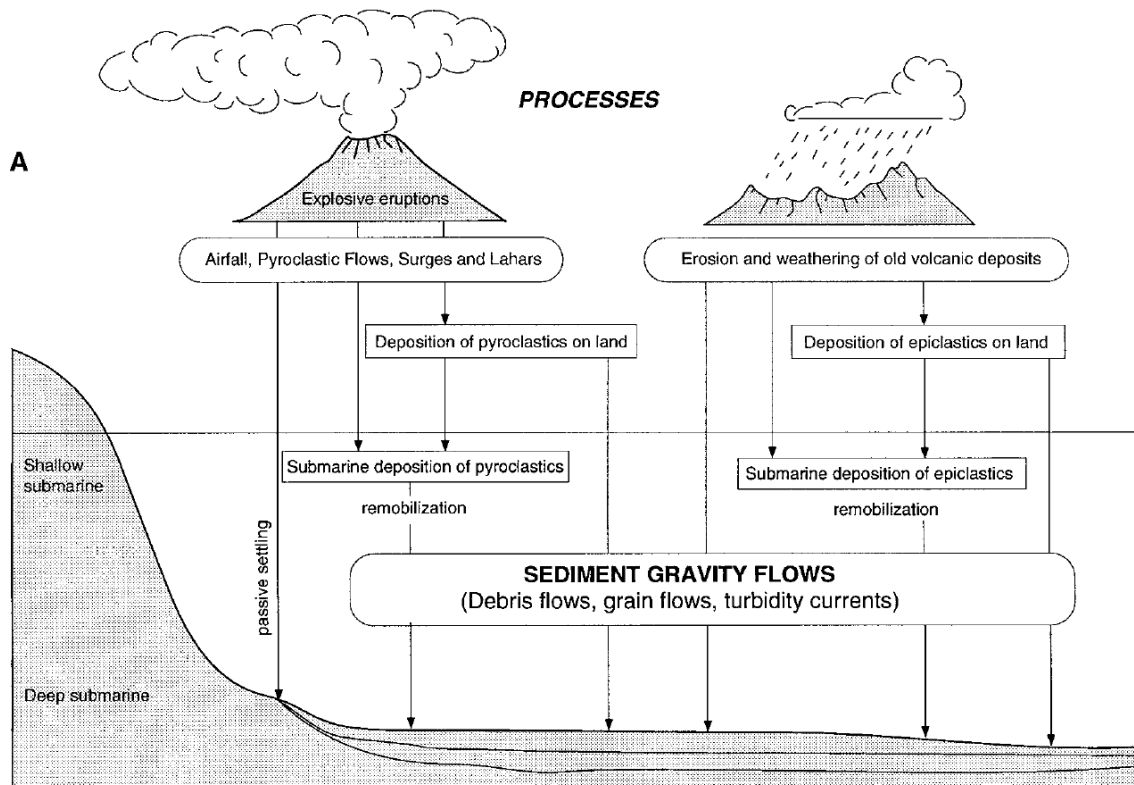


Figure 15. An illustration of the sources, transport, and processes of volcanic materials in the coastal area (Source: Carey, 2000).

1.3. Impacts of volcanic materials at sea

1.3.1. High sedimentation due to volcanic activity

Volcanic eruptions may trigger high sedimentation rates and modify the former geomorphology or landscape conditions. Gordon (2011) mentions that volcanic eruption, for example from Mt. Hood in the Cascade Range of the Pacific Northwest and Mt. Pinatubo in the Philippines, can add hazardous sediment into rivers and cause widespread damage to downstream areas. The eruptions of Mt. St. Helens in 1980 CE also result in extensive landscape disturbance. Furthermore, enormous quantities of sediment were deposited on hillslopes and river corridors in the watersheds near the volcano (Major, 2004).

A sedimentary material of volcanic eruptions has a complex and unique system (Cuitiño and Scasso, 2013). In general, the system describes the amount of material from the eruption, as well as the transport and deposition processes that occur from upstream to the sea (Fisher and Smith, 1991; McPhie et al., 1993; Manville et al., 2009), as a result of weathering, erosion, or the production of the biogenic material. Sediment supply through eruption instantly impacts systems, and in large volumes, pre-existing systems overwhelm them during transport (Fisher and Smith, 1991; Major et al., 1996; Manville et al., 2005, Manville et al., 2009). For example, since 1995 in the Soufriere Hills volcano, numerous pyroclastic flows have traveled down to the downstream area through the Tar River Valley and depositing almost 70% of the volcanic material into the submarine environment (Le Friant et al., 2009; Le Friant et al., 2010). The material that deposited close to the coast is characterized by coarse and denser grained fraction, while the fine volcanic ash may spread out over long distances along with the turbidity current (Karstens et al., 2013).

1.3.2. Volcanic eruption-induced tsunami

The word tsunami comes from the Japanese terms, "*Tsu*" (port) and "*nami*" (wave). In general, the tsunami may be interpreted as an ocean wave or series of waves with a long period generated by inevitable disturbances that occur in the marine environment and can affect the coastal environment. These disturbances are can in the form of a tectonic earthquake with its epicenter in the ocean floor, submarine volcanic eruptions, submarine landslides, meteor, or bomb at the ocean. Therefore, the tsunami also is known as a secondary hazard, while the primary hazard is the geophysical phenomenon as mentioned above (Smart et al., 2016). Paris et al. (2013) mention that there are several causes of the volcanic eruption-induced tsunami, such as an underwater explosion, airwave generated by the blast, pyroclastic flows that entered to

the sea, the collapse of an underwater caldera, subaerial failure, and submarine failure (Figure 16).

The global historical tsunami database from National Geophysical Data Center - NOAA shows that volcanic activity triggered at least 139 tsunamis in the world since 2100 BC, and 26 of them were located in Indonesia (Table 1). The most prominent tsunami that triggered by volcanic activity in historical times in the world occurred in Thera Island, Santorini, Greece (1610 BC) and in W. Hokkaido Island, Japan on 29 August 1741 CE. Both tsunamis reached 90-meter maximum run-up. The most recent volcanic eruption-induced tsunami occurred in Kadovar Island, Papua New Guinea on 9 February 2018. The collapse of the lava dome at Kadovar's SE Coastal Vent caused 5 - 6 minor tsunamis with less than 1-meter run-up (National Geophysical Data Center / World Data Service (NGDC/WDS), 2018).

Tsunamis caused by volcanic activities have resulted in the death of more than 54,000 persons, which is equal to 25% of total victims due to volcanism (Latter, 1981). Although volcanic eruption-induced tsunami events rarely happen, however, some events ever had a major impact, e.g., the Krakatoa tsunami in 1883 CE (36,000 death tolls), the 1792 CE of dome collapse of the Mayuyama volcano in Kyushu (15,030 death tolls), and the 1741 CE eruption of Oshima-Oshima Volcano in the Japan Sea (1,607 death tolls) (Paris, 2012).

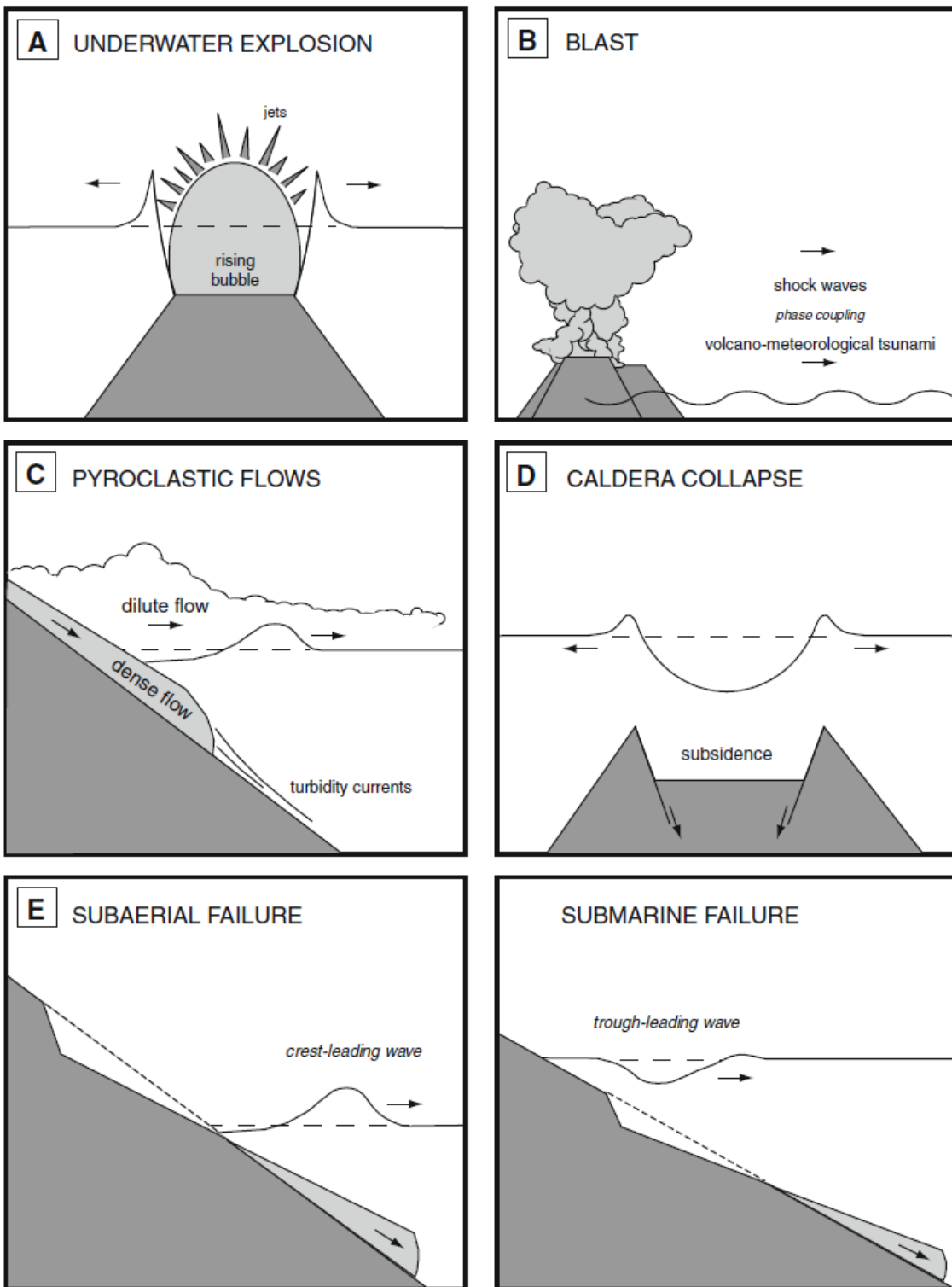


Figure 16. Some causes of the volcanic eruption-induced tsunamis (Source: Paris et al., 2013).

Table 1. Volcanic eruption-induced tsunami in Indonesia since 2100 BC (Latief et al., 2000; Paris et al., 2013; NGDC/WDS, 2018).

| No. | Years | Location | Max Run-up (m) | Cause of tsunami |
|-----|-------|-------------------------------|----------------|-------------------------|
| 1. | 416 | South of Java, Java Island | | Questionable |
| 2. | 1550 | Makian Volcano, Halmahera | | |
| 3. | 1608 | Gamalama, Ternate Island | | |
| 4. | 1659 | Teon Volcano, Banda Sea | 1.5 | Pyroclastic flows? |
| 5. | 1673 | Gamkonora, Halmahera | | Earthquake & landslides |
| 6. | 1771 | North Moluccas Islands | | |
| 7. | 1815 | Tambora, Sumbawa Island | 3.5 | Pyroclastic flows |
| 8. | 1837 | Banda Aceh | | |
| 9. | 1840 | North Moluccas Islands | | |
| 10. | 1845 | Celebes Sea | | |
| 11. | 1856 | Awu Volcano, Sangihe Island | | Pyroclastic flows |
| 12. | 1871 | Ruang, North Sulawesi | 25 | |
| 13. | 1883 | Krakatau, South Lampung | 41 | Pyroclastic flows |
| 14. | 1883 | Krakatau, South Lampung | 35 | |
| 15. | 1884 | Krakatau, South Lampung | | Underwater explosion? |
| 16. | 1889 | North Moluccas Islands | 4 | |
| 17. | 1892 | Awu Volcano, Sangihe Island | 0.75 | Shockwave? |
| 18. | 1918 | Banua Wuhu, Sangihe Island | 0.08 | Underwater explosion |
| 19. | 1919 | Banua Wuhu, Sangihe Island | 5 | Underwater explosion |
| 20. | 1927 | Rokatinda Volcano, Flores | | |
| 21. | 1928 | Paluweh Island, Flores Sea | 10 | Volcanic landslide? |
| 22. | 1928 | Krakatau, South Lampung | | Underwater explosion |
| 23. | 1930 | Krakatau, South Lampung | | Underwater explosion |
| 24. | 1963 | Lesser Sunda, Bali (Agung V.) | | |
| 25. | 1979 | Iliwerung, Lembata | 9 | Volcanic landslide |
| 26. | 1981 | Krakatau, South Lampung | 2 | Volcanic landslide? |
| 27. | 1983 | Iliwerung, Lembata | | Underwater explosion? |

As the most deadly volcanic eruption-induced tsunami in Indonesia, the Krakatoa tsunami in 1883 CE was well studied by several researchers (Francis, 1985; Yokoyama, 1987; van den Bergh et al., 2003; Giachetti, et al., 2012; Paris et al., 2014; Paris et al., 2018). This phenomenon is also well described either by eye-witness descriptions as well as geologic investigations. During two days, several rapid mass transfers from pyroclastics flow entered the sea and produce a tsunami with 42-meter of the maximal run-up in Merak, Banten, Indonesia (Choi et al., 2003; Freundt, 2003). This tsunami reached Colon, Panama about 19,331 km away from the source with maximal run-up up to 0.4-meter (Choi et al., 2003).

Probably the most-frequently volcanic eruption-induced tsunamis occurred in Montserrat, Soufriere Hills Volcano. Since 1997, there are four documented tsunamis due to volcanic activity, i.e., on 26 December 1997, 20 January 1999, 12 July 2003, and 20 May 2006 (Lander et al., 2003; Pelinovsky et al., 2004; Pararas-Carayannis, 2006; Mattioli et al., 2007). In 1997, volcanic debris slide generated a wave with a maximal height up to 3- meter and flooded the Old Bay area which located 10 km from the source of the tsunami (Lander et al., 2003). The height of the 1999-tsunami waves in Soufriere Hills reached two meters but weakened immediately (Pararas-Carayannis, 2006). The 2003 pyroclastic flow material reached the ocean and generated an 8.5-meter high tsunami on the eastern coast of Montserrat and up to 0.5-meter in Guadeloupe (Mattioli et al., 2007). Pelinovsky et al. (2004) also mentioned that the 2003 tsunami had a 4-meter wave height which was identified by its debris at Spanish Point, about 100-150 meters from the shoreline. In 2006, Montserrat Volcano Observatory explained that a 90-million m³ of the lava dome has collapsed and generates a tsunami that reaches Guadeloupe with up to 1-meter of wave height based on tide-gauge measurement.

1.3.3. Disturbances and mortalities of corals

Coral typically live in tropical and subtropical areas with favorable oceanographic conditions, such as water temperatures between 18°-29°C, salinity between 32-42‰, as well as clear water where the intense sunlight still can penetrate it (Lalli and Parsons, 1995). Volcanic materials may reach the sea following to the eruption, and it can result on the disturbances in the ocean environment. Disturbances in the ocean due to volcanic ash, pumice rafts, as well as PDC deposits may affect the coral reefs, e.g., coral bleaching which triggers mortality of corals (Maniwavie et al., 2001; Schils, 2012).

In addition to mortality of corals, there are other negative impacts of lahars, lava flows, and volcanic ash that deposited on coral reefs: 1) sunlight penetration has decreased that affect the coral's photosynthesis, changes in the chemical elements in the ocean (Reuter and Piller, 2011), and 2) nutrient enrichments triggering transformations in the benthic structure (Grigg and Maragos 1974; Tomascik et al., 1996; Vroom and Zgliczynski, 2011; Schils, 2012).

In 1988, the lava from the eruption of Gunung Api in Banda Island, Indonesia entered the sea and buried about 70,000 m² (Casadevall et al., 1989) of coral reef (Sutarna, 1990) to a depth more than 50 m. In other cases, suspended volcanic ash following to the 2003 CE eruption in Anatahan, the Northern Mariana Islands reduced the underwater visibility up to 2-meter (Vroom and Zgliczynski, 2011). Consequently, the maximal living coral cover has decreased by about 35% with poor conditions and most of them displayed signs of stress in the form of coral bleaching (Figure 17) (Vroom and Zgliczynski, 2011). In 1994, volcanic eruption in Rabaul Caldera, Papua

New Guinea produced large volumes of ash and pumice which completely buried the coral reefs around the Rabaul Harbor (Maniwavie et al., 2001).

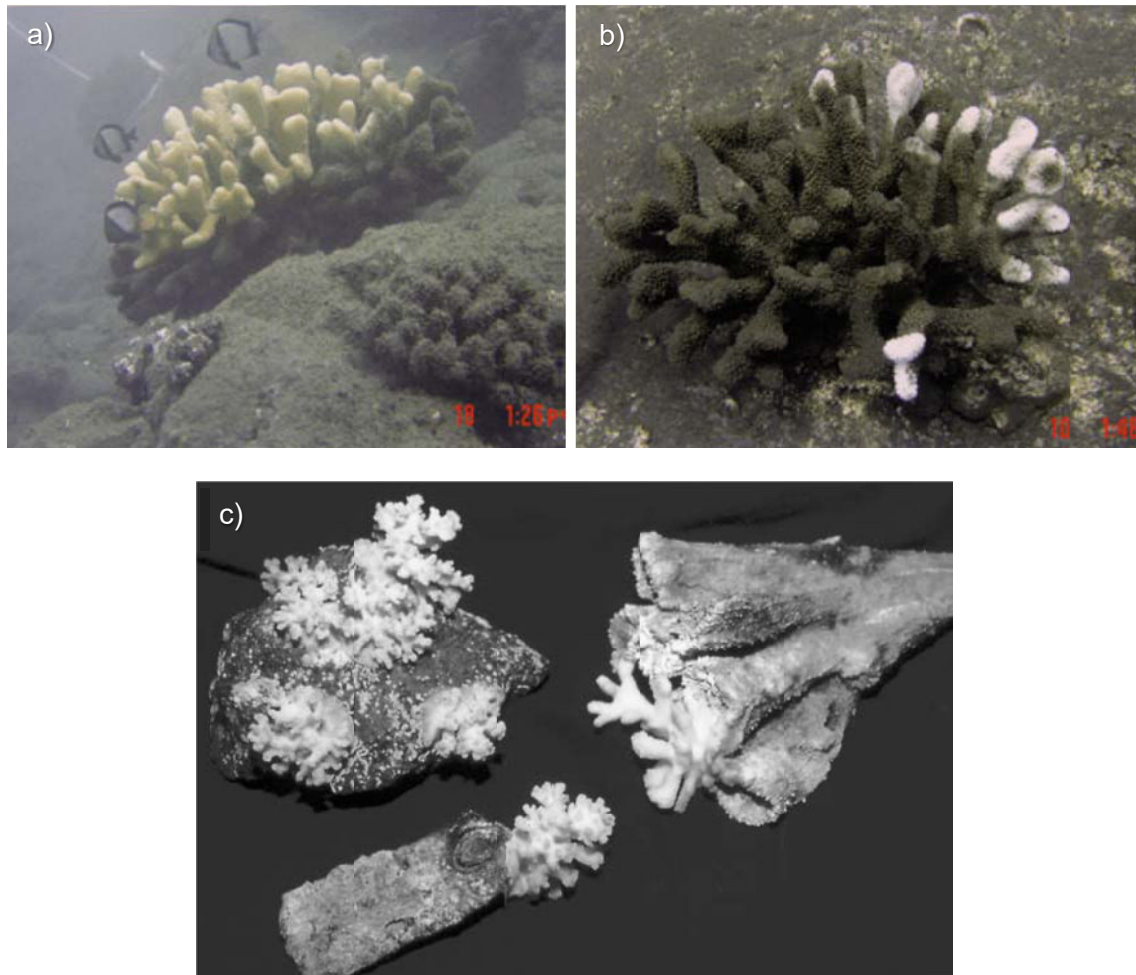


Figure 17. a) and b) Coral bleaching following to the 2003 CE eruption in Anatahan, the Northern Mariana Islands (Source: Vroom and Zgliczynski, 2011); c) Corals condition after the 1994 CE eruption in Rabaul Caldera, Papua New Guinea (Source: Maniwavie et al., 2001).

Although the coral reefs had extensively recolonized in the two years following the eruption, the volcanic ash had succeeded to decrease the live coral cover from 50% before the eruption to 0% in the aftermath of the eruption. Although the coral reefs

had extensively recolonized in the two years following the eruption, the volcanic ash had succeeded to decrease the live coral cover from 50% before the eruption to 0% in the aftermath of the eruption. This rapid recolonization may have happened if the remobilization of volcanic materials from the mainland (i.e., suspended solid sediments and lahars) that reach the sea through the rivers did not disturb the underwater conditions.

1.4. Conclusion

This chapter explains in details that the coastal area, especially in the tropical area, is a very dynamic region in space and time in response to volcanic activities. Volcanic products, in the form of fallout, PDC, and lahars may result in various impacts and changes in the coastal area, such as sedimentation, landscape evolution, tsunami, as well as mortality of corals. In addition to their contributions to fertilizing the soil and providing building materials (e.g., sand, pumice stone), volcanic products, in the form of fallout, PDC, and lahars may also result in various impacts and changes in the coastal area, such as sedimentation, landscape evolution, tsunami, as well as mortality of corals. Everyone who lived in the coastal area should know comprehensively the information related to the impact of volcanic activities in the coastal area. For example in Indonesia, as a country with more than 130 active volcanoes from a total of 400 volcanoes and almost all major cities in Indonesia are located in the coastal area (e.g., Jakarta, Yogyakarta, Surabaya, Mataram, and Bima).

This chapter also presents the importance of the research related to the impact of a major eruption volcanic in the coastal area. For example, volcanic eruption-induced tsunamis in Indonesia are not well-studied yet, their causes nor their consequences. Information scarcity on the impact of volcanic eruptions in coastal areas will raise the

disaster risk on the next major volcanic eruption since the population of the world nowadays is more than 7.5 billion peoples. In this research, we will focus on the impact of 1257 CE eruption of Samalas volcano along the Alas Strait, West Nusa Tenggara, Indonesia, including the local and regional impacts. Figure 18 illustrates the information presented in Chapter 1.

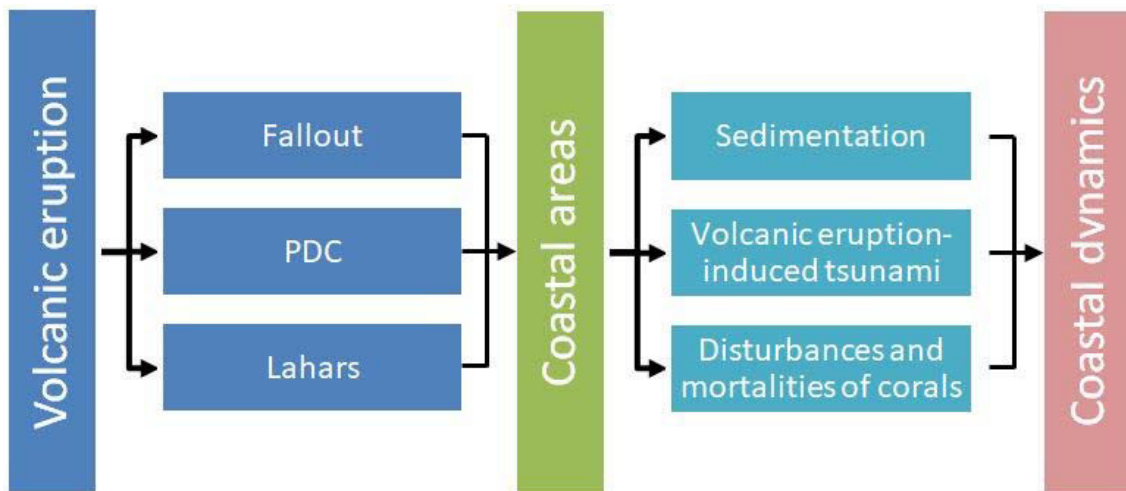


Figure 18. Coastal evolution related to volcanic eruptions.

Chapter 2: Lombok Island, Sumbawa Island, and Samalas volcano

The second chapter presents a description of the study area including geographic information, its geomorphological features, and geological setting, as well as its relation with the 1257 eruption of Samalas volcano in Lombok and Sumbawa Islands, West Nusa Tenggara Province, Indonesia.

2.1. Lombok and Sumbawa Islands

Indonesia, as the largest archipelago country in the world after Canada, has 16,056 registered islands (Sekretariat Kabinet Republik Indonesia, 2017), a coastline approximately 99,093 km in length (Badan Informasi Geospasial, 2015), and 34 provinces. Administratively, Lombok and Sumbawa Islands is part of West Nusa Tenggara Province in Indonesia. West Nusa Tenggara Province is located between 8°10' – 9°5' South Latitude and 115°46' – 119°05' East Longitude, and it is bordered by the Lombok Strait in the West; the Java Sea and the Flores Sea in the North; the Sape Strait in the East; and the Indian Ocean in the South (Figure 19).

There are two main Islands in West Nusa Tenggara (WNT) Province, namely Lombok Island and Sumbawa Island. Lombok Island had an area of 4,738.65 km² (23.52% of total area in WNT Province) which consists of five regencies namely West Lombok, North Lombok, Central Lombok, East Lombok, and Mataram City. Sumbawa Island also consists of five regencies, namely Sumbawa, Dompu, Bima, West Sumbawa, and Bima City. These regencies had a total area of 15,414.5 km² which is about 76.48% of WNT Province areas (Figure 20; Badan Pusat Statistik, 2016).

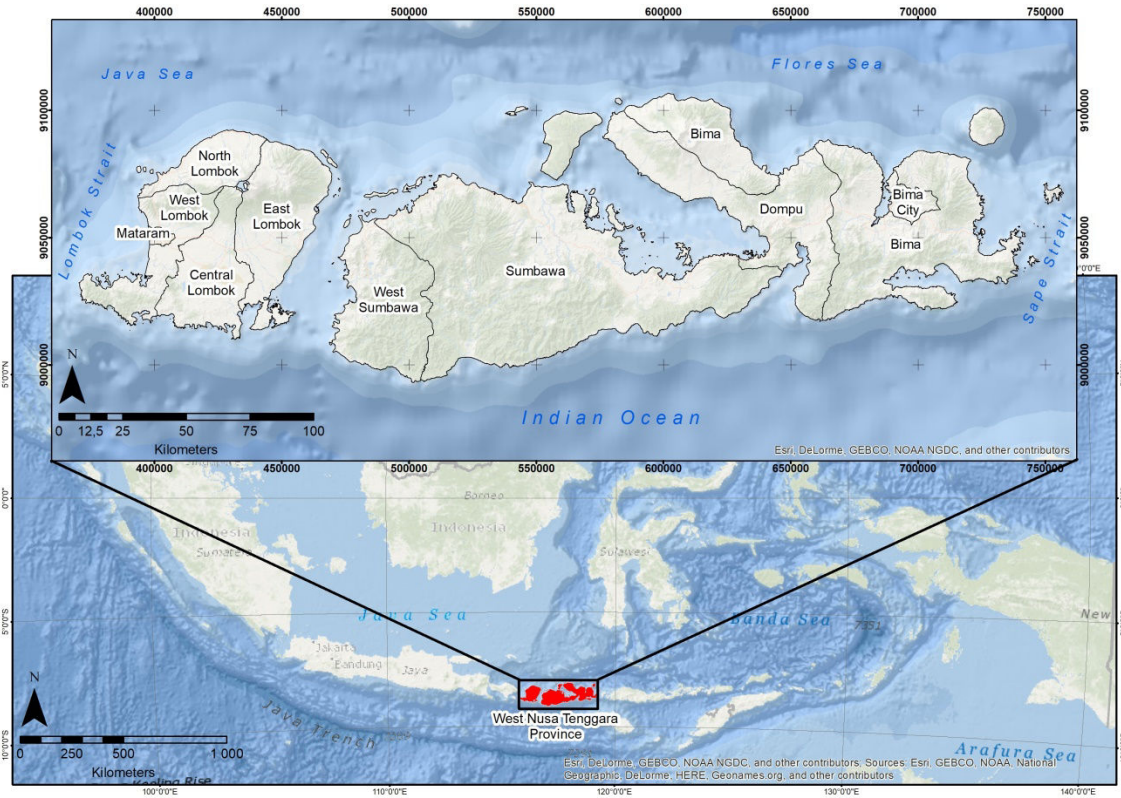


Figure 19. Lombok and Sumbawa Islands located in West Nusa Tenggara Province in Indonesia.

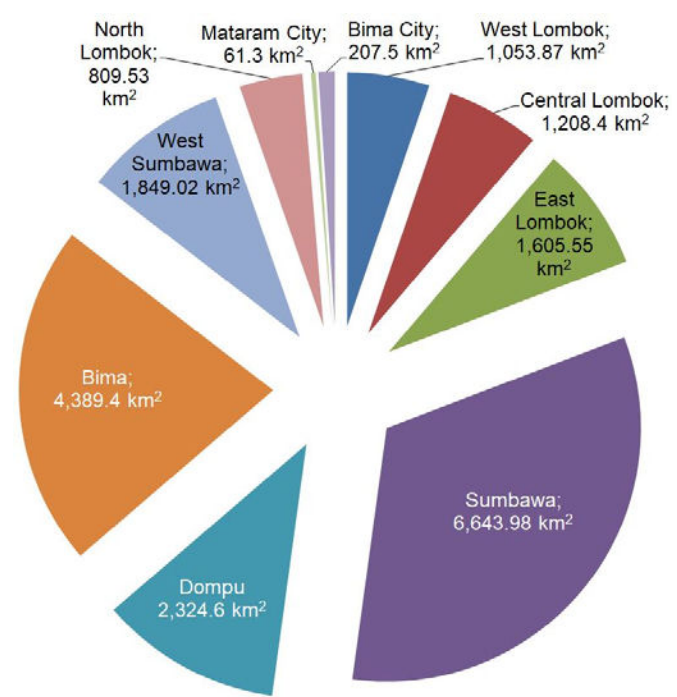


Figure 20. Ten regencies in WNT Province and their superficies (in km²).

The population in WNT Province in 2016 reaches 4,896,162 people, and 70% of them (3,434,708 people) lives in Lombok Island. These numbers of people were increased about 40% since the year 1993 (3,504,006 people), and in 2016 about 34.2% of people in WNT Province (1,173,781 people) mostly live in East Lombok (Badan Pusat Statistik, 2016) (Figure 21).

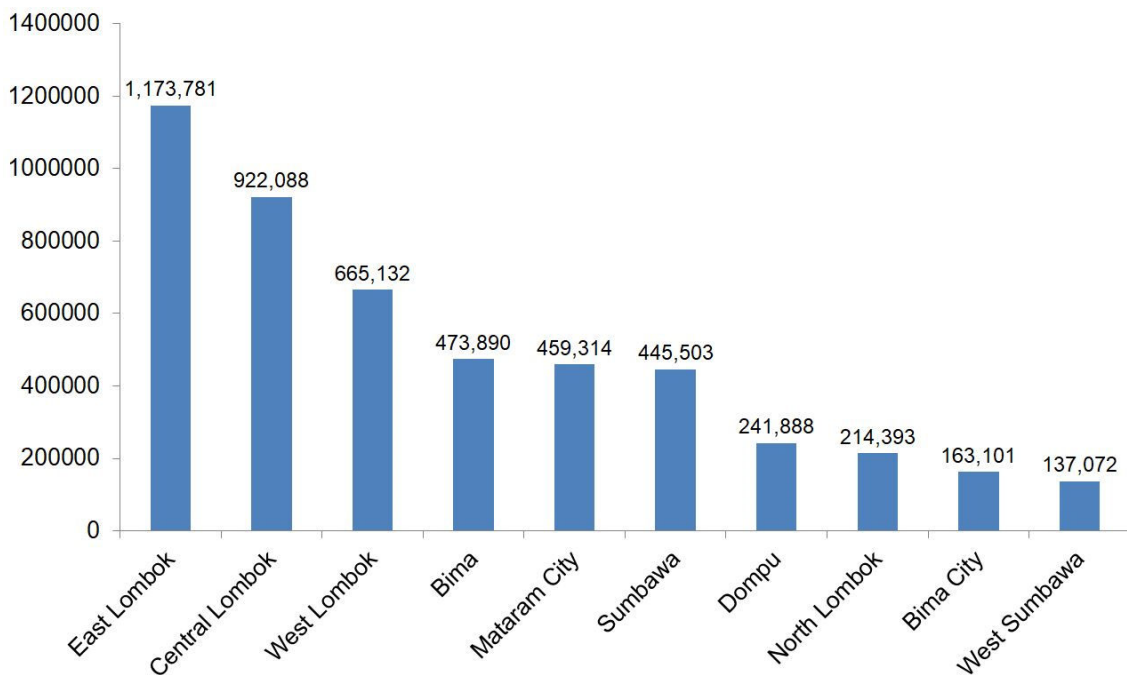


Figure 21. The population of West Nusa Tenggara Province in 2016 by regency (Badan Pusat Statistik, 2016).

Lombok and Sumbawa Islands are located in the inner arc of the Lesser Sunda Islands (LSI), which also include Bali, Komodo, Rinca, Flores, Adonara, Solor, Lomblen, Pantar, Alor, Kambing, Wetar, as well as Romang Island at their easternmost boundary. The LSI area contradicts with the Greater Sunda Islands of Java or Sumatra. The LSI consists of numerous small islands and deep oceanic trenches. In WNT Province, there are 380 small islands of which half of them (193 islands) locates

around Lombok Island. However, there are only 38 islands that are inhabited in WNT Province, i.e., 22 islands in Lombok and 16 in Sumbawa Island. The rest (342 islands) are categorized as the uninhabited island (Figure 22; Badan Pusat Statistik, 2016).

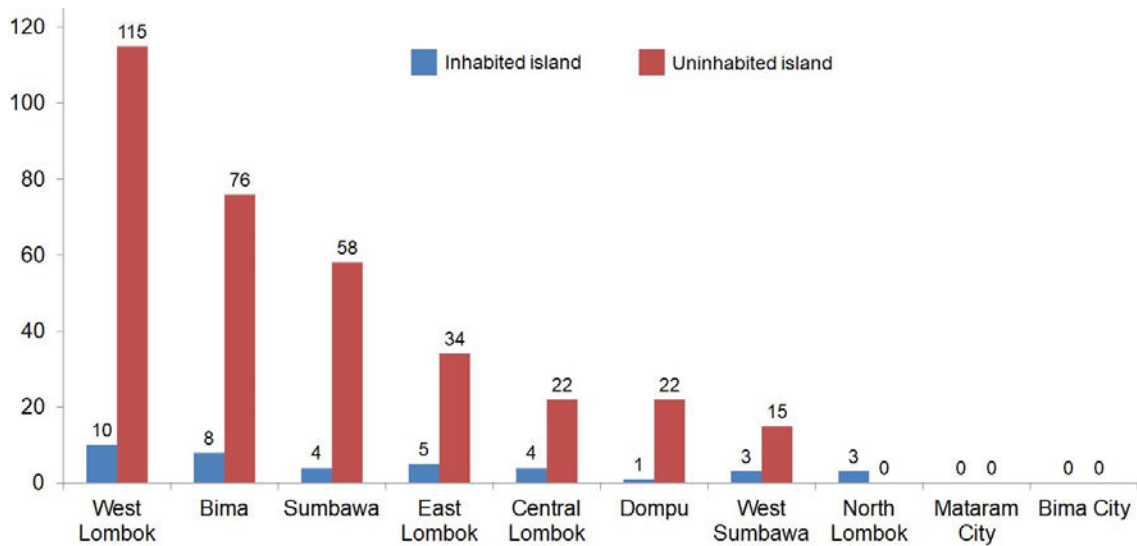


Figure 22. Numbers of inhabited and uninhabited islands in West Nusa Tenggara Province (Badan Pusat Statistik, 2016).

In Lombok, the river stream pattern is radial, dendritic, and parallel, with the basic configuration of lava, pyroclastic, and alluvium materials. As an example of a volcanic island in Indonesia, Lombok is almost wholly composed of volcanic landforms. Wide calderas and an active volcano are combined with fluvio-volcanic slopes, and extensive lowlands then give in easy access to the basis of local agriculture, economy, and civilization in this island (Verstappen, 2005; Tan, 2008). The Alas Strait separates Lombok and Sumbawa Island with an average distance of about 53 km with the current in the north-south direction (Figure 23). The depth of Alas Strait varies from around 15 meters in the nearshore to a maximum depth of 180 meters in the middle of the channel. The sea floor materials in the Alas Strait are dominated by rock and sand

(Schmitz, 1996). Furthermore, the strait was connected by land until about 14ka BP when sea level rose up to 75 meters below the present-day sea level (Voris, 2000; Sathiamurthy and Voris, 2006; Solihuddin, 2014).

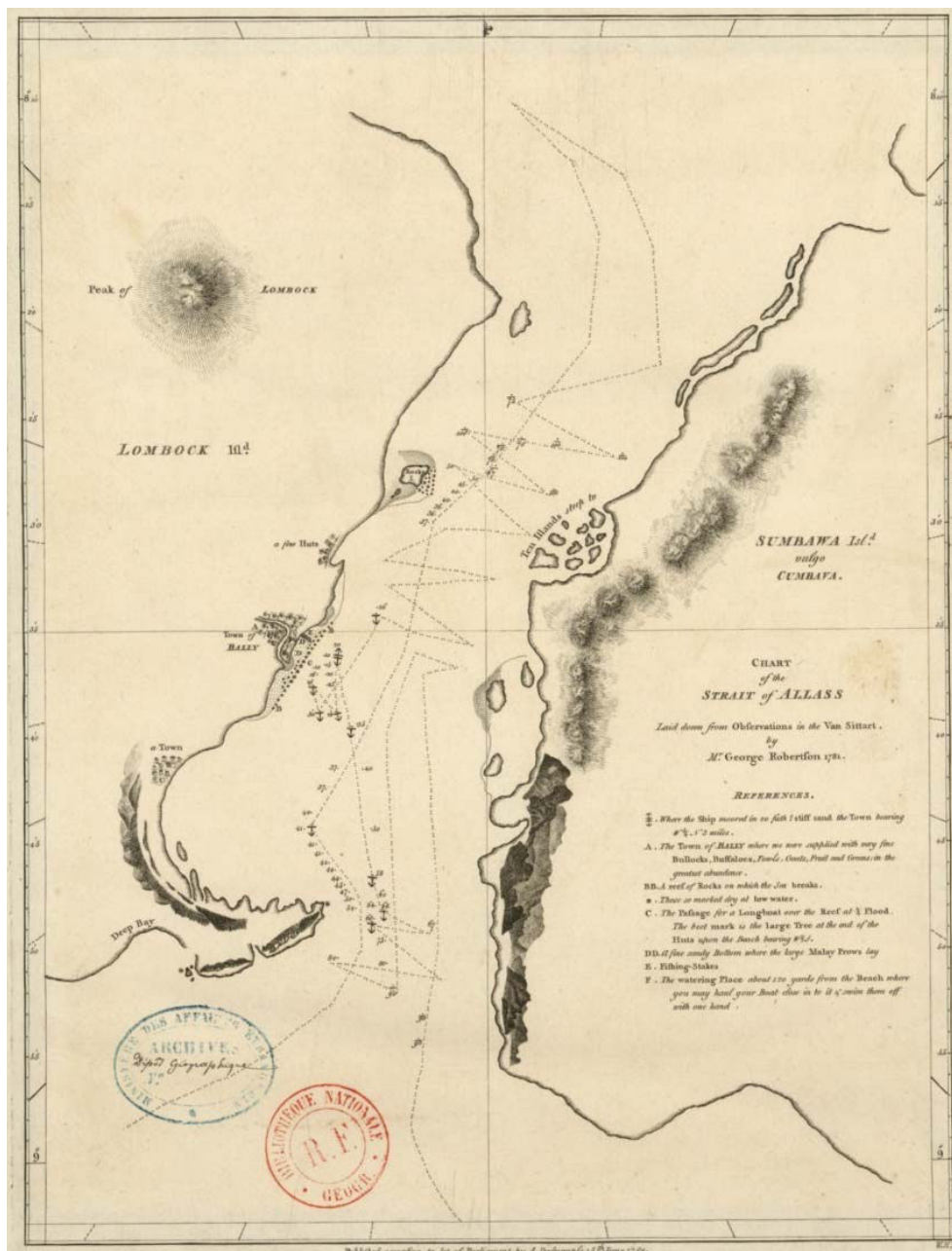


Figure 23. Chart of the strait of Alas that lay down from observations in the Van Sittart by Mr. George Robertson, 1781 (Source: Bibliothèque Nationale de France, 2007).

Sumbawa Island has various profoundly cut bays producing various peninsulas as well as the location of Bima harbor. Submergence coastline characterizes the Saleh Bay, as the biggest bay in Sumbawa and it has divided the island into two parts, i.e., west and east Sumbawa. Sumbawa landform is mostly mountainous areas from early Miocene until Holocene era, with rocky coasts and a few small low plains. The highest elevation in Sumbawa Island is located in the northern part of the island where the famous Tambora Volcano (2,851 m) is situated (Sudrajat et al., 1998).

Lombok and Sumbawa Islands are located in a tectonic setting associated with the northward subduction of the Australian plate beneath the Eurasian plate at a rate of approximately 7 cm/year (Simons et al., 2007). The landscapes in Lombok Island are very diverse, e.g., the lowland plain of Mataram, the tertiary limestones and volcanic breccias in the South, and an active volcanic center in the North (van Bemmelen, 1949). In general, the geology of Sumbawa is characterized by an island arc-type volcano-sedimentary succession of Late Oligocene to Quaternary age. The active volcanic center in Lombok Island is known as the Central Lombok Volcanic Complex (Nasution et al., 2004), or, as it is now referred to, the Rinjani Volcanic Complex (Lavigne et al., 2013; Vidal et al., 2015). The active volcano in Sumbawa Island is Tambora Volcano that erupted in 1815 CE and triggered severe climate disturbance worldwide since it resulted in the year without summer in the northeastern USA, Maritime Provinces of Canada, and Europe the following year (Stothers, 1984; Oppenheimer, 2003). The 1815 CE eruption of Tambora Volcano produced a total volume of about $41 \pm 4 \text{ km}^3$ DRE ($23 \pm 3 \text{ km}^3$ DRE ash fall and $18 \pm 6 \text{ km}^3$ DRE pyroclastic flows) (Kandlbauer and Sparks, 2014).

2.2. Samalas volcano

Indonesia is known as a volcano-rich country, with more than 130 active volcanoes from a total of 400 volcanoes (Figure 24). Most volcanoes in Indonesia are affiliated to the Sunda Arc, as a result of the subduction between three plates, i.e., the Indian plate, the Australian plate, and the Eurasian plate. Samalas volcano collapses following the 1257 CE ultraplinian eruption (Lavigne et al., 2013). The collapse of this volcano has been described in a local written source, namely Babad Lombok, verse number 274: “Rinjani volcano avalanched, and Samalas volcano collapsed, followed by extensive flows of debris as well as boulders rumbling” (Lavigne et al., 2013).



Figure 24. An example of a multiplatform application for geohazard mitigation and assessment for volcanic activities in Indonesia from Indonesian Centre for Volcanology and Geological Hazard Mitigation (CVGHM) <http://magma.vsi.esdm.go.id/>. The color differences of the volcano on the map are related to the current status of the volcano, e.g., normal (green); minor activity (yellow); warning (orange); and erupting (red).

Currently, the Rinjani Volcanic Complex, where the Samalas volcano was located, is composed of three sectors (Figure 25): first, the large stratocone of Rinjani

(currently 3,726 metres a.s.l.); second, the 6.5 x 8 km Samalas caldera, entirely or partly resulting from the 1257 CE Plinian eruption, and now occupied by Lake Segara Anak; and third, the active Barujari cone emerging 320 metres above the lake (Figure 26) (Lavigne et al., 2013; Vidal et al., 2015; Vidal et al., 2016). Since the 1257 CE eruption, the Barujari cone has erupted about 17 times, and the most recent eruption happened in 2016 (Global Volcanism Program, 2013).

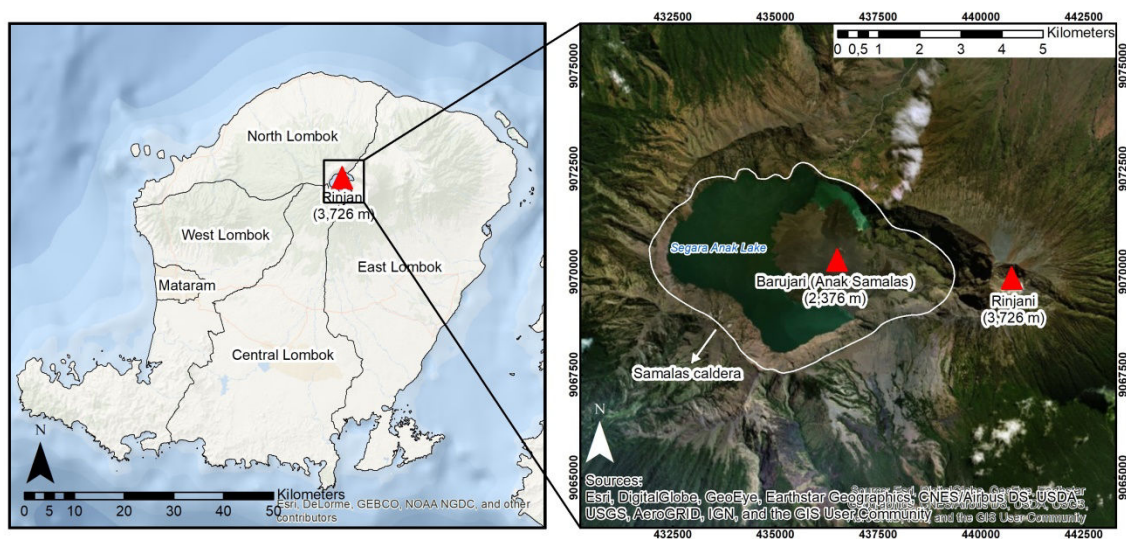


Figure 25. The Rinjani Volcanic Complex in Lombok Island.

The 1257 CE eruption of Samalas had a Volcanic Explosivity Index (VEI) of 7 (Lavigne et al., 2013). This eruption was seven times greater than the eruption of Pinatubo in 1991 CE (Kim and Kim, 2012) and categorized as one of the largest eruptions of the last 7,000 years (Lavigne et al., 2013; Vidal et al., 2015; Vidal et al., 2016). Sigl et al. (2015) also mentioned that the most massive sulfate-producing eruptions in the last 10,000 years originated from the 1257 CE Samalas eruption.



Figure 26. The Segara Anak Lake and the active Barujari cone in the Rinjani Volcanic Complex (Courtesy: P. Guerin, July 2015).

Consequently, the severe impacts have felt by the world's population and the global environment due to the 1257 CE Samalas eruption (Kim and Kim, 2012; Lavigne et al., 2013; Guillet et al., 2017). The impacts of 1257 CE Samalas eruption are famine and death in Europe due to climate anomalies, especially over western Europe in 1258 CE (Lavigne et al. 2013; Guillet et al., 2017). Furthermore, the surface air temperature and the sea surface temperature also decreased by about 1.6°C and 0.8°C, respectively, in response to the 1257 CE Samalas eruption (Kim and Kim, 2012).

2.3. Study area: coastal areas along the Alas Strait

As the most powerful event in Lombok's recent eruptive history with more than 40 km³ dense rock equivalent (DRE) of volcanic deposits, volcanic materials that were expelled by the Samalas volcano in 1257 CE covered the entire of Lombok Island and are widespread in its eastern part. Although there has been some erosion and extensive farming of the eastern part of Lombok (Vidal et al., 2015), this area still contains PDC deposits with a measured thickness of more than 30 metres (Figure 27; Lavigne et al., 2013), as well as lithic fragments measuring up to a maximum of 8–16 mm and pumice fallout fragments measuring up to a maximum of 25–32 mm (Vidal et al., 2015).

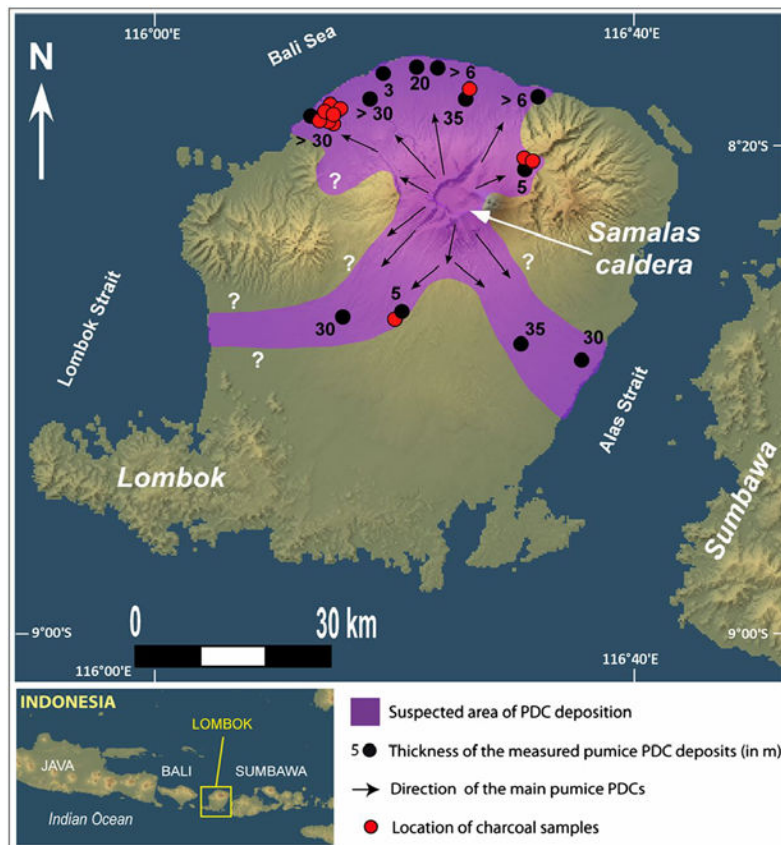


Figure 27. Direction and distribution of PDCs from the 1257 CE eruption of Samalas (Source: Lavigne et al. 2013).

This research focuses on the eastern part of Lombok Island considering that this area had been harshly affected by the PDCs, had a highly dynamic environment with several physical processes, as well as complex landuse. Furthermore, there is a lack of data and information from previous research on the impact of the 1257 CE Samalas eruption on this area. Earlier studies by Lavigne et al. (2013) and Vidal et al. (2015) only focused on areas to the northwest and southwest of the volcano due to the limited amount of field data available. Nevertheless, the people in WNT Province mostly live in East Lombok since 1995 (Figure 28; see also Figure 21 on page 54).

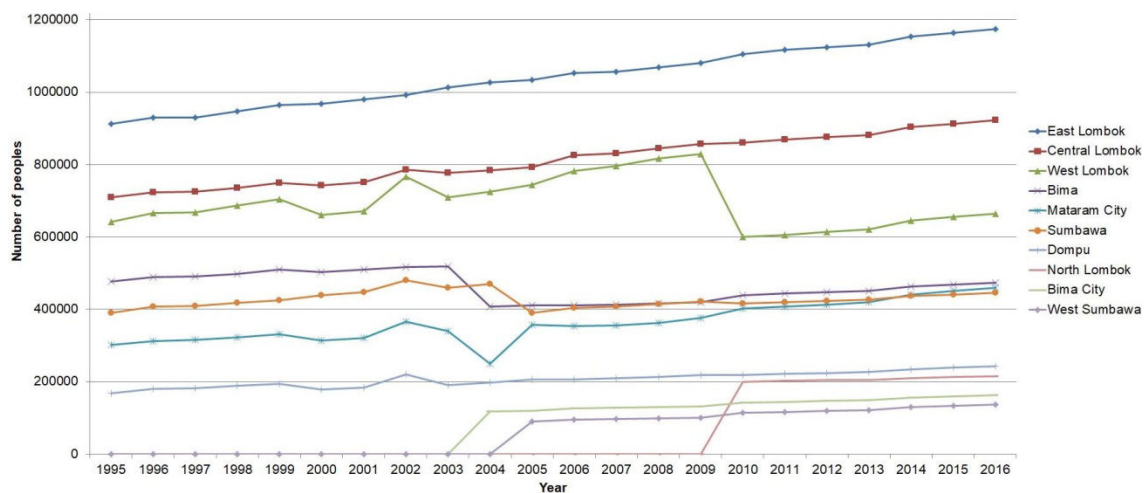


Figure 28. The people in West Nusa Tenggara Province mostly live in East Lombok since 1995 (Badan Pusat Statistik, 2016).

Another factor that makes the eastern part of Lombok scientifically interesting is the fact that the volcanic material in this location entered the sea (Vidal et al., 2015) and may have generated a PDC-triggered tsunami (Choi et al., 2003; Freundt, 2003; Lander et al., 2003; Pelinovsky et al., 2004; Pararas-Carayannis, 2006; Mattioli et al., 2007) in other islands surrounding, e.g., the western coast of Sumbawa. Since 2100 BC at least four tsunamis in Indonesia due to pyroclastic flows were reported to reach

the sea, including the great tsunami in Sunda Strait following the 1883 CE eruption of Krakatau Volcano (Table 2).

Table 2. Tsunamis due to pyroclastic flows that reached the sea in Indonesia since 2100 BC (Paris et al., 2013; NGDC/WDS, 2018).

| No. | Years | Location | Max Run-up (m) | Cause of tsunami |
|-----|-------|-----------------------------|----------------|--------------------|
| 1. | 1659 | Teon Volcano, Banda Sea | 1.50 | Pyroclastic flows? |
| 2. | 1815 | Tambora, Sumbawa Island | 3.50 | Pyroclastic flows |
| 3. | 1856 | Awu Volcano, Sangihe Island | | Pyroclastic flows |
| 4. | 1883 | Krakatau, South Lampung | 41.00 | Pyroclastic flows |

Figure 29 displays the study area of geomorphic impacts of the 1257 CE eruption of Samalas volcano. The morphology on the eastern part of Lombok and western part of Sumbawa is various; from in the form of gently undulating plains to mountains with varying elevations, ranging from 0 m to the highest that located in the Rinjani Volcanic Complex (3,726 m) with the slope that ranges between 0 - 2% (near the shore, i.e., Pringgabaya, Labuhan Haji, Taliwang) until more than 40% (e.g., in the Rinjani Volcanic Complex).

Based on the geological map issued by the Indonesian Geological Agency, the eastern part of Lombok is composed by Lekopiko Formation (pumiceous tuff, laharc breccia, and lava), Kalipalung Formation (alternating calcareous breccia and lava), Kalibabak Formation (breccia and lava), undifferentiated volcanic rocks, as well as alluvium materials that located near the shore. Meanwhile, the geology of the western coast of Sumbawa is composed of several materials, first, andesitic volcanic breccia, with sandy tuff, pumiceous tuff, and tuffaceous sandstone; second, well bedded

coralline limestone, containing chert in the lower part; and third, alluvium and coastal deposits along the coast which mostly comprising an andesitic material and locally containing magnetite. Furthermore, there are several uplifted coral reef in the nearshore of West Sumbawa, consisting of coral reef and coralline clastic limestone (Sudrajat et al., 1998).

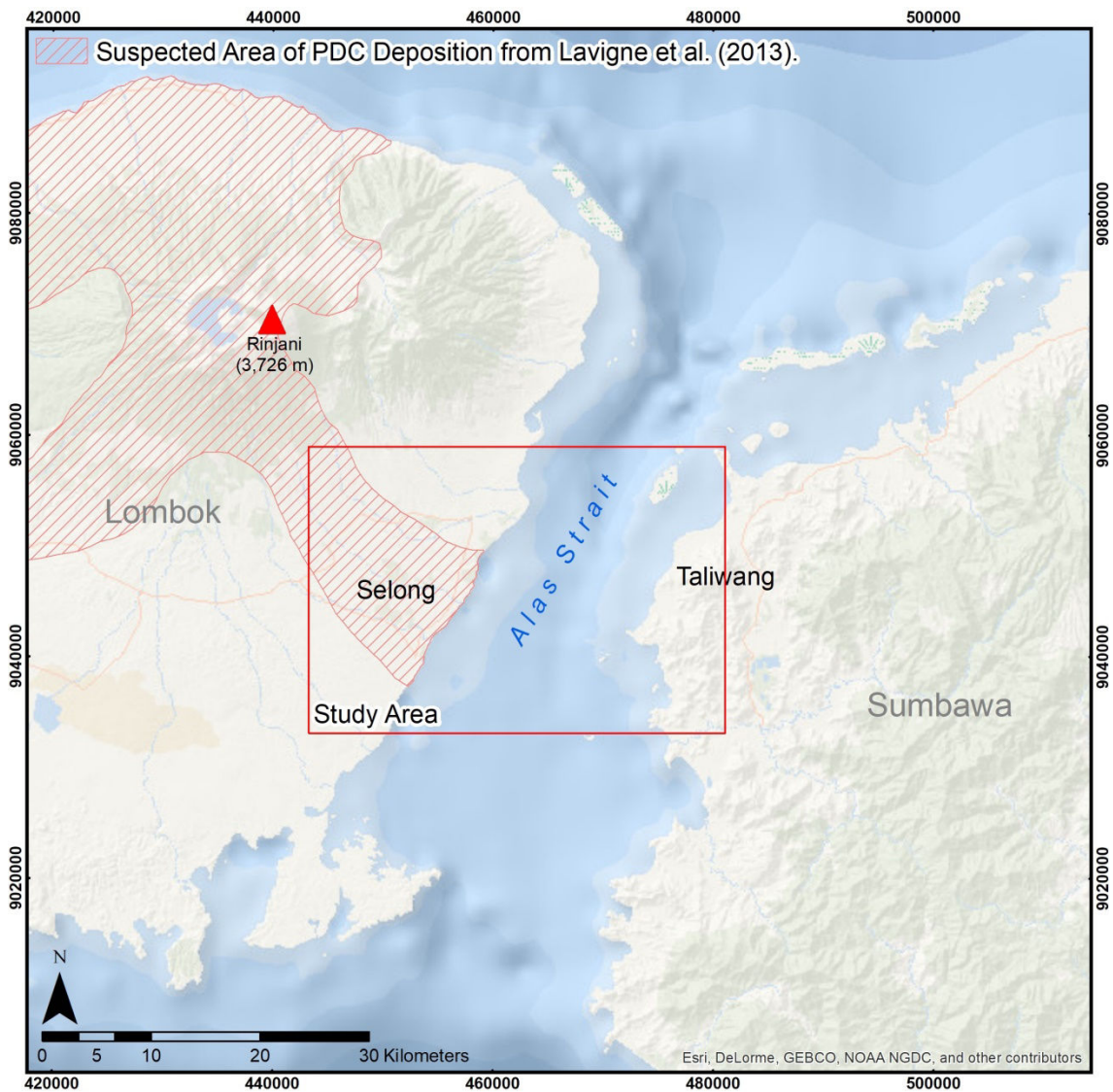


Figure 29. The study area of geomorphic impacts of the 1257 CE eruption of Samalas volcano.

2.4. Conclusion

This chapter describes in details the condition in the study area, such as geographic and demographic information, its geomorphological characteristics and geological setting, as well as its relation with the eruption of Samalas volcano in 1257 CE. Furthermore, this chapter also presents the scientific reason why the coastal area along the Alas Strait in West Nusa Tenggara is fascinating to study. The eastern part of Lombok selected as the study area since this area had been severely affected by volcanic materials from Samalas and there is a lack of data and information from previous studies by Lavigne et al. (2013) and Vidal et al. (2015). Volcanic materials from the 1257 CE eruption of Samalas volcano resulted in a highly dynamic environment with numerous physical processes and complex landuse. These materials entered the sea and may have generated a PDC-triggered tsunami on the western part of Sumbawa.

Chapter 3: Research methodology

The third chapter explains in detail about the methods of this study, data collection, field investigations, and data analyses. A combination of stratigraphic information, present-day topography, geophysical measurement with two-dimensional resistivity profiling technique (Dipole-dipole array), local written sources, as well as laboratory and computational analysis, were used to obtain detailed information concerning geomorphic impacts of the 1257 CE eruption of Samalas volcano on the coastal area along the Alas Strait in West Nusa Tenggara Province, Indonesia.

3.1. Field measurements

3.1.1. Stratigraphic data

Field data were collected from more than 1,300 points in order to gather geomorphological, geological, and geochemical information on the eastern part of Lombok for the last millennium (Figure 30; see Appendix 1). These points consisted of 335 outcrops, 987 wells, eight core drillings and five locations where two-dimensional resistivity profiling was carried out. This information is useful in providing clues on the period in which the material was deposited, and the processes that triggered their transportation (Vogel and Märker, 2010; Vogel et al., 2011; Jordan et al., 2016). Stratigraphic data measurements provided several essential pieces of information, such as the coordinates of stratigraphic data, as well as the elevation of the present-day topography and thickness of the volcanic deposits resulting from the 1257 CE eruption, the difference between these two providing the elevation of the pre-1257 CE topography (Figure 31).

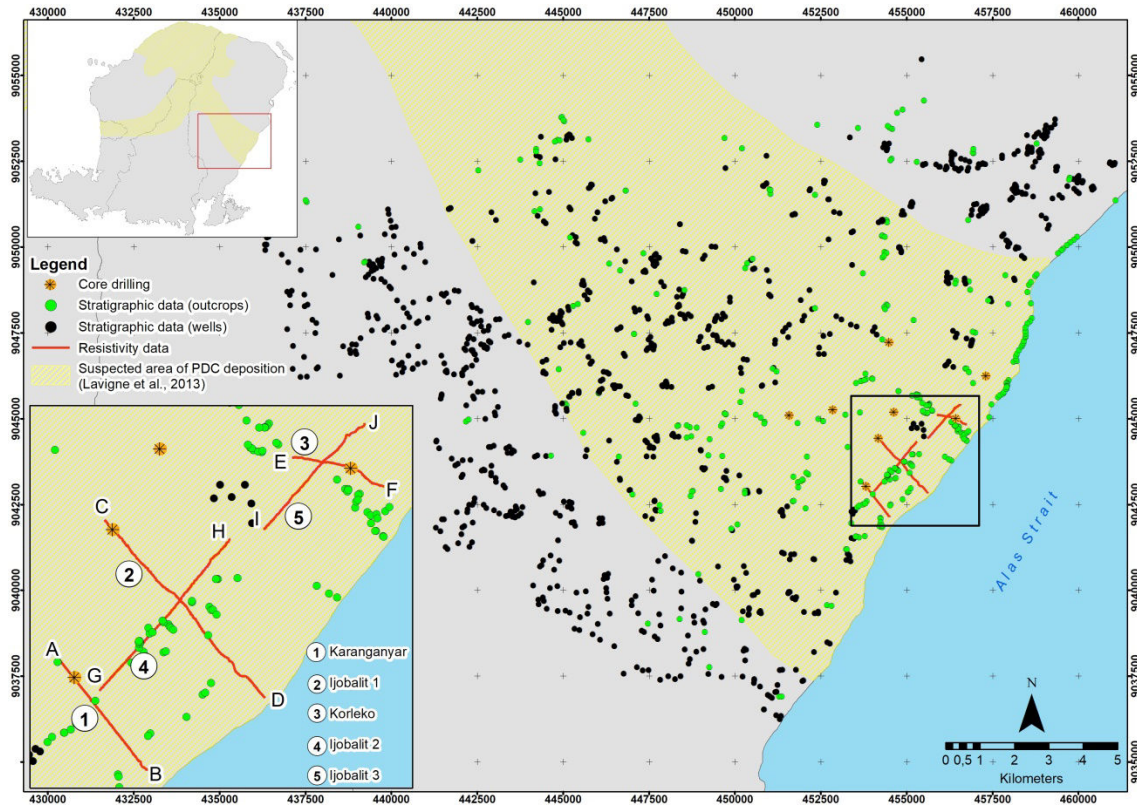


Figure 30. Stratigraphic information and thickness data on the eastern part of Lombok.

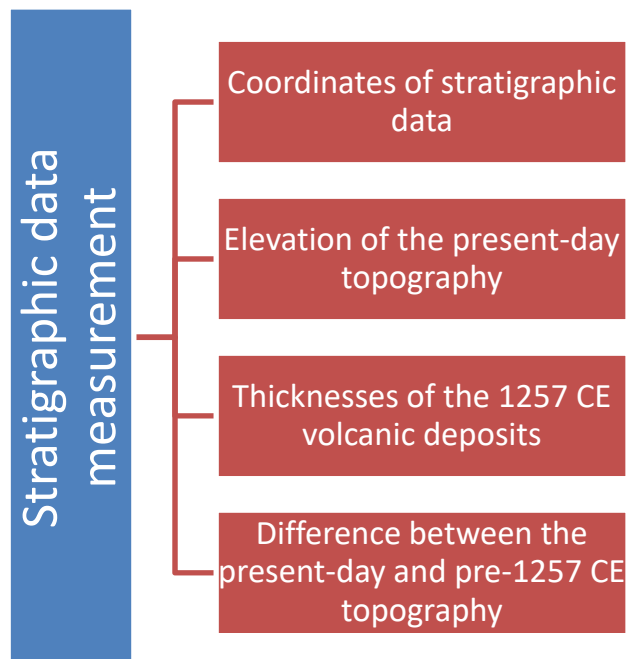


Figure 31. Information from stratigraphic data measurement.

First, we took field measurements using GPS and laser telemetry with an accuracy of up to 3.0 m and 0.2 m respectively in order to obtain stratigraphic information, such as the coordinates of stratigraphic data and PDC thickness, from natural cliffs, riverbanks outcrops, and human-made outcrops in quarries.

Second, we also collected stratigraphic data from cores. A total of eight core drillings were carried out in the research area using the equipment and expertise of local drillers, who usually use their skills to provide groundwater to locals (Figure 32). This technique can reach depths of up to 20 or 30 m, which wells do not usually extend as far as such depths. Furthermore, while not as efficient (more time-consuming) as drills specifically designed to sample cores, this technique allowed us to both sample cores and measured the thickness of the layer up to an accuracy of one meter.



Figure 32. New cores drilling were conducted in the research area using the material and expertise of local drillers (Courtesy: B. Septiangga, July 2017).

Finally, we obtained additional semi-quantitative data by interviewing well owners and local drillers, as well as measured the well coordinates by GPS (Figure 33). The local drillers in Lombok always keep records of each well they work on, including such information as the type of material, the depth of the well, and the depth of water table. They also have good knowledge of types of material in their areas, especially for pumices material due to its originality, characteristics, as well as very specific and easy to recognize. Although the level of accuracy of the data obtained through this “participatory stratigraphy” is lower than that of the data obtained through the other methods, this complementary method allowed us to reduce the error margin or approximation due to spatial data extrapolation.

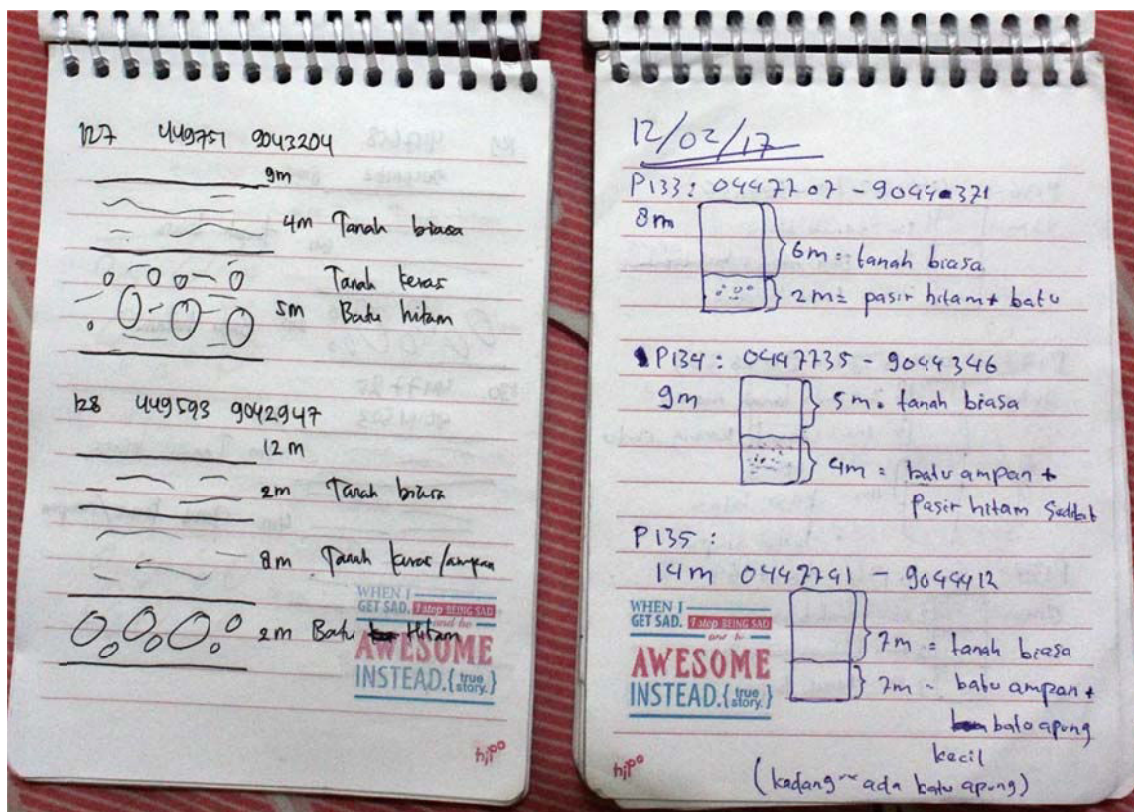


Figure 33. An example of semi-quantitative data through interviews with the well’s owners and local drillers.

3.1.2. Geophysical measurements

In collaboration with the experts from Universitas Mataram, geophysical measurements to obtain the resistivity profiles in the study area were performed using a multi-electrode geophysical tool from Research Center for Geotechnology, Indonesian Institute of Sciences (P2G LIPI), namely SuperSting (Figure 34). The resistivity data was then added to the data collected from cores and wells. This measurement is beneficial to respond the first objective in this study, i.e., to accurately reconstruct the landscape evolution since the 13th century (before, during, and after the 1257 CE eruption of Samalas volcano).



Figure 34. Geophysical measurements using a resistivity meter namely SuperSting
(Courtesy: Y. Sudrajat, September 2015).

SuperSting is used to record the resistivity of the ground up to 120 meters, as the material response varies depending on its composition and level of humidity. The system is connected to 56 stainless steel electrodes, which were laid out in a straight line at equal distances apart using a multi-core cable. Resistivity lines should be arranged in flat and open areas, without any buildings or obstacles along the measurement line (Nazaruddin et al., 2017).

Profile models display resistivity distributions along each line up to a depth of about 100 meters. High resistivity values (orange to red) indicate that the material is less able to transmit electricity. Examples of highly resistive rocks include massive limestone, granite, basalt, dry sand, gravel, ice and pumices (Telford et al., 1990; Reynolds, 1997; Jaramillo et al., 2005; Gómez-Ortiz et al., 2007). Meanwhile, low resistivity values mean that the subsurface material allows electric current to flow through it easily. Rocks with low resistivity include tuff, clay soil and weathered rock (Keller and Frischknecht, 1966; Maury and Balaji, 2014; Nazaruddin et al., 2017; Hiden et al., 2017). Low resistivity layers can also be associated with aquifers (Telford et al., 1990).

Five survey lines – Karanganyar, Ijobalit 1, Korleko, Ijobalit 2, and Ijobalit 3 – were selected based on the morphology and topography of the research area (Figure 35). Frequently, we required a full day of measurement to obtain one resistivity profile. Measured observation data were edited using AGI Administrator software. We then used AGI Earth Imager for inverse modeling to obtain the subsurface resistivity profiles.

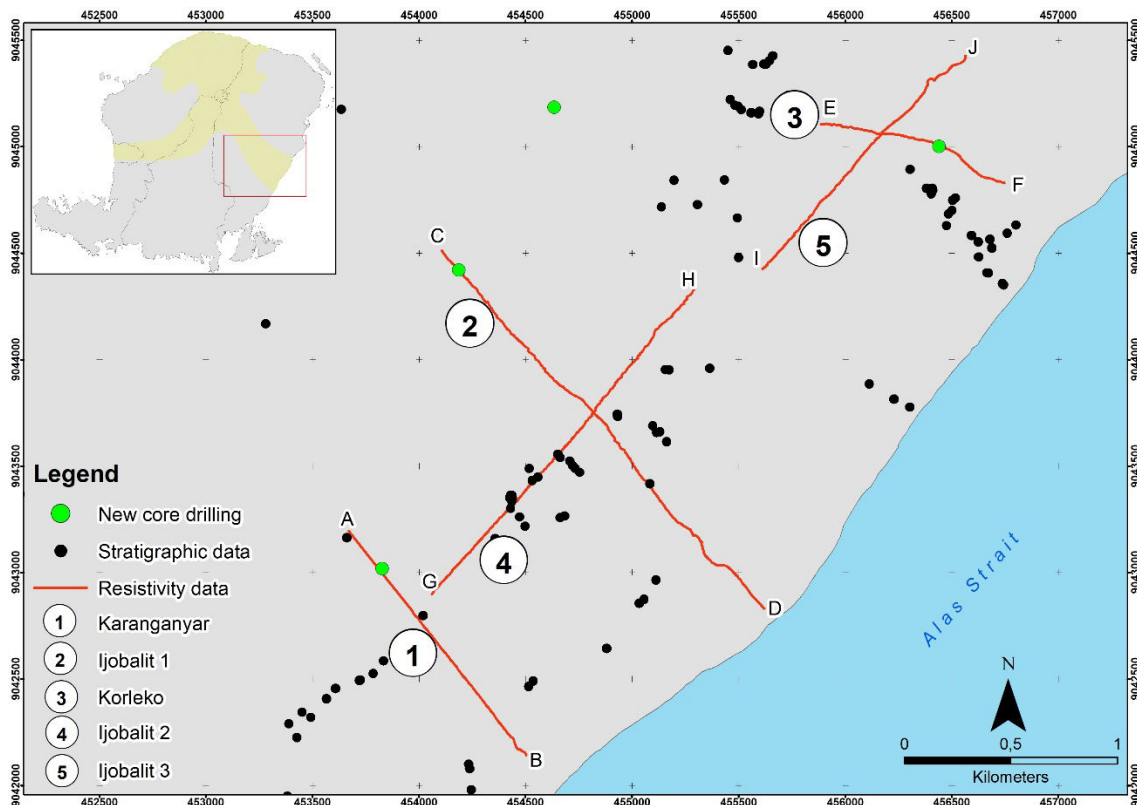


Figure 35. Resistivity lines on the eastern part of Lombok.

A comparison of the resistivity values, stratigraphic information obtained by drilling, and the participatory stratigraphy results, was valuable in terms of interpreting and fix the resistivity ranges for various types of sediment deposit. Furthermore, this stratigraphic interpretation of the resistivity profiles allowed us to reconstruct the history of different phases of the sedimentation process.

3.1.3. Tsunami deposits

Samples of tsunami deposits had been collected in Kiantar Village (T1 – T5) and Belang Island (T6) on the western coast of West Sumbawa. In abandoned fishponds located between 100 and 300 m from the coastline, we found tsunami deposits consisting of sand, volcanic ash, pumice, and coral rubble (T1 – T5) (Figure 36). At

selected locations, vertically contiguous sand samples, as well as ancient coral fragments and seashells, were collected for radiocarbon dating, and to recognize and interpret tsunami deposits (Figure 37).

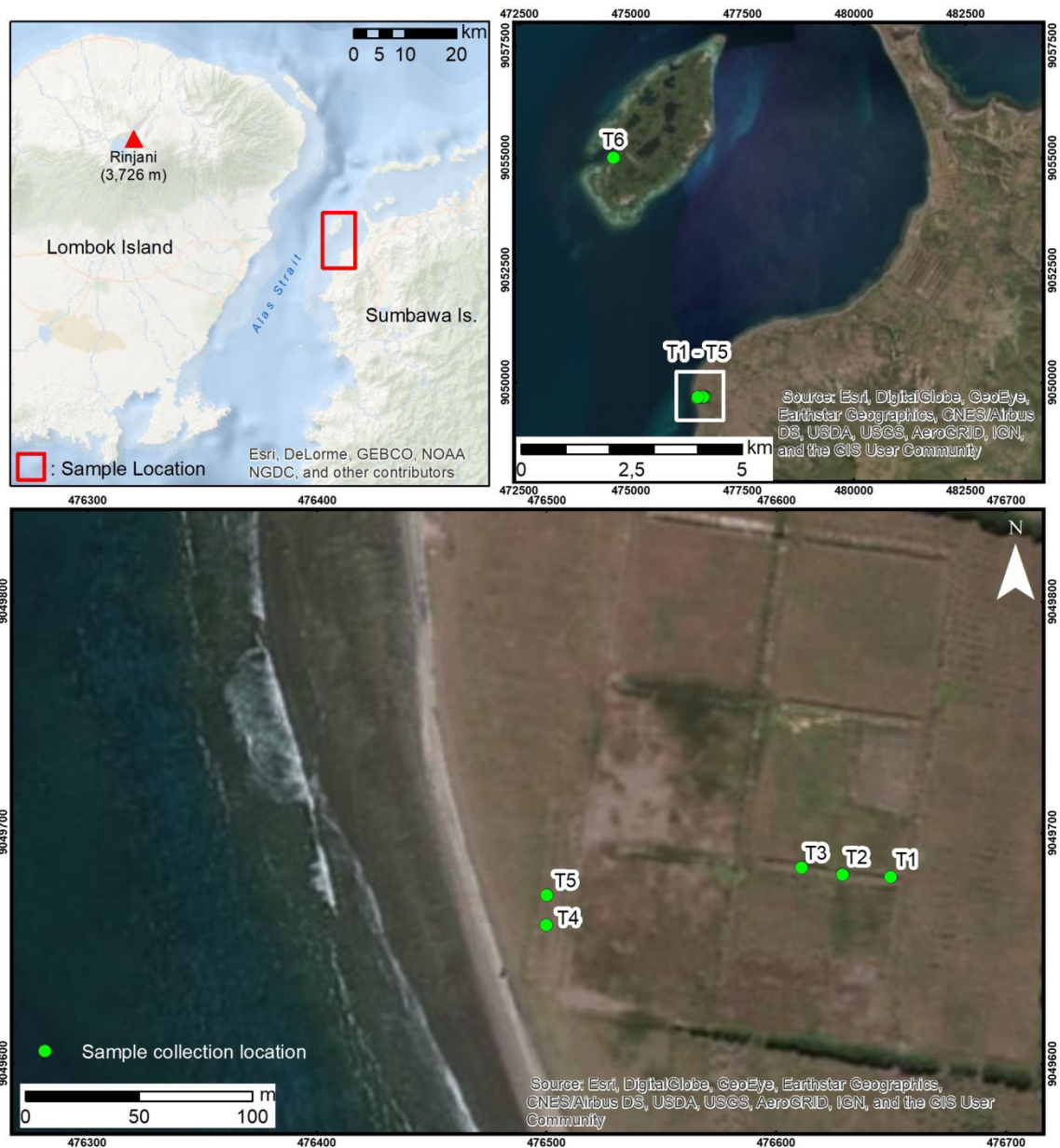


Figure 36. Sample collection location in abandoned fishponds in Kiantar Village (T1 – T5) and Belang Island (T6) on the western coast of West Sumbawa.



Figure 37. Sample collection for radiocarbon dating, and to recognize and interpret tsunami deposits (Courtesy: P. Guerin, February 2016).

We investigated six sample location points (T1 - T6) in February 2016 and February 2017. We collected multiple samples for grain-size analysis in the Laboratory of Soil Analysis and Superficial Training, Ecole et Observatoire des Sciences de la Terre – University of Strasbourg. These samples were obtained from each layer with differences in texture and formation of the sediments on sample location number 4 (T4). We performed a grain size analysis using a Beckman Coulter LS-13-320 Laser Diffraction Particle Size Analyzer device (Figure 38). This laser-based technology uses the flagship multi-wavelength system and may analyze the sediment distributions that range from 0.017 μm to 2,000 μm without the risk of sediment lost, either the largest or the smallest particles in the sediment sample.



Figure 38. Beckman Coulter LS-13-320 Laser Diffraction Particle Size Analyzer device
(Courtesy: Beckman Coulter website, June 2018).

Grain size analysis results encompass granulometric parameters, such as grain size average (mean), sorting degree (variance and standard deviation), and form of the grain size distribution (skewness and kurtosis). The grain size class intervals determine the values of each granulometric parameters. Sediment grain size characteristics may be used to analyze the features of tsunami deposits (Szczuciński et al., 2012; Chagué-Goff et al., 2012). Multiple samples in the form of coral fragments and seashells have been analyzed for radiocarbon dating at Laboratoire de Mesure du Carbone 14 (LMC14) - CNRS France, Beta Analytic Radiocarbon Dating, and DirectAMS Radiocarbon Dating Service in the United States.

3.2. Laboratory and computational analysis

3.2.1. Geochemical analysis

We collected pumice sample for geochemical analysis to verify the concordance of the pumice deposits, as well as charcoal in PDC deposits for radiocarbon dating (Figure 39). Geochemical analyses were done for the samples of pumices from quarries at Dasan Geres (Figure 39b). A total of 3 samples from different layers (i.e., layer 1, 2, and 3) (Figure 40) has been analyzed at the Centre de Recherches Pétrographiques et Géochimiques, Université de Lorraine, Nancy, France. The geochemical analyses included major, minor, and trace elements. The results were compared with previous research conducted by Lavigne et al. (2013) and Vidal et al. (2016).



Figure 39. Pumice and charcoal sampling: (a) from natural cliffs at Korleko coast (Courtesy: F. Lavigne, using a MavicPro drone, August 2017); and (b) from human-made outcrops in quarries at Dasan Geres (Courtesy: F. Lavigne, July 2015).



Figure 40. Samples of pumices for geochemical analysis (layer 1, 2, and 3) (Courtesy: F. Lavigne, July 2015).

3.2.2. Radiocarbon dating

Based on rapid observation in the field, the materials in layer 2 and 3 have different color and texture (see Figure 40). Therefore, two charcoals from each layer have been analyzed for radiocarbon dating at Beta Analytic Radiocarbon Dating, Miami, Florida, United States. This analysis aims to verify the conventional radiocarbon age (BP) of our charcoal samples (Figure 41). Beta Analytic performs all work on these samples, under a strict chain of custody and quality control under ISO/IEC 17025:2005 Testing Accreditation PJLA #59423 accreditation protocols. The results were corrected for total isotopic fractionation effects (natural and laboratory-induced). The radiocarbon dating results have been calibrated using SHCal13 Southern Calibration from Hogg et al. (2013).

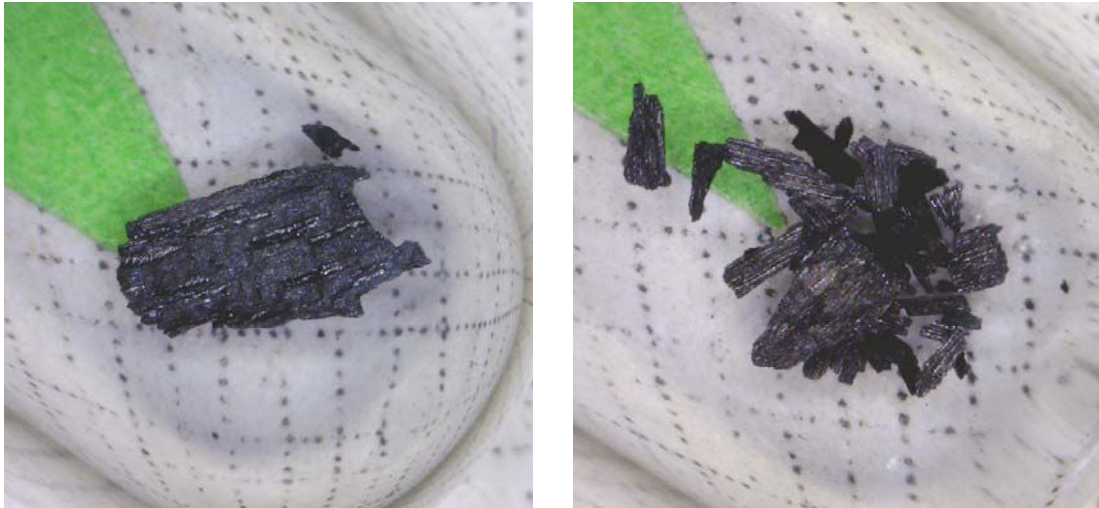


Figure 41. Charcoal samples from layer number 2 (left) and 3 (right).

3.2.3. Geospatial database using ArcGIS

A digital elevation model (DEM) extracted from a 1998 topographic map of Indonesia at a scale of 1:25,000, produced by the country's Geospatial Information Agency (BIG), was used to represent the present-day topography. Lombok's pre-1257 CE topography was reconstructed using a GIS method that subtracts interpolated isobase values from the present-day topography. Besides, this method provides further quantitative analyses of the results, for example, calculation of the difference in volume of deposits between the present-day and pre-1257 CE topography based on the same grid size (12.5 m in our study). Since the root mean square error (RMSE) value is the mean difference between the real and predicted values in the DEM, the RMSE can be used as an indicator of DEM quality (Li, 1988). The smallest RMSE means that the model has reliably predicted the measured values. The model can be categorized as a valid model if the mean standardized error is close to 0, the average standard error value is close to the root mean squared prediction error value, and the root mean squared standardized error value is close to 1 (Li and Tang, 2011).

In this study, we were able to gather data from 1,330 paleo-topographic points that were then interpolated to produce a pre-eruption DEM using the simple kriging method, first order of trend removal, and an exponential semivariogram model. Kriging is a method of geostatistical interpolation that produces a predicted topography (i.e., z-values) from the widespread points. The kriging method was used for the purposes of interpolation in this study, as it has been shown that it performs better than other contemporary methods on several different terrain types since it had the smallest RMSE values (Zimmerman et al., 1999; Schwendel et al., 2012; Arun, 2013).

A total of 26 transects were made manually, both parallel and perpendicular to the shoreline, in order to better reconstruct the thickness distribution of the 1257 CE deposits, as well as predict landscape evolution following the eruption. These profile diagrams were made by plotting the upper and the lower limit of the pumice-rich PDC deposits at various points along its course. Pre-1257 CE elevation also allowed us to determine the types of material below the pumice-rich PDC deposits – that is, from before the 1257 CE eruption – for example, bedrock, pebble, clay or coral. Furthermore, these transects allowed us to predict river networks and the location of laharc corridors based on the types of material found in them, such as pumice-rich PDC, lahar and flood-derived sand deposits.

3.3. Exegesis of written sources

The word "Babad" in Javanese and Balinese culture can define as a chronicle or a story about past events that were written on palm leaves in Old Javanese language. In this research, we used two babad from Museum of West Nusa Tenggara Province namely Babad Lombok and Babad Suwung (Figure 42). Babad Lombok, as mentioned by Lavigne et al. (2013), describes the process of Samalas eruption, the formation of

Segara Anak caldera, and the impacts of voluminous ash fall and pyroclastic flow in Lombok Island. Meanwhile, Babad Suwung describes the history of Lombok Kingdom as well as the impacts of a volcanic eruption in Talkuwang (Taliwang), on the western coast of Sumbawa Island.



Figure 42. a) The popular version of Babad Lombok that translated to Bahasa Indonesia by Lalu Wacana in 1979; b) the original version of Babad Suwung; and c) Mr. Haji, the interpreter of old Javanese language in Mataram, Lombok (Courtesy: F. Lavigne, July 2015).

In the Museum of West Nusa Tenggara Province, access to some babads is restricted only to the babads keeper, museum employee, or some linguists. Therefore, first, we requested permission from the chief of the museum to analyze these babads with their interpreter. Interpretation of Babad in Javanese culture means sing performance from the interpreter (Figure 43). Second, we analyzed the interpretation results and compared it with field observation results and previous researches.



Figure 43. Song performance from the interpreter of Babad Suwung (Courtesy: P. Guerin, July 2016).

Several field observations were conducted in Lombok and Sumbawa during 2014 - 2017 to obtain more information related to Samalas eruption and its impact on the society. In addition to physical aspect measurement (Figure 44a), multiple interviews with old Javanese linguist and museum employee were done to clarify the meanings of some words as well as the history of the Babads (Figure 44b). The results from field

observation and interviews were analyzed and compared with previous research conducted by Lavigne et al. (2013); Vidal et al. (2015); and Vidal et al. (2016).



Figure 44. a) Field observation of pumice deposits in Talkuwang (Taliwang), Sumbawa and b) interviews with museum employee in Mataram (Courtesy: P. Guerin, July 2016).

3.4. Conclusion

This chapter describes extensively the methodology that used during the research, including what was done during and after the fieldworks. We were able to reconstruct in detail the landscape evolution on the eastern part of Lombok based on the information from more than 1,300 stratigraphic data, which was obtained from several sources, such as the outcrops, wells, core drillings, and two-dimensional resistivity profiling. Furthermore, the combination of stratigraphic data and geophysical data was advantageous to obtain an accurate landscape reconstruction on the eastern part of Lombok following the 1257 CE eruption of Samalas volcano. We used kriging method as an interpolation method to reconstruct the landscape evolution in the

research area since 1) it performs better when compared to other contemporary methods in several terrain variations and 2) it can provide a measure of the uncertainty which would have a significant impact on the research results.

At several locations, we took numerous samples in the form of pumices, charcoal, ancient coral fragments, and seashells. These samples were then analyzed in the laboratory to obtain some clues about the period in which the volcanic material was deposited, the processes that triggered the transportation of the material, and to recognize and interpret tsunami deposits following the 1257 CE eruption. Lastly, we had analyzed and compared the field observation results with several written sources that related to the 1257 CE eruption. Figure 45 illustrates the information presented in Chapter 3.

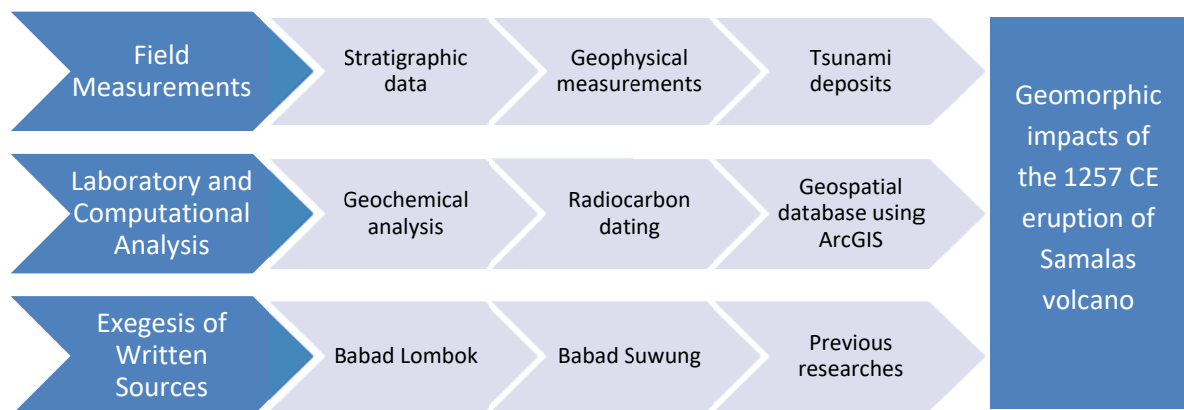


Figure 45. The research methodology that used to understand geomorphic impacts of the 1257 CE eruption of Samalas volcano.

PART 2
Geomorphic impacts of the 1257 CE
eruption of Samalas volcano along
the Alas Strait

Chapter 4: Local impacts of the 1257 CE eruption in East Lombok

The main goal of this chapter is, therefore, to reconstruct the paleo-topography of the eastern part of Lombok Island prior to the eruption of the Samalas volcano in 1257 CE and to analyze the subsequent landscape evolution in the aftermath of this eruption. By reconstructing the paleo-topography prior to the 1257 CE eruption, we can identify the condition of past environments more precisely. This information can also be used to assess, simulate and understand the geological conditions, as well as the geomorphological impact, of the 1257 CE eruption on the research area (Mann et al., 1999; Leverington et al., 2000; Leverington et al., 2002). Here, we present a significant stratigraphic data on the 1257 CE eruption with reference to five detailed studies which are very important in terms of understanding the geomorphological impact of the Samalas eruption in 1257 CE. Our results may serve to build on and complete the results obtained by Lavigne et al. (2013) and Vidal et al. (2015).

4.1. Field data

Examination of all the stratigraphic data obtained from outcrops, wells, and core drilling provided us with detailed information on the elevation of the present-day topography, the 1257 CE deposits and the depth at which the pre-1257 CE topography on the eastern part of Lombok lies. This information was then analyzed and combined with the perpendicular and parallel transects in the research area. The long profile and cross-profile for the perpendicular and parallel transects (see Appendix 2) show gradient changes in the topography from upstream to downstream and from southwest to northeast respectively. The stratigraphic data from the measurements and 26

stratigraphic profiles for the eastern part of Lombok can be divided into four categories based on material type (Figure 46):

- (i) 444 stratigraphic data with the information of pumice-rich PDC deposits only;
- (ii) sand with pumice fragments later referred to as lahar deposits (177 locations) (Figure 47);
- (iii) Flood-derived sand deposits at 188 locations. Flood-derived sand deposits refer to high-discharge streamflows with the material of sand without any pumice fragments. It happens when the volume of eroded material is not sufficient to trigger a hyper-concentrated flow or a debris flow (lahar), i.e., when the bulking effect is limited. It usually happens when the rainfall occurs at the bottom of the volcanic slopes.
- (iv) 521 stratigraphic data with the information of few or no pumice-rich PDC deposits.

We distinguished between these types of deposit based on the volcanic material linked to post-eruptive landscape evolution, especially those materials deposited during phase P4; that is, pumice-rich PDC and co-PDC ash fall deposits. In Lombok, the visual aspect of pumice-rich PDC deposits may vary regarding color and cohesion. Therefore, geochemical analysis from pumice samples and radiocarbon dating from charcoal samples were done to verify the concordance of pumice-rich PDC deposits. With this aim, we extracted pumice and charcoal samples from different layers of the Dasan Geres pumice quarry.

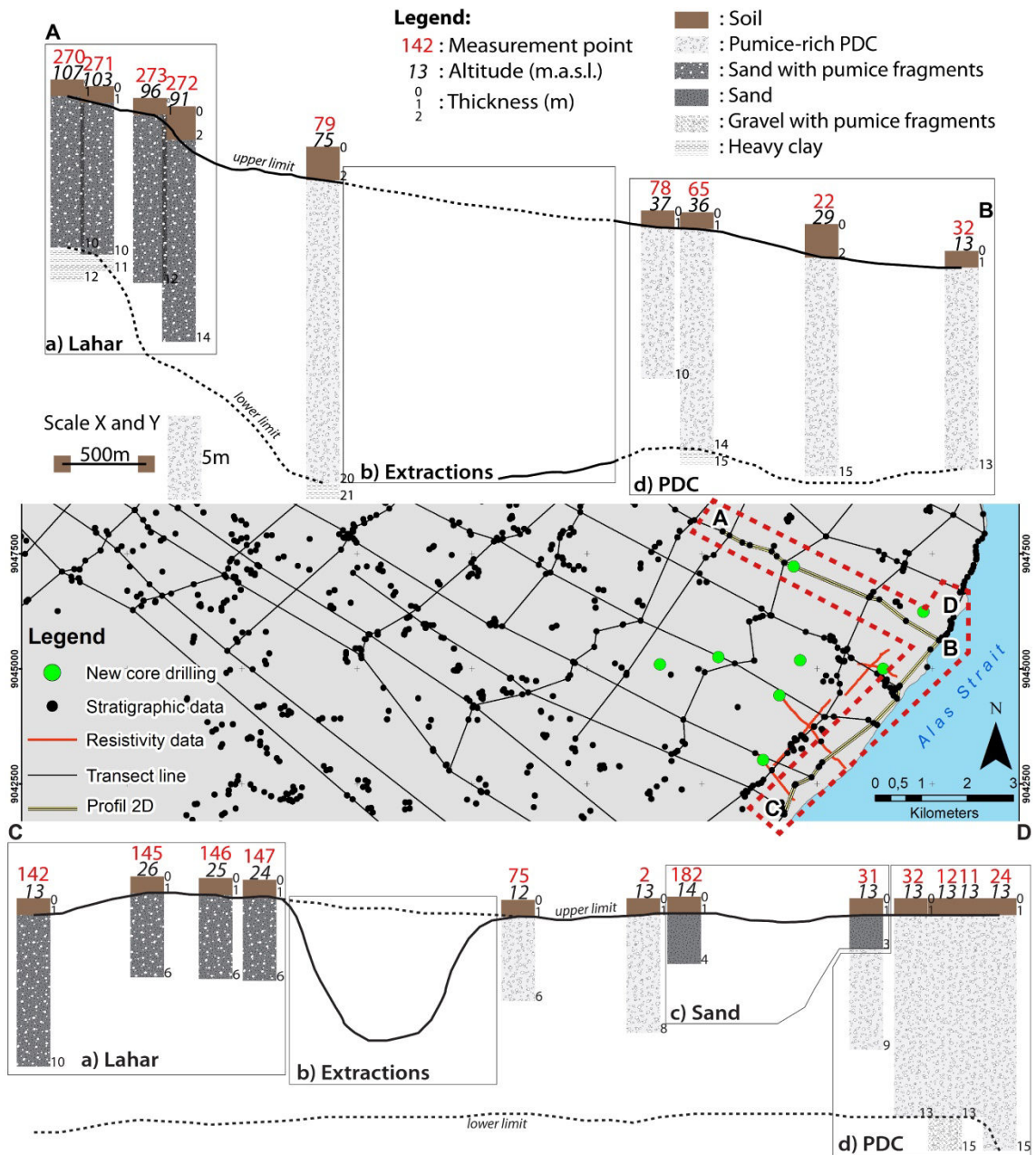


Figure 46. Examples of stratigraphic data with the information of: a) lahar deposits, b) no volcanic material due to extraction, c) flood-derived sand deposits, and d) pumice-rich PDC deposits in Korleko (red box with dashed lines).



Figure 47. An example of lahar deposits near Selong. We used the term of “lahar” for the material of sand with pumice fragments since the lahars on Lombok at that time were pumiceous. For lahars that contain pumice after a large eruption ($VEI \geq 4$), there is a mixture between a normal granulation for lithic and a lack of granulation for pumice vesicles, evenly distributed within the deposit (Fisher and Schmincke, 1984).

The comparison of geochemical results with previous research by Lavigne et al. (2013) and Vidal et al. (2016) aims to verify the origin of sediment deposits in the research area. Although the contents of major, minor, and trace elements are quite similar between the recent research results and the previous ones, there are some differences of geochemical value between pumices samples in layer 1 (DG1), layer 2 (DG2), and layer 3 (DG3) (Figure 48) with the results from previous research (Table 3). Therefore, radiocarbon dating was performed to verify if the conventional radiocarbon age (BP) of all pumice-rich PDC deposits in East Lombok match with the age of the 1257 CE eruption.



Figure 48. The layer of pumice-rich PDC (DG1, DG2, and DG3) in Dasan Geres quarry
(Courtesy: F. Lavigne, July 2015).

Table 3. Geochemical analysis results at Dasan Geres (DG).

| Elements | DG1 | DG2 | DG3 | Lavigne et al. (2013) | Vidal et al. (2016) |
|--------------------------------|--------|--------|--------|-----------------------|---------------------|
| SiO ₂ | 62.58 | 62.48 | 57.73 | 66.66 | 62.30 |
| Al ₂ O ₃ | 16.70 | 16.77 | 15.79 | 16.04 | 16.60 |
| Fe ₂ O ₃ | 4.46 | 4.57 | 4.19 | 2.77 | 4.70 |
| MnO | 0.14 | 0.14 | 0.13 | 0.14 | 0.14 |
| MgO | 1.42 | 1.43 | 1.36 | 0.74 | 1.39 |
| CaO | 4.07 | 3.86 | 5.74 | 2.22 | 3.65 |
| Na ₂ O | 4.65 | 4.68 | 4.27 | 3.99 | 4.09 |
| K ₂ O | 3.48 | 3.42 | 3.14 | 4.04 | 3.38 |
| TiO ₂ | 0.63 | 0.63 | 0.57 | 0.47 | 0.63 |
| P ₂ O ₅ | 0.23 | 0.23 | 0.22 | 0.29 | 0.24 |
| As | 3.61 | 3.66 | 3.46 | - | 3.60 |
| Ba | 747.79 | 741.56 | 704.62 | - | 707.00 |
| Be | 1.36 | 1.32 | 1.25 | - | 1.50 |
| Bi | 0.30 | 0.19 | 0.16 | - | - |
| Cd | 0.14 | 0.12 | 0.15 | - | 0.26 |
| Ce | 49.39 | 49.50 | 46.06 | - | 48.00 |
| Co | 6.23 | 6.83 | 6.22 | - | 6.70 |
| Cr | 5.09 | 3.19 | 3.31 | - | - |
| Cs | 3.05 | 3.03 | 2.80 | - | 3.00 |
| Cu | 16.56 | 16.20 | 7.13 | - | 13.00 |
| Dy | 5.09 | 4.95 | 4.60 | - | 4.60 |
| Er | 3.13 | 3.06 | 2.83 | - | 2.80 |
| Eu | 1.36 | 1.34 | 1.25 | - | 1.27 |
| Ga | 17.67 | 17.66 | 16.60 | - | 17.70 |
| Gd | 4.82 | 4.66 | 4.41 | - | 4.60 |
| Ge | 1.49 | 1.46 | 1.37 | - | 1.50 |
| Hf | 5.78 | 5.65 | 5.26 | - | 5.70 |
| Ho | 1.10 | 1.07 | 1.00 | - | 0.98 |
| In | 0.04 | 0.04 | 0.04 | - | - |
| La | 24.62 | 24.55 | 22.78 | - | 24.10 |
| Lu | 0.53 | 0.51 | 0.48 | - | 0.50 |
| Mo | 3.20 | 3.12 | 2.90 | - | 3.20 |
| Nb | 8.79 | 8.64 | 8.06 | - | 8.70 |
| Nd | 23.21 | 22.91 | 21.56 | - | 22.50 |
| Ni | 2.77 | - | 2.08 | - | - |
| Pb | 9.63 | 11.24 | 12.23 | - | 14.00 |
| Pr | 5.80 | 5.73 | 5.37 | - | 5.70 |
| Rb | 86.98 | 86.46 | 80.61 | - | 83.00 |
| Sc | 10.07 | 9.63 | 8.95 | - | 9.70 |
| Sb | 0.28 | 0.27 | 0.29 | - | 0.29 |
| Sm | 5.15 | 5.03 | 4.76 | - | 5.00 |
| Sn | 1.54 | 1.64 | 1.63 | - | - |
| Sr | 352.03 | 358.39 | 368.64 | - | 351.00 |
| Ta | 0.77 | 0.75 | 0.70 | - | 0.75 |
| Tb | 0.79 | 0.77 | 0.71 | - | 0.74 |
| Th | 9.73 | 9.64 | 8.88 | - | 9.50 |
| Tm | 0.47 | 0.46 | 0.42 | - | 0.45 |
| U | 2.58 | 2.55 | 2.35 | - | 2.50 |
| V | 56.76 | 59.83 | 55.10 | - | 65.00 |
| W | 1.38 | 1.34 | 1.41 | - | - |
| Y | 29.60 | 29.23 | 26.50 | - | 28.80 |
| Yb | 3.32 | 3.29 | 3.02 | - | 3.12 |
| Zn | 68.35 | 71.59 | 66.24 | - | - |
| Zr | 222.18 | 221.38 | 201.53 | - | 224.70 |

Conventional radiocarbon age for charcoal in layer 2 (DG2) is 810 ± 30 BP (1217 – 1286 cal AD with 95.4% probability). While for layer 3 (DG3) is 870 ± 30 BP (1162 – 1270 cal AD with 95.4% probability) (Figure 49). This result corresponds with the year of Samalas volcano eruption in 1257 CE. The radiocarbon dating results for pumices samples from DG2 and DG3 shows that these pumices samples originated from the same eruption of Samalas in 1257 CE, then it can be concluded that there is only one eruption source for all sediment deposits in the research area.

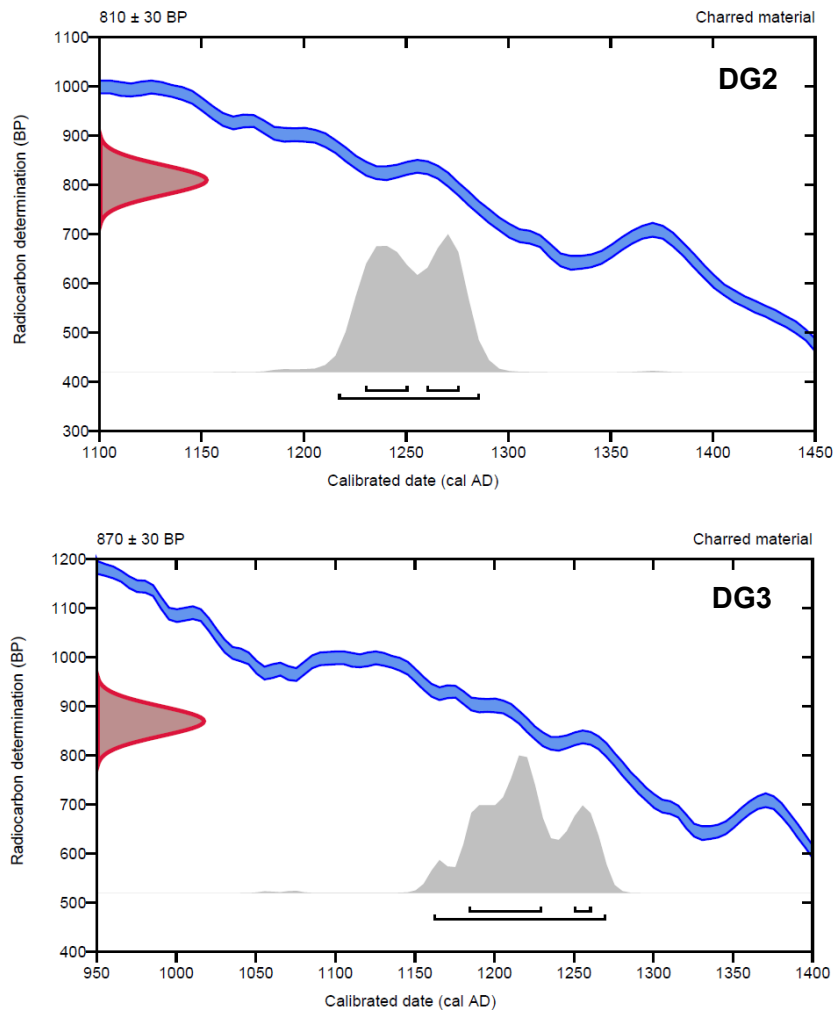


Figure 49. Calibration of radiocarbon age to calendar years with the high probability density range method (HPD - SHCAL13).

Since based on radiocarbon dating results, pumice-rich PDC deposits in Dasan Geres pumice quarry is from the same eruption, it is important to understand that the geochemical values may vary from one phase to another in the same eruption (i.e., between DG1, DG2, and DG3). The variations of color and cohesion observed between different pumice-rich PDC deposits are the result from the evolution of geochemical composition of the ascending magma during the 1257 CE eruption of Samalas volcano. Furthermore, in the study area, the thickness of pumice-rich PDC deposits ranges from 1 to 30 meters, while the average depth is 7.8 meters.

The interpretation of material types on the resistivity lines (Figure 50) were determined based on the results of core drilling. In general, pumice-rich PDC deposits in eastern Lombok produced the highest resistivity values, above $\sim 300 \Omega\text{m}$ (Hiden et al., 2017). Such materials are represented here by orange to dark red colors on the resistivity profiles.

Resistivity profile number 1-AB is located in Karanganyar and runs NW-SE along a length of 1,500 m (Figure 51a). The highest resistivity values, ranging between $300 \Omega\text{m}$ and $2,000 \Omega\text{m}$, are distributed along this line, and the deposits have therefore been interpreted as pumice-rich PDC with a thickness of about 20 m. Differences in pumice distribution in the resistivity profiles may be due to erosion processes, which could be either natural and caused by post-eruptive lahars or floods, or human-made, such as caused by extensive pumice extraction. Along resistivity line 1 AB, there was one core drilling in A+240 m with a depth of about 18 m. The type of material in this core was homogenous, made up of pumice-rich PDC deposits. This result may explain the situation in area A+0 m to A+600 m, which, according to the interviews conducted with local people, has no good source of water. People in this area do not have any wells, and they have to buy their water from the local water company in East Lombok.



Figure 50. Five resistivity lines profiles in: a) AB-Karanganyar, b) CD-Ijobalit 1, c) EF-Korleko, d) GH-Ijobalit 2, and e) IJ-Ijobalit 3.

Along resistivity line number 2-CD Ijobalit 1 (Figure 51b), there was one core drilling in C+130 m with a depth of about 21 m. The type of material in this core was also homogenous and made up of pumice-rich PDC deposits. The orange to dark red colors on the resistivity profile represent the pumice-rich PDC deposits with resistivity values ranging between 300 Ω m and 2,000 Ω m. While resistivity was being measured along this line, the local people were drilling a well in C+360 m with a depth of more than 40 m. They found pumice-rich PDC deposits up to a depth of 16 m ($>300 \Omega$ m), sand with pumice fragments at a depth of 16–20 m ($\sim 30\text{--}300 \Omega$ m), and a sandy clay material at a depth of 20–41 m ($<30 \Omega$ m).

The highest resistivity values in the resistivity profile number 3-EF Korleko (Figure 51c) are represented by orange to dark red colors and have been interpreted as pumice-rich PDC deposits. The medium resistivity values ranging from about 30 Ω m to 300 Ω m, represented by the light green to dark yellow colors, have been interpreted as bedrock, pebble or wet sand. Lower resistivity values (<30 Ω m) are indicated by the dark blue to light blue colors. Based on the core drilling carried out in E+580 m, the part of the resistivity profile with a resistivity of less than 30 Ω m was interpreted as a potential source of groundwater in unconfined aquifers. We had to stop drilling at a depth of 11 m due to the fact that the water flow moving in a SE direction was too strong at this depth.

In resistivity profile number 4-GH Ijobalit 2 (Figure 51d), there are two wells in G+1060 m and G+1780 m with depths of about 15 m and 9 m respectively. Based on interviews with the wells' owner, the material in the wells is sand with pumice fragments. This would make sense since the wells in G+1060 m and G+1780 m were built on the site of former pumice extraction, where about 13 m and 12 m respectively of pumice-rich PDC deposits were removed. The highest resistivity values, which are more than 300 Ω m, are distributed along resistivity line number 5-IJ Ijobalit 3 (Figure 51e) and have been interpreted as pumice-rich PDC deposits based on the information obtained during the participatory stratigraphy process. An outcrop in I+750 m also shows a 12 m layer of pumice-rich PDC deposits. These deposits are represented by orange to dark red colors. Based on the results of direct measurement, participatory stratigraphy, drilling, and the resistivity profiles, we were able to summarize the relationship between resistivity value and type of material on the eastern part of Lombok (Table 4).

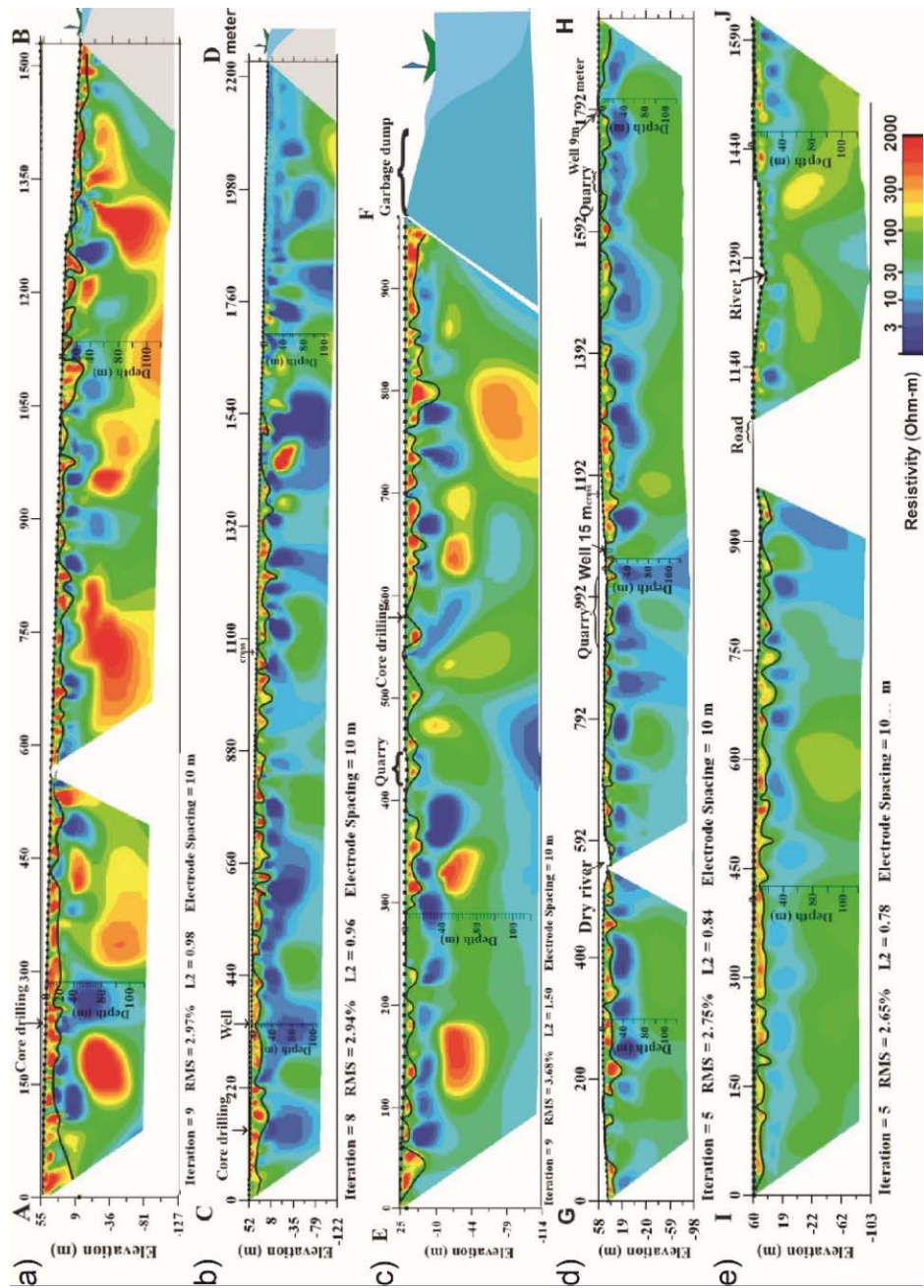








Figure 51. Resistivity profiles in: a) AB-Karanganyar, b) CD-Ijobalit 1, c) EF-Korleko, d) GH-Ijobalit 2, and e) JJ-Ijobalit 3. Orange to dark red colors ($\rho \geq 300 \Omega\text{m}$) represents pumices or dry sand. Fine black lines mark the possible depth of the pumice layer.

Table 4. Interpretation of how resistivity values corresponding to types of material on the eastern part of Lombok.

| Resistivity values (ρ) | Color | Types of materials |
|---|---|--|
| $\rho < 3 \Omega\text{m}$ |  | Very fine sandy clay, sea sediments (suspected), poor water quality. |
| $3 \Omega\text{m} \leq \rho < 10 \Omega\text{m}$ |  | Fine sandy clay, sea sediments (suspected), poor water quality. |
| $10 \Omega\text{m} \leq \rho < 30 \Omega\text{m}$ |  | Sandy tuff, aquifers (suspected). |
| $30 \Omega\text{m} \leq \rho < 100 \Omega\text{m}$ |  | Very fine sand (wet sand), tuff, aquifers (suspected). |
| $100 \Omega\text{m} \leq \rho < 300 \Omega\text{m}$ |  | Fine sand (wet sand), gravel, and the possibility of an aquifer. |
| $\rho \geq 300 \Omega\text{m}$ |  | Pumices, dry sand. |

4.2. Computational Analysis

4.2.1. Reconstruction of the pre-1257 CE topography

Figure 52a and 52b compare the present-day topography extracted from the 1998 topographic map of Indonesia (at a scale of 1:25,000) with the reconstructed pre-1257 CE topography (at a resolution of 12.5 m). The RMSE, average standard error, mean standardized error, and root mean squared standardized error values for the present-day and the reconstructed pre-1257 CE topography are shown in Table 5.

Table 5. Cross-validation for the present-day and reconstructed pre-1257 CE topography.

| Prediction Errors | Present-day | Reconstructed pre-1257 CE |
|---------------------------------------|-------------|---------------------------|
| RMSE | 2.81 | 3.43 |
| Average standard errors | 2.12 | 2.80 |
| Mean standardized errors | -0.01 | 0.00 |
| Root mean squared standardized errors | 1.03 | 1.05 |

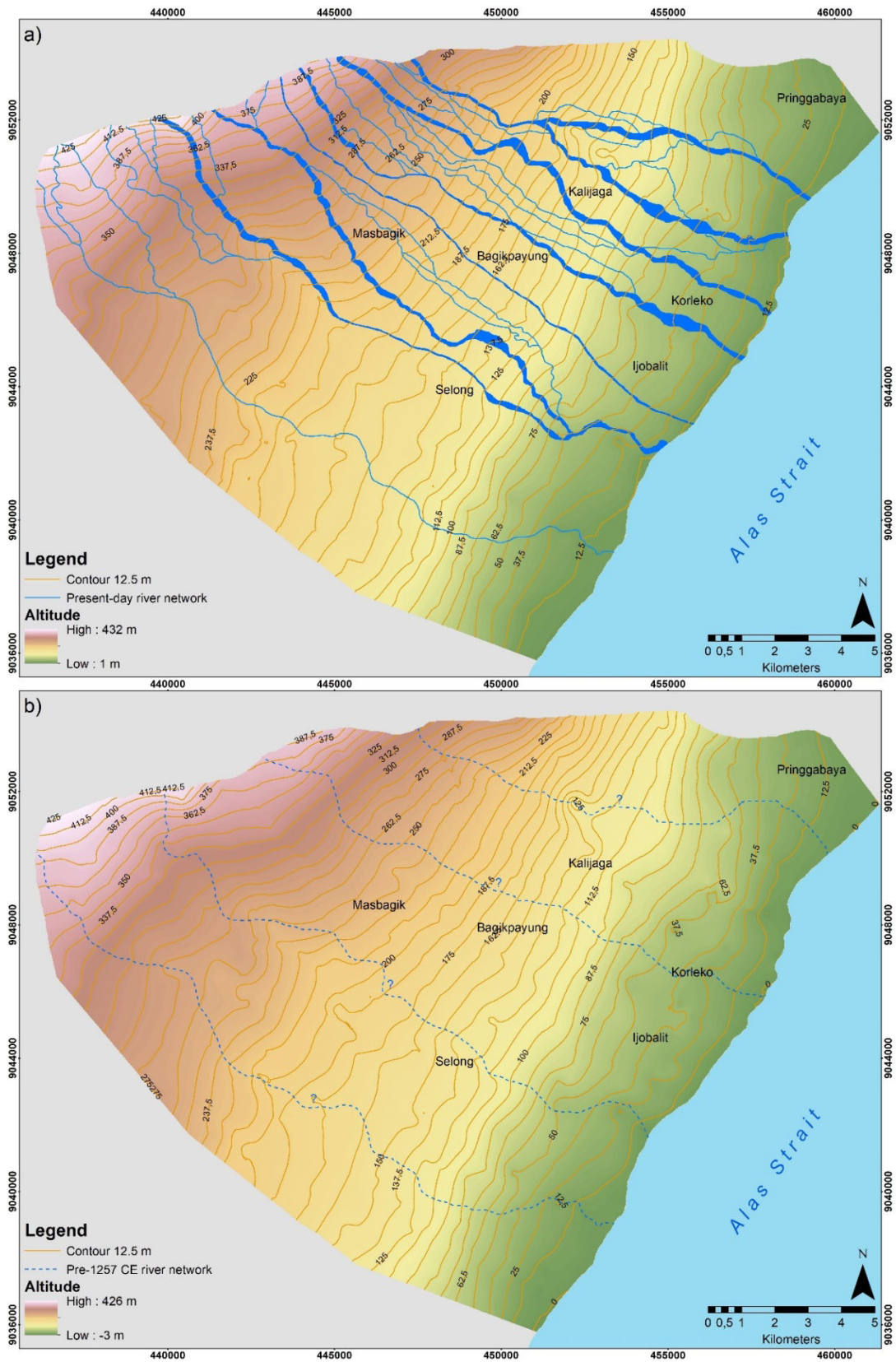


Figure 52. (a) Present-day topography and (b) reconstructed pre-1257 CE topography.

Almost the entire landscape on the eastern part of Lombok, with the exception of the north and south of this area, differs today from the landscape prior to the 1257 CE eruption (Figure 53a). The pre-1257 CE river network was predicted using the reconstructed pre-1257 CE topography and information from the 1994 Geological Map of Indonesia (at a scale of 1:250,000) produced by the Indonesian Geological Agency. The pre-1257 CE river network in the eastern part of Lombok consisted of four major rivers draining a basin 18 km long. Two hilly landscapes bordered this basin in the northern and southern part. In the northern part, there is early Holocene material in the form of undifferentiated volcanic rocks (e.g., lava, breccia, and tuff) from the Pusuk and Nangi volcanos to the east of the Rinjani volcano.

The pre-1257 CE material in the middle part is made up of alternating layers of calcareous breccia and lava dating from the end of the Pliocene to mid-Pleistocene, which is later overlaid by pumice-rich PDC and co-PDC ash fall deposits from phase P4 of the 1257 CE eruption. The core drilling data (FR7) also show that there is breccia material at a depth of 13 m, which forced us to stop drilling. The participatory stratigraphy results also support this information: when drilling their wells, locals claimed to have found a "hard material" which they call "*batu ampan*" below the pumice-rich PDC material. The hilly landscape in the southern part of the basin was formed by a large debris avalanche deposit dated at 16,490 \pm 50 BP (Beta Analytic, uncal).

4.2.2. Primary volcanic deposits

Pumice-rich PDCs covered the eastern part of Lombok in the aftermath of the 1257 CE eruption. Pre-eruptive valleys were filled with the newly deposited volcanic material as it followed the contours of the pre-eruption topography (Figure 53b). Based

on the several pumice quarries and outcrops in the area, we surmised that at least three massive pumice-rich PDCs reached the sea during the P4 phase (column collapse) of the eruption. One of these crossed the Alas Strait and deposited its pumice fragments on the western coast of Sumbawa, 50 km from the Samalas volcano (Vidal et al., 2015).

As a result of this rapid pumice-rich PDC deposition, there was aggradation at some points along the shoreline, and volcanic (PDC, tephra fallout) and volcanoclastic (lahar) material buried most of the pre-eruption coral reef, probably up to several kilometers from the pre-1257 coast. During interviews, local people also maintained that the area's high cliffs jutted out further into the sea a few decades ago, and pumice-rich PDC deposits were much more widespread. Since the eruption occurred during the dry season (Lavigne et al., 2013), there was very little erosion of pumice-rich PDC deposits in the aftermath of the eruption. Furthermore, based on field evidence, we can conclude that there was no syn-eruptive lahar deposition in the aftermath of the 1257 CE eruption. During the dry season in Lombok, there was not enough water to trigger lahars since there are no rains for several weeks or even months. Although it was raining, it is still difficult since the rainwater was either evaporated due to hot tephra or seeps into the very permeable pumice-rich PDC deposits (Klug and Cashman, 1996; Wright et al., 2006; Douillet et al., 2015).

We estimated the volume of pumice-rich PDC deposits based on the information from 444 stratigraphic data and eight core drillings, which are categorized as the first type of stratigraphic data (see 4.1.), i.e., pumice-rich PDC deposits. The values for RMSEs, average standard errors, mean standardized errors and root mean squared standardized errors are 2.90, 2.25, 0.00 and 1.08 respectively. Having performed a raster calculation using ArcGIS, the volume of pumice-rich PDCs in the aftermath of the

1257 CE eruption was found to be approximately $4,435 \times 10^6 \pm 5.5 \text{ m}^3$ over a surface of 171 km^2 .

4.2.3. Erosion of PDC deposits

From the end of the 13th to the beginning of the 20th century, the main cause of landscape evolution was fluvial erosion. We were able to reconstruct the post-1257 river network based on: 1) the second and third type of the stratigraphic data (i.e., flood-derived sand and lahar deposits; see 4.1.), 2) the 1998 topographic map of Indonesia at a scale of 1:25,000, and 3) the present-day topography. We delineated the area of erosion manually based on the spatial distribution of the stratigraphic data which has the information of lahar and flood-derived sand deposits.

Over the course of at least one or two decades (compared with the 1991 CE eruption of Pinatubo as a reference), wide lahar corridors were created at a width of approximately 1-4 km. Unlike the lahars resulting from the erosion of block-and-ash flows that can be found at the Merapi or Semeru volcanoes (Lavigne and Thouret, 2003; Lavigne et al., 2007), the lahars on Lombok at that time were pumiceous, due to the very easily erodible source material. Consequently, a new hydrographic network appeared fairly quickly – probably just a few months after the emplacement of the pumiceous deposit – with broad main valleys mostly located where the original pre-1257 valleys were, and new shorter tributaries located where pumice-rich PDC deposits were found. The deposited volcanic material has been progressively eroded following intense rainfall events by mountain streams carrying sand, pebbles, and pumices (Figure 53c).

In the midstream area, variations were observed between areas with erosion and those with excellent preservation of pumice-rich PDC deposits. Furthermore, in the downstream area, there are no lahars or flood-derived sand deposits except in the post-1257 river networks. We estimate the volume of pumice-rich PDC deposits after erosion to be approximately $625 \times 10^6 \pm 5.5 \text{ m}^3$ over a surface of 89 km^2 . Since then, the coastline has also begun to retreat inland due to marine erosion (Figure 53d). All this means that although there have been numerous erosion processes in the time range between 1257 and 2018, 14% of eastern Lombok's initial volume of volcanic material from the 1257 CE Samalas eruption remains.

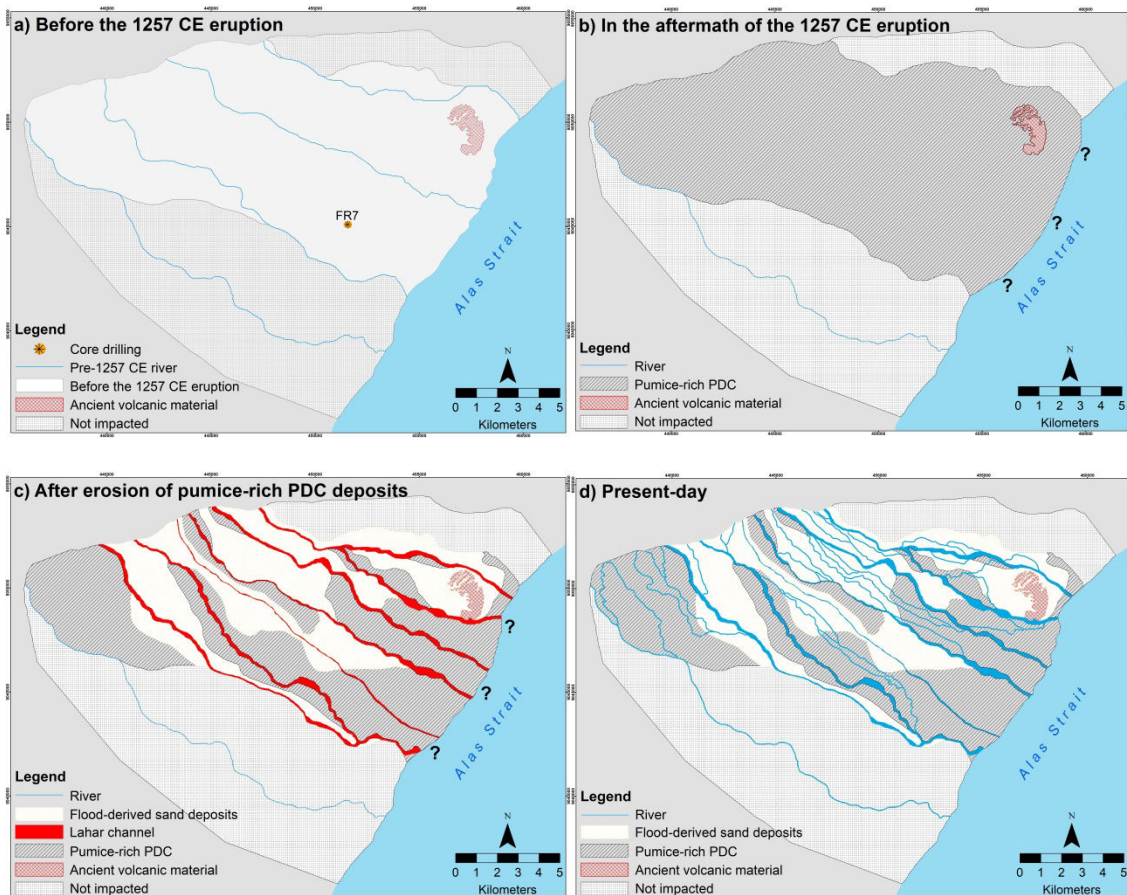


Figure 53. Modeled post-eruptive landscape evolution.

4.3. Discussion

Only the stratigraphic data with the information of pumice-rich PDC deposits was used as the basis for reconstructing the paleo-topography and calculating the volume of pumice-rich PDC deposits on the eastern part of Lombok. Since in some areas the land has been partly reworked and covered by lahar and flood-derived sand deposits, or other areas no longer contain pumice-rich PDC deposits, the participatory and resistivity data play an important role in accurately predicting and deriving post-eruptive landscape evolution, as well as in calculating the volume of pumice-rich PDC deposits on the eastern part of Lombok.

In order to interpolate the pre-1257 CE topography from isobase values, the accuracy of the DEM is crucial. Several factors affect DEM quality, these being: a) the number of samples (1,330 points in our study) compared to the total area (295 km²), and the precision of position measurement and spatial distribution of sampling points (the average distance between data points was 128 m) (Erdogan, 2009; Heritage et al., 2009; Chen et al., 2013); b) the characteristics of the terrain, i.e., either regular or chaotic pre- and post-eruption topographic, which would affect how easily the real surfaces could be found (Skidmore, 1989; Carrara et al., 1997; Schwendel et al., 2012; Chen et al., 2013; Zhang et al., 2015); and c) the interpolation techniques used (Carrara et al., 1997; Heritage et al., 2009; Schwendel et al., 2012; Arun, 2013; Chen et al., 2013; Yang et al., 2015). Topography models can be categorized as valid in our study since the mean standardized error is close to 0, the average standard error value is close to the root mean squared prediction error value, and the root mean squared standardized error value is close to 1 (see Table 5).

Several studies have sought to reconstruct volcanic landscape evolution following major eruptions using a variety of different methods, including modelling the pre-eruptive landscape prior to the major eruption (Daag and Van Westen, 1996; Vogel and Märker, 2010; Cimarelli et al., 2013), modelling the former shape of a collapsed volcano (Salvany et al., 2012; Platz et al., 2012; Lavigne et al., 2013; Karátson et al., 2016), or using historical maps, remote sensing and GIS (Lahitte et al., 2012; Marsella et al., 2012; Torrecillas et al., 2012; Gomez, 2014; Germa et al., 2015; Kubanek et al., 2015). As the Pinatubo eruption was recent, Daag and Van Westen (1996) used a multi-temporal DEM from 1986–1994, derived from a topographic map and oblique and vertical photos, to analyze the geomorphologic situation from prior to the eruption up until the third rainy season in 1993 CE. In this study, we used a similar approach; although reconstructing Samalas’s pre-eruptive topography was more challenging than Pinatubo’s since the Samalas eruption occurred 734 years before the 1991 CE eruption of Pinatubo. In contrast to the research conducted by Vogel and Märker (2010), which used Topo to Raster as the interpolation method, we used kriging for this study, since it can provide a measure of the uncertainty, which would have a significant impact on the inferred volume of pumice-rich PDC deposits on the eastern part of Lombok.

Our results show that the topography on the eastern part of Lombok has changed dramatically over the course of the last millennium (Figure 54). As with all relief-forming geomorphic processes, the spatial distribution of volcanic deposits is influenced by natural factors, such as elevation and hydrological variables (Vogel & Märker, 2010). We surmised that volcanic and volcanoclastic material had buried most of the pre-1257 coral reef, since this phenomenon has also occurred following several other eruptions, including the 1991 CE eruption of the Pinatubo volcano in the Philippines (Wu et al., 2018), the 1994 CE volcanic eruption of the Rabaul caldera in Papua New Guinea

(Maniwavie et al., 2001) and the 2003 CE volcanic eruption of Anatahan in the Northern Mariana Islands (Vroom and Zgliczynski, 2011).



Figure 54. Pumice-rich PDC covered all the current plain in the aftermath of the 1257 CE eruption. Based on an interview with a local people, the PDC deposits were widespread a few decades ago. A sudden natural shift from the main rivers in Dasan Geres (Geres River), as well as intense quarrying activity, are both responsible for the accelerated erosion (Courtesy: F. Lavigne, July 2015).

The area of eastern Lombok covered by pumice-rich PDC deposits turns out to be different from the one previously mapped by Lavigne et al. (2013) and Vidal et al. (2015). Their findings were an estimation based on less than ten measurement points, which is why Lavigne et al. (2013) referred to the area as one of suspected PDC deposition. Our estimation is more detailed than these previous results, especially for

the eastern part of Lombok, since we used around 1,330 measurement points and valid topography models.

In addition to differences in the spatial distribution of pumice-rich PDC deposits from the 1257 CE eruption, we also compared the volume of pumice-rich PDC deposits on eastern Lombok with the total volume of these deposits across all of Lombok, taken from previous research by Vidal et al. (2015), who arrived at this volume using fewer data (eight measurement points). As previously mentioned, we estimated the volume of pumice-rich PDC deposits at about 4.5 km^3 , which represents approximately 28% of the total volume of pumice-rich PDC deposits estimated by Vidal et al. in 2015 (16 km^3). Table 6 compares the volume of pumice-rich PDC deposits on eastern Lombok following the 1257 CE Samalas eruption with those following other eruptions with a VEI ≥ 6 . Although known as the most active volcano in the Cascade Range during the Holocene era (Global Volcanism Program, 2013), the eruption of Mount St. Helens in 1980 only had a VEI of 5, with the volume of pumice-rich PDC deposits is less than 1 km^3 (Lipman and Mullineaux, 1981; Sulpizio, 2005; Belousov, et al., 2007; Nathenson, 2017). Hence, it is not comparable to other eruptions listed in Table 6.

Vidal et al. (2015) estimated the total volume of pumice-rich PDC deposits based on three isopach values from eight measurement points in the southwest and southeast of Lombok and ten in the north of Lombok, as well as an assumption that there are two very distal fine ashes at Lake Logung in East Java and on the flanks of Merapi in Yogyakarta. However, the uncertainty applying to the total volume of pumice-rich PDC deposits from the 1257 CE eruption estimated by Vidal et al. (2015) is still significant. Our study's more recent and detailed dataset, therefore, provides better constraints, even if it is on the lower area, on the volume of pumice-rich PDC deposits compared to the previous one, especially with regard to the eastern part of Lombok.

Table 6. Comparison of the volume of pumice-rich PDC deposits on eastern Lombok with those of other eruptions with a VEI \geq 6.

| Volcano name | Eruption year | VEI | Volume (km ³) | References |
|-----------------------|---------------|-----|---------------------------|---|
| Pinatubo, Philippines | 1991 CE | 6 | 1.28 | Daag and Van Westen (1996) |
| Krakatoa, Indonesia | 1883 CE | 6 | 9 - 19 | Self and Rampino (1981); Sigurdsson et al. (1991); Mandeville et al. (1996); Yokoyama (2015) |
| Tambora, Indonesia | 1815 CE | 7 | ~18 | Kandlbauer and Sparks (2014) |
| Samalas, Indonesia | 1257 CE | 7 | 16 | Vidal et al. (2015) |

The landscape on the eastern part of Lombok still evolved until the present time. The exploitation of pumice from Samalas eruption started intensively since the early 1980's in this area. The pumices material has been exported mainly to Asia (China 59.4%, South Korea 20.1%, Vietnam 8.7%, and Thailand 3.2%) as building materials in the manufacture of concrete, and as an abrasive material (Badan Pusat Statistik, 2017) (Figure 55). The pumice extraction (Figure 56) which is widespread all over Lombok Island has accelerated the natural landscape evolution. As a result, their exploitation allows the extension of cultivated areas from under-exploited land to large rice fields (Figure 57). The pumice extraction also causes the pollution of the rivers, which then flows into the sea and leads to coral reef damage.



Figure 55. Exploitation of pumices material on the eastern part of Lombok (Courtesy: F. Lavigne, April 2016).



Figure 56. Pumice extraction in Ijobalit (Courtesy: F. Lavigne, using a MavicPro drone, August 2017).



Figure 57. Rice fields with the residue of pumice extraction as a background in a) Korleko and b) Ijobalit (Courtesy: b) F. Lavigne, July 2015).

The physical (mechanical) action of the strong waves sturdily erodes the 1257 CE volcanic and volcanoclastic deposits along the coast. The cliffs moved up to 2 km landward since the 1980's (Figure 58), due to the combination of strong waves and

human (illegal) destruction of the natural barrier (i.e., coral reef for lime production). The eroded material is then exported southward by the longshore currents in the Alas Strait. The Marine Geological Institute of Indonesia measured the velocity of the current in 2006. The results show that during springtime the velocity of the current at the water depth of 4 m is higher than 1.7 m/s during the first (15:00 - 17:00 PM) and second (2:00 - 6:00 AM) low water tides. The maximum velocity in the same location is about 2.59 m/s during the lowest tide and flowing towards the south.



Figure 58. Cliffs in Korleko nowadays which is eroded by the strong waves.

4.4. Conclusion

The pre- and post-1257 CE topographies were reconstructed using the kriging method, with the same grid size, based on more than 1,300 paleo-topographic points, consisting of 335 outcrops, 987 wells, eight core drillings, and five two-dimensional

resistivity profiles. The predicted pre-1257 CE topography is a valid model and has the smallest RMSE; it can, therefore, be concluded that the derived pre-1257 CE river system is relatively accurate. Nonetheless, our results only provide a model for landscape evolution pre- and post-1257 based on the hypothesis detailed above. Consequently, the pre-1257 CE river networks are still an estimation and may need to be validated by further research. Taking into account the present geomorphology of Lombok, we have identified two main geomorphological periods over the last millennium. The first is in the aftermath of the 1257 CE eruption of the Samalas volcano. During this period, volcanic material buried the pre-1257 CE river system, and rapid pumice-rich PDC deposition resulted in the aggradation of the shoreline at various points. There has been little erosion of the approximately $4,435 \times 10^6 \pm 5.5 \text{ m}^3$ of pumice-rich PDC deposits due to the fact that the 1257 CE eruption occurred during the dry season.

The second period consists of a long-lasting erosional period dominated by fluvial erosion. The valleys were at first filled with volcanic material, after which a new hydrographic network appeared that has continued to evolve to the present day. After a long erosional period of eight centuries, we estimate the volume of pumice-rich PDC deposits to be $625 \times 10^6 \pm 5.5 \text{ m}^3$ over a surface of 89 km^2 . Our study provides a more recent and detailed dataset for calculating the volume of pumice-rich PDC deposits than was used in previous research, especially with regard to the eastern part of Lombok. Further investigation will have to be carried out to assess the impact of the eruption on water resources and coral growth, as well as to analyze human impact – from sand mining in particular – on the landscape over the last half-century. Furthermore, a combination of the pre-1257 CE topography and archaeological information could be used to determine the location of the ancient capital of the Lombok Kingdom, Pamatan, which was buried by material from the 1257 CE eruption.

Chapter 5: Regional impacts of the 1257 CE eruption in West Sumbawa

This chapter presents the regional impacts of the 1257 CE eruption of Samalas in West Sumbawa. The relation between local written sources with the 1257 CE eruption processes, such as volcanic ash, PDCs, and lahars, is discussed in this chapter, as well as the long-term impacts of this event in West Sumbawa.

5.1. Evidence of volcanic deposits from the 1257 CE eruption of Samalas volcano along the west coast of Sumbawa

Based on previous research from Vidal et al. (2015), the P3 fallout deposits and the P4 PDC deposits were laid down all along the west part of Sumbawa, at least as far as 60 km from the former Samalas volcano (Figure 59). These materials are overtopped by the current soil and the material from Tambora eruption in 1815 CE. In Sumbawa, the fallout deposits of Samalas have 7-cm of thickness along the coast and display scattered pumice clasts which have 3-cm of diameter (outcrop RIN-1386 and RIN-1391 in Figure 59). Microlites existence in the pumice materials of RIN-1386 deposit is evidence that the P3 fallout deposits were extensively dispersal, not only in Lombok but also in Sumbawa Island.

Vidal et al. (2015) explained that following the deposition of PDCs, the prolonged coastal steam blasts, as well as numerous turbulent dilute PDCs, were produced due to the entrance of P4 PDC deposits into the sea. The dilute PDCs on the eastern part of Lombok Island were capable of crossing the Alas Strait and produced a thin deposit on the western coast of Sumbawa (outcrop RIN-1386 and RIN-1391 in Figure 59).

Dilute PDC deposits located far away from their source are somehow very challenging to interpret. Hence, it should be cross-checked with other evidence, e.g., observations in written sources.

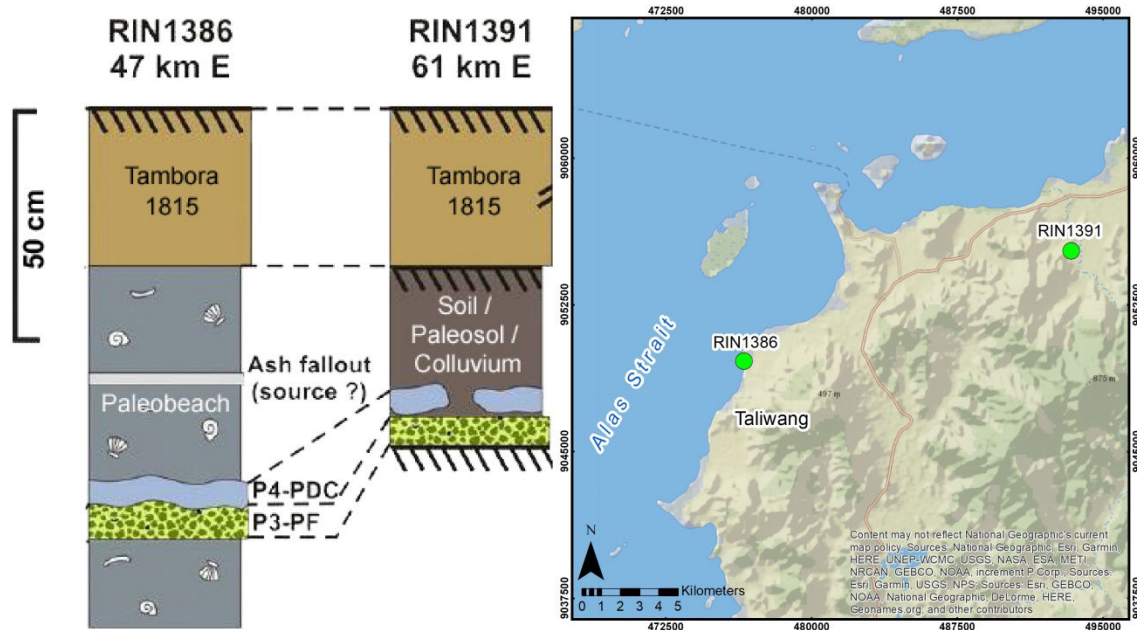


Figure 59. The P3 fallout deposits and the P4 PDC deposits were laid down all along the west part of Sumbawa (Source: Vidal et al., 2015).

5.2. Information from Babad Lombok and Babad Suwung

Here we present two written sources that undoubtedly refer to the 1257 CE ultraplinian eruption of Samalas volcano.

5.2.1. Babad Lombok

The recent translation of Babad Lombok describes the volcanic processes that were observed in 1257 CE (Lavigne et al., 2013). Based on the original text from the manuscript in old Javanese language and the English translation as well as field

observation and data, Lavigne et al. (2013) explained that there are at least four descriptions of eruption sequences of the Samalas eruption (Figure 60):

1. A catastrophic caldera-forming eruption of Mount Samalas, a volcano adjacent to Mount Rinjani (Lombok Island).
2. The Segara Anak caldera establishment with the 6×8.5-km-wide and 800-m-deep.
3. The horseshoe-shaped collapse structure that profoundly incises the western flank of Rinjani volcano.
4. Sequences of volcanic phenomena that have destroyed the fields and settlements nearby the volcano, as well as the Pamatan Kingdom, whereby, kill thousands of people.

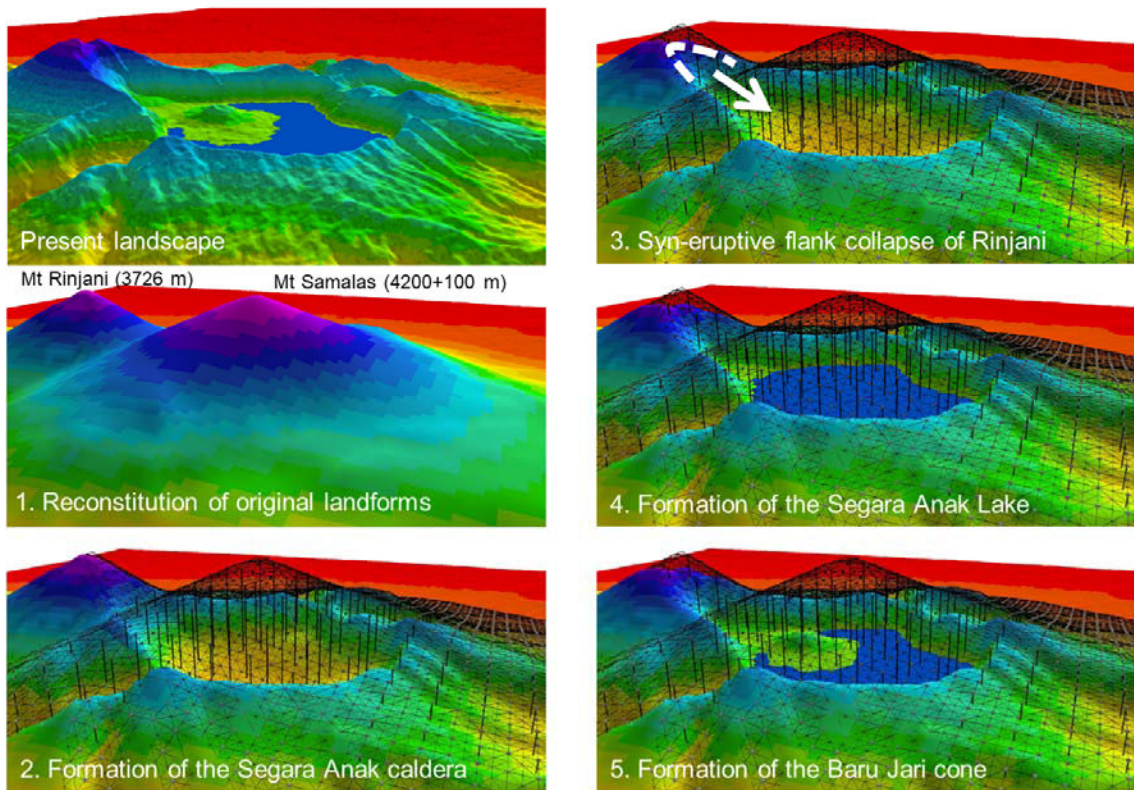


Figure 60. Reconstruction of original landforms in Rinjani Volcanic Complex based on the descriptions in Babad Lombok (Courtesy: P. Lahitte, 2015).

5.2.2. New relevant information from Babad Suwung

The recent translation of another forgotten Babad called Babad Suwung provides additional description of this eruption in the neighbor island of Sumbawa. The term "Suwung" is a word in old Javanese which means quiet and without life. It may refer by itself to the consequences of this dramatic eruption as also mentioned in Babad Lombok (Figure 61).

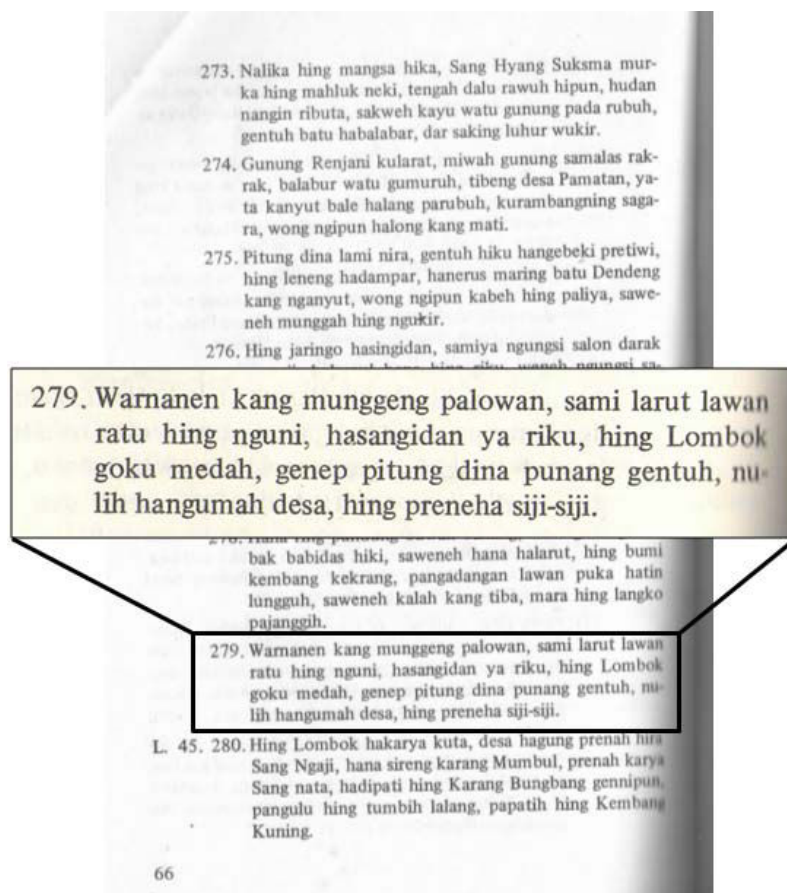


Figure 61. The description in Babad Lombok about the consequences of the 1257 CE eruption of Samalas volcano. The English translation of this text is: "The King and their peoples took refuge simultaneously; Lombok became very quiet, even seven days after the earthquakes happened, and afterward, they rebuilt their own homes" (Wacana, 1979; Lavigne et al., 2013).

Babad Suwung is not accessible to the local people who do not have access. This babad may be found only in the Museum of West Nusa Tenggara Province in Mataram, or in the Leiden library in the Netherlands. Also, they could not understand the texts, which is restricted and limited to a very few old people.

Babad Suwung explains that Talkuwang is the name of one of the children from Batara Indra and Dewi Sinta. As an emperor of the Selaparang Kingdom in Lombok Island, Batara Indra ordered Amaq Talkuwang to build a village in Sumbawa Island which was named Talkuwang and later renamed Taliwang. However, eventually, Taliwang villagers had to flee since the rain and fire from the sky, as well as the hot winds coming from the West and destroyed their village.

Here is the explanation of some sentences in Babad Suwung that relate to the 1257 CE Samalas eruption.

*“...hing Talkuwang, saking takdiring hyang Sukseme lantasturun
hudan geni haneng langit...”*

[Original text].

“...in Talkuwang, due to the destiny of the Almighty, rain and fire felt
on the ground...”

[English translation].

The description of rain and fire that felt on the ground is undoubtedly referred to the fallout deposits which reached Taliwang. Another text in Babad Suwung mentions that:

“...*geni angin hiku lintas binakur dese Takuwang...*”

[Original text].

“...and the hot wind burned everything in Talkuwang...”

[English translation].

The description of hot wind in Babad Suwung is unquestionably referring to hot dilute materials that traveled the Alas Strait between Lombok and Sumbawa Island and then deposited in Taliwang. This hot dilute material was also known as pyroclastic surge which is a low particle concentration and a strongly turbulent PDC. The eruption intensity combined with turbulence and low bulk density generates a high-velocity which allows transporting the PDCs across the Alas Strait. The PDCs remained hot even after crossing 16 km of the sea (Figure 62).

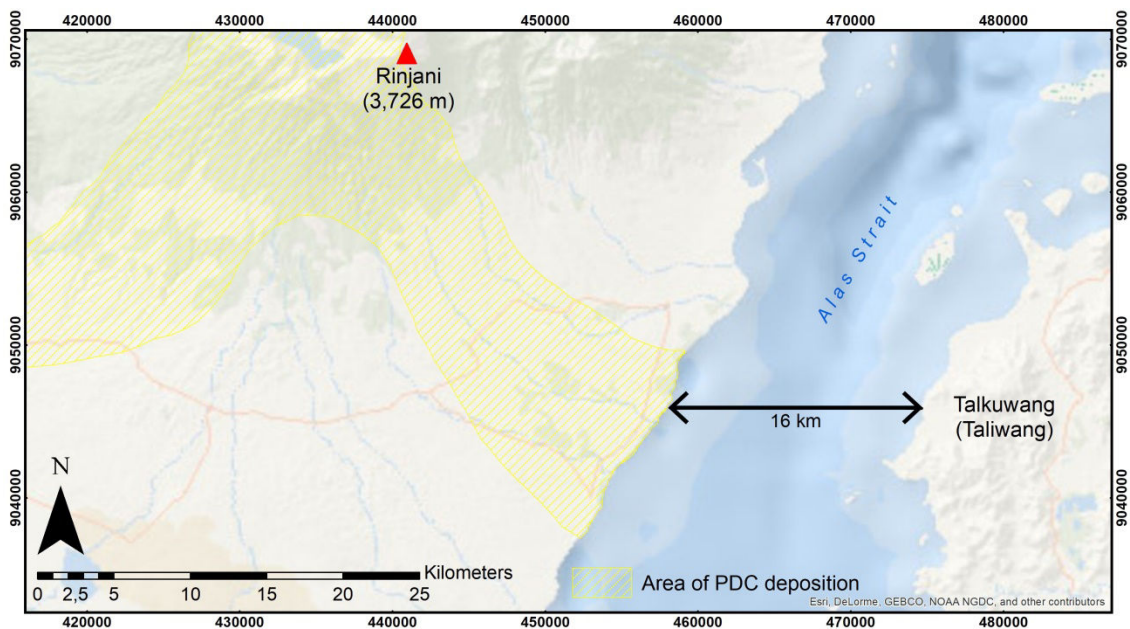


Figure 62. The PDCs remained hot even after crossing 16 km of the sea.

Another text in Babad Suwung mentions that:

*“...malik waktu sino iye laeq sopoq desa Taliwang dai Selaparang,
ndeq naraq laut lalangne...”*

[Original text].

*“...at that time, there is no sea between Taliwang dan Selaparang
villages...”*

[English translation] (Figure 63).

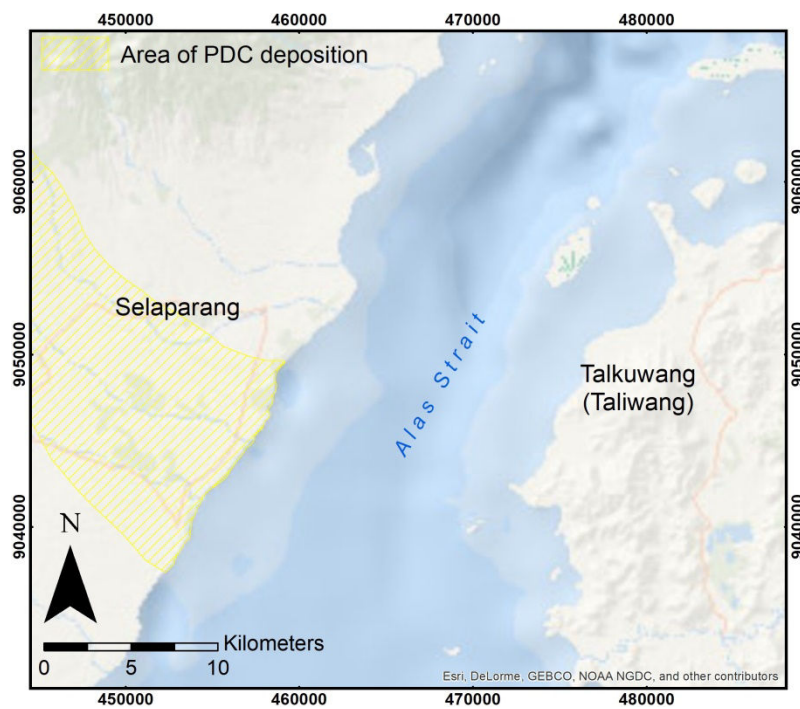


Figure 63. The sentence in Babad Suwung mentioned that there is no sea between Selaparang (Lombok Island) and Taliwang (Sumbawa Island).

This description undoubtedly refers to additional volcanic deposits in the sea from the littoral explosions with the formation of the co-ignimbrite clouds, pyroclastic flow

over water, and the pumices from PDCs. The interaction between pyroclastic materials from the volcanic eruption and the water at the ocean may result in the widespread volcanoclastic deposit in the nearshore (Cas and Wright, 1991; Freundt, 2003; Dufek et al., 2007). Furthermore, immense quantities of pumice that fall into the water may generate floating banks of pumice known as pumice rafts.

5.3. Discussion

5.3.1. Description of a volcanic eruption in written sources

The first written sources referring to volcanic eruptions appear in the Greek and Roman mythology. They relate to the God of fire Hephaistos or Vulcan. The eye of the Cyclops broken by Ulysses from which sprang blood in the *Odysseus* had been attributed to the visual observations of Stromboli eruptions by Greek sailors. Later on, the ca. 3200 BP Minoan eruption of Santorini (Thera) left the first reliable eyewitness accounts of a major explosive volcanic event.

However, should we consider the description of volcanic processes found in the Greek Hellenistic literature as credible evidence? What is the respective proportion of actual visual observations and myths and legends? We need to wait for the 79 CE eruptions of Vesuvius to get the first detailed and reliable description of Pyroclastic Density Currents by Pliny the Younger. His letters that have discovered in the 16th century describe his experience during the eruption while he was staying in his Uncle houses, Pliny the Elder (Allen, 1915; Maiuri, 1960; Radice, 1969).

The description in Babad Suwung that refers to the fallout deposits is also quite similar to the letters of Pliny the Younger related to volcanic fallout (Figure 64). The description in Babad Suwung and the letters of Pliny the Younger can relate to the

volcanic ash that may fall instantly from eruption columns. Furthermore, the last sentences in the letters of Pliny the Younger also relate to another description in Babad Suwung about additional volcanic deposits in the sea from the littoral explosions.

EPISTVLARVM VI. 16 71

nisi navibus fuga); ut se tanto discrimini eriperet, orabat. Vertit ille consilium et, quod studioso animo inchoaverat, obit 9 maximo. Deducit quadriremes, ascendit ipse non Rectinae modo, sed multis (erat enim frequens amoenitas orae) laturus auxilium. Properat illuc, unde alii fugiunt, rectumque cursum, 10 recta gubernacula in periculum tenet adeo solutus metu, ut omnes illius mali motus, omnes figuras, ut deprehenderat oculis, dictaret enotaretque. Iam navibus cinis incidebat, quo propius 11 accederent, calidior et densior, iam pumices etiam nigrique et ambusti et fracti igne lapides, iam vadum subitum ruinaque montis litora obstantia. Cunctatus paulum, an retro flecteret, mox gubernatori, ut ita faceret, monenti 'Fortes' inquit 'fortuna iuvat: Pomponianum pete.' Stabiis erat diremptus 12 sinu medio (nam sensim circumactis curvatisque litoribus mare infunditur); ibi quamquam nondum periculo adpropinquante, conspicuo tamen et, cum cresceret, proximo sarcinas contulerat in naves certus fugae, si contrarius ventus resedisset; quo tunc avunculus meus secundissimo invectus complectitur trepidantem, consolatur, hortatur, utque timorem eius sua securitate leniret, deferri in balineum iubet: lotus accubat, cenat aut hilaris aut, quod est aequae magnum, similis hilari. Interim 13 e Vesuvio monte pluribus locis latissimae flammae altaque incendia relucebant, quorum fulgor et claritas tenebris noctis excitabatur. Ille agrestium trepidatione ignes relictos desertasque villas per solitudinem ardere in remedium formidinis dictitabat. Tum se quieti dedit et quievit verissimo quidem somno. Nam meatus animae, qui illi propter amplitudinem corporis gravior et sonantior erat, ab iis, qui limini obversabantur, audiebatur.

Figure 64. The description in letters of Pliny related to the volcanic fallout following the 79 CE Vesuvius eruption (Source: Allen, 1915).

"...iam navibus cinis incidebat, quo propius accederent, calidior et densior; iam pumices etiam nigrique et ambusti et fracti igne lapides; iam vadum subitum ruinaque montis litora obstantia..."

[Original text].

"...The ashes were starting to fall on the boats, together with pumice-stones and black pieces of burning rock, which became thicker and hotter the nearer they approached the mountain. They were in danger due to the unexpected retreat of the sea, as well as the shores obstruction by the large fragments which moved down from the mountain..."

[English translation].

The description of hot wind in Babad Suwung is quite similar to the ones made by Pliny the Younger in 79 CE as an eyewitness during the Vesuvius eruption (Figure 65); as well as during the eruption of Krakatoa by the Dutch shippers in 1883 CE. They all refer to dilute PDCs or hot pyroclastic surges that crossed the sea.

"...ab altero latere nubes atra et horrenda ignei spiritus tortis vibratisque discursibus rupta in longas flammaram figuras dehiscebat: fulguribus illae et similes et maiores erant..."

[Vesuvius eruption - original text].

Profecto avunculo ipse reliquum tempus studiis (ideo enim 2
 remanseram) impendi; mox balineum, cena, somnus inquietus
 et brevis. Praecesserat per multos dies tremor terrae minus 3
 formidolosus, quia Campaniae solitus; illa vero nocte ita in-
 valuit, ut non moveri omnia, sed verti crederentur. Inrumpit 4
 cubiculum meum mater: surgebam invicem, si quiesceret,
 excitaturus. Resedimus in area domus, quae mare a tectis
 modico spatio dividebat. Dubito, constantiam vocare an im- 5
 prudentiam debeam (agebam enim duodevicensimum annum):
 posco librum Titi Livi et quasi per otium lego atque etiam, ut
 coeperam, excerpo. Ecce amicus avunculi, qui nuper ad eum
 ex Hispania venerat, ut me et matrem sedentes, me vero etiam
 legentem videt, illius patientiam, securitatem meam corripit.
 Nihilo segnius ego intentus in librum. Iam hora diei prima, 6
 et adhuc dubius et quasi languidus dies. Iam quassatis circum-
 iacentibus tectis, quamquam in aperto loco, angusto tamen,
 magnus et certus ruinae metus. Tum demum excedere oppido 7
 visum: sequitur vulgus attonitum, quodque in pavore simile
 prudentiae, alienum consilium suo praefert ingentique agmine
 abeuntes premit et impellit. Egressi tecta consistimus. Multa 8
 ibi miranda, multas formidines patimur. Nam vehicula, quae
 produci iusseramus, quamquam in planissimo campo, in con-
 trarias partes agebantur ac ne lapidibus quidem fulta in eodem
 vestigio quiescebant. Praeterea mare in se resorberi et tremore 9
 terrae quasi repelli videbamus. Certe processerat litus mul-
 taque animalia maris siccis harenis detinebat. Ab altero latere
 nubes atra et horrenda ignei spiritus tortis vibratisque discursibus
 rupta in longas flammaram figuras dehiscebat: fulguribus
 illae et similes et maiores erant. Tum vero idem ille ex Hi- 10
 spania amicus acrius et instantius 'Si frater' inquit 'tuus, tuus
 avunculus vivit, vult esse vos salvos; si periit, superstites voluit:
 proinde quid cessatis evadere?' Respondimus non commissuros
 nos, ut de salute illius incerti nostrae consuleremus. Non 11
 moratus ultra proripit se effusoque cursu periculo aufertur. Nec

Figure 65. The description in letters of Pliny related to the pyroclastic surge following the 79 CE Vesuvius eruption (Source: Allen, 1915).

"...a fearful black cloud which was rent by forked and quivering bursts
of flame and parted to reveal great tongues of fire, like flashes of
lightning magnified in size..."

[Vesuvius eruption - English translation].

*"...and a red fiery glare was visible in the sky above the burning
mountain..."*

[Krakatoa eruption - Simkin and Fiske, 1983].

There were two stages during the 79 CE Vesuvius eruption, i.e., the Plinian stage which generated pumice fallouts; and the "Peléan" stage that consists of six destructive pyroclastic surges and flows (Bradley, 2013). In his letter to Cornelius Tacitus, Pliny the Younger reported that he and his mother saw the sixth pyroclastic surges of Vesuvius eruption during the second stage at Misenum (Figure 66) which later sank down to the ground and reached the sea (Radice, 1969; Sigurdsson, 2009).

For comparison, with VEI of 6, the 1883 CE eruption of Krakatoa generated PDCs which also traveled over the sea and remained hot at distances of 65 km in Lampung Bay, Sumatra, so that caused burn fatalities on the southern coast of Sumatra (Carey et al., 1996). Field deposits of these pyroclastic surges as mentioned in Babad Suwung were described in Taliwang province up to 50 km from the vent (Vidal et al., 2015). These pyroclastic surges may categorize as the far-traveled pyroclastic surges, along with the pyroclastic surges of St. Helens in 1980 CE and Krakatoa in 1883 CE which reaches about 35 km and 80 km, respectively.



Figure 66. Pliny the Younger and his mother as the eyewitnesses of the sixth pyroclastic surges of Vesuvius eruption at Misenum.

During the Middle Age, references to visual observations of volcanic processes during explosive eruptions are insufficient. The Vikings described the major Eldgjá eruption in 934 CE, which led to a major disaster in Iceland (Stothers, 1998). Japan's first documented historical eruption was from Aso volcano in 553 CE, the year after Buddhism had entered the country from Korea in 552 CE (Bowring, 2005). There is documentation about more than 17 Japanese volcanoes that erupted during the Middle Age, including the largest historical eruption in 915 CE by Towada volcano, and valuable data on the activity of Mount Fuji dating from the 8th century onwards (Koyama, 2007).

Eyewitness accounts describe a wide range of volcanic processes; including caldera-forming, pumice fallout, pyroclastic flows, and lahars. Babad Suwung describes dilute PDCs traveling across the sea 40 km from the vent, 626 years before the 1883 CE eruption of Krakatoa on the same country. This historical account becomes the oldest observation of pyroclastic surges since those by Pliny the Younger in 79 CE.

Although there are several eruptions in the Lesser Sunda Islands during 1257 - 1815 CE (Table 7) (Global Volcanism Program, 2013), there is no documentation about the eruption near Taliwang in West Nusa Tenggara Province before the eruption of Tambora volcano in 1815 CE (Figure 67). The hot wind that mentioned in Babad Suwung cannot be produced from volcanic ashfall deposits. The hot dilute materials may be generated only from the pyroclastic surges; then the eruption source is more likely from Lombok Island since the other closest active volcano in Sumbawa, in this case, is Tambora Volcano, located far away from Taliwang. Hence the description in Babad Suwung mentioned above undoubtedly refers to the 1257 CE eruption of Samalas volcano in Lombok Island.

Table 7. List of volcanic eruption during 1257 – 1815 CE in the Lesser Sunda Islands.

| No. | Volcano Name | Year of Eruption (CE) | Location |
|-----|-----------------|-----------------------|----------------------|
| 1. | Samalas | 1257 | Lesser Sunda Islands |
| 2. | Gunungapi Wetar | 1512, 1699 | Lesser Sunda Islands |
| 3. | Sangeang Api | 1512, 1715 | Lesser Sunda Islands |
| 4. | Iya | 1671 | Lesser Sunda Islands |
| 5. | Paluweh | 1650 | Lesser Sunda Islands |
| 6. | Lewotolo | 1660 | Lesser Sunda Islands |
| 7. | Lewotobi | 1675 | Lesser Sunda Islands |
| 8. | Batur | 1804 | Lesser Sunda Islands |
| 9. | Agung | 1808 | Lesser Sunda Islands |
| 10. | Tambora | 1815 | Lesser Sunda Islands |

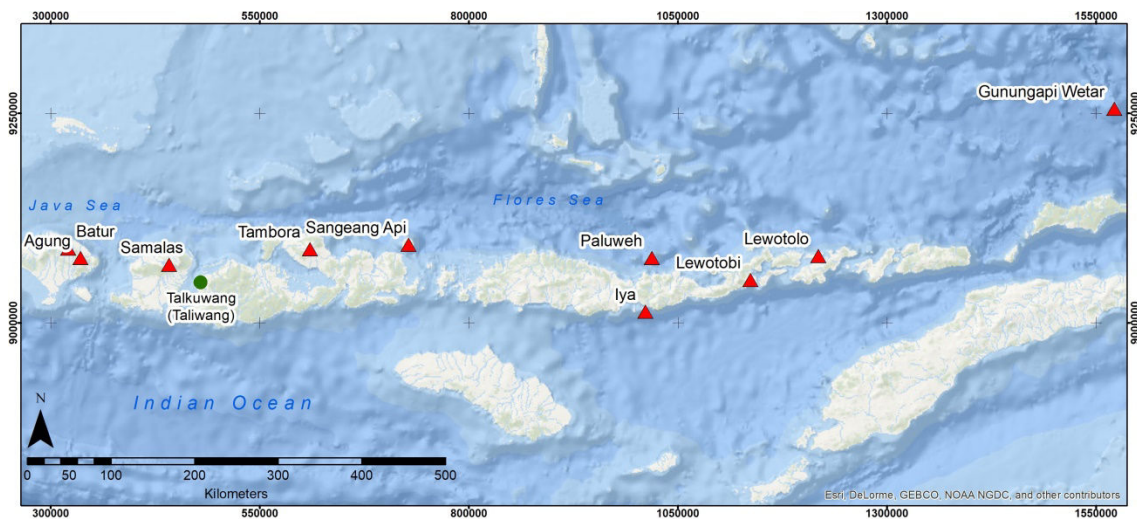


Figure 67. The eruption near Talkuwang during 1257 – 1815 CE.

5.3.2. Long-term impacts of the eruption on population and land use on the west coast of Sumbawa

Administratively, the west coast of Sumbawa is located in West Sumbawa Regency. Surprisingly the west coast of Sumbawa is very poorly populated. In 2016, the populations in West Sumbawa are about 137,072 peoples, which is only 2.8% of total populations in West Nusa Tenggara Province (Figure 68).

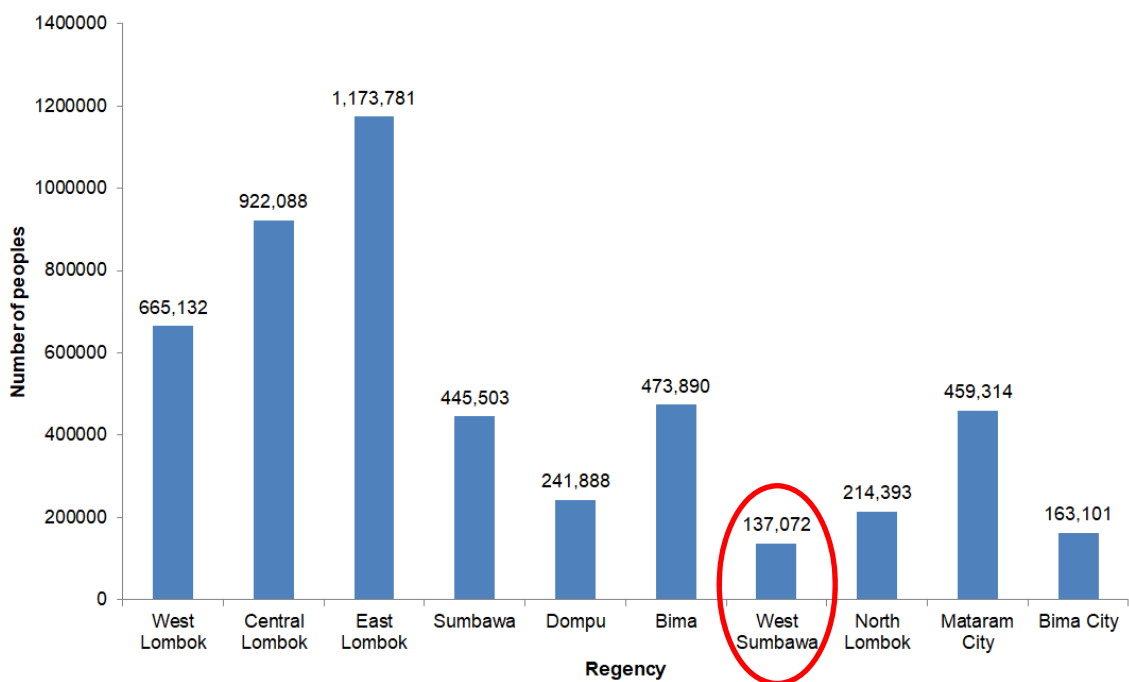


Figure 68. The number of peoples in West Nusa Tenggara Province. The populations in West Sumbawa are about 137,072 peoples, which is only 2.8% of total populations.

In 2015, the non-agricultural area (e.g., settlements and office complex) in West Sumbawa was only about 112.02 km² (6.1%), from the total area of 1,849.02 km². Almost 70% (1,291.4 km²) areas in West Sumbawa are still in the form of forest (Badan Pusat Statistik, 2016). Based on the interviews with the local people, they revealed that the lowlands on the west coast of Sumbawa, including Taliwang, are considered as a

“forbidden area”, i.e., a dangerous area. This situation can relate to the impact of Samalas eruption in Talkuwang as mentioned in Babad Suwung.

*“...sedanging negere telas melayu tebeng ngalas, hikulah asal dese
nare hingriku...”*

[Original text].

“...The people who are still alive have fled to the jungle that is not
exposed to fire rain and does not go back to Talkuwang...”

[English translation].

The 1257 CE eruption of Samalas volcano in Lombok forced local peoples in Taliwang at that time to evacuate to the forest and the mountain. The situation in 1257 CE was passed down by word of mouth for generations. Hence, they prefer to live in the higher lands, away from the coast. We conclude, based on interviews with local people, that oral tradition remains vivid in Sumbawa in the time range between 1257 and 2018, 761 years after the 1257 CE eruption of Samalas. Since the eruption, the eyewitnesses have transmitted their observations and experiences to their descendants. On the contrary, the 1257 CE eruption of Samalas has absent on the oral traditions of Lombok, where almost nobody was aware of the 1257 CE eruption until the massive media coverage of the Babad Lombok since the publication of Lavigne et al. in PNAS (2013).

This situation is easily understandable insofar as most of the people of Lombok did not survive the eruption, except a few eyewitnesses. As a result, the east coast of Lombok is much more densely populated than the west coast of Sumbawa, which

suffered from the two largest volcanic eruptions in history, i.e., Samalas in 1257 CE and Tambora in 1815 CE.

5.4. Conclusion

In conclusion, heretofore, the written sources of visual observations related to the volcanic processes during the eruptions, especially in Indonesia, are insufficient. Hence, we believed that the integrations between local written sources and previous research from several researchers could give a better understanding of the 1257 CE eruption of Samalas. Furthermore, the discovery of local written sources (i.e., Babad Lombok and Babad Suwung) and its explanation with the 1257 CE eruption of Samalas can make the Babad Lombok and Babad Suwung as the oldest observation of pyroclastic surges and volcanic fallout, following those by Pliny the Younger in 79 CE.

Chapter 6: Did the 1257 CE eruption of Samalas trigger a tsunami?

The main goal of this chapter is to answer the last scientific question in our study related to tsunami events following the 1257 CE eruption of Samalas volcano. Furthermore, this chapter also presents the results of our fieldwork on the west coast of Sumbawa since 2015. We collected and analyzed several samples of coral and seashell from tsunami deposits so that we can identify the tsunami sources and the occurrence period of these events. This information is helpful for understanding if there were any tsunamis triggered by the 1257 CE eruption of Samalas volcano or not since enormous amounts of volcanic materials from this eruption have reached the Alas Strait between Lombok and Sumbawa Island.

The west coast of Sumbawa is one of the best locations to look for tsunami deposits following the 1257 CE eruption of Samalas volcano. Large amounts of P4-PDCs from this eruption reached the Alas Strait, and as it is now, it formed 10 - 15 meters cliffs of non-welded deposits. As mentioned in Chapter 4 and 5, this massive pumice-rich PDC crossed the Alas Strait and deposited its pumice fragments on the western coast of Sumbawa, 50 km from the Samalas volcano (Vidal et al., 2015). Volcanic materials that entered the sea may have triggered tsunami events (Latief et al., 2000; Paris, 2012; Paris et al., 2013). Here we present our analysis of tsunami deposits in two locations along the western coast of Sumbawa, i.e., Belang Island and in abandoned fishponds in Kiantar Village (Figure 69).



Figure 69. Tsunami deposits in Belang Island and abandoned fishponds in Kiantar Village. a) As a small uninhabited island located in Gili Balu conservation area on the western coast of Sumbawa, this island dominated by mangrove ecosystems with several sandy areas; b) Sample collection location in abandoned fishponds in Kiantar Village; and c) Abandoned fishponds in Kiantar Village with the location of T4 and T5 sampling points as well as Alas Strait and Lombok Island on the west (left side).

6.1. Belang Island

We found a tsunami deposit in the one meter-thick natural outcrop located on the west part of Belang Island (see Figure 69). Belang Island is one of the small uninhabited islands in Gili Balu district, 5 km from the main harbor of Poto Tano on the western coast of Sumbawa. In this outcrop, the first layer is 15 cm-thick of dark brown volcanic ashes from the 1815 CE eruption of Tambora Volcano, located below the 15

cm-thick of topsoil. The layer below the volcanic ash is fine sand materials with the 50 cm-thick; contains well-rounded pumice with the diameter of 3-4 cm and numerous coral fragments. We collected two coral samples from this layer for further analyses. The last layer at the bottom is sand materials with neither pumice nor coral fragments presence. Figure 70 shows the stratigraphic profile of an outcrop in Belang Island.

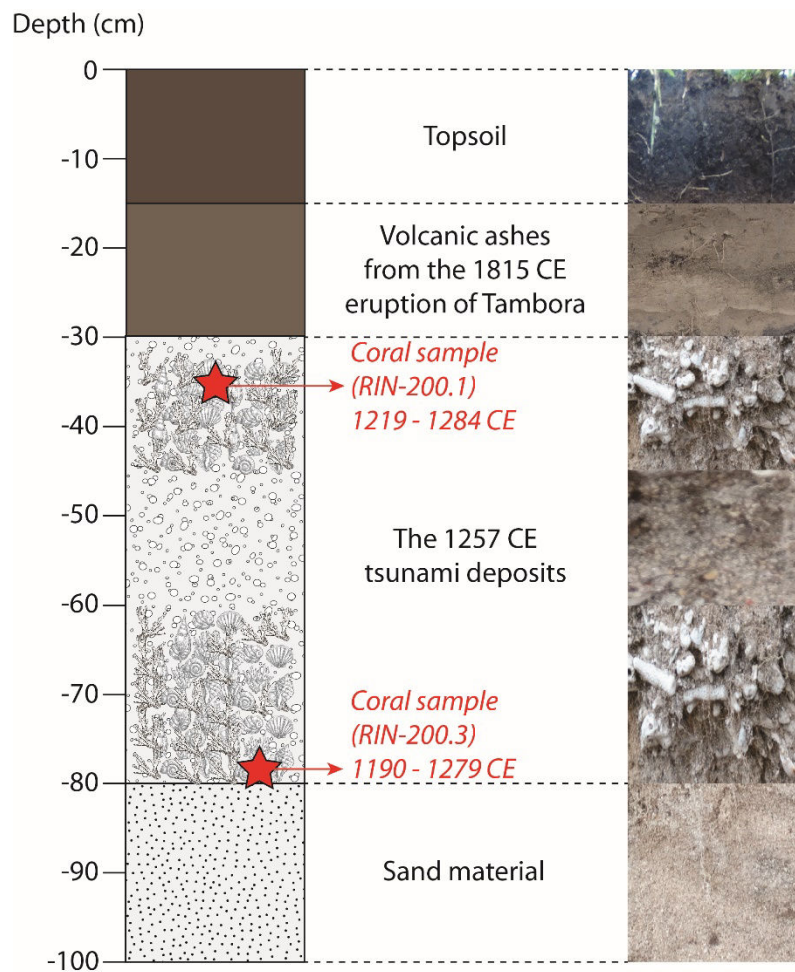


Figure 70. The stratigraphic profile of an outcrop in Belang Island.

We dated two samples of coral deposited in the 50 cm-thick of tsunami deposit in Belang Island in 2016 at Laboratoire de Mesure du Carbone 14 (LMC14) - CNRS France. These coral samples were located -35 cm (RIN-200.1) and -80 cm (RIN-200.3)

respectively from the surface. Table 8 and Figure 71 show radiocarbon dating results for coral samples in Belang Island.

Table 8. Radiocarbon dates for samples from Belang Island.

| Sample name | Date of analysis | Sample type | Uncal age BP | Cal. age CE |
|-------------|------------------|-------------|--------------|-------------|
| RIN-200.1 | 2 August 2016 | Coral | 760 ± 30 | 1219 – 1284 |
| RIN-200.3 | 2 August 2016 | Coral | 790 ± 30 | 1190 - 1279 |

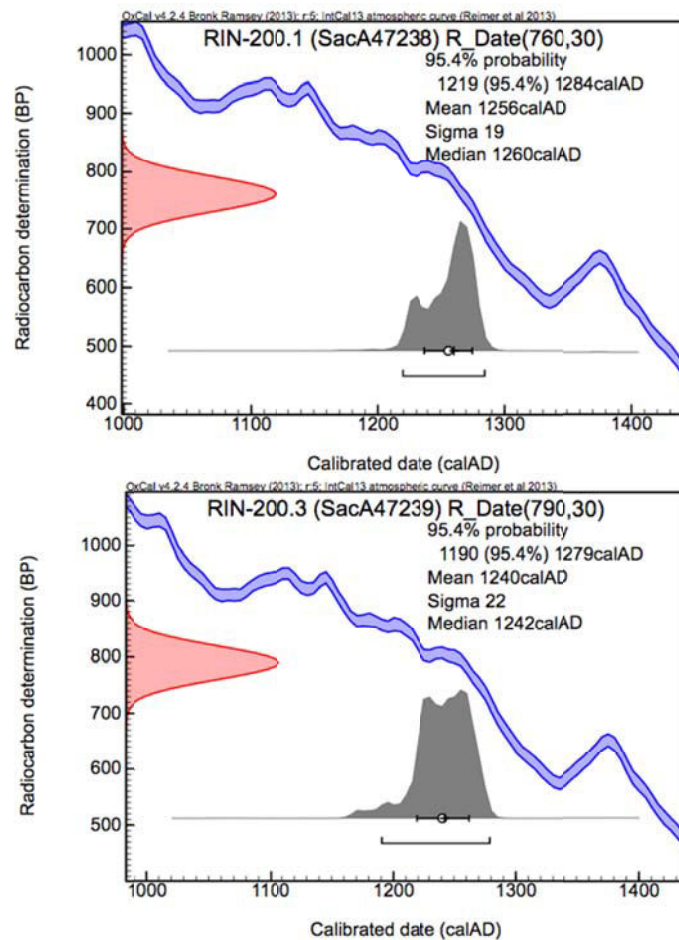


Figure 71. Calibration of radiocarbon age to calendar years for two coral samples in Belang Island. The result shows the 50 cm-thick of tsunami deposit in the island results from the 1257 CE eruption-induced tsunami.

6.2. Abandoned fishponds

We also found a tsunami deposit in abandoned fishponds in Kiantar Village. In the area of $3.3 \times 10^4 \text{ m}^2$, we analyzed five outcrops (i.e., T1-T5; see Figure 69), collected vertically contiguous sand samples from the location of T4, and collected ancient coral fragments and seashells from each outcrop. Their basic sedimentological characteristics which were analyzed are as follows:

- (i) On sampling point of T1, T2, and T3, an old massive tsunami deposit with a single ~1.5 m thick layer composed of a mixture of abundant big coral fragments, shells, sand and other 10 - 20 cm rounded boulders of unknown origin (probably of fluvial origin) (Figure 72);
- (ii) On sampling point of T4 and T5, additional thick tsunami deposits are composed of three different layers. Each of these layers, 0.5 m thick on average, consists on coral fragments mixed with boulders and capped by sand; and
- (iii) The uppermost geologic unit for all sampling points consists of 2 cm-thick of pumice originated from the 1257 CE eruption of Samalas; 0.2 m tephra fall originated from the 1815 CE eruption of Tambora and covered by topsoil. On the other side of the Alas Strait, tsunami deposits from this eruption were also identified in several sites in Lombok.

Figure 73 illustrates stratigraphic profiles for all sampling points in abandoned fishponds in Kiantar Village.

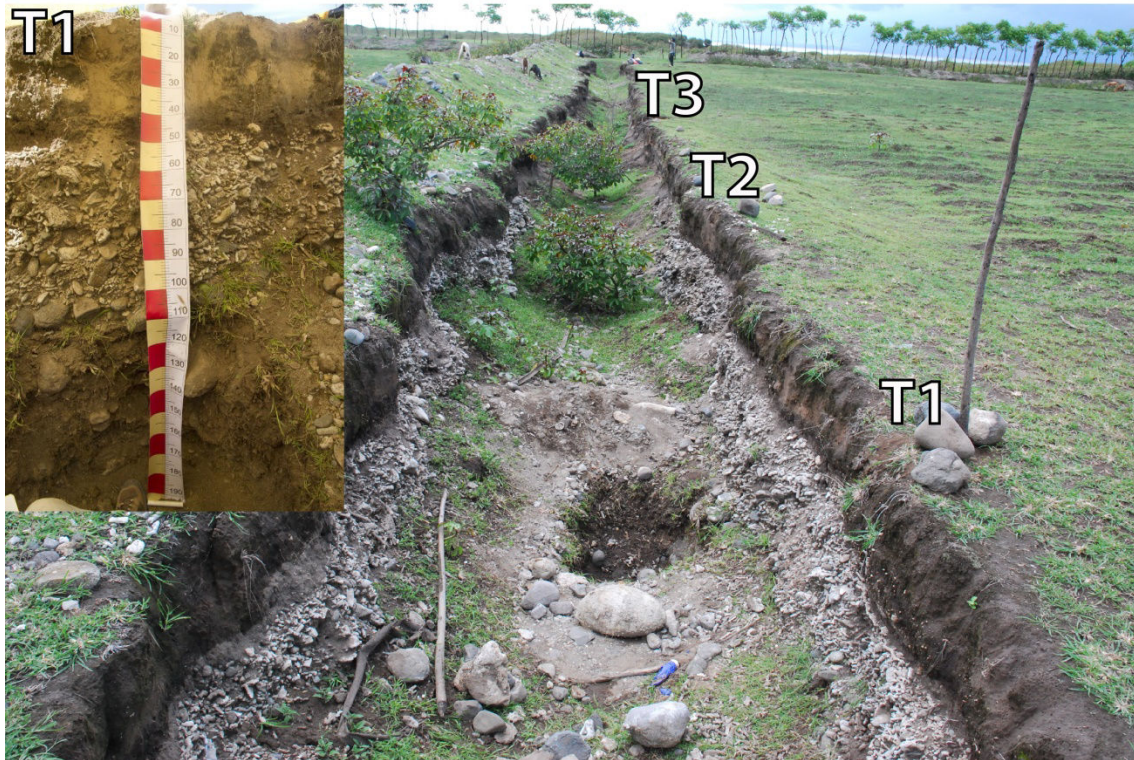


Figure 72. The location of T1, T2, and T3 sampling points in an abandoned fishpond in Kiantar Village with an example of an old massive tsunami deposit with a single ~1.5 m thick layer on sampling point of T1.

Grain size analysis is one of the main criteria to identify tsunami deposits (Goff et al., 2012) since it shows both the origin of sediments and the hydrodynamic conditions during sedimentation processes. Grain-size characteristics of tsunami deposits are commonly fining inland and upwards within the deposits (Moore et al., 2007; Goff et al., 2012; Dura et al., 2014) and poorly sorted (Grauert et al., 2001; Donato et al., 2009; Szczuciński et al., 2011). Grain-size analyses (Appendix 3) were performed for eight sediment samples collected on sample location T4 (Figure 74).

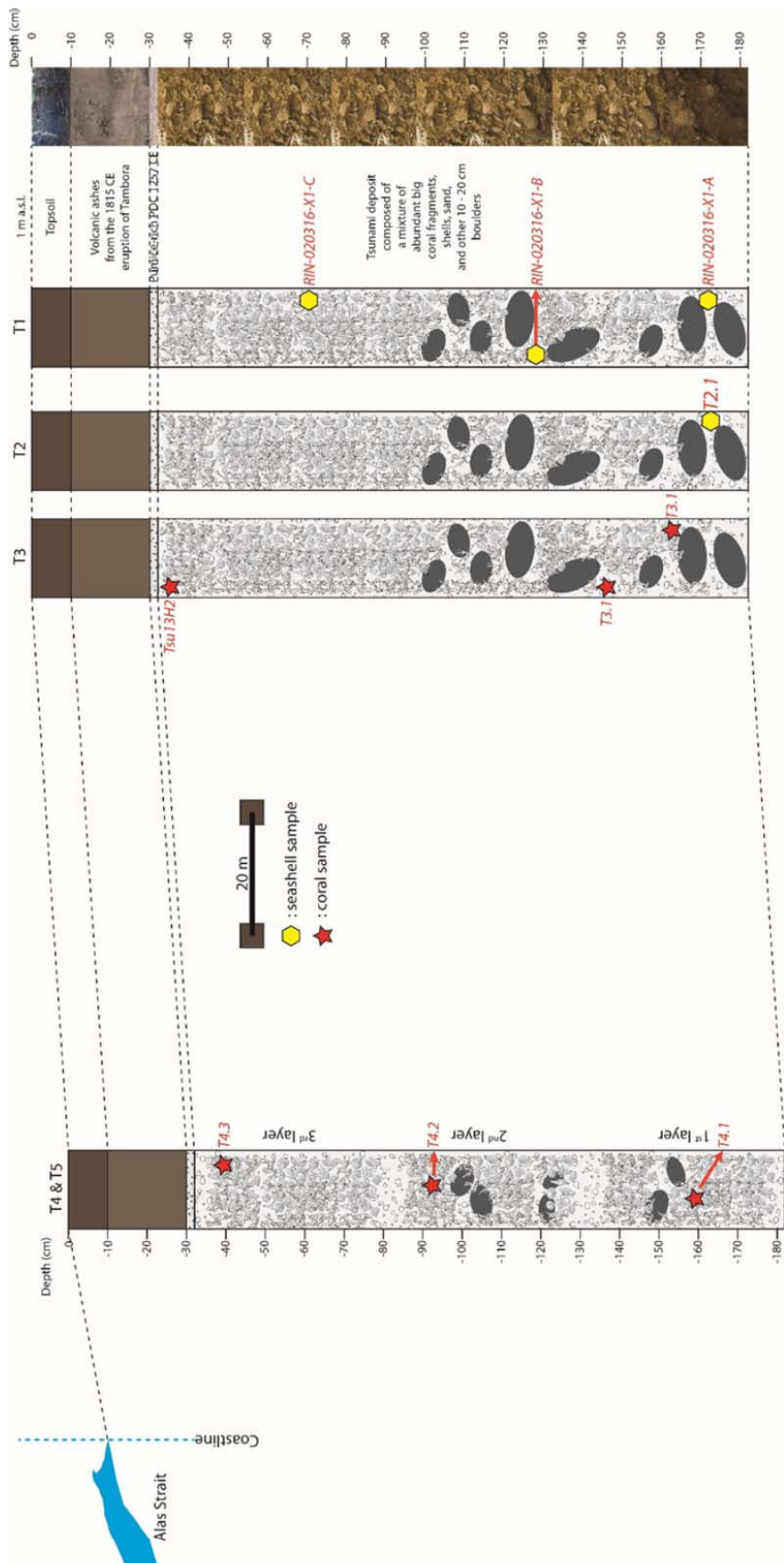


Figure 73. Stratigraphic profiles for all sampling points in abandoned fishponds in Kiantar Village.

The result presented in Table 9 show that deposits consist of medium sand to fine sand. The standard deviation of eight sediment layers ranges from σ_ϕ 0.91 to 2.40, which classified as interval σ_ϕ 0.71 to 4.00 (Folk and Ward, 1957), indicating the moderately sorted to very poorly sorted sediment layers (Folk and Ward, 1957; Blott and Pye, 2001), as usually discovered in debris flow (Major, 1997) and tsunami deposits (Kortekaas and Dawson, 2007). Skewness ranges from Sk_i -0.60 to -0.06 means that the sediment layers are generally composed of strongly coarse skewed to near symmetrical particles (Folk and Ward, 1957; Blott and Pye, 2001). Furthermore, the range of kurtosis (K_G 1.02 to 3.02) displays the curves between mesokurtic (K_G 0.90 to 1.11) and extremely leptokurtic ($K_G > 3.00$) (Folk and Ward, 1957; Blott and Pye, 2001). Figure 75 and Table 10 show the soil classification and triangle of textures from the sample collected from the T4 sampling point.

Table 9. Grain-size distribution for the sample collected from the T4 sampling point.

| Sample Name | Depth (cm) | Mean Grain-size | | Standard Deviation | Skewness | Kurtosis |
|-------------|---------------|-----------------|---------------|-----------------------|----------|----------|
| | | ϕ | μm | | | |
| KANG_T4_1 | -35 | 2.95 | 234.83 | 2.40 | -0.60 | 1.36 |
| KANG_T4_2 | -55 | 2.45 | 225.60 | 1.81 | -0.59 | 3.02 |
| KANG_T4_3 | -80 | 2.50 | 223.54 | 1.76 | -0.57 | 2.25 |
| KANG_T4_4 | -102 | 1.70 | 347.67 | 1.29 | -0.40 | 1.91 |
| KANG_T4_5 | -125 | 1.70 | 342.80 | 0.91 | -0.10 | 1.28 |
| KANG_T4_6 | -133 | 1.33 | 446.53 | 0.95 | -0.18 | 1.14 |
| KANG_T4_7 | -157 | 1.56 | 389.93 | 0.98 | -0.06 | 1.02 |
| KANG_T4_8 | -172 | 1.38 | 548.53 | 2.01 | -0.48 | 1.61 |

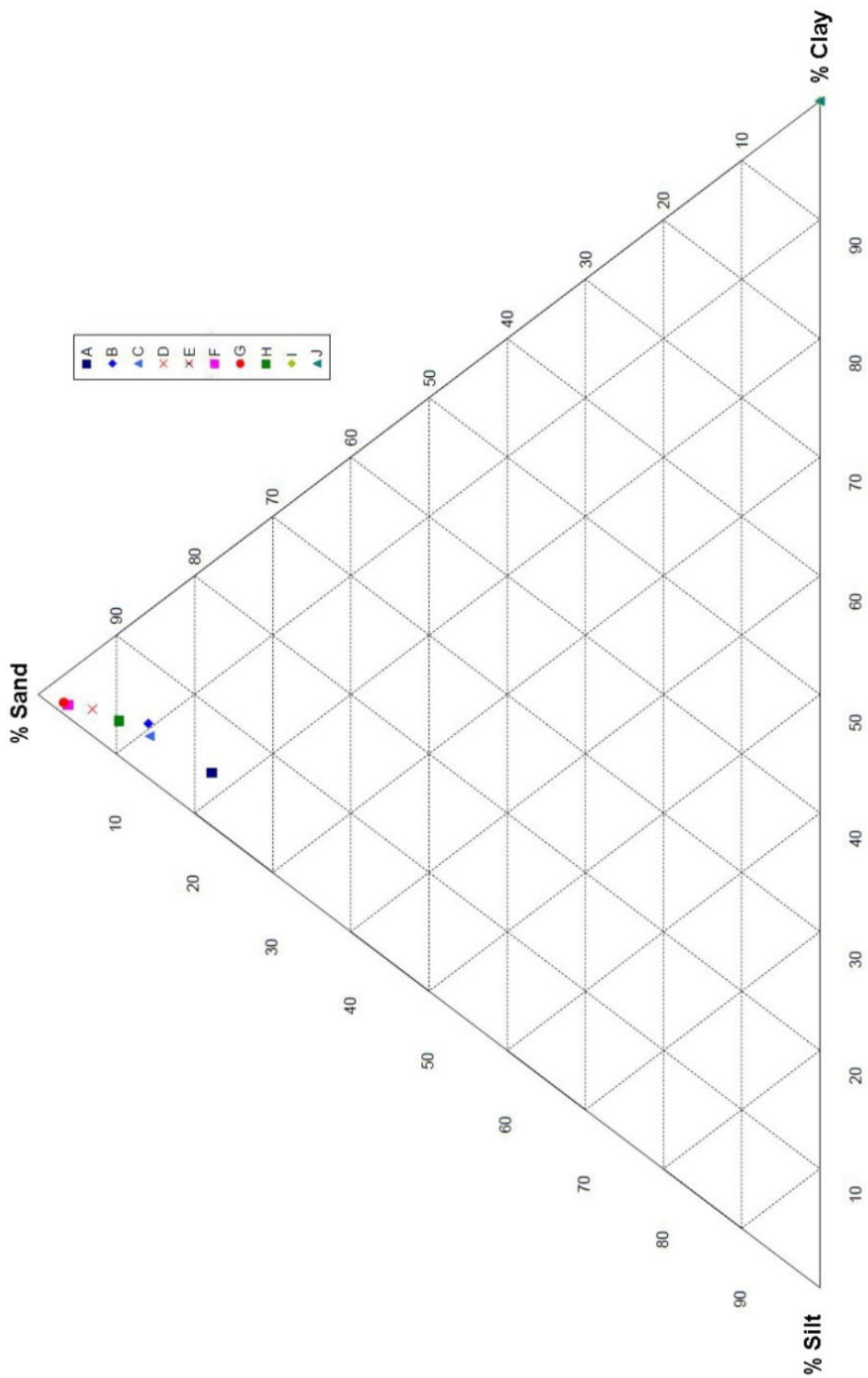


Figure 75. Triangle of textures from the sample collected from the T4 sampling point.

Table 10. Soil classification for the sample collected from the T4 sampling point.

| Sample Name | Sample Code | % Sand | % Silt | % Clay | Soil classification | | | |
|-------------|-------------|--------|--------|--------|---------------------|------------|------------|------------|
| | | | | | CDA | USDA | SSEW | INTL |
| KANG_T4_1 | A | 77.80 | 17.71 | 4.49 | Loamy sand | Loamy sand | Loamy sand | Loamy sand |
| KANG_T4_2 | B | 85.90 | 9.50 | 4.60 | Loamy sand | Loamy sand | Loamy sand | Loamy sand |
| KANG_T4_3 | C | 85.73 | 10.65 | 3.62 | Loamy sand | Loamy sand | Loamy sand | Loamy sand |
| KANG_T4_4 | D | 93.06 | 4.71 | 2.23 | Sand | Sand | Sand | Sand |
| KANG_T4_5 | E | 96.32 | 2.75 | 0.93 | Sand | Sand | Sand | Sand |
| KANG_T4_6 | F | 96.16 | 2.78 | 1.07 | Sand | Sand | Sand | Sand |
| KANG_T4_7 | G | 96.73 | 2.32 | 0.95 | Sand | Sand | Sand | Sand |
| KANG_T4_8 | H | 89.64 | 7.41 | 2.95 | Sand | Sand | Sand | Loamy sand |

Note :

- CDA : Canadian Department of Agriculture.
- USDA : U.S. Department of Agriculture.
- SSEW : Soil Survey for England and Wales.
- INTL : International Soil Association.

We dated six samples of coral and four samples of seashell obtained in abandoned fishponds during fieldworks in Kiantar Village in the time range between 2016 and 2018 (see Figure 73) with details are as follows:

- (i) Three samples of seashell (RIN-020316-X1-A, RIN-020316-X1-B, and RIN-020316-X1-C) were collected in February 2016 and analyzed at Laboratoire de Mesure du Carbone 14 (LMC14) - CNRS France in the same year;
- (ii) Four samples of coral (T3.1, T4.1, T4.2, and T4.3) were collected in February 2017 and analyzed at Beta Analytic Radiocarbon Dating, the United States in 2017;
- (iii) Two samples of coral (T3.1 and Tsu13H2) and one sample of seashell (T2.1) were collected in February 2017 and February 2018 and analyzed at DirectAMS, the United States in 2017 and 2018.

In 2016, we started taking coral fragments randomly from the tsunami deposit since we assumed that all deposits in abandoned fishponds were deposited due to the tsunami following the 1257 CE eruption. Radiocarbon dating results for 2016 samples have no significant results since it shows very old material. Therefore, we changed the sampling protocol with the very fresh red coral fragments to obtained better results. Table 11, Figure 76, and Figure 77 show radiocarbon dating results for coral and seashell samples in Kiantar Village.

Table 11. Radiocarbon dates for samples from abandoned fishponds in Kiantar Village.

| Sample name | Date of analysis | Sample type | Uncal age BP | Cal. Age BCE/CE |
|-----------------|------------------|-------------|--------------|-----------------|
| RIN-020316-X1-A | 08/2016 | Seashell | 2375 ± 30 | 541 – 390 BCE |
| RIN-020316-X1-B | 08/2016 | Seashell | 2145 ± 30 | 232 – 89 BCE |
| RIN-020316-X1-C | 08/2016 | Seashell | 2250 ± 30 | 321 – 206 BCE |
| T3.1 | 10/2017 | Coral | 2050 ± 30 | 278 – 508 CE |
| T4.1 | 10/2017 | Coral | 1520 ± 30 | 840 – 1030 CE |
| T4.2 | 10/2017 | Coral | 1540 ± 30 | 815 – 1015 CE |
| T4.3 | 10/2017 | Coral | 1560 ± 30 | 790 – 995 CE |
| T2.1 | 12/2017 | Seashell | 2137 ± 34 | 213 – 53 BCE |
| T3.1 | 12/2017 | Coral | 2169 ± 40 | 364 – 105 BCE |
| Tsu13H2 | 03/2018 | Coral | 1740 ± 28 | 239 – 382 CE |

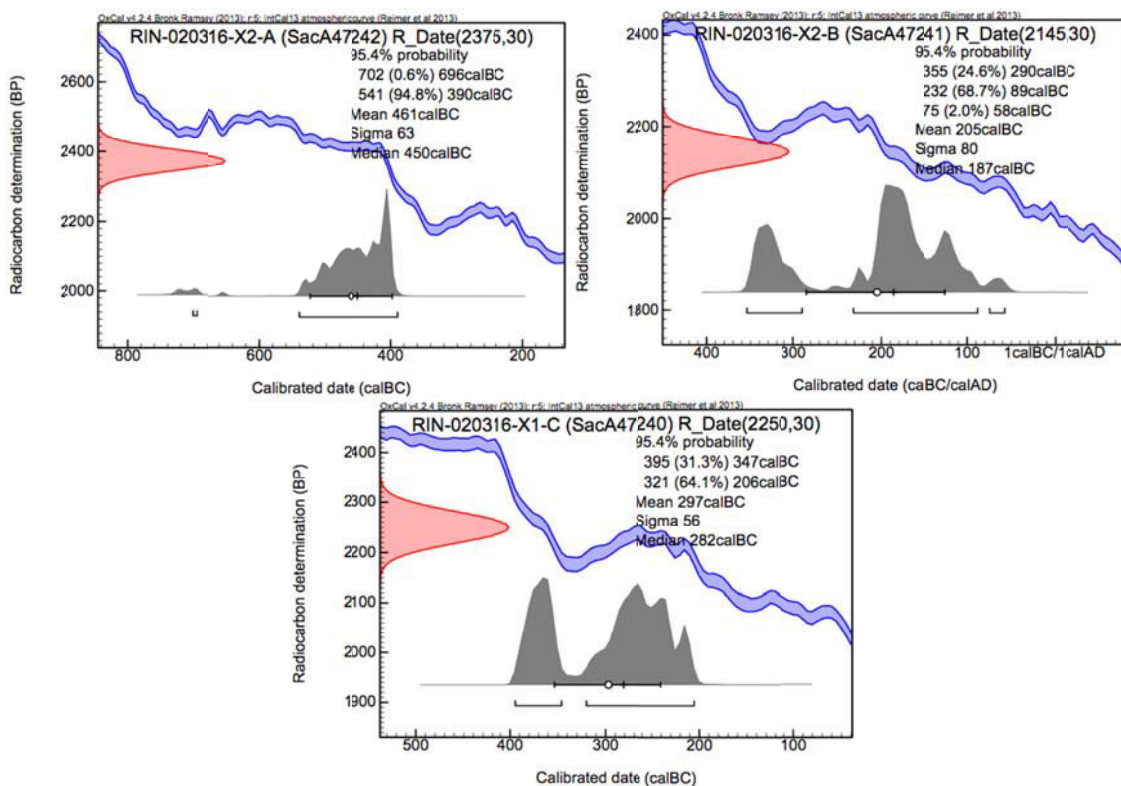


Figure 76. Calibration of radiocarbon age to calendar years for three samples of seashell (RIN-020316-X1-A, RIN-020316-X1-B, and RIN-020316-X1-C).

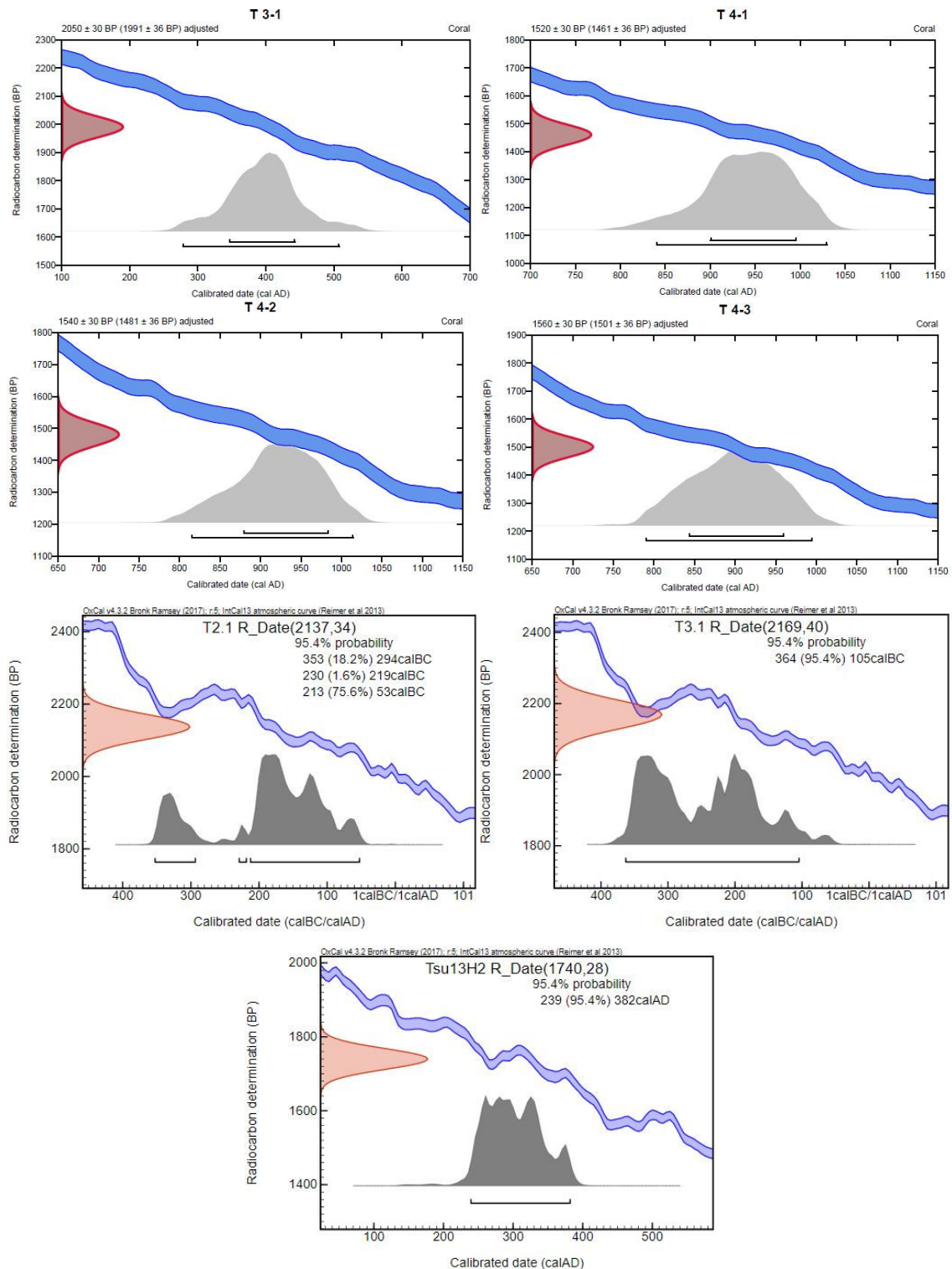


Figure 77. Calibration of radiocarbon age to calendar years with the high probability density range method (HPD - SHCAL13) for sample T3.1, T4.1, T4.2, and T4.3; and with calibration curve IntCal 13 in OxCal 4.3 program (Ramsey, 2009) for sample T2.1, T3.1, and Tsu13H2.

were found in the middle of the Belang Island. Furthermore, we used a tsunami model following the 1257 CE eruption in Alas Strait by C. Gomez from Kobe University, Japan (Figure 79) to confirm our hypotheses related to the tsunami along the western coast of Sumbawa.

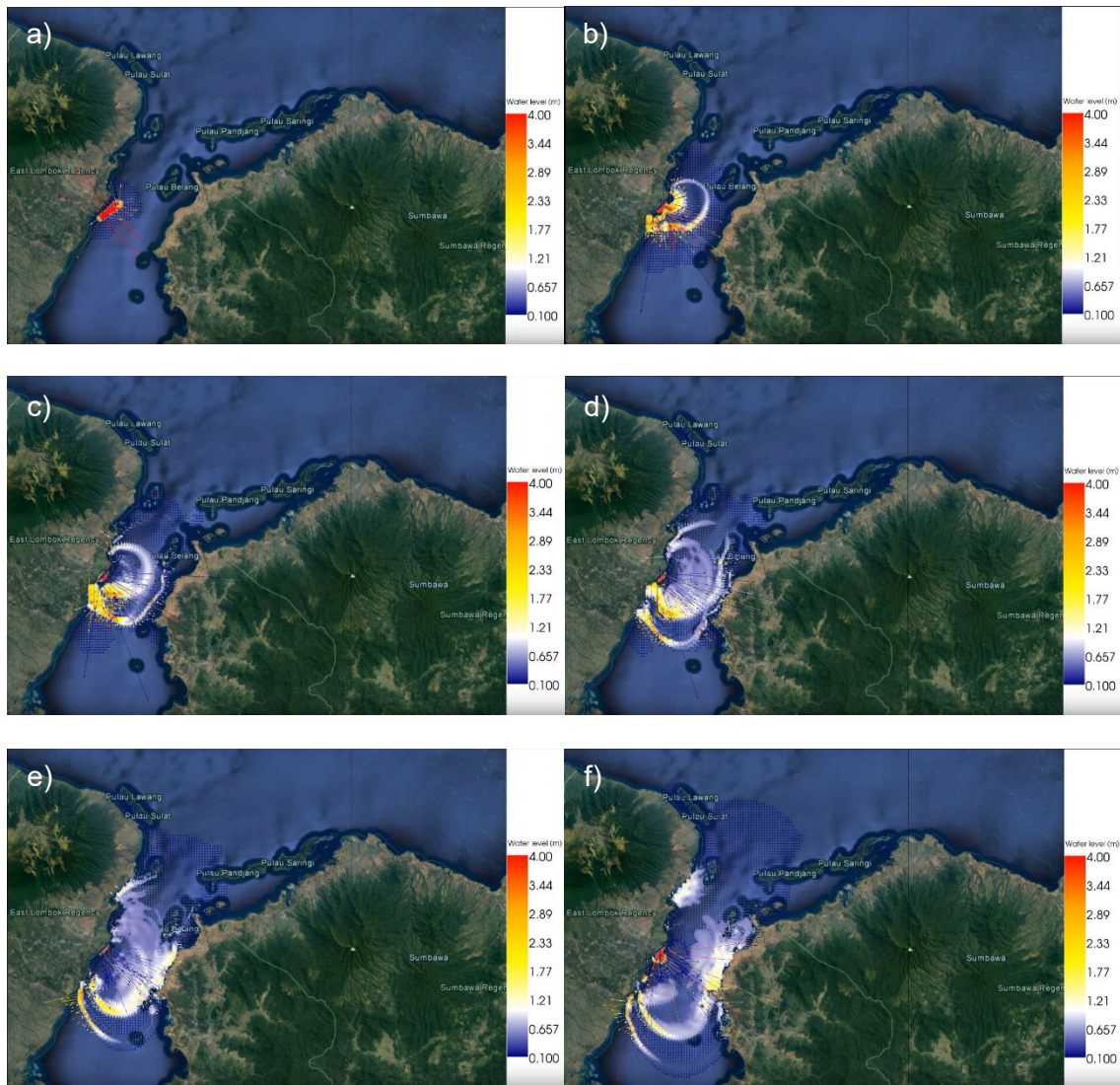


Figure 79. Tsunami simulation in the Alas Strait by C. Gomez from Kobe University.

This simulation has built using Cornell Multi-grid Coupled Tsunami Model (COMCOT), a tsunami modeling package able to simulate the tsunami processes in

coastal areas (Liu et al., 1998). COMCOT has been widely used to analyze numerous tsunami events since the last 20 years, such as the 1992 CE tsunami in Flores Islands, Indonesia (Liu et al., 1994, 1995), the 2003 CE tsunami in Algeria (Wang and Liu, 2005), the 2004 CE Indian Ocean tsunami (Wang and Liu, 2006, 2007), and the 1755 CE tsunami in Morocco coast (Ramalho et al., 2018).

Based on this model, the tsunami that occurred following the 1257 CE eruption hit Belang Island with approximately 1-meter run-up and then affected the western coast of Sumbawa in Kiantar Village with less than 1-meter run-up. Several factors, such as bathymetry, tsunami source velocity, and coral barrier presence, may cause this situation. The tsunami source: PDCs (or lahars) that triggered the small tsunami in 1257 CE already had a limited velocity when reaching the Alas Strait, about 30 km away from the Samalas crater. In addition, the nature of the PDC deposits (very light pumice fragments) certainly did not provide sufficient strength to push the seawater efficiently. Furthermore, coral reefs along the Alas Strait serve as an effective barrier against tsunamis and can reduce its impact on the coastal area (Marris, 2005; Fernando et al., 2005; Kunkel et al., 2006; Baba et al., 2008).

There are presently no living coral reefs near the coast on the eastern part of Lombok (Figure 80). We conclude that pre-1257 CE coral reefs, especially near Selong, are buried by volcanic materials since the participatory stratigraphy results show that there are dead corals and white sands below pumices on several wells near the coast. Furthermore, the regular input of acid pumice material transported in suspension by the main rivers in this area affects coral reefs presence since then. Contrarily, coral reefs on the western coast of Sumbawa are in good condition, and we assumed that the pre-1257 CE coral reef in this area was also in good condition since, as mentioned in the Babad Suwung, there was no human civilization until Amaq

Talkuwang arrived in this area. Therefore, anthropogenic pressures that cause coral bleaching or direct destruction does not exist in this area. Coral reef as a barrier within two meters of the surface and located at least a few hundred meters separated from the main island can perform a significant role in reducing tsunami effect (Gabrie and Salvat, 1985; Paulay, 1997; Kunkel et al., 2006). Figure 81 shows the general landscape on the western coast of Sumbawa, especially in Kiantar Village, that plays an essential role in reducing the impact of tsunami events.

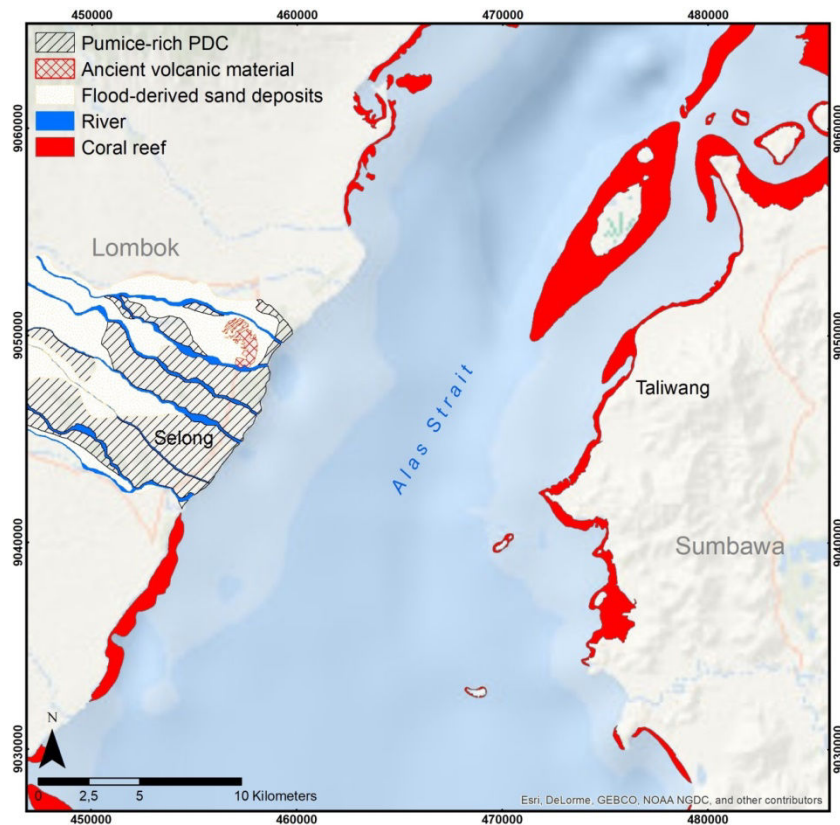


Figure 80. Spatial distribution of coral reefs along the Alas Strait in the present-day. Although the present-day condition of coral reef on the eastern part of Lombok and the western part of Sumbawa is very different, we assumed that before the eruption of Samalas volcano in 1257 CE, coral reefs in this area were in good conditions. This condition has maybe resulted in the absence of tsunami deposits from the 1257 CE eruption in this area.

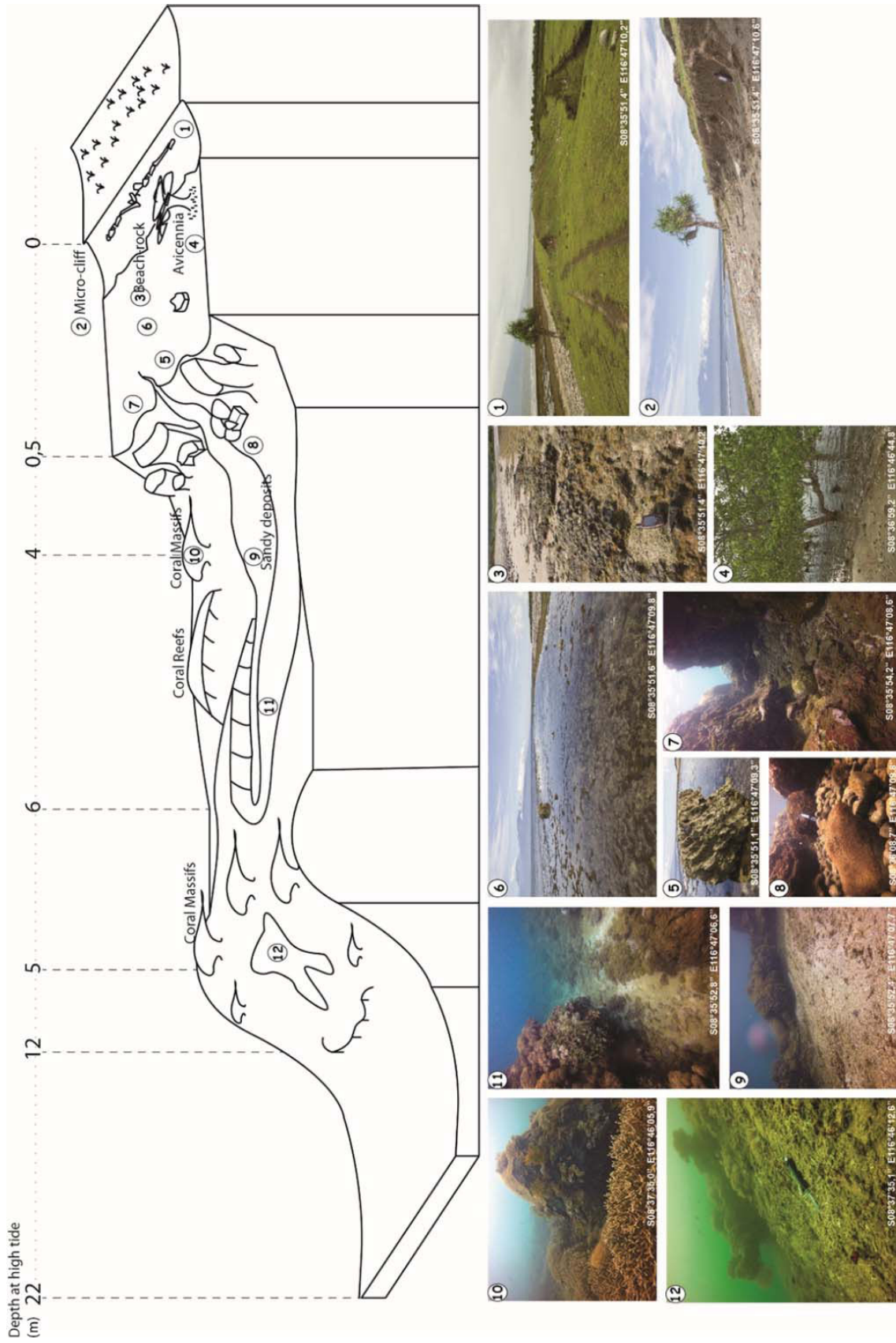


Figure 81. General landscapes on the western coast of Sumbawa (Courtesy: A. Landa, 2016).

Based on radiocarbon dating results, we conclude that at least three tsunamis occurred in historical time along the western coast of Sumbawa, dated on 4th century CE and 9th century CE, located in abandoned fishponds in Kiantar Village; and dated on 13th century CE, located in Belang Island. Tsunami deposits in abandoned fishponds are interpreted as sediments deposited by earthquake-triggered tsunamis since there were no volcanic eruptions occurred in the area at that time (Takada et al., 2003; Nasution et al., 2004).

6.4. Conclusion

Grain-size information on the tsunami deposits is the important factor for tsunami identification since most of the paleo tsunami studies use grain-size in the analysis. Deposits that found on the western coast of Sumbawa have common characteristics of tsunami deposits such as fining upwards within the deposits as well as poorly sorted sediments. Another common characteristic is fining inland deposits, however, there was no information related to inland sediment since we cannot find other deposits than in abandoned fishponds.

Until now, three tsunamis has strike the western coast of Sumbawa, dated on 4th century CE, 9th century CE, and 13th century CE. One tsunami is categorized as a volcanic eruption-induced tsunami, i.e., the tsunami in the 13th century CE following the 1257 CE eruption of Samalas volcano. We conclude that others tsunamis are earthquake-triggered tsunamis since there were no volcanic eruptions occurred in the area at that time. Although the 1257 CE eruption of Samalas volcano generated more than 4 km³ of volcanic materials, the material that reached the sea only triggers a minor tsunami along the western coast of Sumbawa Island due to many factors, such as

bathymetry, tsunami source velocity, type of tsunami source material, as well as coral reefs presence in that area.

Furthermore, further in-depth studies related to paleo earthquake-triggered tsunamis are needed since 1) there were no studies yet about these events, 2) it is very important for current earthquake context where people dread with the tsunami, and 3) it also can provide detailed information on paleo tsunami events along the western coast of Sumbawa. This information is handy to disaster risk reduction in Sumbawa as well as Lombok Island in the future.

Conclusion

For the last 800 years, volcanic materials from one of the world's greatest and most powerful eruptions during the Holocene era, namely the 1257 CE eruption of Samalas volcano, have contributed towards the excellent preservation of the paleo topography especially on the eastern part of Lombok. However, the geomorphological impact of this eruption remains unknown. Through several detailed field measurement accompanied by a laboratory and computational analysis, this thesis proposed to take into account the combination of stratigraphic information, DEM, geophysical measurement, spatial analysis in GIS, local written sources analysis, and radiocarbon dating, in order to better understand the geomorphic impacts of the 1257 CE eruption of Samalas volcano along the Alas Strait in West Nusa Tenggara, Indonesia.

The first objective of this study was to precisely reconstruct the landscape evolution of Lombok Island since the early 13th century, i.e., before, during, and after the 1257 CE eruption of Samalas volcano. In this study, we were capable of obtaining a valid model of pre- and post-1257 CE topographies through reconstruction of more than 1,300 paleo-topographic points using the kriging interpolation method. There are four phases related to the landscape evolution on the eastern part of Lombok, namely:

- (i) Before the 1257 CE eruption; the pre-1257 CE material on the eastern part of Lombok is made up of alternating layers of calcareous breccia and lava dating from the end of the Pliocene to mid-Pleistocene; with two hilly landscapes bordered this area in the northern and southern part.
- (ii) In the aftermath of the 1257 CE eruption; pumice-rich PDCs covered the eastern part of Lombok in the aftermath of the 1257 CE eruption. Pre-eruptive valleys were

filled with the newly deposited volcanic material as it followed the contours of the pre-eruption topography.

- (iii) After erosion of pumice-rich PDC deposits; a new hydrographic network appeared fairly quickly with broad main valleys mostly located where the original pre-1257 valleys were, and new shorter tributaries located where pumice-rich PDC deposits were found. The deposited volcanic material has been progressively eroded following intense rainfall events by mountain streams carrying sand, pebbles, and pumices.
- (iv) Present-day; the pumice extraction which is widespread all over Lombok Island has accelerated the natural landscape evolution, such as the extension of cultivated areas from under-exploited land to large rice fields, the pollution of the rivers, and coral reef damage.

The study results show that the landscape on the eastern part of Lombok is still evolved until the present time. It can be shown by the volume of volcanic material from the 1257 CE Samalas eruption that still remains about 14% (i.e., $625 \times 10^6 \pm 5.5 \text{ m}^3$) from the initial volume (i.e., $4,435 \times 10^6 \pm 5.5 \text{ m}^3$), even though there were numerous erosion processes happened in the time range between 1257 and 2018.

The second objective was to find and analyze local written sources related to the 1257 CE eruption of Samalas volcano, as well as its impacts on Lombok and surrounding islands. Local written sources in Indonesia have proven to be able to provide detailed information related to historical events, including volcanic activities. For example, volcanic processes of Samalas volcano in 1257 CE are well described in the Babad Lombok as mentioned in Lavigne et al. (2013). In this study, discovery and recent translation of another forgotten local source called Babad Suwung, provide additional description of Samalas eruption in the neighbor island of Lombok, namely Sumbawa Island. Furthermore, we believed that the description of volcanic processes

during the 1257 CE eruption of Samalas volcano in Babad Lombok and Babad Suwung might become the oldest visual observation of pyroclastic surges and volcanic fallout, following those by Pliny the Younger in 79 CE.

The third objective was to investigate whether a tsunami had been triggered by the 1257 CE eruption of Samalas volcano. Besides the tsunami following the 1883 CE eruption of Krakatoa volcano, in general, volcanic eruption-induced tsunamis in Indonesia are not well-studied yet, neither their causes nor their consequences. Nevertheless, we were able to find two tsunami deposits along the west coast of Sumbawa, i.e., in Belang Island and abandoned fishponds in Kiantar Village. Based on radiocarbon dating results on coral and seashell samples, the 1257 CE eruption of Samalas volcano had triggered a minor tsunami that hit Belang Island. Another tsunami deposits located in abandoned fishponds dated 4th century CE and 9th century CE. We conclude that a big earthquake triggered these tsunamis since no volcanic eruption occurred near the Alas Strait at that time that may trigger a tsunami.

This study provides new information related to the geomorphic impact of a major eruption volcanic in coastal areas, in this case, on the eastern part of Lombok as well as on the western coast of Sumbawa. This information is very important since Indonesia is known as a volcano-rich country, with more than 130 active volcanoes. Furthermore, almost all major cities in Indonesia are located in the coastal areas. Lack of information related to the geomorphic impact of volcanic eruptions in coastal areas will boost the risk on the subsequent major volcanic eruption; moreover, the population of Indonesia nowadays is more than 250 million peoples.

Notwithstanding, this study may have inadequacies and limitations, such as follows:

- (i) Limited access to archives of other "*lontars*" (Babads) due to museum policies (e.g., related to religion, taboo, or disgraces) and language barriers (Babad was written in old Javanese). Analyses of other archives (Babad) in the Museum of West Nusa Tenggara Province and the Museum of Bali will be very useful to provide additional description of the 1257 CE eruption of Samalas volcano.
- (ii) There was no data and sample of marine sediment due to limitations of survey equipment. Marine sediment sample will be useful in understanding maximal distance from the coastline, volcanic materials from the 1257 CE eruption of Samalas volcano that entered the sea. Furthermore, this information is handy to update the volume of pumice-rich PDC generated by this eruption.
- (iii) Tsunami deposits studies were only carried out on the west coast of Sumbawa. Further study to discover the 1257 CE tsunami evidence in other areas, such as Kangean Island in Madura and on the southwest coast of Sumbawa is necessary for understanding the tsunami coverage following the 1257 CE eruption of Samalas volcano.

Hence, weaknesses resulted from this study open new opportunities for performing an advanced study related to the 1257 CE eruption of Samalas volcano.

References

- Alizadeh, K., Cohen, M., and Behling, H. (2015). Origin and dynamics of the northern South American coastal savanna belt during the Holocene - the role of climate, sea-level, fire, and humans. *Quaternary Science Reviews*. 122, 51-62. <https://doi.org/10.1016/j.quascirev.2015.05.009>.
- Allen, G. (1915). *Selected Letters of Pliny* (1 ed.). Oxford: Clarendon Press.
- Allen, S.R. (2001). Reconstruction of a major caldera-forming eruption from pyroclastic deposit characteristics: Kos Plateau Tuff, eastern Aegean Sea. *Journal of Volcanology and Geothermal Research*, 105(1-2), 141-162. [https://doi.org/10.1016/S0377-0273\(00\)00222-5](https://doi.org/10.1016/S0377-0273(00)00222-5).
- Annamala, K., Walsh, R., Bidin, K., Blake, W. (2013). The use of multi-proxy sediment fingerprinting to explore changes in sedimentation rate and sediment sources with rotational selective logging and oil palm conversion in the Segama Catchment, Malaysian Borneo. *Geophysical Research Abstracts Vol. 15*, EGU2013-13277, EGU General Assembly.
- Anthony, E. J. (2015). Wave influence in the construction, shaping, and destruction of river deltas: A review. *Marine Geology*. 361, 53–78. <https://doi.org/10.1016/j.margeo.2014.12.004>.
- Aretano, R., Parlagreco, L., Semeraro, T., Zurlini, G., Petrosillo, I. (2017). Coastal dynamics vs beach users attitudes and perceptions to enhance environmental conservation and management effectiveness. *Marine Pollution Bulletin*. 123, 142–155. <https://doi.org/10.1016/j.marpolbul.2017.09.003>.

- Arun, P. (2013). A comparative analysis of different DEM interpolation methods. *The Egyptian Journal of Remote Sensing and Space Sciences*(16), 133-139. <https://doi.org/10.1016/j.ejrs.2013.09.001>.
- Baba, T., Mleczko, R., Burbidge, D., Cummins, P. R., Thio, H. K. (2008). The Effect of the Great Barrier Reef on the Propagation of the 2007 Solomon Islands Tsunami Recorded in Northeastern Australia. *Pure Appl. Geophys.*, 165, 2003–2018. <https://doi.org/10.1007/s00024-008-0418-5>.
- Badan Informasi Geospasial. (2015). Pentingnya Informasi Geospasial untuk Menata Laut Indonesia. Available at: <http://big.go.id/berita-surta/show/pentingnya-informasi-geospasial-untuk-menata-laut-indonesia> (accessed on 26 March 2015).
- Badan Pusat Statistik. (2016). *Nusa Tenggara Barat dalam Angka*. Badan Pusat Statistik, Indonesia.
- Badan Pusat Statistik. (2017). *Ekspor Menurut Kelompok Komoditi dan Negara*. Buletin Statistik Perdagangan Luar Negeri. Jakarta: CV Josevindo.
- Bartolini, S., Geyer, A., Marti, J., Pedrazzi, D., and Aguirre-Diaz, G. (2014). *Journal of Volcanology and Geothermal Research*. 285, 150-168. <https://doi.org/10.1016/j.jvolgeores.2014.08.009>.
- Baxter, P. J. (2000). Impacts of Eruptions on Human Health. In Sigurdsson, H., Houghton, B., Rymer, H., Stix, J., and McNutt, S. *Encyclopedia of Volcanoes*. London: Academic Press.
- Beatley, T., Brower, D., and Schwab, A. (2002). *An Introduction to Coastal Zone Management (éd. 2e)*. Washington DC: Island Press.
- Belousov, A., Voight, B., Belousova, M. (2007). Directed blasts and blast-generated pyroclastic density currents: a comparison of the Bezymianny 1956, Mount St Helens 1980, and Soufrière Hills, Montserrat 1997 eruptions and deposits. *B. Volcanol.* 69, 701-740. <https://doi.org/10.1007/s00445-006-0109-y>.

- Bibliothèque Nationale de France. (2007). *Chart of the strait of Alas / laid down from observations in the Van Sittart by Mr. George Robertson, 1781.* <http://catalogue.bnf.fr/ark:/12148/cb40668553n>.
- Bird, E. (2008). *Coastal Geomorphology: An Introduction.* John Wiley & Sons Ltd, West Sussex, England.
- Blott, S. J. and Pye, K. (2001). GRADISTAT: a grain size distribution and statistics package for the analysis of unconsolidated sediments. *Earth Surface Processes and Landforms*, 26 (11), 1237-1248. <https://doi.org/10.1002/esp.261>.
- Bowring, R. (2005). *The Religious Traditions of Japan, 500–1600* (1 ed.). Cambridge: Cambridge University Press.
- Bradley, P. (2013). *Cities of Vesuvius: Pompeii and Herculaneum.* Cambridge: Cambridge University Press.
- Bryan, S. E., Cook, A., Evans, J. P., Colls, P. W., Wells, M. G., Lawrence, M. G., Jell, J. S., Greig, A., Leslie, R. (2004). Pumice rafting and faunal dispersion during 2001–2002 in the Southwest Pacific: record of a dacitic submarine explosive eruption from Tonga. *Earth and Planetary Science Letters*. 227, 135 – 154. <https://doi.org/10.1016/j.epsl.2004.08.009>.
- Carey, S. (2000). Volcaniclastic Sedimentation around Island Arcs. In Sigurdsson, H., Houghton, B., Rymer, H., Stix, J., and McNutt, S. *Encyclopedia of Volcanoes.* London: Academic Press.
- Carey, S., Sigurdsson, H., Mandeville, C., and Bronto, S. (1996). Pyroclastic flows and surges over water: an example from the 1883 Krakatoa eruption. *Bulletin of Volcanology*. 57, 7, 493-511. <https://doi.org/10.1007/BF00304435>.
- Carrara, A., Bitelli, G., & Carla, R. (1997). Comparison of techniques for generating digital terrain models from contour lines. *International Journal of Geographical Information Science*, 11(5), 451-473. <https://doi.org/10.1080/136588197242257>.

- Carrasco, A. R., Ferreira, Ó., Matiasa, A., Freire, P. (2012). Natural and human-induced coastal dynamics at a back-barrier beach. *Geomorphology*. 159-160, 30–36. <https://doi.org/10.1016/j.geomorph.2012.03.001>.
- Cas, R., and Wright, J. (1988). *Volcanic Successions Modern and Ancient: A geological approach to processes, products, and successions*. Springer Netherlands. <http://dx.doi.org/10.1007/978-94-009-3167-1>.
- Cas, R. A. F., and Wright, J. V. (1991). Subaqueous pyroclastic flows and ignimbrites: an assessment. *Bulletin of Volcanology*. 53, 5, 357-380. <https://doi.org/10.1007/BF00280227>.
- Casadevall, T., Pardyanto, L., Abas, H., and Tulus. (1989). The 1988 eruption of Banda Api volcano, Maluku, Indonesia. *Geologi Indonesia*. 12, 1, 603-635.
- Chagué-Goff, C., Niedzielski, P., Wong, H. K. Y., Szczuciński, W., Sugawara, D., Goff, J. (2012). Environmental impact assessment of the 2011 Tohoku-Oki tsunami on the Sendai Plain. *Sedimentary Geology*. 282, 175-187. <https://doi.org/10.1016/j.sedgeo.2012.06.002>.
- Chen, C., Li, Y., & Yue, T. (2013). Surface modeling of DEMs based on a sequential adjustment method. *International Journal of Geographical Information Science*, 27(7), 1272-1291. <https://doi.org/10.1080/13658816.2012.704037>.
- Choi, B. H., Pelinovsky, E., Kim, K. O., and Lee, J. S. (2003). Simulation of the trans-oceanic tsunami propagation due to the 1883 Krakatoa volcanic eruption. In Tsunamis, Tinti, S., and Pelinovsky, E. *Nat. Hazards Earth Syst. Sci.* 3, 5, 321-332. <https://doi.org/10.5194/nhess-3-321-2003>.
- Cimarelli, C., Di Traglia F., de Rita, D., Gimeno Torrente, D., Fernandez Turiel, J.-L. (2013). Space–time evolution of monogenetic volcanism in the mafic Garrotxa Volcanic Field (NE Iberian Peninsula). *B. Volcanol.* 75 (11), 758. <https://doi.org/10.1007/s00445-013-0758-6>.

- Cioni, R., Marianelli, P., Santacroce, R., and Sbrana, A. (2000). Plinian and Subplinian Eruptions. In Sigurdsson, H., Houghton, B., Rymer, H., Stix, J., and McNutt, S. *Encyclopedia of Volcanoes*. London: Academic Press.
- Cole, P. D., Guest, J. E., Duncan, A. M., Pacheco, J.-M. (2001). Capelinhos 1957-1958, Faial, Azores: deposits formed by an emergent surtseyan eruption. *Bull Volcanol.* 63, 204-220. <https://doi.org/10.1007/s004450100136>.
- Coombs, D. S., and Landis, C. A. (1966). Pumice from the South Sandwich Eruption of March 1962 reaches New Zealand. *Nature.* 209, 289–290. <https://doi.org/10.1038/209289b0>.
- Costa, M. B. S. F., Araújo, M., Araújo, T. C. M., Siegle, E. (2016). Influence of reef geometry on wave attenuation on a Brazilian coral reef. *Geomorphology.* 253, 318–327. <https://doi.org/10.1016/j.geomorph.2015.11.001>.
- Crandell, D. R. (1971). Postglacial Lahars from Mount Rainier Volcano. *Report: USGS Numbered Series* (677). U.S. Govt. Print. Off: Washington.
- Cuitiño, J., and Scasso, R. A. (2013). Reworked pyroclastic beds in the early Miocene of Patagonia: Reaction in response to high sediment supply during explosive volcanic events. *Journal of Sedimentary Geology.* 289, 194–209. <https://doi.org/10.1016/j.sedgeo.2013.03.004>.
- Daag, A., & Westen, C. (1996). Cartographic modelling of erosion in pyroclastic flow deposits of Mount Pinatubo, Philippines. *ITC Journal*, 2, 110-124.
- Davidson-Arnott, R. (2010). *An Introduction to Coastal Processes and Geomorphology*. Cambridge University Press, New York.
- Davis, R. A. (1996). *Coasts*. Prentice-Hall, Englewood Cliffs, NJ.
- de Castro, M., Gómez-Gesteira, M., Costoya, X., and Santos, F. (2014). Upwelling influence on the number of extreme hot SST days along the Canary upwelling ecosystem. *J. Geophys. Res. Oceans.* 119, 3029–3040. <https://doi.org/10.1002/2013JC009745>.

- Dehn, J., and McNutt, S. R. (2000). Volcanic Materials in Commerce and Industry. In Sigurdsson, H., Houghton, B., Rymer, H., Stix, J., and McNutt, S. *Encyclopedia of Volcanoes*. London: Academic Press.
- Deng, J., Harff, J., Li, Y., Zhao, Y., and Zhang, H. (2016). Morphodynamics at the Coastal Zone in the Laizhou Bay, Bohai Sea. *Journal of Coastal Research*. SI (74), 59-69. <https://doi.org/10.2112/SI74-006.1>.
- Divins, D. L. (2003). *Total Sediment Thickness of the World's Oceans & Marginal Seas*, NOAA National Geophysical Data Center, Boulder, CO.
- Divins, D. L., and Rabinowitz, P. D. (1990). Thickness of Sedimentary Cover for the South Atlantic, in *International Geological-Geophysical Atlas of the Atlantic Ocean*, edited by G.B. Udinstev, Intergovernmental Oceanographic Commission, Moscow.
- Donato, S. V., Reinhardt, E. G., Boyce, J. I., Pilarczyk, J. E., Jupp, B. P. (2009). Particle-size distribution of inferred tsunami deposits in Sur Lagoon, Sultanate of Oman. *Marine Geology*, 257 (1-4), 54-64. <https://doi.org/10.1016/j.margeo.2008.10.012>.
- Doranzo, D. M., and Dellino, P. (2014). Pyroclastic density currents and local topography as seen with the conveyor model. *Journal of Volcanology and Geothermal Research*. 278–279, 25–39. <http://dx.doi.org/10.1016/j.jvolgeores.2014.03.012>.
- Douillet, G. A., Taisne, B., Tsang-Hin-Sun, È., Müller, S. K., Kueppers, U., Dingwell, D. B. (2015). Syn-eruptive, soft-sediment deformation of deposits from dilute pyroclastic density current: triggers from granular shear, dynamic pore pressure, ballistic impacts and shock waves. *Solid Earth* 6, 553–572. <https://doi.org/10.5194/se-6-553-2015>.
- Du, J-L., Yang, S-L., Feng, H. (2016). Recent human impacts on the morphological evolution of the Yangtze River delta foreland: A review and new perspectives.

Estuarine, Coastal and Shelf Science. 181, 160-169.

<https://doi.org/10.1016/j.ecss.2016.08.025>.

Dufek, J., Manga, M., Staedter, M. (2007). Littoral blasts: Pumice-water heat transfer and the conditions for steam explosions when pyroclastic flows enter the ocean.

J. Geophys. Res., 112, B11201. <https://doi.org/10.1029/2006JB004910>.

Duggen, S., Olgun, N., Croot, P., Hoffmann, L., Dietze, H., Delmelle, P., and Teschner, C. (2010). The role of airborne volcanic ash for the surface ocean biogeochemical iron-cycle: a review. *Biogeosciences.* 7, 827–844.

<https://doi.org/10.5194/bg-7-827-2010>.

Dura, T., Cisternas, M., Horton, B. P., Ely, L. L., Nelson, A. R., Wesson, R. L., Pilarczyk, J. E. (2014). Coastal evidence for Holocene subduction-zone earthquakes and tsunamis in central Chile. *Quaternary Science Reviews*, 113,

93-111. <https://doi.org/10.1016/j.quascirev.2014.10.015>.

Duxbury, A. B., Duxbury, A. C., and Sverdrup, K. A. (2002). *Fundamentals of Oceanography*. McGraw-Hill, Singapore.

Encinas, A., Maksaev, V., Pinto, L., Le Roux, J. P., Munizaga, F., and Zentilli, M. (2006). Pliocene lahar deposits in the Coastal Cordillera of central Chile: Implications for uplift, avalanche deposits, and porphyry copper systems in the Main Andean Cordillera. *Journal of South American Earth Sciences.* 20, 4, 269-

381. <https://doi.org/10.1016/j.jsames.2005.08.007>.

Erdogan, S. (2009). A comparison of interpolation methods for producing digital elevation models at the field scale. *Earth Surface Processes and Landforms*, 34(3), 366-376. <https://doi.org/10.1002/esp.1731>.

FAO. (2000). *Global River Sediment Yields Database*. FAO's Information System on Water and Agriculture.

- Fernando, H. J. S., McCulley, J. L., Mendis, S. G., Perera, K. (2005). Coral poaching worsens tsunami destruction in Sri Lanka, *Eos*, 86 (33), 301–304. <https://doi.org/10.1029/2005EO330002>.
- Ferrario, F., Beck, M. W., Storlazzi, C. D., Micheli, F., Shepard, C. C., and Airoidi, L. (2014). The effectiveness of coral reefs for coastal hazard risk reduction and adaptation. *Nature Communications*. 5:3794. <https://doi.org/10.1038/ncomms4794>.
- Fisher, R. V., Heiken, G., Mazzoni, M. (2006). Where do Tuffs Fit into the Frameworks of Volcanoes? in Heiken, G. *Tuffs: Their Properties, Uses, Hydrology, and Resources, Numéro 408*. Geological Society of America.
- Fisher R. V., and Schmincke H. U. (1984). *Pyroclastic rocks*. Springer-Verlag, Berlin. 472p. <https://doi.org/10.1007/978-3-642-74864-6>.
- Fisher, R. V., and Smith, G. A. (1991). Volcanism, Tectonics, and Sedimentation. In: Fisher, R. V., and Smith, G. A. *Sedimentation in Volcanic Settings*. SEPM Special Publication, Tulsa, Oklahoma USA.
- Fiske, R. S., Naka, J., Iizasa, K., Yuasa, M., Klaus, A. (2001) Submarine silicic caldera at the front of the Izu-Bonin arc, Japan: voluminous seafloor eruptions of rhyolite pumice. *Geological Society of America Bulletin*. 113, 7, 813–824. [https://doi.org/10.1130/0016-7606\(2001\)113<0813:SSCATF>2.0.CO;2](https://doi.org/10.1130/0016-7606(2001)113<0813:SSCATF>2.0.CO;2).
- Folk, R. L. and Ward, W. C. (1957). A Study in the Significance of Grain-Size Parameters. *Journal of Sedimentary Petrology*, 27, 3-26. <https://doi.org/10.1306/74D70646-2B21-11D7-8648000102C1865D>.
- Francis, P. W. (1985). The origin of the 1883 Krakatau tsunamis. *Journal of Volcanology and Geothermal Research*. 25, 3-4, 349-363. [https://doi.org/10.1016/0377-0273\(85\)90021-6](https://doi.org/10.1016/0377-0273(85)90021-6).
- French, P. W. (1997). *Coastal and Estuarine Management*. Routledge. London.

- Freundt, A. (2003). Entrance of Hot Pyroclastic Flows into the Sea: Experimental Observations. *Bulletin of Volcanology*, 65, 2-3, 144-164. <https://doi.org/10.1007/s00445-002-0250-1>.
- Freundt, A., Wilson, C. J. N., and Carey, S. N. (2000). Ignimbrites and Block-and-ash Flow Deposits. In Sigurdsson, H., Houghton, B., Rymer, H., Stix, J., and McNutt, S. *Encyclopedia of Volcanoes*. London: Academic Press.
- Gabrie, C., and Salvat, B. (1985). General features of French Polynesian islands and their coral reefs. *The 5th International Coral Reef Congress*, Tahiti, vol. 1, edited by Delesalle, B., Galzin, R., and Salvat, B., 1–16, Antenne du Mus. Natl. d'Hist. Nat. et de l'Ecole Pratique des Hautes Etudes, Moorea, French Polynesia.
- Garrels, R. M., and Mackenzie, F. T. (1971). *Evolution of Sedimentary Rocks*, W.W. Norton, New York.
- Germa, A., Lahitte, P., and Quidelleur, X. (2015). Construction and destruction of Mont Pelée volcano: Volumes and rates constrained from a geomorphological model of evolution. *Journal of Geophysical Research: Earth Surface*, 120, 7. <https://doi.org/10.1002/2014JF003355>.
- Giachetti, T., Paris, R., Kelfoun, K., Ontowirjo, B. (2012). Tsunami hazard related to a flank collapse of Anak Krakatau Volcano, Sunda Strait, Indonesia. *Geological Society*, London, Special Publications 361, 79-90. <https://doi.org/10.1144/SP361.7>.
- Global Volcanism Program. (2013). *Volcanoes of the World*, v. 4.6.7. Venzke, E (ed.). Smithsonian Institution. Downloaded 09 April 2018. <https://dx.doi.org/10.5479/si.GVP.VOTW4-2013>.
- Goff, J., Chagué-Goff, C., Nichol, S., Jaffe, B., Dominey-Howes, D. (2012). Progress in paleotsunami research. *Sedimentary Geology*, 243-244, 70-88. <https://doi.org/10.1016/j.sedgeo.2011.11.002>.

- Gomez, C. (2014). Digital photogrammetry and GIS-based analysis of the biogeomorphological evolution of Sakurajima Volcano, diachronic analysis from 1947 to 2006. *Journal of Volcanology and Geothermal Research*. 280, 1-13. <https://doi.org/10.1016/j.jvolgeores.2014.04.015>.
- Gomes, G., and Silva, A. C. (2014). Coastal Erosion Case at Candeias Beach (NE-Brazil). *Journal of Coastal Research*. 71, pp30-40. <https://doi.org/10.2112/SI71-004.1>.
- Gómez-Ortiz, D., Martín-Velázquez, S., Martín-Crespo, T., Márquez, A., Lillo, J., López, I., Carreño, F., Martín-González, F., Herrera, R., De Pablo, M. A. (2007). Joint application of ground penetrating radar and electrical resistivity imaging to investigate volcanic materials and structures in Tenerife (Canary Islands, Spain). *Journal of Applied Geophysics*. 62, 287–300. <https://doi.org/10.1016/j.jappgeo.2007.01.002>.
- Gordon, L. (2011). *Small Volcanic Eruption Can Add Hazardous Sediment to Rivers*. USGS, <http://www.usgs.gov/newsroom/article.asp?ID=2750>.
- Grauert, M., Björck, S., Bondevik, S. (2001). Storegga tsunami deposits in a coastal lake on Suouroy, the Faroe Islands. *Boreas*, 30 (4), 263-271. <https://doi.org/10.1111/j.1502-3885.2001.tb01045.x>.
- Grigg, R. W., and Maragos, J. E. (1974) Recolonization of hermatypic corals on submerged lava flows in Hawaii. *Ecology*. 55, 387–395. <https://doi.org/10.2307/1935226>.
- Guannel, G., Arkema, K., Ruggiero, P., Verutes, G. (2016). The Power of Three: Coral Reefs, Seagrasses, and Mangroves Protect Coastal Regions and Increase Their Resilience. *PLoS ONE* 11(7): e0158094. <https://doi.org/10.1371/journal.pone.0158094>.
- Guillet, S., Corona, C., Stoffel, M., Khodri, M., Lavigne, F., Ortega, P., Eckert, N., Sielenou, P.D., Daux, V., Churakova (Sidorova), O.V., Davi, N., Edouard, J.L.,

- Zhang, Y., Luckman, B.H., Myglan, V.S., Guiot, J., Beniston, M., Masson-Delmotte, V., Oppenheimer, C. (2017). Climate response to the Samalas volcanic eruption in 1257 revealed by proxy records. *Nature Geoscience*. 10, 123-128. <http://dx.doi.org/10.1038/ngeo2875>.
- Harris, D. L., Rovere, A., Casella, E., Power, H., Canavesio, R., Collin, A., Pomeroy, A., Webster, J. M., Parravicini, V. (2018). Coral reef structural complexity provides important coastal protection from waves under rising sea levels. *Science Advances*. 4, 2, eaao4350. <https://doi.org/10.1126/sciadv.aao4350>.
- Harrison, P., and Pearce, F. (2000). *AAAS Atlas of Population and Environment*. Victoria Dompka Markham, editor. American Association for the Advancement of Science and the University of California Press. 215p.
- Hayes, D. E., and LaBrecque, J. L. (1991). Sediment Isopachs: Circum-Antarctic to 30S, in *Marine Geological and Geophysical Atlas of the Circum-Antarctic to 30S*, edited by D.E. Hayes, American Geophys. Union, Washington, D.C.
- Heritage, G., Milan, D., Large, A., & Fuller, I. (2009). Influence of survey strategy and interpolation model on DEM quality. *Geomorphology*(112), 334-344. <https://doi.org/10.1016/j.geomorph.2009.06.024>.
- Hidden, H., Brotopuspito, K., Hadmoko, D., Lavigne, F., Boillot-Airaksinen, K., Mutaqin, B.W., Hananto, N.D., Handayani, L., Sudrajat, Y., Suryanto, W. (2017). The Isopach Mapping of Volcanic Deposits of Mount Samalas 1257 AD Based on the Values of Resistivity and Physical Properties. *Geosciences*, 7(3), 67. <https://doi.org/10.3390/geosciences7030067>.
- Hogg, A., Hua, Q., Blackwell, P., Niu, M., Buck, C., Guilderson, T., Heaton, T. J., Palmer, J. G., Reimer, P. J., Reimer, R. W., Turney, C. S. M., Zimmerman, Z. (2013). SHCal13 Southern Hemisphere calibration, 0–50,000 years cal BP. *Radiocarbon*, 55(4), 1889-1903. https://doi.org/10.2458/azu_js_rc.55.16783.

- Hongo, C., Kurihara, H., and Golbuu, Y. (2018). Coral boulders on Melekeok reef in the Palau Islands: An indicator of wave activity associated with tropical cyclones. *Marine Geology*. 399, 14–22. <https://doi.org/10.1016/j.margeo.2018.02.004>.
- Inman, D., and Nordström, C. (1971). On the tectonic and morphological classification of coasts. *Journal of Geology*. 79:1–21. <https://doi.org/10.1086/627583>.
- Jackson, N. L., Nordstrom, K. F., Farrell, E.J. (2017). Longshore sediment transport and foreshore change in the swash zone of an estuarine beach. *Marine Geology*. 386, p88–97. <https://doi.org/10.1016/j.margeo.2017.02.017>.
- Jakobsson, S. P., and Gudmundsson, G. (2003). Rof Surtseyjar. Mælingar 1967-2002 og framtíðarspá (The marine abrasion of Surtsey, Iceland: Area changes 1967-2002 and future development). *Náttúrufræðingurinn*. 71: 138–144.
- Jaramillo, E.C., Vega, X., Monsalve, H. (2005). Application of gravimetry and electric tomography methods to obtain stratigraphic profiles: a case study at the University of Quindío and Puerto Espejo area, Armenia—Colombia. *Earth Sci. Res. J.* 9, 73–84. <http://dx.doi.org/10.15446/esrj>.
- Johnson, D. W. (1919). *Shore Processes and Shoreline Development*. John Wiley, New York.
- Jordan, H., Holbrook, H., & Lawley, R. (2016). Early Holocene geomorphology of the Great Yarmouth area, Norfolk, UK. *Journal of Maps*, 12(S1), 122-130. <https://doi.org/10.1080/17445647.2016.1169951>.
- Julien, P. Y. (2010). *Erosion and Sedimentation*. Cambridge University Press. New York.
- Kandlbauer, J., and Sparks, R. S. J. (2014). New estimates of the 1815 Tambora eruption volume. *Journal of Volcanology and Geothermal Research*. 286, 93–100. <https://doi.org/10.1016/j.jvolgeores.2014.08.020>.
- Karátson, D., Yepes, J., Favalli, M., Rodríguez-Peces, M. J., Fornaciai, A. (2016). Reconstructing eroded paleovolcanoes on Gran Canaria, Canary Islands, using

advanced geomorphometry. *Geomorphology* 253, 123-134.
<https://doi.org/10.1016/j.geomorph.2015.10.004>.

Karstens, J., Crutchley, G. J., Berndt, C., Talling, P. J., Watt, S. F. L., Hühnerbach, V., Le Friant, A., Lebas, E., Trofimovs, J. (2013). Emplacement of pyroclastic deposits offshore Montserrat: Insights from 3D seismic data. *Journal of Volcanology and Geothermal Research*. 257, 1-11.
<https://doi.org/10.1016/j.jvolgeores.2013.03.004>.

Kataoka, K. S., Manville, V., Nakajo, T., Urabe, A. (2009). Impacts of explosive volcanism on distal alluvial sedimentation: Examples from the Pliocene–Holocene volcanoclastic successions of Japan. *Sedimentary Geology*. 220, 306–317.
<https://doi.org/10.1016/j.sedgeo.2009.04.016>.

Kataoka, K. S., Urabe, A., Nagahashi, Y. (2016). Millennial-scale reworking of tephra in alluvial to shallow marine settings: Distinguishing pseudo-isochrons from genuine ones. *Quaternary International*. 397, 173-193.
<https://doi.org/10.1016/j.quaint.2015.03.022>.

Kay, R., and Alder, J. (1999). *Coastal Planning and Management (éd. 2nd)*. New York: Taylor and Francis.

Keller, G., and Frischknecht, F. (1966). *Electrical Methods in Geophysical Prospecting*. New York: Pergamon Press. 517p.

Kim, S-J., and Kim, B-M. (2012). Ocean Response to the Pinatubo and 1259 Volcanic Eruptions. *Ocean and Polar Research*. 34 (3), 305-323.
<http://doi.org/10.4217/OPR.2012.34.3.305>.

King, C. A. M. (1959). *Beaches and Coasts*. Edward Arnold, London.

Kitamura, A., and Kobayashi, K. (2014). Geologic evidence for prehistoric tsunamis and coseismic uplift during the AD 1854 Ansei-Tokai earthquake in Holocene sediments on the Shimizu Plain, central Japan. *The Holocene*. 24, 7, p814-827.
<https://doi.org/10.1177/0959683614530447>.

- Klug, C., and Cashman, K. V. (1996). Permeability development in vesiculating magmas: implications for fragmentation. *B. Volcanol.* 58 (2-3), 87-100. <https://doi.org/10.1007/s004450050128>.
- Kobayashi, N., Agarwal, A., and Johnson, B. D. (2007). Longshore Current and Sediment Transport on Beaches. *Journal of Waterway, Port, Coastal, and Ocean Engineering.* 133, 4. [https://doi.org/10.1061/\(ASCE\)0733-950X\(2007\)133:4\(296\)](https://doi.org/10.1061/(ASCE)0733-950X(2007)133:4(296)).
- Komar, P. D., and Inman, D. L. (1970). Longshore Sand Transport on Beaches. *Journal of Geophysical Research.* 75, 30. <https://doi.org/10.1029/JC075i030p05914>.
- Kortekaas, S. and Dawson, A. G. (2007). Distinguishing tsunami and storm deposits: An example from Martinhal, SW Portugal. *Sedimentary Geology*, 200 (3-4), 208-221. <https://doi.org/10.1016/j.sedgeo.2007.01.004>.
- Koyama, M. (2007). Database of eruptions and other activities of Fuji Volcano, Japan, based on historical records since AD 781. In S. Aramaki, T. Fujii, S. Nakada, & N. Miyaji (Eds.), *Fuji volcano* (pp. 119-136). Yamanashi: Yamanashi Institute of Environmental Sciences.
- Kubanek, J., Richardson, J. A., Charbonnier, S. J., Connor, L. J. (2015). Lava flow mapping and volume calculations for the 2012–2013 Tolbachik, Kamchatka, fissure eruption using bistatic TanDEM-X InSAR. *Bulletin of Volcanology.* 77, 106. <https://doi.org/10.1007/s00445-015-0989-9>.
- Kunkel, C. M., Hallberg, R. W., Oppenheimer, M. (2006). Coral reefs reduce tsunami impact in model simulations. *Geophysical Research Letters*, 33, L23612, <https://doi.org/10.1029/2006GL027892>.
- Kusky, T. M. (2008). *Volcanoes: The Hazardous Earth*. Infobase Publishing.
- Lahitte, P., Samper, A., and Quidelleur, X. (2012). DEM-based reconstruction of southern Basse-Terre volcanoes (Guadeloupe archipelago, FWI): Contribution to the Lesser Antilles Arc construction rates and magma production.

Geomorphology. 136, 1, 148-164.

<https://doi.org/10.1016/j.geomorph.2011.04.008>.

Lalli, C. M., and Parsons, T. R. (1995). *Biological Oceanography: An Introduction*. Oxford, UK: Butterworth-Heinemann Ltd.

Lander, J. F., Whiteside, L. S., and Lockridge, P. A. (2003). Two Decades of Global Tsunamis, 1982-2002. *Science of Tsunami Hazards*. 21(1), 3-88.

Latief, H., Puspito, N. T., and Imamura, F. (2000). Tsunami Catalog and Zones in Indonesia. *Journal of Natural Disaster Science*. 22, 1, 25-43.

<https://doi.org/10.2328/jnds.22.25>.

Latter, J. H. (1981). Tsunamis of volcanic origin: Summary of causes, with particular reference to Krakatoa, 1883. *Bulletin Volcanologique*. 44, 3, 467-490.

<https://doi.org/10.1007/BF02600578>.

Lavigne, F., Degeai, J.-P., Komorowski, J.-C., Guillet, S., Robert, V., Lahitte, P., Oppenheimer, C., Stoffel, M., Vidal, C.M., Surono, Pratomo, I., Wassmer, P., Hajdas, I., Hadmoko, D.S., de Belizal, E. (2013). Source of the great A.D. 1257 mystery eruption unveiled, Samalas volcano, Rinjani Volcanic Complex, Indonesia. *PNAS*. 110(42), 16742-16747.

<https://doi.org/10.1073/pnas.1307520110>.

Lavigne, F. and Thouret J.-C. (2000). Les lahars, dépôts, occurrence et dynamique : une revue des écoulements volcano-hydrologiques. *Bulletin de la Société géologique de France*. 171, 5, 545-558.

Lavigne, F. and Thouret, J.-C. (2003). Sediment transportation and deposition by rain-triggered lahars at Merapi Volcano, Central Java, Indonesia. *Geomorphology*. 49(1-2), 45-69. [https://doi.org/10.1016/S0169-555X\(02\)00160-5](https://doi.org/10.1016/S0169-555X(02)00160-5).

Lavigne, F., Thouret, J.-C., Hadmoko, D., & Sukatja, C. (2007). Lahars in Java: Initiations, Dynamics, Hazard Assessment, and Deposition Processes. *Forum Geografi*. 21(1), 17-32. <https://doi.org/10.23917/forgeo.v21i1.1822>.

- Le Friant, A., Deplus, C., Boudon, G., Feuillet, N., Trofimovs, J., Komorowski, J-C., Sparks, R. S. J., Talling, P., Loughlin, S., Palmer, M., Ryan, G. (2010). Eruption of Soufriere Hills (1995–2009) from an offshore perspective: insights from repeated swath bathymetry surveys. *Geophysical Research Letters*. 37, 19. <https://doi.org/10.1029/2010GL043580>.
- Le Friant, A., Deplus, C., Boudon, G., Sparks, R. S. J., Trofimovs, J., Talling, P. (2009). Submarine deposition of volcanoclastic material from the 1995–2005 eruptions of Soufriere Hills volcano, Montserrat. *Journal of the Geological Society*. 166, 171–182. <https://doi.org/10.1144/0016-76492008-047>.
- Leverington, D. W., Teller, J. T., & Mann, J. D. (2002). A GIS method for reconstruction of late Quaternary landscapes from isobase data and modern topography. *Computers & Geosciences*, 28, 631–639. [https://doi.org/10.1016/S0098-3004\(01\)00097-8](https://doi.org/10.1016/S0098-3004(01)00097-8).
- Leverington, D., Mann, J., & Teller, J. (2000). Changes in the Bathymetry and Volume of Glacial Lake Agassiz between 9200 and 7700 14C yr B.P. *Quaternary Research*, 57, 244-252. <https://doi.org/10.1006/qres.2001.2311>.
- Li, Z. (1988). On the measure of digital terrain model accuracy. *Photogram Rec*. 12, 873–877. <https://doi.org/10.1111/j.1477-9730.1988.tb00636.x>.
- Li, F., and Tang, G. (2011). DEM-based Terrain Factor of Soil Erosion at Regional Scale and Soil Erosion Mapping. In Ruas, A. *Advances in Cartography and GIScience (Volume 2)*. Springer-Verlag Berlin Heidelberg. <https://doi.org/10.1007/978-3-642-19214-2>.
- Lipman, P. W., and Mullineaux, D. R. (1981). *The 1980 eruptions of Mount St. Helens, Washington: Professional Paper 1250*. Washington, D.C.: US Government Printing Office. 844p.
- Liu, P. L. F., Cho, Y. S., Yoon, S. B., Seo, S. N. (1994). Numerical simulations of the 1960 Chilean tsunami propagation and inundation at Hilo, Hawaii. In: Tsuchiya

- Y., Shuto N. (eds) *Tsunami: Progress in Prediction, Disaster Prevention and Warning*. Advances in Natural and Technological Hazards Research, vol 4. Springer, Netherlands, pp. 99–115. https://doi.org/10.1007/978-94-015-8565-1_7.
- Liu, P. L. F., Cho, Y. S., Briggs, M. J., Kanoglu, U., Synolakis, C. E. (1995). Runup of solitary waves on a circular island. *J. Fluid Mech.* 302, 259–285. <https://doi.org/10.1017/S0022112095004095>.
- Liu, P. L. F., Woo, S. B., Cho, Y. S. (1998). *Computer Programs for Tsunami Propagation and Inundation*. School of Civil and Environmental Engineering, Cornell University, USA. Available at: http://223.4.213.26/archive/tsunami/cornell/comcot_down.htm.
- Ludwig, W. J., and Houtz, R. E. (1979). *Isopach Map of the Sediments in the Pacific Ocean Basin*, color map with text, Am. Assoc. Pet. Geol., Tulsa, OK.
- Maiuri, A. (1960). *Pompeian Wall Paintings* (1 ed.). Berne: Hallwag.
- Major, J. J. (1997). Depositional Processes in Large-Scale Debris-Flow Experiments. *The Journal of Geology*, 105 (3), 345-366. <https://doi.org/10.1086/515930>.
- Major, J. J. (2004). Post-eruption suspended sediment transport at Mount St. Helens: Decadal-scale relationships with landscape adjustments and river discharges. *J. Geophys. Res.* 109, F01002. <https://doi.org/10.1029/2002JF000010>.
- Major, J. J., Janda, R. J., and Daag, A. S. (1996). Watershed Disturbance and Lahars on the East Side of Mount Pinatubo during the Mid-June 1991 Eruptions. In: Newhall, C. G., and Punongbayan, R. S. *Fire and Mud, Eruptions and Lahars of Mount Pinatubo, Philippines*. PHIVOLCS Press, Quezon City, and University of Washington Press, Seattle.
- Major, J. J., Pierson, T. C., Dinehart, R. L., & Costa, J. E. (2000). Sediment yield following severe volcanic disturbance - a two-decade perspective from Mount St. Helens. *Geology*. 28(9), 819-822. [https://doi.org/10.1130/0091-7613\(2000\)28%3C819:SYFSVD%3E2.0.CO;2](https://doi.org/10.1130/0091-7613(2000)28%3C819:SYFSVD%3E2.0.CO;2).

- Mandeville, C. W., Carey, S., and Sigurdsson, H. (1996). Sedimentology of the Krakatau 1883 submarine pyroclastic deposits. *B. Volcanol.*, 57, 512-529. <https://doi.org/10.1007/BF00304436>.
- Maniwavie, T., Rewald, J., Aitsi, J., Wagner, T. P., and Munday, P. L. (2001). Recovery of corals after volcanic eruptions in Papua New Guinea. *Coral Reefs*. 20:24. <https://doi.org/10.1007%2Fs003380100114>.
- Mann, J., Leverington, D., Rayburn, J., & Teller, J. (1999). The volume and paleobathymetry of glacial Lake Agassiz. *Journal of Paleolimnology*, 22(1), 71-80. <https://doi.org/10.1023/A:1008090015161>.
- Manville, V., Németh, K., Kano, K. (2009). Source to Sink: A Review of Three Decades of Progress in the Understanding of Volcaniclastic Processes, Deposits, and Hazards. *Sedimentary Geology*. 220, 136–161. <https://doi.org/10.1016/j.sedgeo.2009.04.022>.
- Manville, V., Newton, E. H., and White, J. D. L. (2005). Fluvial Responses to Volcanism: Resedimentation of the 1800a Taupo Ignimbrite Eruption in the Rangitaiki River Catchment, North Island, New Zealand. *Geomorphology*. 65, 49–70. <https://doi.org/10.1016/j.geomorph.2004.07.007>.
- Marris, E. (2005). Tsunami damage was enhanced by coral theft. *Nature*, 436, 1071. <https://doi.org/10.1038/4361071a>.
- Marsella, M., Baldi, P., Coltelli, M., Fabris, M. (2012). The morphological evolution of the Sciara del Fuoco since 1868: reconstructing the effusive activity at Stromboli volcano. *B. Volcanol.* 74 (1), 231-248. <https://doi.org/10.1007/s00445-011-0516-6>.
- Matthias, P. K., Rabinowitz, P. D., and Dipiazza, N. (1988). *Sediment Thickness Map of the Indian Ocean*, Map 505, Am. Assoc. Pet. Geol., Tulsa, OK.
- Mattioli, G. S., Voight, B., Linde, A. T., Sacks, I. S., Watts, P., Widiwijayanti, C., Young, S. R., Hidayat, D., Elsworth, D., Malin, P. E., Shalev, E., Van Boskirk, E.,

- Johnston, W., Sparks, R. S. J., Neuberg, J., Bass, V., Dunkley, P., Herd, R., Syers, T., Williams, P., and Williams, D. (2007). Unique and remarkable dilatometer measurements of pyroclastic flow-generated tsunamis. *Geology*. 35 (1), 25–28. <https://doi.org/10.1130/G22931A.1>.
- Maury, S. and Balaji, S. (2014). Geoelectrical method in the investigation of groundwater resource and related issues in Ophiolite and Flysch formations of Port Blair, Andaman Island, India. *Environ. Earth Sci.* 71, 183–199. <https://doi.org/10.1007/s12665-013-2423-y>.
- McCoy, F. W., and Heiken, G. 2000. Tsunami Generated by the Late Bronze Age Eruption of Thera (Santorini), Greece. *Pure and Applied Geophysics*. 157, 6-8, 1227-1256. <https://doi.org/10.1007/s000240050024>.
- McKee, C. O., Johnson, R. W., Lowenstein, P. L., Riley, S. J., Blong, R. J., De Saint Ours, P., Talai, B. (1985). Rabaul Caldera, Papua New Guinea: Volcanic hazards, surveillance, and eruption contingency planning. *Journal of Volcanology and Geothermal Research*. 23, 3-4, 195-237. [https://doi.org/10.1016/0377-0273\(85\)90035-6](https://doi.org/10.1016/0377-0273(85)90035-6).
- McPhie, J., Doyle, M., and Allen, R. (1993). *Volcanic Textures: A Guide to the Interpretation of Textures in Volcanic Rocks*. Hobart, CODES Key Centre. The University of Tasmania.
- Mei-e, R. (1992). Human Impact on Coastal Landform and Sedimentation - The Yellow River Example. *GeoJournal*. 28, 4, 443-448. <https://doi.org/10.1007/BF00273113>.
- Montserrat Volcano Observatory, Montserrat, West Indies. (2006). *Interim report for the period midday 19 May to midday 22 May 2006*. The Caribbean Disaster Emergency Response Agency News Centre at <http://www.cdera.org/cunews/>
- Moore, A. L., McAdoo, B. G., Ruffman, A. (2007). Landward fining from multiple sources in a sand sheet deposited by the 1929 Grand Banks tsunami,

Newfoundland. *Sedimentary Geology*, 200 (3-4), 336-346.

<https://doi.org/10.1016/j.sedgeo.2007.01.012>.

Mouslopoulou, V., Oncken, O., Hainzl, S., and Nicol, A. (2016). Uplift rate transients at subduction margins due to earthquake clustering. *Tectonics*. 35, p2370–2384.

<https://doi.org/10.1002/2016TC004248>.

Mutaqin, B. W., and Rohmah, F. N. (2013). Biodegradation of Seagrass Ecosystem and its Implication on Coastal Resources in Maratua Island, East Kalimantan – Indonesia. *Proceeding of Ecosystem Disaster Risk Reduction*. Master Program in Planning and Management of Coastal Area and Watershed in cooperation with the Center for Natural Resources and Development (CNRD). ISBN: 978-602-14856-1-5.

Mutaqin, B. W., Agustina, N., and Permatasari, C. W. (2014). Characteristics of waves in Kuwaru waters during the East Monsoon. *IJJSS 2014: The 6th Indonesia Japan Joint Scientific Symposium*. ISBN: 978-979-8786-52-5.

Mutaqin, B. W. (2017). Shoreline Changes Analysis in Kuwaru Coastal Area, Yogyakarta, Indonesia: An Application of the Digital Shoreline Analysis System (DSAS). *International Journal of Sustainable Development and Planning* 12(7):1203-1214, October 2017, WIT Press. <https://doi.org/10.2495/SDP-V12-N7-1203-1214>.

Nasution, A., Takada, A., Rosgandika, M. (2004). The volcanic activity of Rinjani, Lombok Island, Indonesia, during the last thousand years, viewed from 14C datings. In: *Proceedings of the Convention Bandung 2004, the 33rd annual convention & exhibition*, 29 November – 1 October 2004, Bandung, 8-15.

Nathenson, M. (2017). Revised tephra volumes for Cascade Range volcanoes. *J. Volcanol. Geoth. Res.* 341, 42-52.

<https://doi.org/10.1016/j.jvolgeores.2017.04.021>.

- National Geophysical Data Center / World Data Service (NGDC/WDS). (2018). *Global Historical Tsunami Database*. National Geophysical Data Center, NOAA. <https://doi.org/10.7289/V5PN93H7> [3 April 2018].
- Nazaruddin, D., Amiruzan, Z., Hussin, H., & Jafar, M. (2017). Integrated geological and multi-electrode resistivity surveys for groundwater investigation in Kampung Rahmat village and its vicinity, Jeli district, Kelantan, Malaysia. *Journal of Applied Geophysics*, 138, 23-32. <https://doi.org/10.1016/j.jappgeo.2017.01.012>.
- Neall, V. E. (2004). Lahar. In Goudie A.S. (Ed.): *Encyclopedia of Geomorphology*. Routledge Ltd, London.
- Németh, K. and Cronin, S. J. (2007). Syn- and post-eruptive erosion, gully formation, and morphological evolution of a tephra ring in tropical climate erupted in 1913 in West Ambrym, Vanuatu. *Geomorphology*. 86, 115–130. <https://doi.org/10.1016/j.geomorph.2006.08.016>.
- Németh, K., Cronin, S. J., Stewart, R. B., Charley, D. (2009). Intra- and extra-caldera volcanoclastic facies and geomorphic characteristics of a frequently active mafic island–arc volcano, Ambrym Island, Vanuatu. *Sedimentary Geology*. 220, 256–270. <https://doi.org/10.1016/j.sedgeo.2009.04.019>.
- Ogorodov, S. A., Baranskaya, A. V., Belova, N. G., Kamalov, A. M., Kuznetsov, D. E., Overduin, P. P., Shabanova, N. N., Vergun, A. P. (2016). Coastal Dynamics of the Pechora and Kara Seas under Changing Climatic Conditions and Human Disturbances. *Geography, Environment, Sustainability*. 9(3), 53-73. https://doi.org/10.15356/2071-9388_03v09_2016_04.
- Oppenheimer, C. (2003). Climatic, environmental and human consequences of the largest known historic eruption: Tambora volcano (Indonesia) 1815. *Progress in Physical Geography: Earth and Environment*. 27, 2, 230-259. <https://doi.org/10.1191/0309133303pp379ra>.

- Pararas-Carayannis, G. (2006). Risk assessment of tsunami generation from active volcanic sources in the eastern Caribbean region. *Caribbean Tsunami Hazard, Proceedings of the NSF Caribbean Tsunami Workshop*, March 30-31, 2004, Aurelio Mercado-Irizarry and Philip Liu, eds., World Scientific Publishing Co., Singapore, p91-137. https://doi.org/10.1142/9789812774613_0005.
- Paris, R. (2012). Signature morpho-sédimentaire des tsunamis et implications en terme de risques. *Mémoire de l'Habilitation à Diriger des Recherches*. Université Blaise Pascal, Clermont-Ferrand.
- Paris, R., Ramalho, R. S., Madeira, J., Ávila, S., May, S. M., Rixhon, G., Engel, M., Brückner, H., Herzog, M., Schukraft, G., Perez-Torrado, F. J., Rodriguez-Gonzalez, A., Carracedo, J. C., Giachetti, T. (2018). Mega-tsunami conglomerates and flank collapses of ocean island volcanoes. *Marine Geology*. 395, 168-187. <https://doi.org/10.1016/j.margeo.2017.10.004>.
- Paris, R., Switzer, A. D., Belousova, M., Belousov, A., Ontowirjo, B., Whelley, P. L., Ulvrova, M. (2013). Volcanic tsunami: a review of source mechanisms, past events, and hazards in Southeast Asia (Indonesia, Philippines, Papua New Guinea). *Nat Hazards*. 70, 1, 447-470. <https://doi.org/10.1007/s11069-013-0822-8>.
- Paris, R., Wassmer, P., Lavigne, F., Belousov, A., Belousova, M., Iskandarsyah, Y., Benbakkar, M., Ontowirjo, B., Mazzoni, N. (2014). Coupling eruption and tsunami records: the Krakatau 1883 case-study, Indonesia. *Bulletin of Volcanology*. 76, 814. <https://doi.org/10.1007/s00445-014-0814-x>.
- Paskoff, R. (1981). *L'érosion des côtes*. Paris, Presses Universitaires de France.
- Paskoff, R. (1998). *Les littoraux, impacts des aménagements sur leur évolution*. Paris, A. Colin.
- Paulay, G. (1997). Productivity plays a major role in determining atoll life and form: Tarawa, Kiribati. *Proceedings of the 8th International Coral Reef Symposium*, vol.

- 1, edited by Lessios, H. A. and MacIntyre, I. G., 483–488, Smithsonian Trop. Res. Instit., Balboa, Panama.
- Pelinovsky, E., Zahibo, N., Dunkley, P., Edmonds, M., Herd, R., Talipova, T., Kozelkov, A., and Nikokina, I. (2004). Tsunami Generated by the Volcano Eruption on July 12-13, 2003 at Montserrat, Lesser Antilles. *Science of Tsunami Hazards*. 22, 1, 44-57.
- Peterson, D. (1976). Processes of volcanic island growth, Kilauea Volcano, Hawaii, 1969–1973. *Proceedings of the Symposium “Andean and Antarctic Volcanology Problems.”* Spec. Series Internat. Assoc. of Volcanology and Chemistry of the Earth's Interior, pp172–189.
- Radice, B. (1969). *The Letters of the Younger Pliny* (1 ed.). London: Penguin Books Ltd.
- Ramalho, I., Omira, R., El Moussaoui, S., Baptista, M. A., Zaghloul, M. N. (2018). Tsunami-induced morphological change – A model-based impact assessment of the 1755 tsunami in NE Atlantic from the Morocco coast. *Geomorphology*, 319, 78-91. <https://doi.org/10.1016/j.geomorph.2018.07.013>.
- Ramalho, R., Quartau, R., Trenhaile, A., Mitchell, N., Woodroffe, C., & Ávila, S. (2013). Coastal evolution on volcanic oceanic islands: A complex interplay between volcanism, erosion, sedimentation, sea-level change and biogenic production. *Earth-Science Reviews*. (127), 140-170. <https://doi.org/10.1016/j.earscirev.2013.10.007>.
- Ramsey, C. B. (2009). Bayesian analysis of radiocarbon dates. *Radiocarbon*, 51 (1), 337-360. <https://doi.org/10.1017/S0033822200033865>.
- Reguero, B. G., Beck, M. W., Agostini, V. N., Kramer, P. (2018). Coral reefs for coastal protection: A new methodological approach and engineering case study in Grenada. *Journal of Environmental Management*. 210, 146-161. <https://doi.org/10.1016/j.jenvman.2018.01.024>.

- Reuter, M., and Piller, W. E. (2011). Volcaniclastic events in coral reef and seagrass environments: evidence for disturbance and recovery (Middle Miocene, Styrian Basin, Austria). *Coral Reefs*. 30, 889–899. <https://doi.org/10.1007/s00338-011-0798-3>.
- Reynolds, J. M. (1997). *An Introduction to Applied and Environmental Geophysics*. John Wiley and Sons. Chichester. 796p.
- Rodolfo, K. S. (2000). The Hazard from Lahars and Jökulhlaups. In Sigurdsson, H., Houghton, B., Rymer, H., Stix, J., and McNutt, S. *Encyclopedia of Volcanoes*. London: Academic Press.
- Rose, W. I., and Durant, A. J. (2009). Fine ash content of explosive eruptions. *Journal of Volcanology and Geothermal Research*. 186, 1, 32-39. <https://doi.org/10.1016/j.jvolgeores.2009.01.010>.
- Salvany, T., Lahitte, P., Nativel, P., Gillot, P-Y. (2012). Geomorphic evolution of the Piton des Neiges volcano (Réunion Island, Indian Ocean): Competition between volcanic construction and erosion since 1.4 Ma. *Geomorphology*. 136, 1, 132-147. <https://doi.org/10.1016/j.geomorph.2011.06.009>.
- Santos, F., Gómez-Gesteira, M., Varela, R., Ruiz-Ochoa, M., and Días, J. M. (2016). Influence of upwelling on SST trends in La Guajira system. *J. Geophys. Res. Oceans*. 121, 2469–2480. <https://doi.org/10.1002/2015JC011420>.
- Sathiamurthy, E., and Voris, H. K. (2006). Maps of Holocene Sea Level Transgression and Submerged Lakes on the Sunda Shelf. *The Natural History Journal of Chulalongkorn University*, Supplement 2: 1-43.
- Schils, T. (2012). Episodic Eruptions of Volcanic Ash Trigger a Reversible Cascade of Nuisance Species Outbreaks in Pristine Coral Habitats. *PLoS ONE* 7(10): e46639. <https://doi.org/10.1371/journal.pone.0046639>.
- Schmitz, W. J. (1996). On the world ocean circulation: volume II. *Technical report WHOI-96-08*. Woods Hole Oceanographic Institution, December 1996.

- Schneider, J.-L., Torrado, F. J. P., Torrente, D. G., Wassmer, P., Santana, M. D. C. C., Carracedo, J. C. (2004). Sedimentary signatures of the entrance of coarse-grained volcanoclastic flow into the sea: the example of the breccia units of the Las Palmas Detritic Formation (Mio–Pliocene, Gran Canaria, Eastern Atlantic, Spain). *Journal of Volcanology and Geothermal Research*. 138, 295-323. <https://doi.org/10.1016/j.jvolgeores.2004.07.007>.
- Schubel, J. R. (1977). Sediment and the quality of the estuarine environment: Some observations. In: I. H. Suffet. *Fate of pollutants in the air and water environments*. Part 1. Mechanism of interaction between environments and the mathematical modeling and the physical fate of pollutants. John Wiley and Sons, New York.
- Schwartz, M. L. (2005). *Encyclopedia of Coastal Science*. Springer, Dordrecht, the Netherlands.
- Schwendel, A., Fuller, I., & Death, R. (2012). Assessing DEM interpolation methods for effective representation of upland stream morphology for rapid appraisal of bed stability. *River Research and Applications*, 28(5), 567-584. <https://doi.org/10.1002/rra.1475>.
- Searle, M. (2006). Co-seismic uplift of coral reefs along the western Andaman Islands during the December 26th, 2004 earthquake. *Coral Reefs*. 25, 1, p2-2. <https://doi.org/10.1007/s00338-005-0051-z>.
- Segschneider, B., Landis, C. A., Manville, V., White, J. D. L., Wilson, C. J. N. (2002). Environmental response to a large, explosive rhyolite eruption: sedimentology of post-1.8 ka pumice-rich Taupo volcanoclastics in the Hawke's Bay region, New Zealand. *Sedimentary Geology*. 150, 275–299. [https://doi.org/10.1016/S0037-0738\(01\)00200-7](https://doi.org/10.1016/S0037-0738(01)00200-7).
- Sekretariat Kabinet Republik Indonesia. (2017). PBB Verifikasi 16,056 Nama Pulau Indonesia. Available at: <http://setkab.go.id/pbb-verifikasi-16-056-nama-pulau-indonesia> (accessed on 06 April 2018).

- Self, S., and Rampino, M. R. (1981). The 1883 eruption of Krakatau. *Nature*. 294, 699-704. <https://doi.org/10.1038/294699a0>.
- Shepard, F. P. (1973). *Submarine Geology (3rd edition)*. Harper and Row, New York.
- Shore Protection Manual. (1984). *Shore Protection Manual, Volume 1*. Coastal Engineering Research Center, US Army, Washington.
- Sidik, F., Neil, D., Lovelock, C. E. (2016). Effect of high sedimentation rates on surface sediment dynamics and mangrove growth in the Porong River, Indonesia. *Marine Pollution Bulletin*. 107, 355–363. <https://doi.org/10.1016/j.marpolbul.2016.02.048>.
- Sigl, M., Winstrup, M., McConnell, J. R., Welten, K. C., Plunkett, G., Ludlow, F., Büntgen, U., Caffee, M., Chellman, N., Dahl-Jensen, D., Fischer, H., Kipfstuhl, S., Kostick, C., Maselli, O. J., Mekhaldi, F., Mulvaney, R., Muscheler, R., Pasteris, D. R., Pilcher, J. R., Salzer, M., Schüpbach, S., Steffensen, J. P., Vinther, B. M., Woodruff, T. E. (2015). Timing and climate forcing of volcanic eruptions for the past 2,500 years. *Nature*, 523 (7562), 543–549. <http://doi.org/10.1038/nature14565>.
- Sigurdsson, H. (2009). The Environmental and Geomorphological Context of the Volcano. In Dobbins, J. J. and Foss, P. *The World of Pompeii*. London: Routledge.
- Sigurdsson, H., and Carey, S. (1989). Plinian and co-ignimbrite tephra fall from the 1815 eruption of Tambora volcano. *Bulletin of Volcanology*. 51, 4, 243-270. <https://doi.org/10.1007/BF01073515>.
- Sigurdsson, H., Carey, S., Mandeville C. W., and Bronto, S. (1991). Pyroclastic flows of the 1883 Krakatau eruption. *EOS*, 72, 377-392. <https://doi.org/10.1029/90EO00286>.
- Silva, R., Mendoza, E., Mariño-Tapia, I., Martinez, M. L., and Escalante, E. (2016). An artificial reef improves coastal protection and provides a base for coral recovery.

Journal of Coastal Research. SI (75), 467-471. <https://doi.org/10.2112/SI75-094.1>.

Simkin, T., and Fiske, R. (1983). *Krakatau 1883: The Volcanic Eruption and Its Effects*. Washington, D.C.: Smithsonian Institution Press.

Simons, W., Socquet, A., Vigny, C., Ambrosius, B., Haji Abu, S., Promthong, C., Subarya, C., Sarsito, D. A., Matheussen, S., Morgan, P., Spakman, W. (2007). A decade of GPS in Southeast Asia: Resolving Sundaland motion and boundaries. *Journal of Geophysical Research*, 112(B06420). <https://doi.org/10.1029/2005JB003868>.

Skidmore, A. (1989). A comparison of techniques for calculating gradient and aspect from a gridded digital elevation model. *International Journal of Geographical Information Systems*, 3(4), 323-334. <https://doi.org/10.1080/02693798908941519>.

Smart, G. M., Crowley, K. H. M., and Lane, E. M. (2016). Estimating tsunami run-up. *Natural Hazards*. 80, 3, 1933-1947. <https://doi.org/10.1007/s11069-015-2052-8>.

Smith, G., and Fritz, W. (1989). Volcanic influence on terrestrial sedimentation. *Geology*. 17, 375-376. [https://doi.org/10.1130/0091-7613\(1989\)017<0375:VIOTS>2.3.CO;2](https://doi.org/10.1130/0091-7613(1989)017<0375:VIOTS>2.3.CO;2).

Smith G. A., and Lowe D. R. (1991). Lahars: Volcano-hydrologic events and deposition in the debris flow—hyperconcentrated flow continuum. In *Sedimentation in Volcanic Settings*. Fisher R.V., Smith G.A. (Eds.), Soc. Sediment. Geol. (SEPM), Spec. Publ. 45 (1991), pp. 59-70.

Solihuddin, T. (2014). A Drowning Sunda Shelf Model during Last Glacial Maximum (LGM) and Holocene: A Review. *Indonesian Journal on Geoscience*. 1, 2. <https://doi.org/10.17014/ijog.v1i2.182>.

- Soloviev, S. L., and Go, C. N. (1974). *A Catalogue of Tsunami on the Western Shore of the Pacific Ocean*, translated by Canada Institute for Scientific and Technical Information, National Research Council Ottawa, Nauka House, Moscow.
- Stix, J., and Gaonac'h, H. (2000). Gas, Plume, and Thermal Monitoring. In Sigurdsson, H., Houghton, B., Rymer, H., Stix, J., and McNutt, S. *Encyclopedia of Volcanoes*. London: Academic Press.
- Stothers, R. B. (1984). The Great Tambora Eruption in 1815 and Its Aftermath. *Science*. 224, 4654, 1191-1198. <https://doi.org/10.1126/science.224.4654.1191>.
- Stothers, R. B. (1998). Far Reach of the Tenth Century Eldgjá Eruption, Iceland. *Climatic Change* (39), 715-726.
- Stothers, R. B. (2000). Climatic and demographic consequences of the massive volcanic eruption of 1258. *Climatic Change*. 45, 361-374. <https://doi.org/10.1023/A:1005523330643>.
- Su, M., Yao, P., Wang, Z. B., Zhang, C. K., Stive, M. J. F. (2017). Exploratory morphodynamic hindcast of the evolution of the abandoned Yellow River Delta, 1578–1855 CE. *Marine Geology*. 383, 99–119. <https://doi.org/10.1016/j.margeo.2016.11.007>.
- Sudrajat, A., Mangga, A., Suwarna, N. (1998). *Geological Map of the Sumbawa Quadrangle, Nusa Tenggara*. Geological Research and Development Centre, Indonesian Geological Agency, Bandung.
- Sukardi, Y. (2010). Permasalahan Kawasan Segara Anakan. *Majalah Perencanaan Pembangunan*. BAPPENAS.
- Sulpizio, R. (2005). Three empirical methods for the calculation of distal volume of tephra-fall deposits. *J. Volcanol. Geoth. Res.* 145 (3-4), 315-336. <https://doi.org/10.1016/j.jvolgeores.2005.03.001>.
- Sulpizio, R., Dellino, P., Doronzo, D. M., Sarocchi, D. (2014). Pyroclastic density currents: state of the art and perspectives. *Journal of Volcanology and*

<http://dx.doi.org/10.1016/j.jvolgeores.2014.06.014>.

- Sunarto. (2000). Kausalitas Poligenetik dan Ekuilibrium Dinamik sebagai Paradigma dalam Pengelolaan Ekosistem Pesisir. *Prosiding Seminar Nasional Pengelolaan Ekosistem Pantai dan Pulau-pulau Kecil Dalam Konteks Negara Kepulauan*. Badan Penerbit Fakultas Geografi, UGM, Yogyakarta. 84-90.
- Sutarna, I. N. (1990). Shape and condition of living coral colonies in the waters around Banda Islands, Central Maluku. In: Praseno D. P., Atmadja, W. S. (eds) *Waters of the Maluku and its Environments*. Indonesian Institute of Sciences (LIPI), Ambon. 135-147.
- Szczuciński, W., Kokociński, M., Rzeszewski, M., Chagué-Gof, C., Cachão, M., Goto, K., Sugawara, D. (2012). Sediment sources and sedimentation processes of 2011 Tohoku-Oki tsunami deposits on the Sendai Plain, Japan — Insights from diatoms, nannoliths and grain size distribution. *Sedimentary Geology*. 282, 40-56.
<https://doi.org/10.1016/j.sedgeo.2012.07.019>.
- Takada, A., Nasution, A., Rosgandika, M. (2003). Eruptive history during the last 10ky for the caldera-forming eruption of Rinjani volcano. In: *Abstracts of Japan Earth and Planet Sci. Joint Meet*, Chiba, Japan, 26–29 May 2003.
- Tan, K. H. (2008). *Soils in the Humid Tropics and Monsoon Region of Indonesia*. CRC Press. Florida, USA.
- Tani, K., Fiske, R. S., Tamura, Y., Kido, Y., Naka, J., Shukuno, H., Takeuchi, R. (2008). Sumisu volcano, Izu-Bonin arc, Japan: site of a silicic caldera-forming eruption from a small open-ocean island. *Bulletin of Volcanology*. 70, 5, 547-562.
<https://doi.org/10.1007%2Fs00445-007-0153-2>.
- Telford, W. M., Geldart, L. P., Sheriff, R. E. (1990). *Applied Geophysics*. Cambridge University Press.

- Tomascik, T., van Woesik, R., and Mah, A. J. (1996) Rapid coral colonization of a recent lava flow following a volcanic eruption, Banda Islands, Indonesia. *Coral Reefs*. 1, 169–175. <https://doi.org/10.1007/BF01145887>.
- Torrecillas, C., Berrocoso, M., Felpeto, A., Torrecillas, M. D., Garcia, A. (2013). Reconstructing palaeo-volcanic geometries using a Geodynamic Regression Model (GRM): Application to Deception Island volcano (South Shetland Islands, Antarctica). *Geomorphology*. 182, 79-88. <https://doi.org/10.1016/j.geomorph.2012.10.032>.
- Torrecillas, C., Berrocoso, M., Pérez-López, R., Torrecillas, M. D. (2012). Determination of volumetric variations and coastal changes due to historical volcanic eruptions using historical maps and remote-sensing at Deception Island (West-Antarctica). *Geomorphology*. 136, 1, 6-14. <https://doi.org/10.1016/j.geomorph.2011.06.017>.
- Udinstev, G. B. (2003). *International Geological-Geophysical Atlas of the Pacific Ocean*, 192p. Intergovernmental Oceanographic Commission, Moscow-Saint Petersburg.
- Valentin, H. (1952). *Die Küsten der Erde*. Petermanns Geografische Mitteilungen Ergänzungshft 246. Justies Perthes, Gotha.
- Vallance, J. W. (2000). Lahars. In Sigurdsson, H., Houghton, B., Rymer, H., Stix, J., and McNutt, S. *Encyclopedia of Volcanoes*. London: Academic Press.
- Vallance, J. W. (2005). Volcanic Debris Flow. In Jacob, M., and Hungr, O. (Ed.): *Debris-flow Hazards and Related Phenomena*. Praxis Publishing Ltd, Chichester.
- Vallance, J. W., and Iverson, R. M. (2000). Lahars and Their Deposits. In Sigurdsson, H., Houghton, B., Rymer, H., Stix, J., and McNutt, S. *Encyclopedia of Volcanoes*. London: Academic Press.

- van Bemmelen, R. W. (1949). *The Geology of Indonesia (Volume IA – General Geology of Indonesia and Adjacent Archipelagoes)*. Government Printing Office, The Hague.
- van den Bergh, G. D., Boer, W., de Haas, H., van Weering, Tj. C. E., van Wijhe, R. (2003). Shallow marine tsunami deposits in Teluk Banten (NW Java, Indonesia), generated by the 1883 Krakatau eruption. *Marine Geology*. 197, 1-4, 13-34. [https://doi.org/10.1016/S0025-3227\(03\)00088-4](https://doi.org/10.1016/S0025-3227(03)00088-4).
- Verstappen, H. Th. (2005). Volcanic Islands. In Gupta, A. *The Physical Geography of Southeast Asia, Volume 4 de Oxford Regional Environments*. OUP Oxford.
- Vidal, C. M., Komorowski, J.-C., Métrich, N., Pratomo, I., Kartadinata, N., Prambada, O., Michel, A., Carazzo, G., Lavigne, F., Rodysill, J., Fontijn, K., Surono. (2015). Dynamics of the major Plinian eruption of Samalas in 1257 A.D. (Lombok, Indonesia). *Bulletin of Volcanology*. 77(9), 73. <https://doi.org/10.1007/s00445-015-0960-9>.
- Vidal, C. M., Métrich, N., Komorowski, J.-C., Pratomo, I., Michel, A., Kartadinata, N., Robert, V., Lavigne, F. (2016). The 1257 Samalas eruption (Lombok, Indonesia): the single greatest stratospheric gas release of the Common Era. *Scientific Reports*. 6(34868). <https://doi.org/10.1038/srep34868>.
- Vieux, C., Chancrelle, Y., Aubanel, A., and Salvat, B. (2008). Les modifications de la ligne de rivage dans les îles de la Société (Polynésie française) : un indicateur des pressions anthropiques en zone côtière. *Le Journal de la Société des Océanistes*. 126-127, p59-66. <https://doi.org/10.4000/jso.3162>.
- Vogel, S., & Märker, M. (2010). Reconstructing the Roman topography and environmental features of the Sarno River Plain (Italy) before the AD 79 eruption of Somma–Vesuvius. *Geomorphology*(115), 67-77. <https://doi.org/10.1016/j.geomorph.2009.09.031>.

- Vogel, S., Märker, M., & Seiler, F. (2011). Revised modeling of the post-AD 79 volcanic deposits of Somma-Vesuvius to reconstruct the pre-AD 79 topography of the Sarno River plain (Italy). *Geologica Carpathica*, 62(1), 5-16. <https://doi.org/10.2478/v10096-011-0001-3>.
- von Huene, R., Miller, J. J., Klaeschen, D., Dartnell, P. (2016). A Possible Source Mechanism of the 1946 Unimak Alaska Far-Field Tsunami: Uplift of the Mid-Slope Terrace above a Splay Fault Zone. *Pure Appl. Geophys.* 173, p4189–4201. <https://doi.org/10.1007/s00024-016-1393-x>.
- Voris, H. K. 2000. Maps of Pleistocene Sea Levels in South East Asia: Shorelines, River Systems, Time Durations. *Journal of Biogeography*. 27:1153-1167.
- Vroom, P. S., and Zgliczynski, B. J. (2011). Effects of volcanic ash deposits on four functional groups of a coral reef. *Coral Reefs*. 30, 1025–1032. <https://doi.org/10.1007/s00338-011-0793-8>.
- Wacana, L. (1979). *Babad Lombok*. Jakarta: Departemen Pendidikan dan Kebudayaan Republik Indonesia.
- Walker, G. P. L. (1981). Generation and dispersal of fine ash and dust by volcanic eruptions. *J. Volcanol. Geotherm. Res.* 11: 81-92. [https://doi.org/10.1016/0377-0273\(81\)90077-9](https://doi.org/10.1016/0377-0273(81)90077-9).
- Wang, X., Liu, P. L. F. (2005). A numerical investigation of Boumerdes-Zemmouri (Algeria) earthquake and tsunami. *Comput. Model. Eng. Sci.* 10 (2), 171. <https://doi.org/10.3970/cmesc.2005.010.171>.
- Wang, X., Liu, P. L. F. (2006). An analysis of 2004 Sumatra earthquake fault plane mechanisms and Indian Ocean tsunami. *J. Hydraul. Res.* 44 (2), 147–154. <https://doi.org/10.1080/00221686.2006.9521671>.
- Wang, X., Liu, P. L. F. (2007). Numerical simulations of the 2004 Indian Ocean tsunamis—coastal effects. *J. Earthq. Tsunami* 1 (03), 273–297. <https://doi.org/10.1142/S179343110700016X>.

- Wang, Z. B., van Maren, D. S., Ding, P. X., Yang, S. L., van Prooijen, B. C., de Vet, P. L. M., Winterwerp, J. C., de Vriend, H. J., Stive, M. J. F., He, Q. (2015). Human impacts on morphodynamic thresholds in estuarine systems. *Continental Shelf Research*. 111, 174–183. <https://doi.org/10.1016/j.csr.2015.08.009>.
- Wilson, C. J. N., and Houghton, B. F. (2000). Pyroclastic Transport and Deposition. In Sigurdsson, H., Houghton, B., Rymer, H., Stix, J., and McNutt, S. *Encyclopedia of Volcanoes*. London: Academic Press.
- Wright, H. M. N., Roberts, J. J., Cashman, K. V. (2006). Permeability of anisotropic tube pumice: Model calculations and measurements. *Geophys. Res. Lett.* 33, L17316. <https://doi.org/10.1029/2006GL027224>.
- Wu, C-C., Shen, C-C., Chang, C-C., Yu, K-F., Chou, Y-M, Pallister, J., Burr, G., Lo, L. (2018). Pinatubo Volcanic Eruption Exacerbated an Abrupt Coral Mortality Event in 1991 Summer. Poster in *AOGS 15th Annual Meeting*, 3-8 June 2018, Honolulu, Hawaii.
- Yang, H., Wang, C., Ma, T., & Guo, W. (2015). Accuracy assessment of interpolation methods in grid DEMs based on a variance-scale relation. *Environmental Earth Sciences*(74), 6525-6539. <https://doi.org/10.1007/s12665-015-4388-5>.
- Yang, L., Meng, X., & Zhang, X. (2011). SRTM DEM and its application advances. *International Journal of Remote Sensing*, 32(14), 3875-3896. <https://doi.org/10.1080/01431161003786016>.
- Yokoyama, I. (1987). A scenario of the 1883 Krakatau tsunami. *Journal of Volcanology and Geothermal Research*. 34, 1-2, 123-132. [https://doi.org/10.1016/0377-0273\(87\)90097-7](https://doi.org/10.1016/0377-0273(87)90097-7).
- Yokoyama, I. (2015). Eruption products of the 1883 eruption of Krakatau and their final settlement. *Annals of Geophysics*, 58, 2, S0220. <https://doi.org/10.4401/ag-6529>.

- Zhang, T., Xu, X., & Xu, S. (2015). Method of establishing an underwater digital elevation terrain based on kriging interpolation. *Measurement* (63), 287-298. <https://doi.org/10.1016/j.measurement.2014.12.025>.
- Zhong, G., Geng, J., Wong, H. K., Ma, Z., & Wu, N. (2004). A semi-quantitative method for the reconstruction of eustatic sea level history from seismic profiles and its application to the southern South China Sea. *Earth and Planetary Science Letters*(223), 443-459. <https://doi.org/10.1016/j.epsl.2004.04.039>.
- Zhu, L., He, Q., Shen, J., Wang, Y. (2016). The influence of human activities on morphodynamics and alteration of sediment source and sink in the Changjiang Estuary. *Geomorphology*. 273, 52–62. <https://doi.org/10.1016/j.geomorph.2016.07.025>.
- Zimmerman, D., Pavlik, C., Ruggles, A., & Armstrong, M. (1999). An Experimental Comparison of Ordinary and Universal Kriging and Inverse Distance Weighting. *Mathematical Geology*, 31(4), 375-390. <https://doi.org/10.1023/A:1007586507433>.

Table of Contents

| | |
|--|----|
| Abstract..... | 2 |
| Sommaire | 4 |
| Executive Summary in French..... | 6 |
| Acknowledgments..... | 12 |
| Introduction..... | 16 |
| PART 1 | 22 |
| State of the art, field presentation, and research methodology | 22 |
| Chapter 1: Coastal evolution related to volcanic eruptions..... | 24 |
| 1.1. Coastal dynamics in the tropical area | 24 |
| 1.1.1. Conceptual framework and terminology..... | 24 |
| 1.1.2. Typology of the coastal area | 27 |
| 1.1.3. Factors influencing coastal dynamics | 29 |
| 1.2. Coastal sedimentation caused by volcanism | 35 |
| 1.2.1. Fallout | 35 |
| 1.2.2. Pyroclastic density currents (PDCs)..... | 37 |
| 1.2.3. Lahars | 40 |
| 1.3. Impacts of volcanic materials at sea | 43 |
| 1.3.1. High sedimentation due to volcanic activity | 43 |
| 1.3.2. Volcanic eruption-induced tsunami | 44 |
| 1.3.3. Disturbances and mortalities of corals | 49 |
| 1.4. Conclusion..... | 51 |
| Chapter 2: Lombok Island, Sumbawa Island, and Samalas volcano..... | 54 |
| 2.1. Lombok and Sumbawa Islands | 54 |
| 2.2. Samalas volcano | 60 |
| 2.3. Study area: coastal areas along the Alas Strait | 63 |
| 2.4. Conclusion..... | 67 |
| Chapter 3: Research methodology | 68 |
| 3.1. Field measurements..... | 68 |
| 3.1.1. Stratigraphic data | 68 |
| 3.1.2. Geophysical measurements..... | 72 |

| | | |
|---|--|-----|
| 3.1.3. | Tsunami deposits | 74 |
| 3.2. | Laboratory and computational analysis | 78 |
| 3.2.1. | Geochemical analysis | 78 |
| 3.2.2. | Radiocarbon dating | 80 |
| 3.2.3. | Geospatial database using ArcGIS | 81 |
| 3.3. | Exegesis of written sources | 82 |
| 3.4. | Conclusion | 85 |
| PART 2 | | 88 |
| Geomorphic impacts of the 1257 CE eruption of Samalas volcano along the Alas Strait | | 88 |
| Chapter 4: Local impacts of the 1257 CE eruption in East Lombok | | 90 |
| 4.1. | Field data | 90 |
| 4.2. | Computational Analysis | 101 |
| 4.2.1. | Reconstruction of the pre-1257 CE topography | 101 |
| 4.2.2. | Primary volcanic deposits | 103 |
| 4.2.3. | Erosion of PDC deposits | 105 |
| 4.3. | Discussion | 107 |
| 4.4. | Conclusion | 114 |
| Chapter 5: Regional impacts of the 1257 CE eruption in West Sumbawa | | 116 |
| 5.1. | Evidence of volcanic deposits from the 1257 CE eruption of Samalas volcano along the west coast of Sumbawa | 116 |
| 5.2. | Information from Babad Lombok and Babad Suwung | 117 |
| 5.2.1. | Babad Lombok | 117 |
| 5.2.2. | New relevant information from Babad Suwung | 119 |
| 5.3. | Discussion | 123 |
| 5.3.1. | Description of a volcanic eruption in written sources | 123 |
| 5.3.2. | Long-term impacts of the eruption on population and landuse on the west coast of Sumbawa | 131 |
| 5.4. | Conclusion | 133 |
| Chapter 6: Did the 1257 CE eruption of Samalas trigger a tsunami? | | 134 |
| 6.1. | Belang Island | 135 |
| 6.2. | Abandoned fishponds | 138 |
| 6.3. | Discussion | 148 |
| 6.4. | Conclusion | 153 |
| Conclusion | | 156 |

| | |
|--|-----|
| References | 160 |
| Table of Contents | 194 |
| List of Figures | 198 |
| List of Tables | 204 |
| APPENDICES..... | 206 |
| Appendix 1: Stratigraphic data | 208 |
| Appendix 2: Perpendicular and parallel transects | 254 |
| Appendix 3: Grain-size analysis | 256 |

List of Figures

| | |
|--|----|
| Figure 1. Onshore distribution of PDC deposits emplaced during phase P4, and isopach contours of associated P4 co-PDC ash fallout (in cm) (Source: Vidal et al., 2015). | 18 |
| Figure 2. Ph.D. thesis outline. | 21 |
| Figure 3. Coastal populations, marine protected areas, and large marine ecosystems around the world. The number of coastal population is a proportion of the population living within 100 km of the coast in 2000 (Source: Harrison and Pearce, 2000). | 25 |
| Figure 4. Coastal terminology (Source: Bird, 2008). | 26 |
| Figure 5. The processes series in the coastal area..... | 27 |
| Figure 6. The classification of coastal systems by Shepard (1973). | 29 |
| Figure 7. Factors influencing coastal dynamics. | 30 |
| Figure 8. Amount of sediment transported to the ocean (Source: Garrels and Mackenzie, 1971). | 33 |
| Figure 9. Total sediment thickness database for the world's oceans and marginal seas (Source: Divins, 2003). | 34 |
| Figure 10. Volcanic ash deposits are thick and coarse in particle size near the volcano. However, at a distance, the deposit gets thinner and finer. | 36 |
| Figure 11. Pumice raft in Tonga Islands, South Pacific from Aqua MODIS satellite on 10 August 2006 (Courtesy: NASA Earth Observatory, 2006). | 37 |
| Figure 12. Examples of PDCs generation from various eruptive processes (Source: Sulpizio et al., 2014). | 39 |
| Figure 13. Illustration of several scenarios where pyroclastic flows formed on land enters the sea (Source: Freundt, 2003). | 40 |
| Figure 14. The stratification of a volcanoclastic deposit (lahars) (Source: Fisher et Schmincke, 1984). | 42 |
| Figure 15. An illustration of the sources, transport, and processes of volcanic materials in the coastal area (Source: Carey, 2000). | 43 |
| Figure 16. Some causes of the volcanic eruption-induced tsunami (Source: Paris et al., 2013). | 46 |

| | |
|---|----|
| Figure 17. a) and b) Coral bleaching following to the 2003 CE eruption in Anatahan, the Northern Mariana Islands (Source: Vroom and Zgliczynski, 2011); c) Corals condition after the 1994 CE eruption in Rabaul Caldera, Papua New Guinea (Source: Maniwavie et al., 2001). | 50 |
| Figure 18. Coastal evolution related to volcanic eruptions..... | 52 |
| Figure 19. Lombok and Sumbawa Islands located in West Nusa Tenggara Province in Indonesia..... | 55 |
| Figure 20. Ten regencies in WNT Province and their superficies (in km ²). | 55 |
| Figure 21. The population of West Nusa Tenggara Province in 2016 by regency (Badan Pusat Statistik, 2016). | 56 |
| Figure 22. Numbers of inhabited and uninhabited islands in West Nusa Tenggara Province (Badan Pusat Statistik, 2016). | 57 |
| Figure 23. Chart of the strait of Alas that lay down from observations in the Van Sittart by Mr. George Robertson, 1781 (Source: Bibliothèque Nationale de France, 2007). | 58 |
| Figure 24. An example of a multiplatform application for geohazard mitigation and assessment for volcanic activities in Indonesia from Indonesian Centre for Volcanology and Geological Hazard Mitigation (CVGHM) http://magma.vsi.esdm.go.id/ . The color differences of the volcano on the map are related to the current status of the volcano, e.g., normal (green); minor activity (yellow); warning (orange); and erupting (red). | 60 |
| Figure 25. The Rinjani Volcanic Complex in Lombok Island. | 61 |
| Figure 26. The Segara Anak Lake and the active Barujari cone in the Rinjani Volcanic Complex (Courtesy: P. Guerin, July 2015). | 62 |
| Figure 27. Direction and distribution of PDCs from the 1257 CE eruption of Samalas (Source: Lavigne et al. 2013). | 63 |
| Figure 28. The people in West Nusa Tenggara Province mostly live in East Lombok since 1995 (Badan Pusat Statistik, 2016). | 64 |
| Figure 29. The study area of geomorphic impacts of the 1257 CE eruption of Samalas volcano. | 66 |
| Figure 30. Stratigraphic information and thickness data on the eastern part of Lombok. | 69 |
| Figure 31. Information from stratigraphic data measurement. | 69 |
| Figure 32. New cores drilling were conducted in the research area using the material and expertise of local drillers (Courtesy: B. Septiangga, July 2017). | 70 |

| | |
|--|----|
| Figure 33. An example of semi-quantitative data through interviews with the well's owners and local drillers..... | 71 |
| Figure 34. Geophysical measurements using a resistivity meter namely SuperSting (Courtesy: Y. Sudrajat, September 2015). | 72 |
| Figure 35. Resistivity lines on the eastern part of Lombok..... | 74 |
| Figure 36. Sample collection location in abandoned fishponds in Kiantar Village (T1 – T5) and Belang Island (T6) on the western coast of West Sumbawa. | 75 |
| Figure 37. Sample collection for radiocarbon dating, and to recognize and interpret tsunami deposits (Courtesy: P. Guerin, February 2016). | 76 |
| Figure 38. Beckman Coulter LS-13-320 Laser Diffraction Particle Size Analyzer device (Courtesy: Beckman Coulter website, June 2018). | 77 |
| Figure 39. Pumice and charcoal sampling: (a) from natural cliffs at Korleko coast (Courtesy: F. Lavigne, using a MavicPro drone, August 2017); and (b) from human-made outcrops in quarries at Dasan Geres (Courtesy: F. Lavigne, July 2015)..... | 79 |
| Figure 40. Samples of pumices for geochemical analysis (layer 1, 2, and 3) (Courtesy: F. Lavigne, July 2015). | 80 |
| Figure 41. Charcoal samples from layer number 2 (left) and 3 (right). | 81 |
| Figure 42. a) The popular version of Babad Lombok that translated to Bahasa Indonesia by Lalu Wacana in 1979; b) the original version of Babad Suwung; and c) Mr. Haji, the interpreter of old Javanese language in Mataram, Lombok (Courtesy: F. Lavigne, July 2015). | 83 |
| Figure 43. Song performance from the interpreter of Babad Suwung (Courtesy: P. Guerin, July 2016). | 84 |
| Figure 44. a) Field observation of pumice deposits in Talkuwang (Taliwang), Sumbawa and b) interviews with museum employee in Mataram (Courtesy: P. Guerin, July 2016). | 85 |
| Figure 45. The research methodology that used to understand geomorphic impacts of the 1257 CE eruption of Samalas volcano. | 86 |
| Figure 46. Examples of stratigraphic data with the information of: a) lahar deposits, b) no volcanic material due to extraction, c) flood-derived sand deposits, and d) pumice-rich PDC deposits in Korleko (red box with dashed lines). | 92 |
| Figure 47. An example of lahar deposits near Selong. We used the term of “lahar” for the material of sand with pumice fragments since the lahars on Lombok at that time were pumiceous. For lahars that contain pumice after a large | |

| | | |
|------------|---|-----|
| | eruption ($VEI \geq 4$), there is a mixture between a normal granulation for lithic and a lack of granulation for pumice vesicles, evenly distributed within the deposit (Fisher and Schmincke, 1984)..... | 93 |
| Figure 48. | The layer of pumice-rich PDC (DG1, DG2, and DG3) in Dasan Geres quarry (Courtesy: F. Lavigne, July 2015)..... | 94 |
| Figure 49. | Calibration of radiocarbon age to calendar years with the high probability density range method (HPD - SHCAL13). | 96 |
| Figure 50. | Five resistivity lines profiles in: a) AB-Karanganyar, b) CD-Ijobalit 1, c) EF-Korleko, d) GH-Ijobalit 2, and e) IJ-Ijobalit 3. | 98 |
| Figure 51. | Resistivity profiles in: a) AB-Karanganyar, b) CD-Ijobalit 1, c) EF-Korleko, d) GH-Ijobalit 2, and e) IJ-Ijobalit 3. Orange to dark red colors ($\rho \geq 300 \Omega m$) represents pumices or dry sand. Fine black lines mark the possible depth of the pumice layer..... | 100 |
| Figure 52. | (a) Present-day topography and (b) reconstructed pre-1257 CE topography. | 102 |
| Figure 53. | Modeled post-eruptive landscape evolution..... | 106 |
| Figure 54. | Pumice-rich PDC covered all the current plain in the aftermath of the 1257 CE eruption. Based on an interview with a local people, the PDC deposits were widespread a few decades ago. A sudden natural shift from the main rivers in Dasan Geres (Geres River), as well as intense quarrying activity, are both responsible for the accelerated erosion (Courtesy: F. Lavigne, July 2015)..... | 109 |
| Figure 55. | Exploitation of pumices material on the eastern part of Lombok (Courtesy: F. Lavigne, April 2016)..... | 112 |
| Figure 56. | Pumice extraction in Ijobalit (Courtesy: F. Lavigne, using a MavicPro drone, August 2017)..... | 112 |
| Figure 57. | Rice fields with the residue of pumice extraction as a background in a) Korleko and b) Ijobalit (Courtesy: b) F. Lavigne, July 2015). | 113 |
| Figure 58. | Cliffs in Korleko nowadays which is eroded by the strong waves. | 114 |
| Figure 59. | The P3 fallout deposits and the P4 PDC deposits were laid down all along the west part of Sumbawa (Source: Vidal et al., 2015). | 117 |
| Figure 60. | Reconstruction of original landforms in Rinjani Volcanic Complex based on the descriptions in Babad Lombok (Courtesy: P. Lahitte, 2015). | 118 |
| Figure 61. | The description in Babad Lombok about the consequences of the 1257 CE eruption of Samalas volcano. The English translation of this text is: "The | |

| | |
|---|-----|
| King and their peoples took refuge simultaneously; Lombok became very quiet, even seven days after the earthquakes happened, and afterward, they rebuilt their own homes" (Wacana, 1979; Lavigne et al., 2013)..... | 119 |
| Figure 62. The PDCs remained hot even after crossing 16 km of the sea..... | 121 |
| Figure 63. The sentence in Babad Suwung mentioned that there is no sea between Selaparang (Lombok Island) and Taliwang (Sumbawa Island)..... | 122 |
| Figure 64. The description in letters of Pliny related to the volcanic fallout following the 79 CE Vesuvius eruption (Source: Allen, 1915)..... | 124 |
| Figure 65. The description in letters of Pliny related to the pyroclastic surge following the 79 CE Vesuvius eruption (Source: Allen, 1915)..... | 126 |
| Figure 66. Pliny the Younger and his mother as the eyewitnesses of the sixth pyroclastic surges of Vesuvius eruption at Misenum. | 128 |
| Figure 67. The eruption near Talkuwang during 1257 – 1815 CE. | 130 |
| Figure 68. The number of peoples in West Nusa Tenggara Province. The populations in West Sumbawa are about 137,072 peoples, which is only 2.8% of total populations..... | 131 |
| Figure 69. Tsunami deposits in Belang Island and abandoned fishponds in Kiantar Village. a) As a small uninhabited island located in Gili Balu conservation area on the western coast of Sumbawa, this island dominated by mangrove ecosystems with several sandy areas; b) Sample collection location in abandoned fishponds in Kiantar Village; and c) Abandoned fishponds in Kiantar Village with the location of T4 and T5 sampling points as well as Alas Strait and Lombok Island on the west (left side). | 135 |
| Figure 70. The stratigraphic profile of an outcrop in Belang Island. | 136 |
| Figure 71. Calibration of radiocarbon age to calendar years for two coral samples in Belang Island. The result shows the 50 cm-thick of tsunami deposit in the island results from the 1257 CE eruption-induced tsunami..... | 137 |
| Figure 72. The location of T1, T2, and T3 sampling points in an abandoned fishpond in Kiantar Village with an example of an old massive tsunami deposit with a single ~1.5 m thick layer on sampling point of T1. | 139 |
| Figure 73. Stratigraphic profiles for all sampling points in abandoned fishponds in Kiantar Village. | 140 |
| Figure 74. Eight sediment samples collected on sample location T4 for grain-size analysis and its histogram of frequency from 0.017 μ m to 2000 μ m..... | 141 |

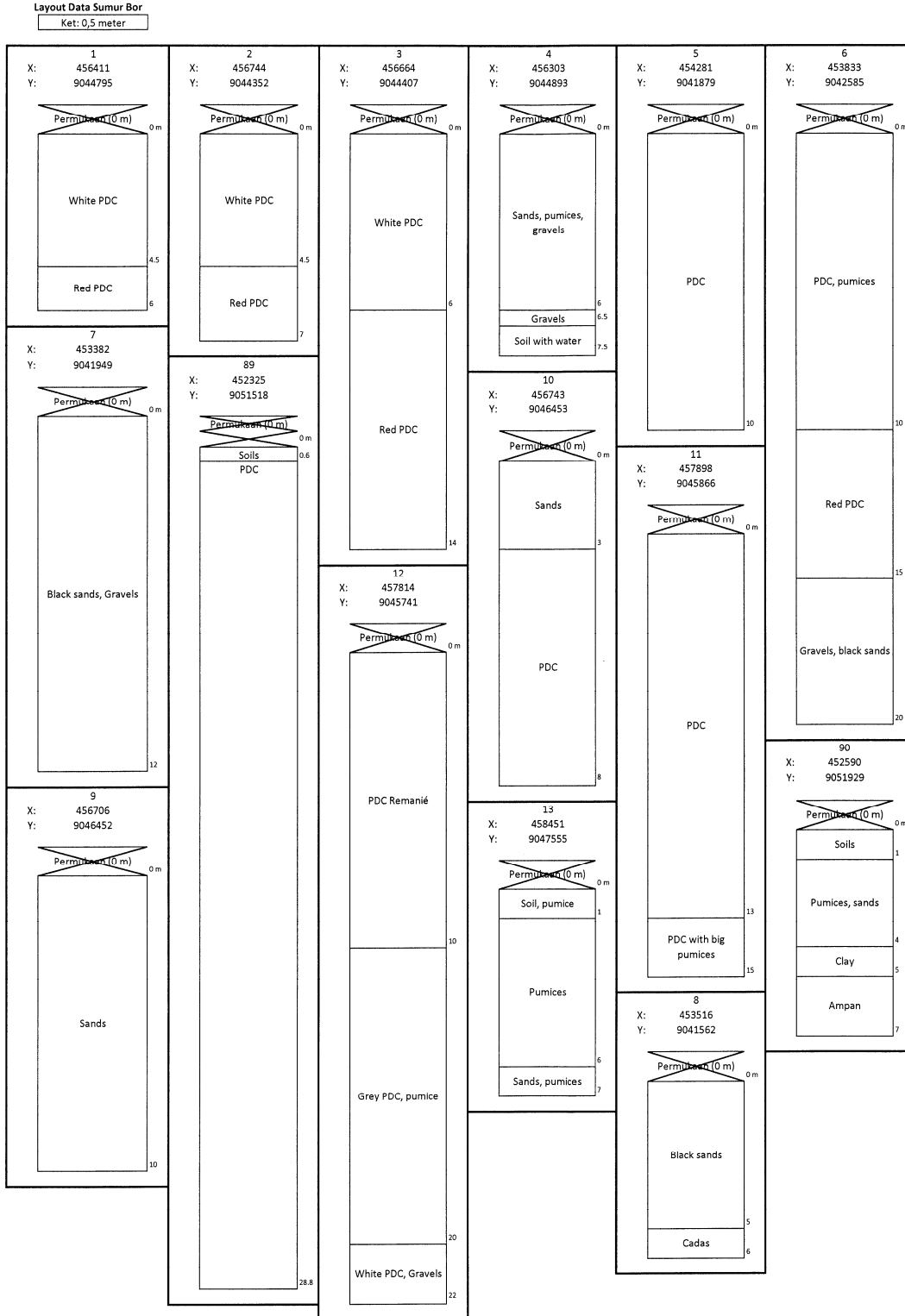
| | |
|--|-----|
| Figure 75. Triangle of textures from the sample collected from the T4 sampling point. | 143 |
| Figure 76. Calibration of radiocarbon age to calendar years for three samples of seashell (RIN-020316-X1-A, RIN-020316-X1-B, and RIN-020316-X1-C). | 146 |
| Figure 77. Calibration of radiocarbon age to calendar years with the high probability density range method (HPD - SHCAL13) for sample T3.1, T4.1, T4.2, and T4.3; and with calibration curve IntCal 13 in OxCal 4.3 program (Ramsey, 2009) for sample T2.1, T3.1, and Tsu13H2. | 147 |
| Figure 78. Dating results for coral and seashell samples in abandoned fishponds. . | 148 |
| Figure 79. Tsunami simulation in the Alas Strait by C. Gomez from Kobe University. | 149 |
| Figure 80. Spatial distribution of coral reefs along the Alas Strait in the present-day. Although the present-day condition of coral reef on the eastern part of Lombok and the western part of Sumbawa is very different, we assumed that before the eruption of Samalas volcano in 1257 CE, coral reefs in this area were in good conditions. This condition has maybe resulted in the absence of tsunami deposits from the 1257 CE eruption in this area. | 151 |
| Figure 81. General landscapes on the western coast of Sumbawa (Courtesy: A. Landa, 2016). | 152 |

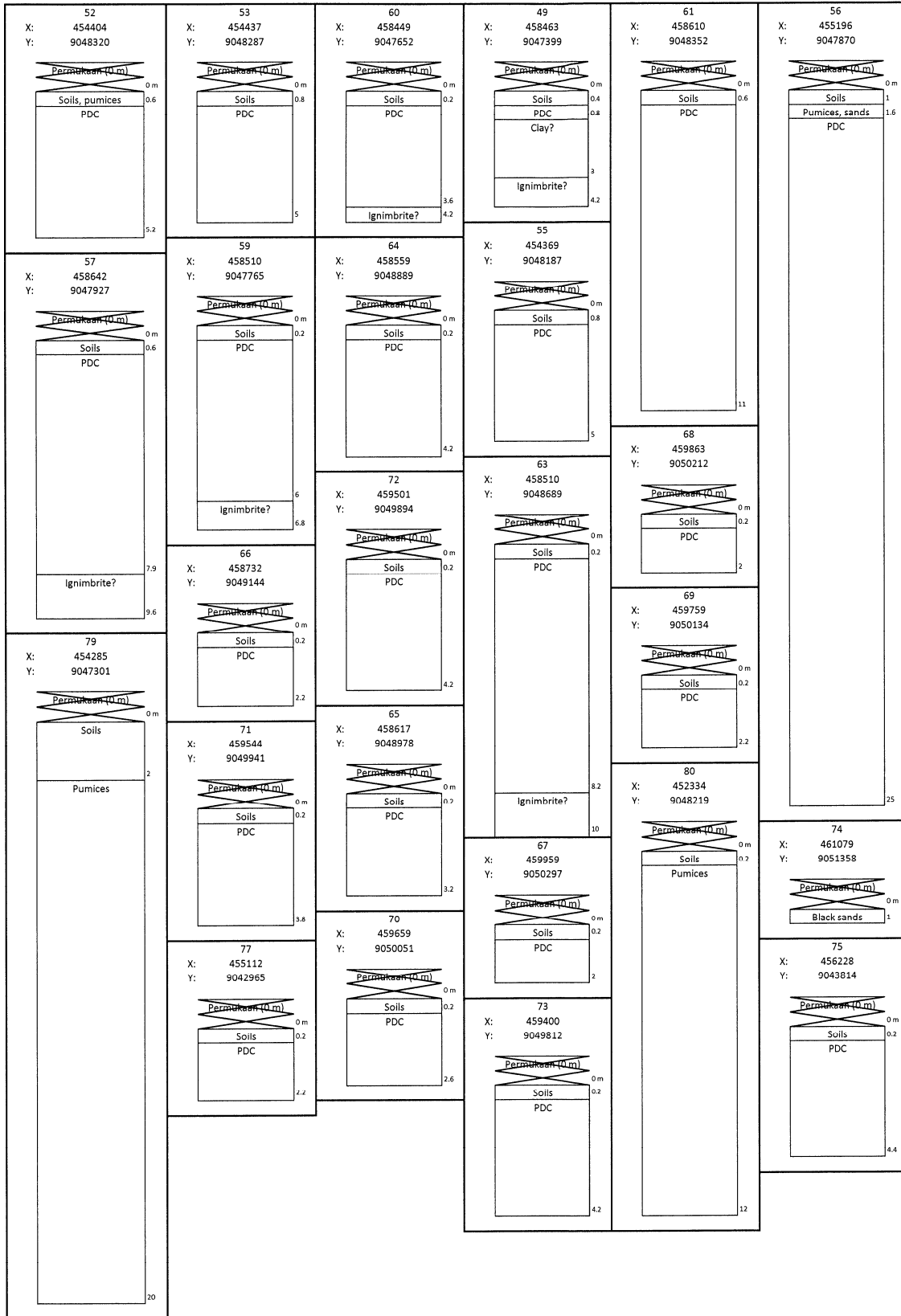
List of Tables

| | |
|---|-----|
| Table 1. Volcanic eruption-induced tsunami in Indonesia since 2100 BC (Latief et al., 2000; Paris et al., 2013; NGDC/WDS, 2018). | 47 |
| Table 2. Tsunamis due to pyroclastic flows that reached the sea in Indonesia since 2100 BC (Paris et al., 2013; NGDC/WDS, 2018). | 65 |
| Table 3. Geochemical analysis results at Dasan Geres (DG). | 95 |
| Table 4. Interpretation of how resistivity values corresponding to types of material on the eastern part of Lombok..... | 101 |
| Table 5. Cross-validation for the present-day and reconstructed pre-1257 CE topography..... | 101 |
| Table 6. Comparison of the volume of pumice-rich PDC deposits on eastern Lombok with those of other eruptions with a VEI \geq 6. | 111 |
| Table 7. List of volcanic eruption during 1257 – 1815 CE in the Lesser Sunda Islands. | 130 |
| Table 8. Radiocarbon dates for samples from Belang Island..... | 137 |
| Table 9. Grain-size distribution for the sample collected from the T4 sampling point. | 142 |
| Table 10. Soil classification for the sample collected from the T4 sampling point..... | 144 |
| Table 11. Radiocarbon dates for samples from abandoned fishponds in Kiantar Village. | 146 |

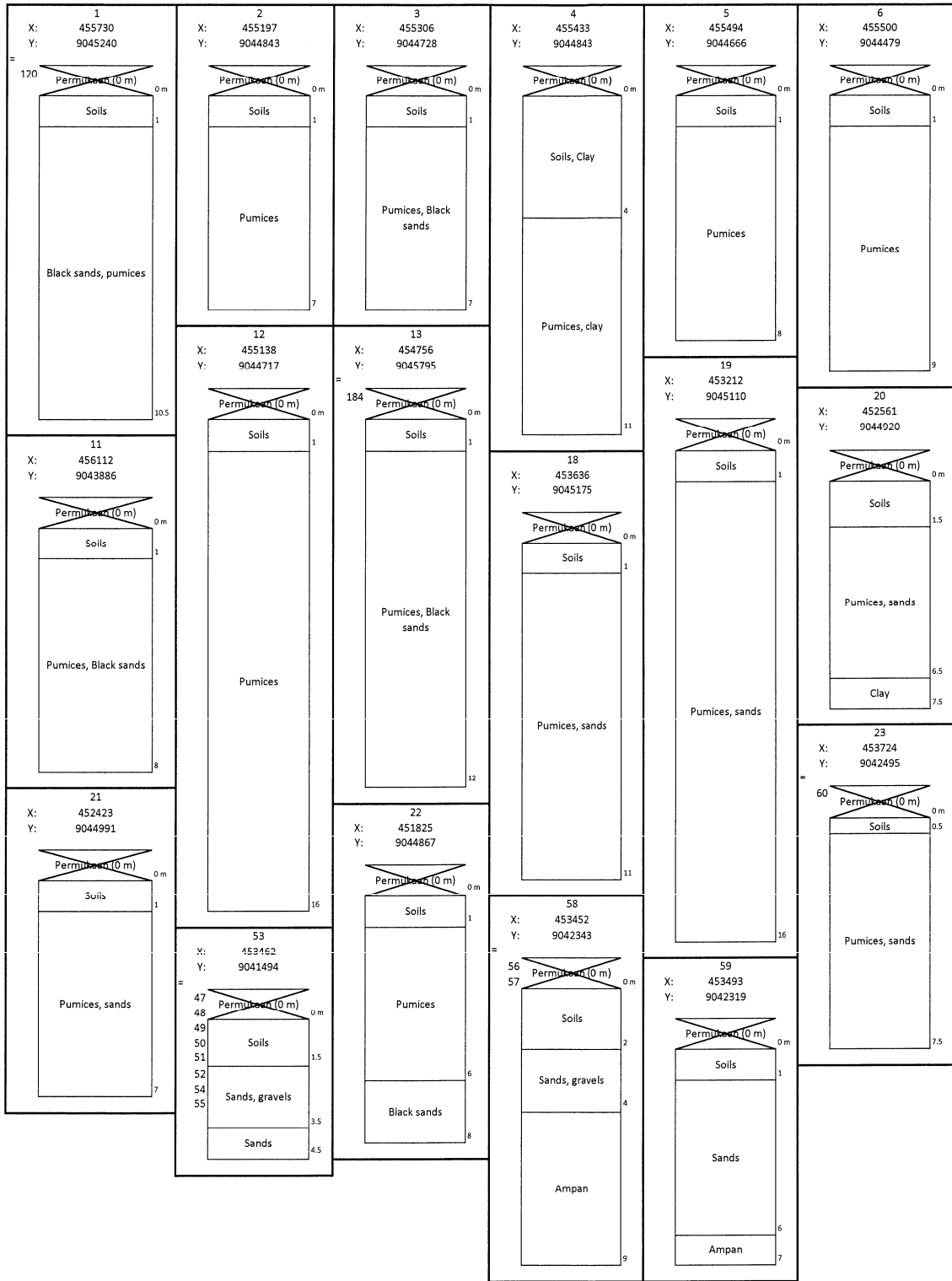
APPENDICES

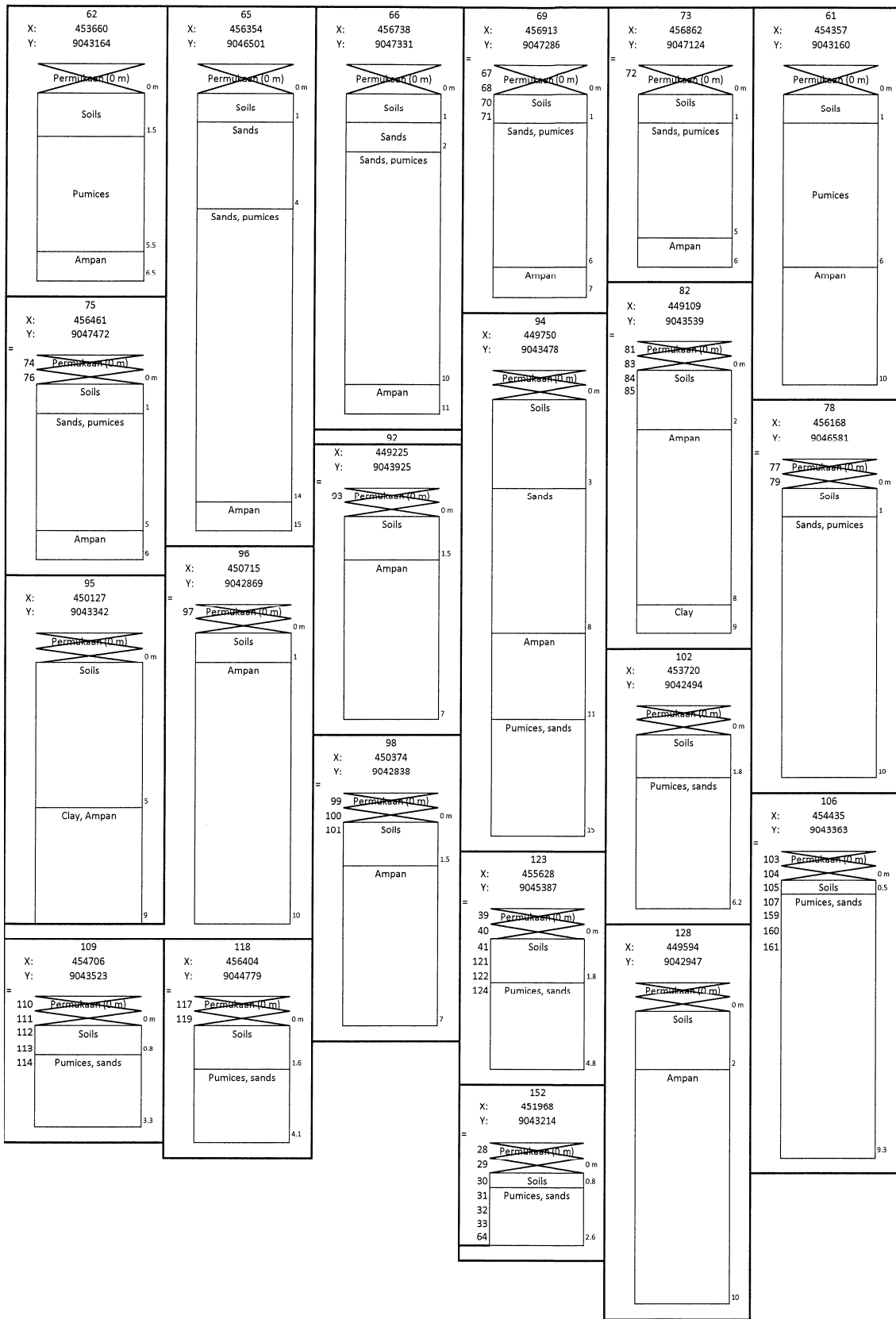
Appendix 1: Stratigraphic data



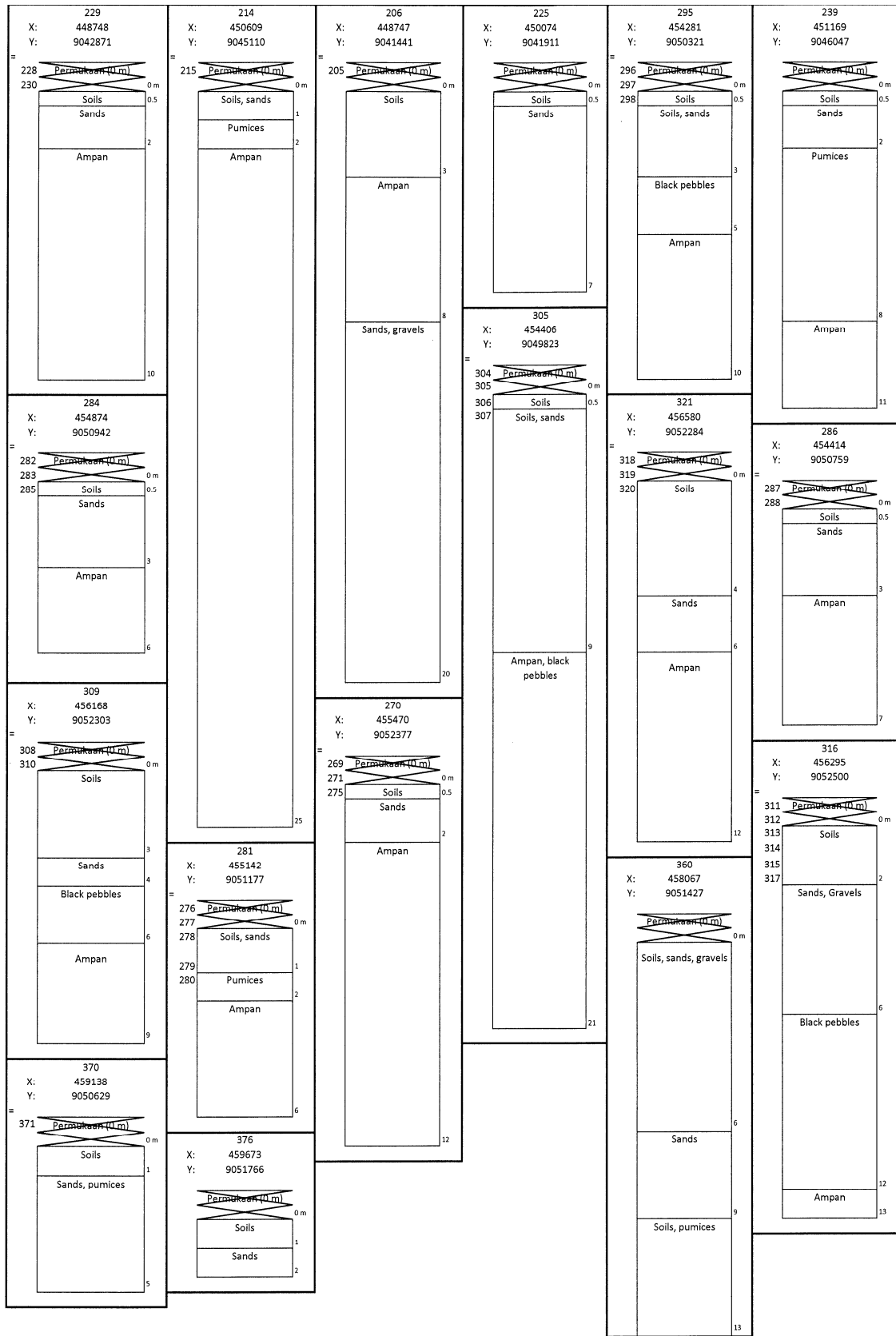


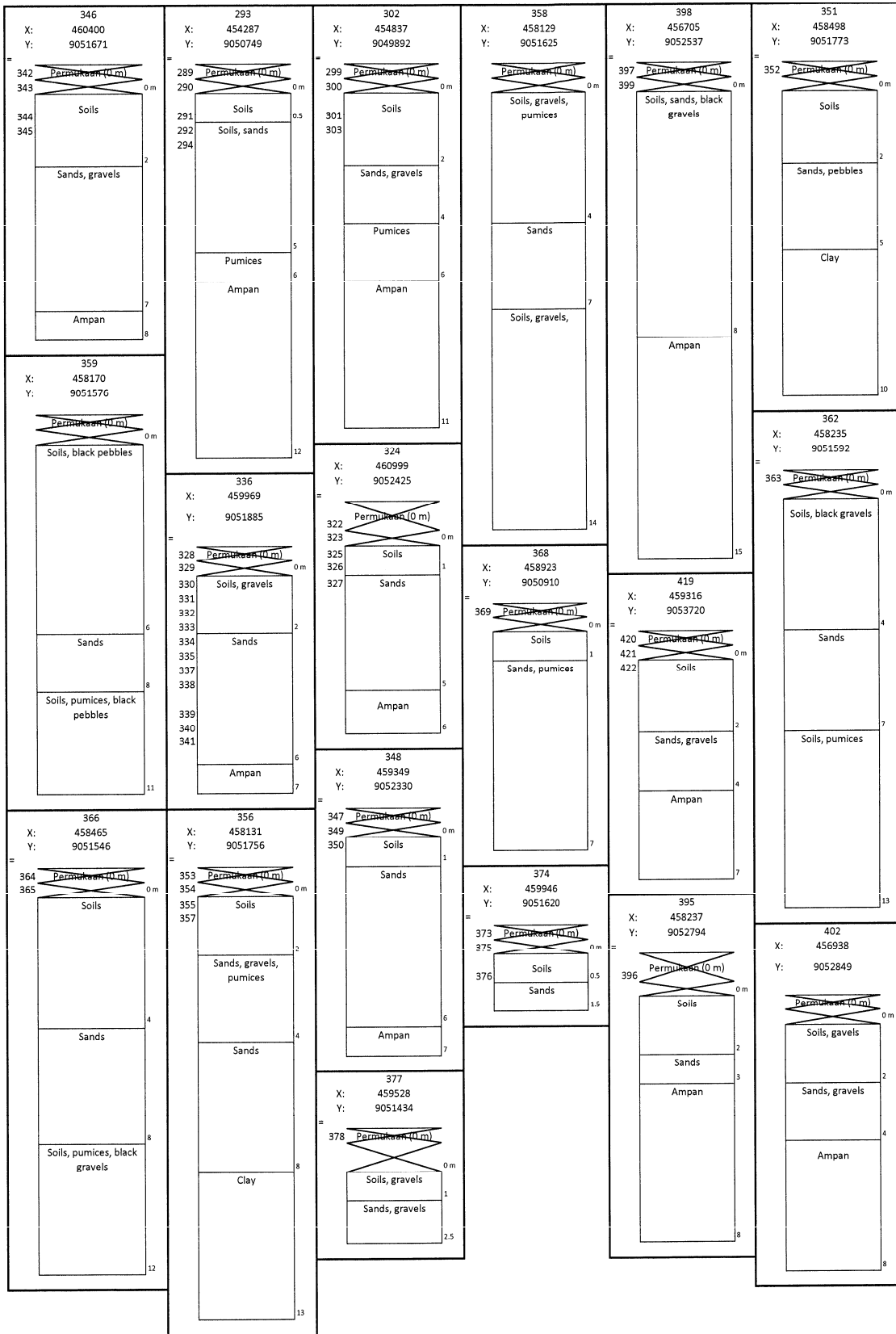
Layout Data Sumur Bor
Ket. 0,5 meter

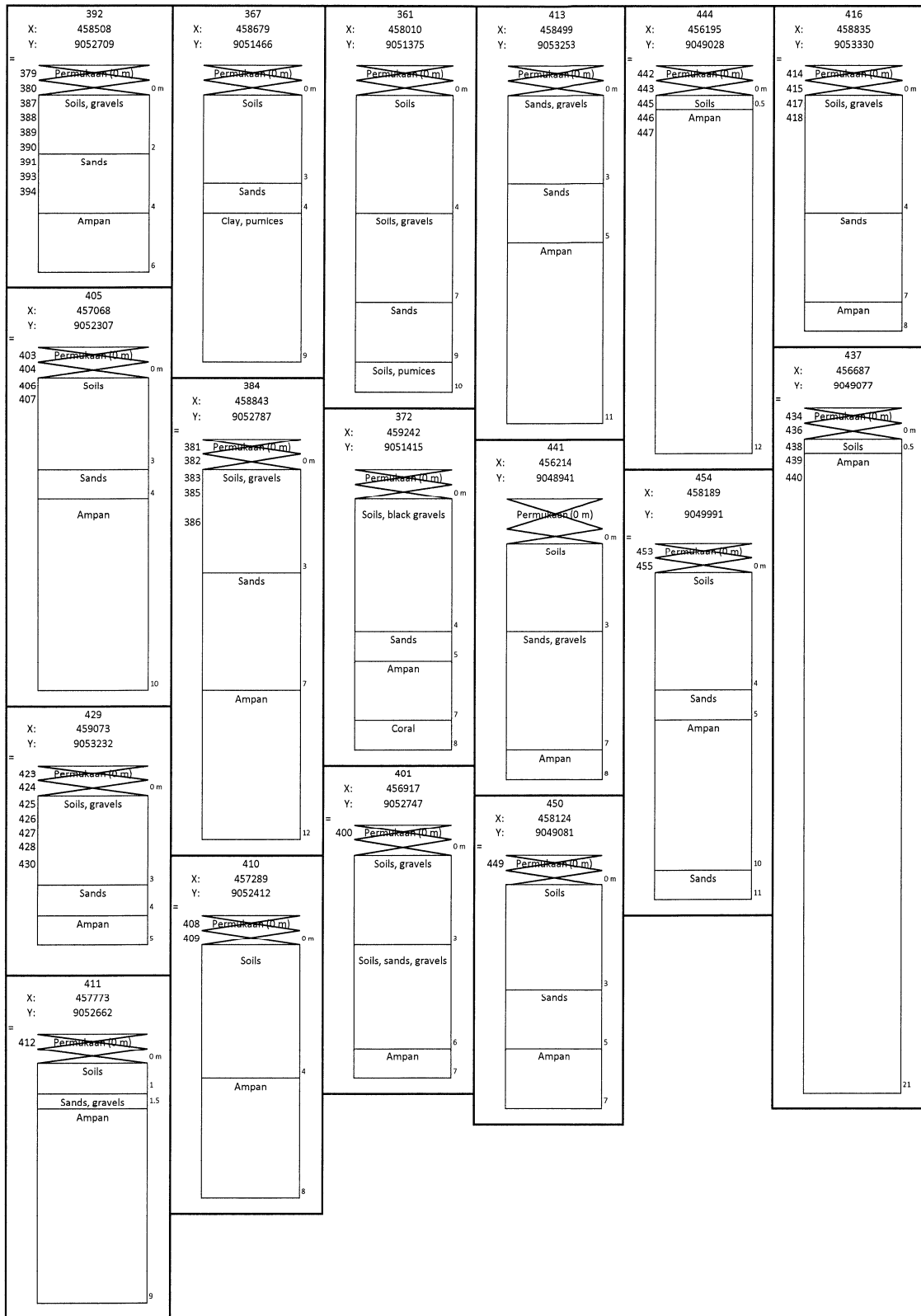


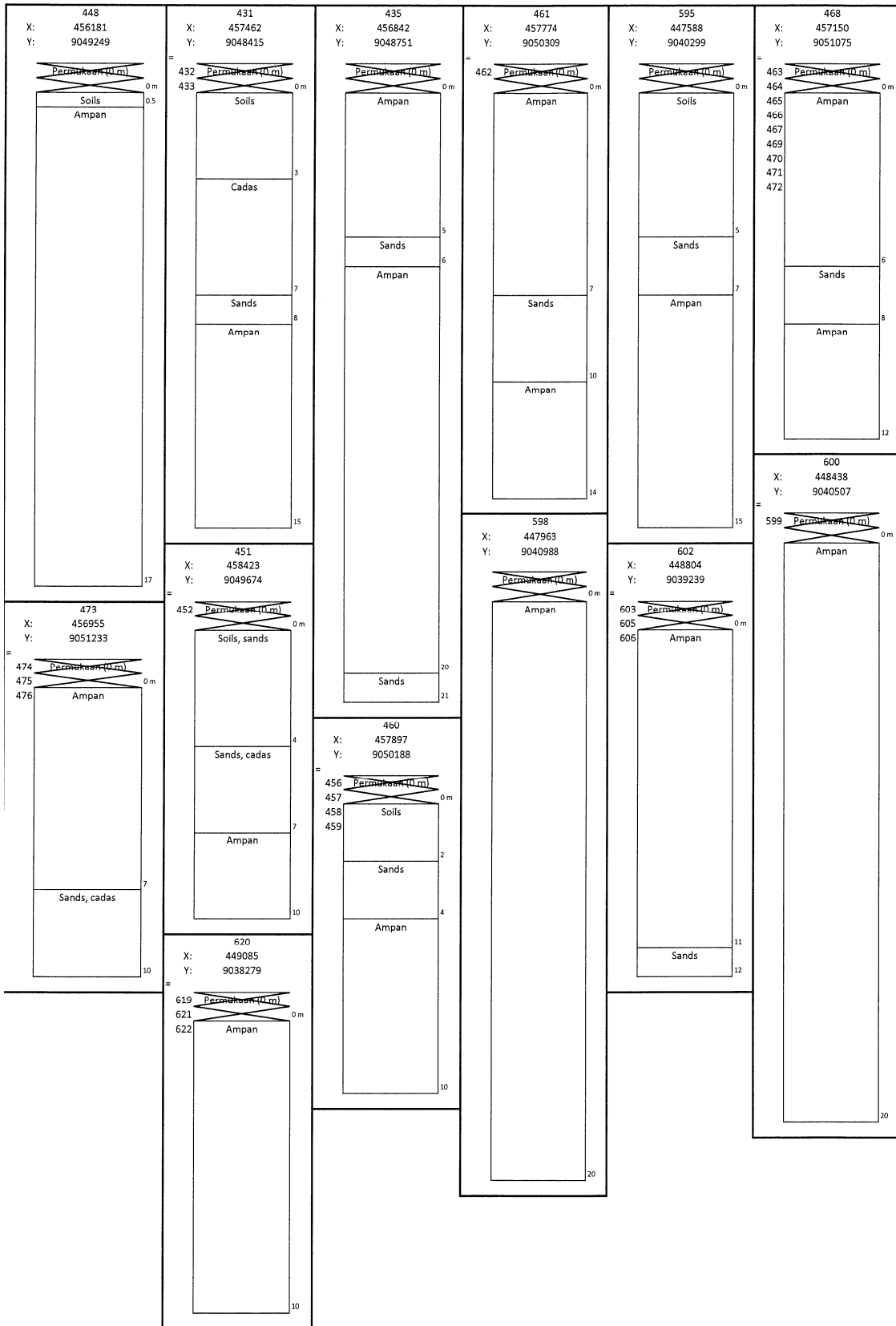




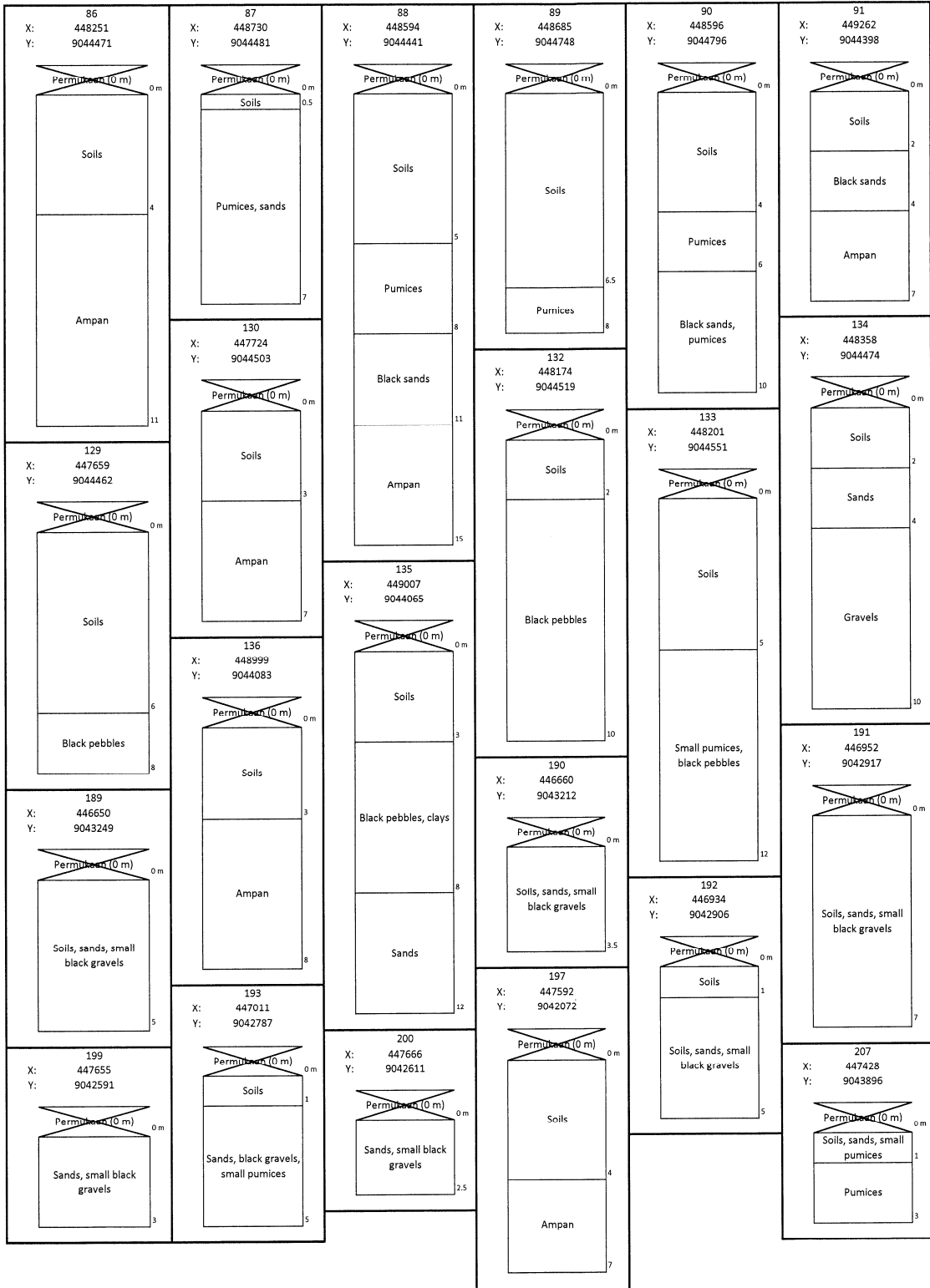


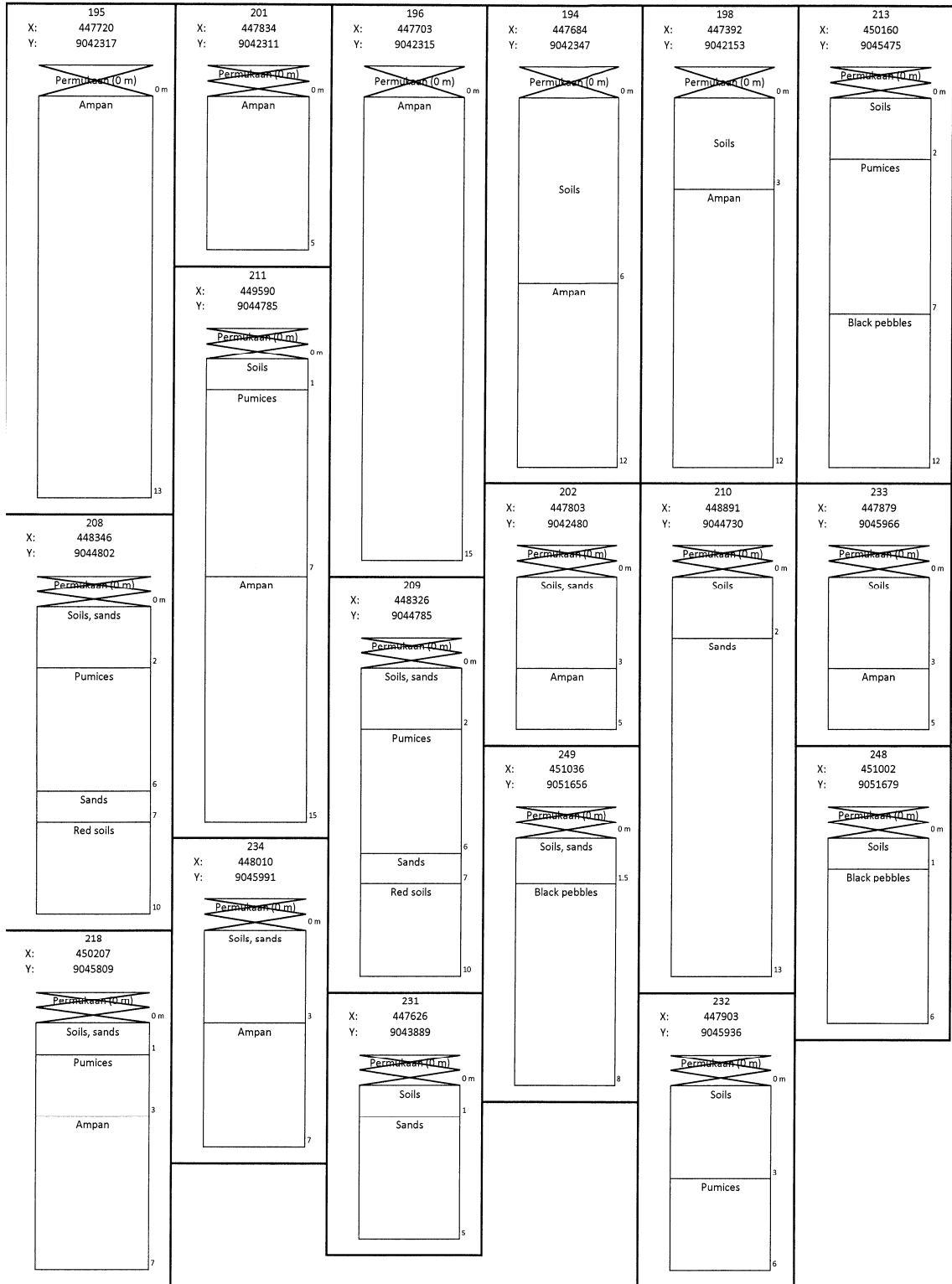


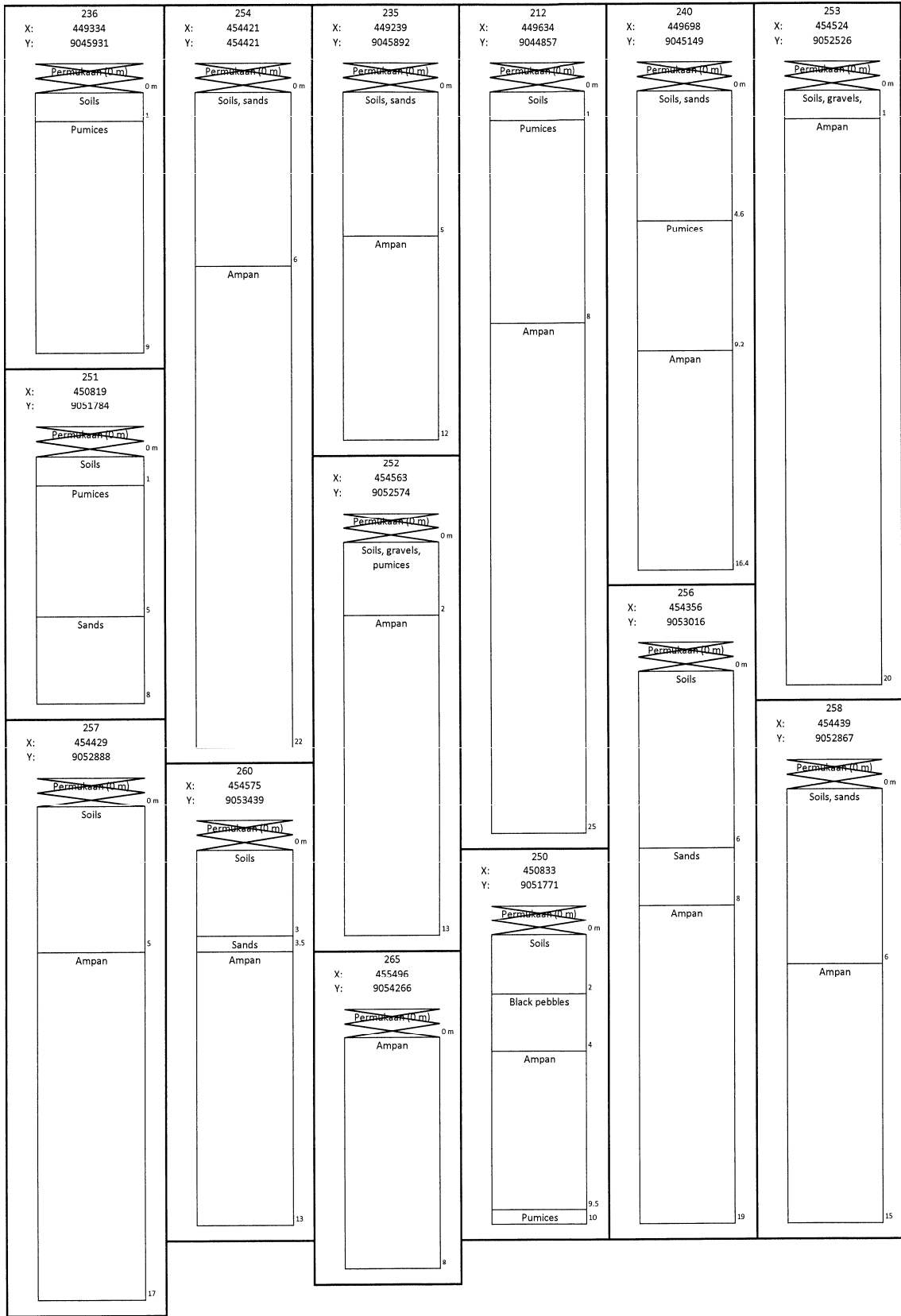


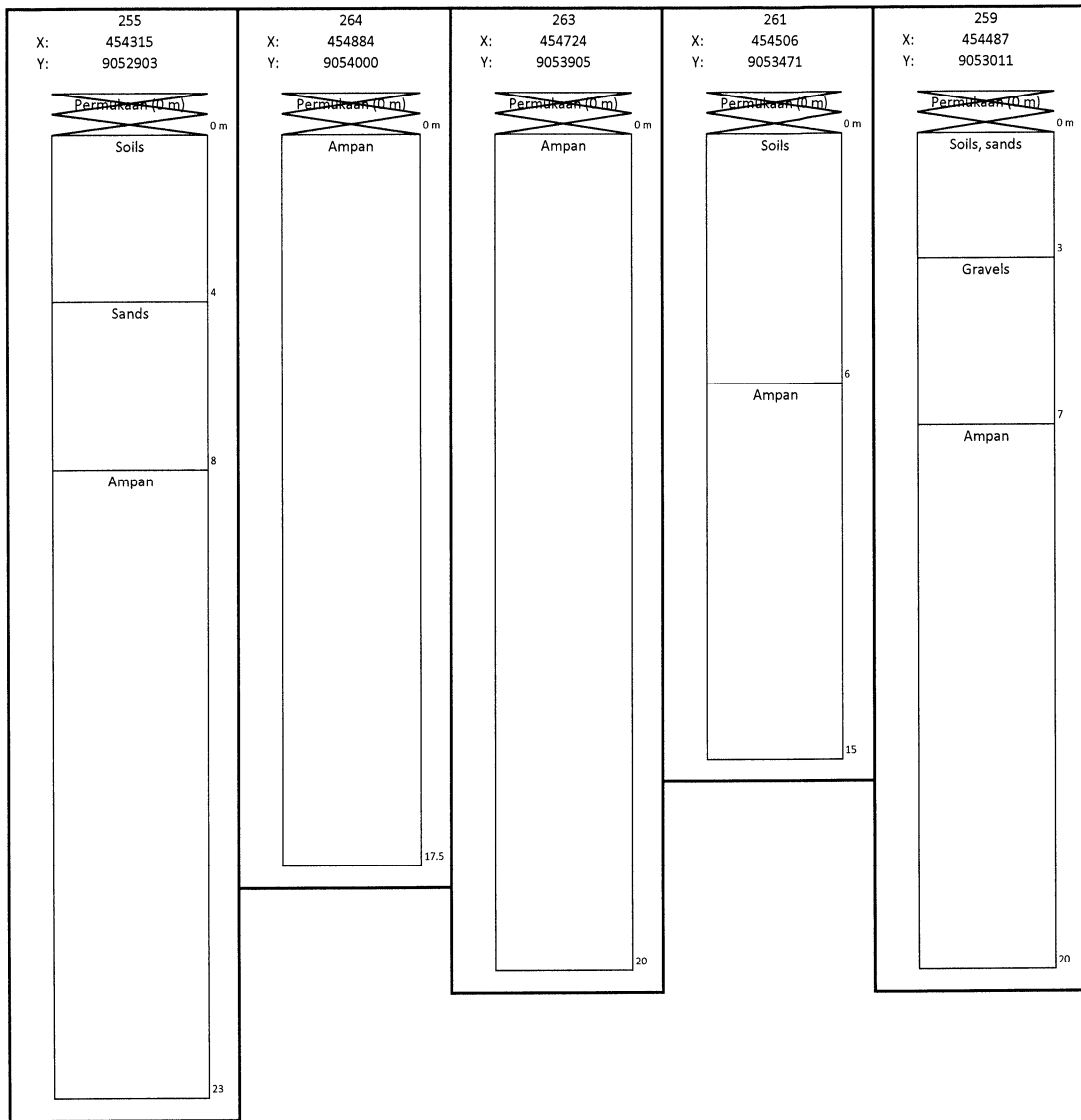


Layout Data Sumur Bor
Ket: 0,5 meter

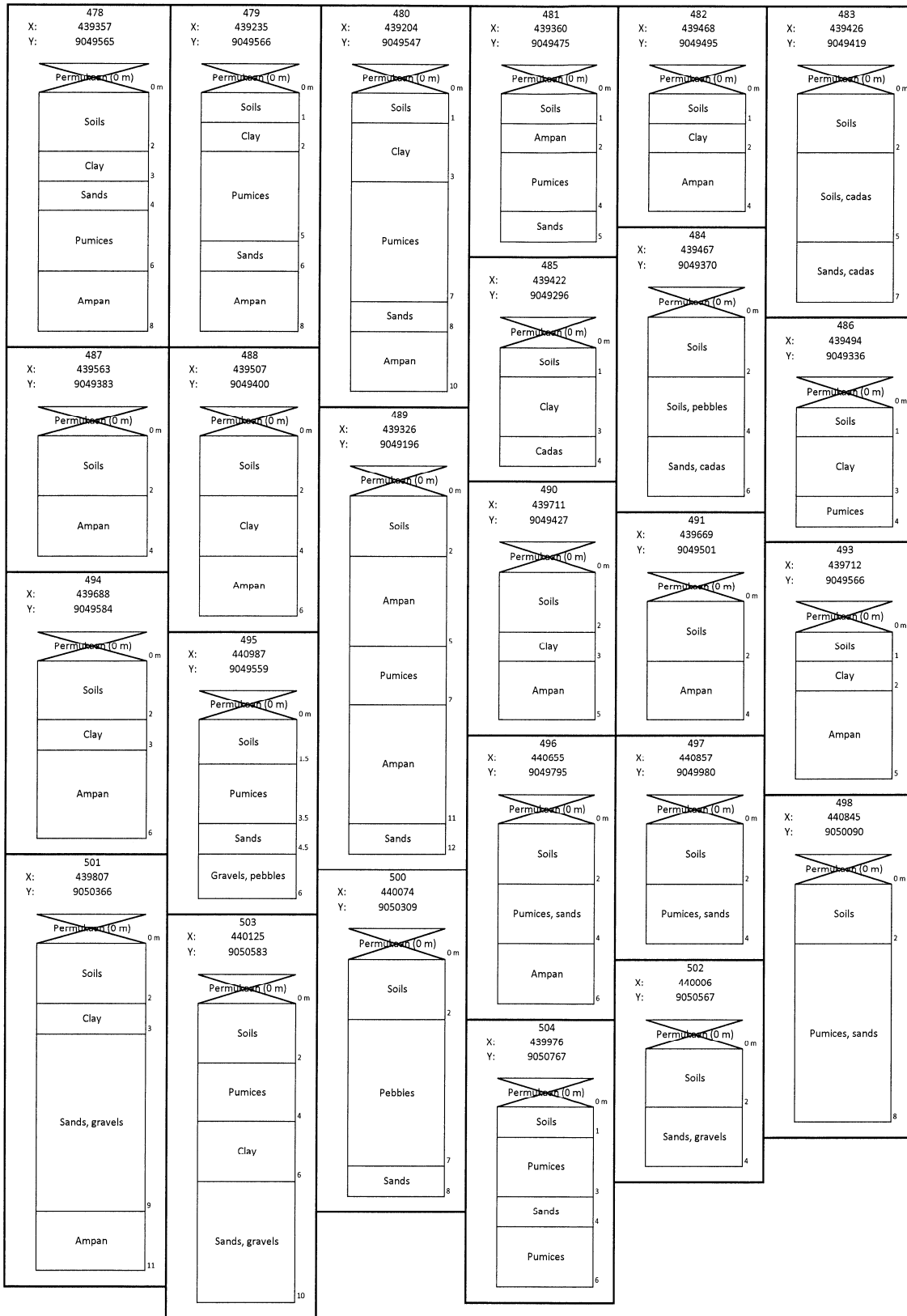


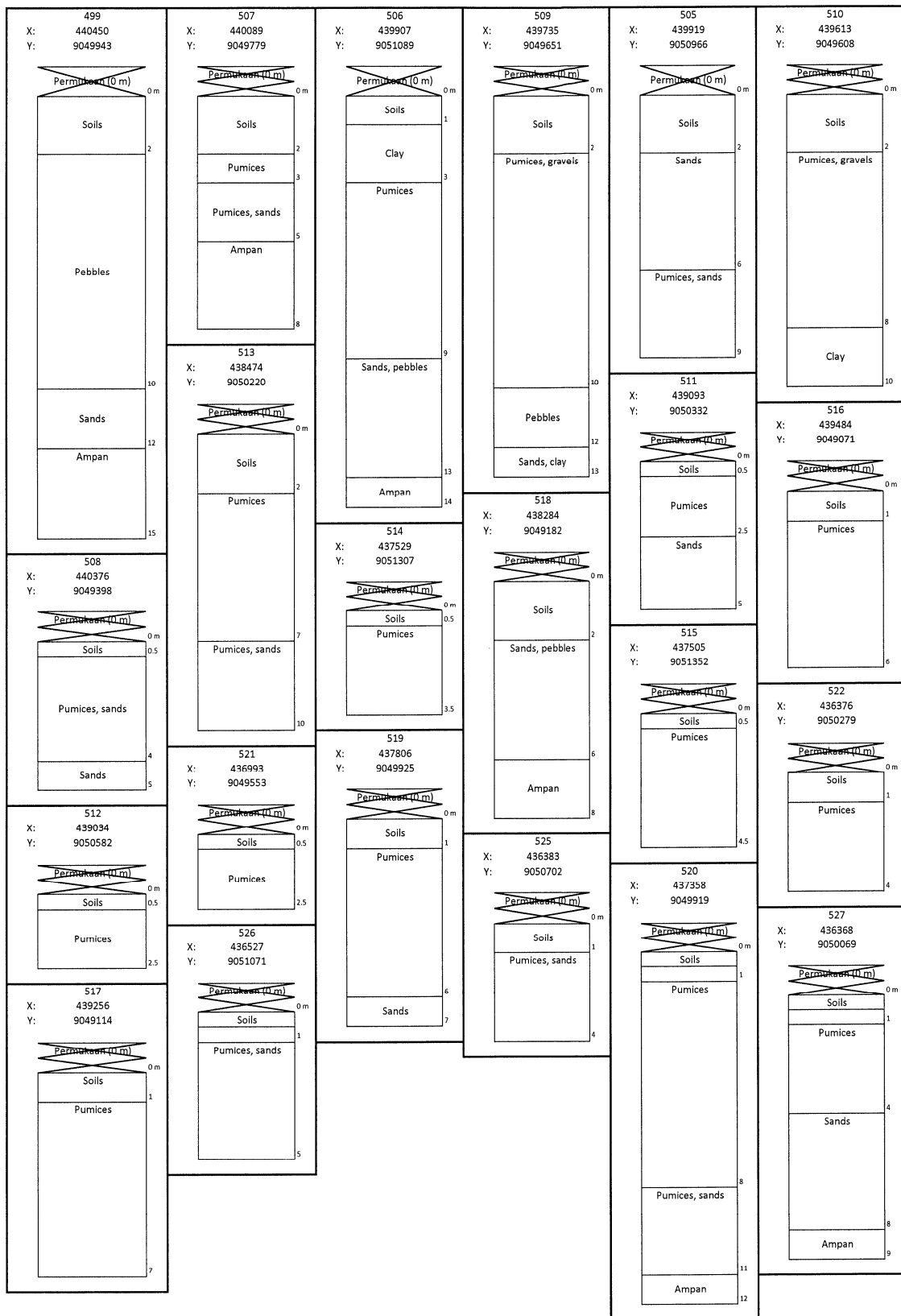


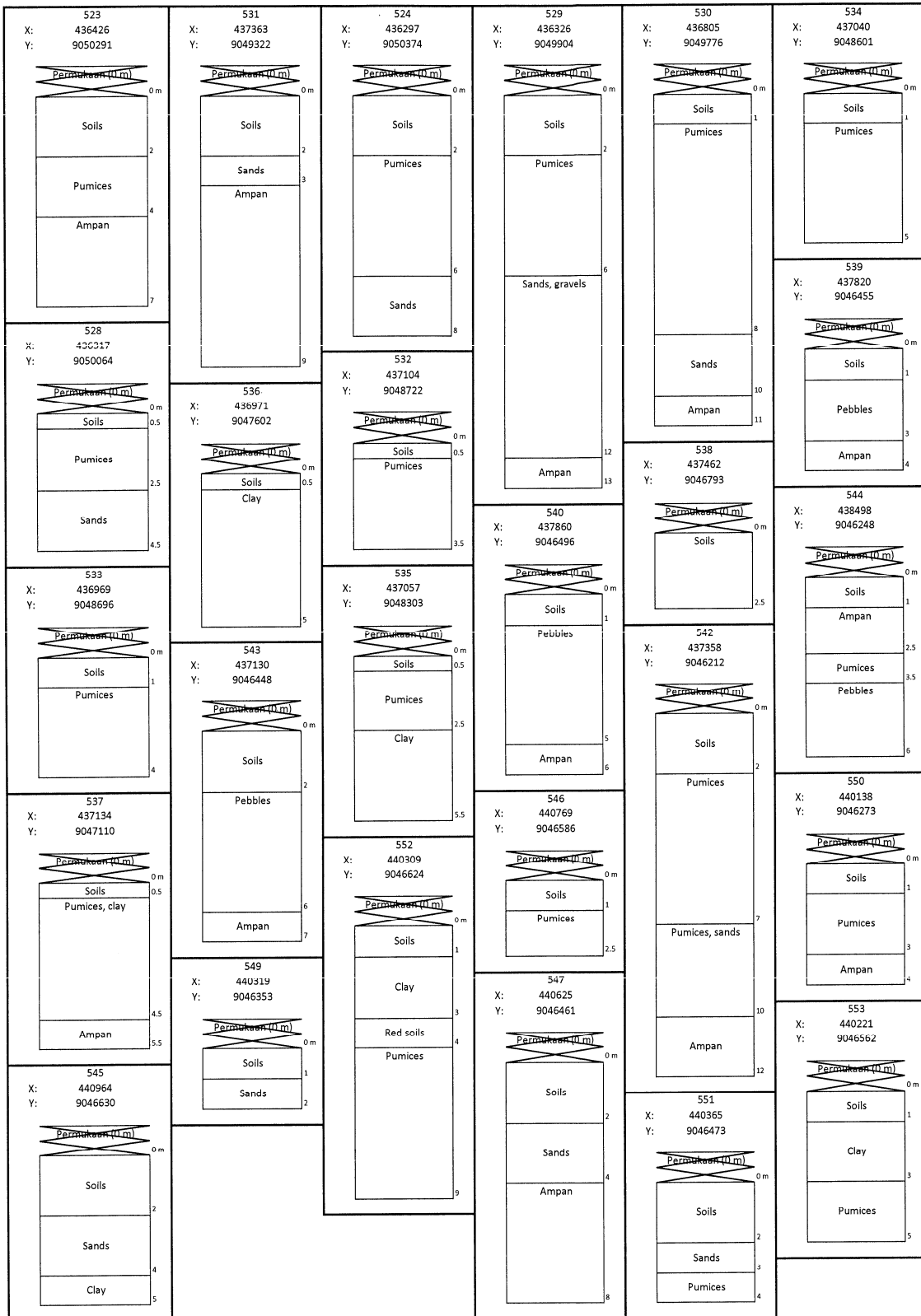


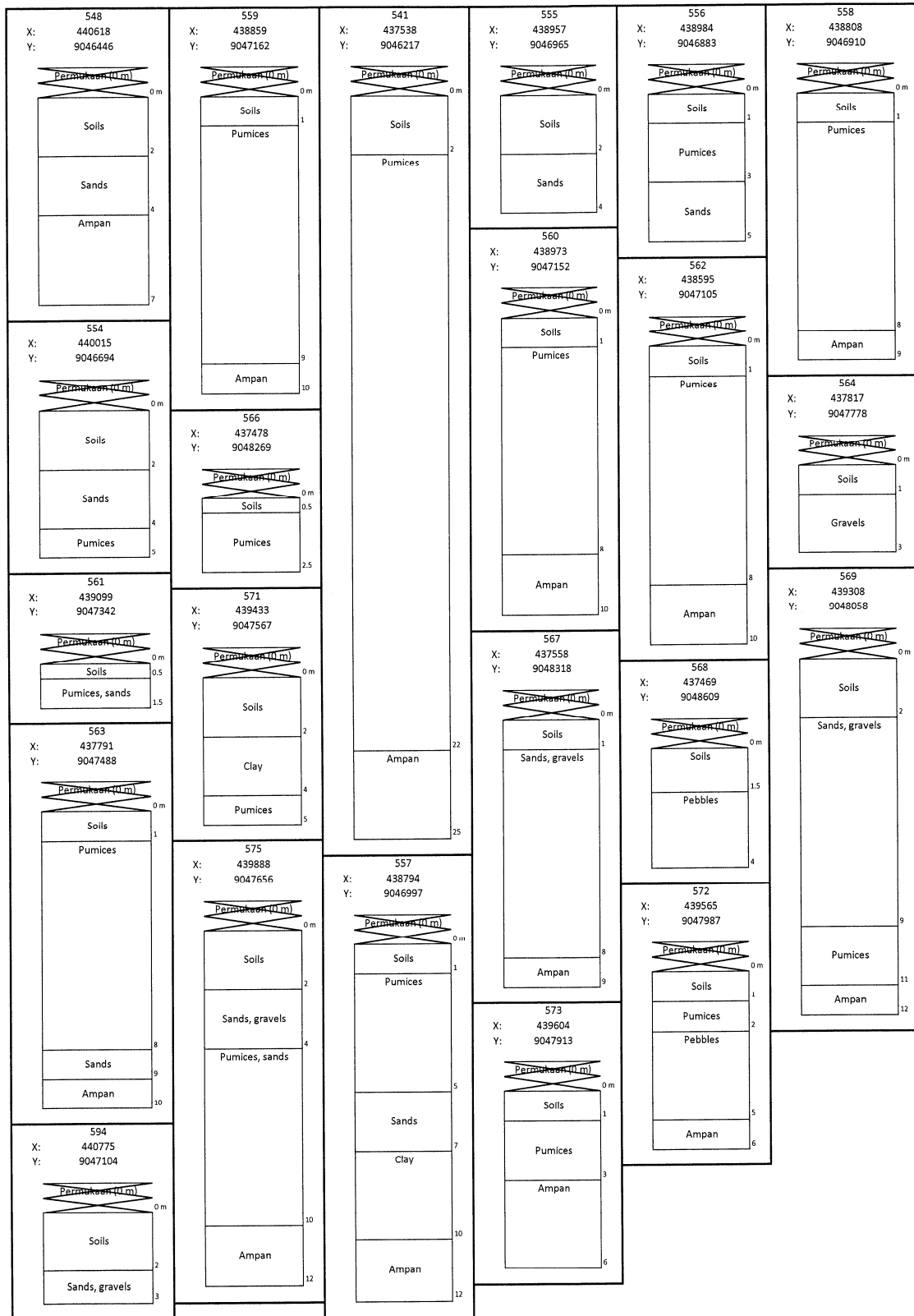


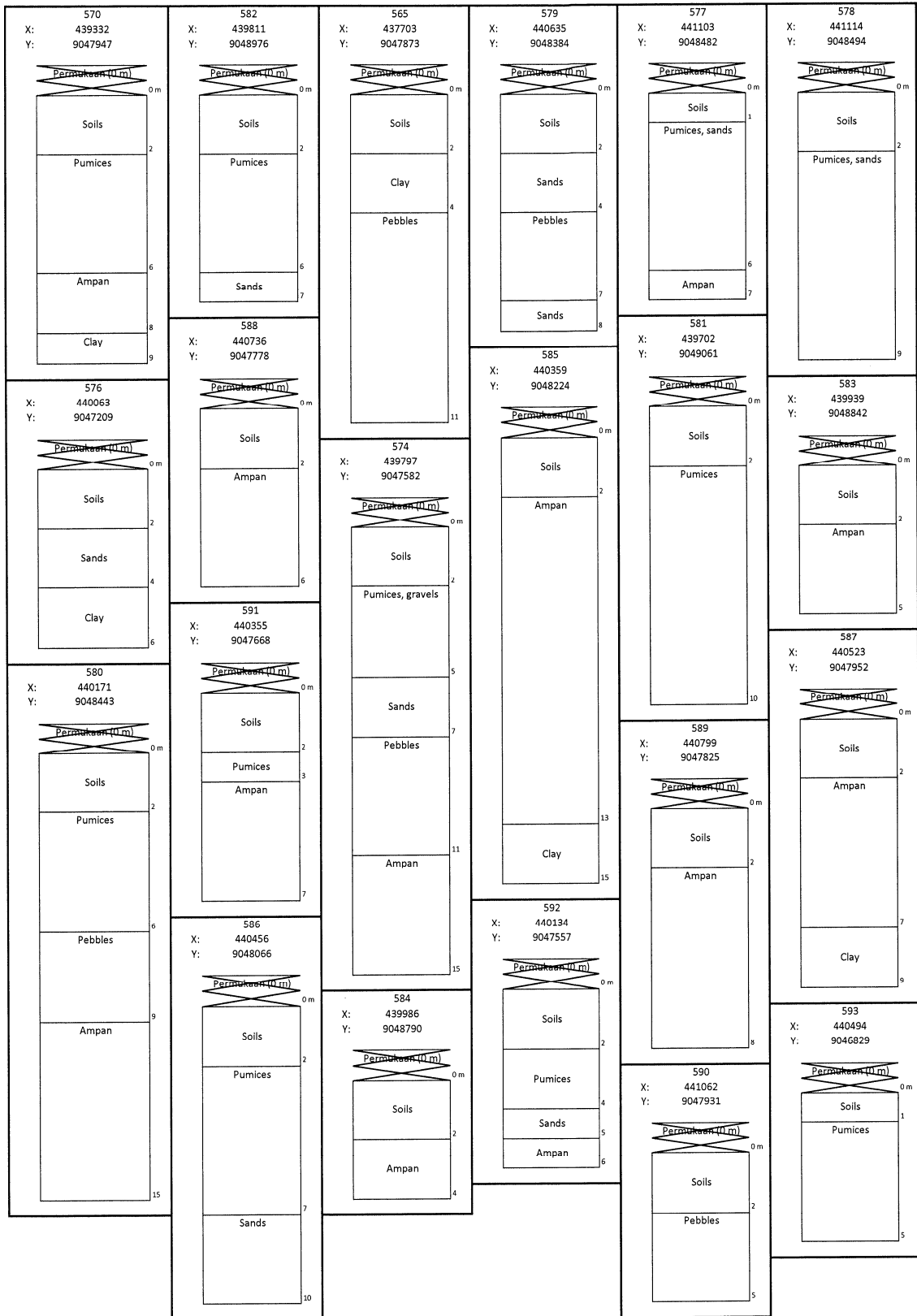
Layout Data Sumur Bor
Ket: 0,5 meter



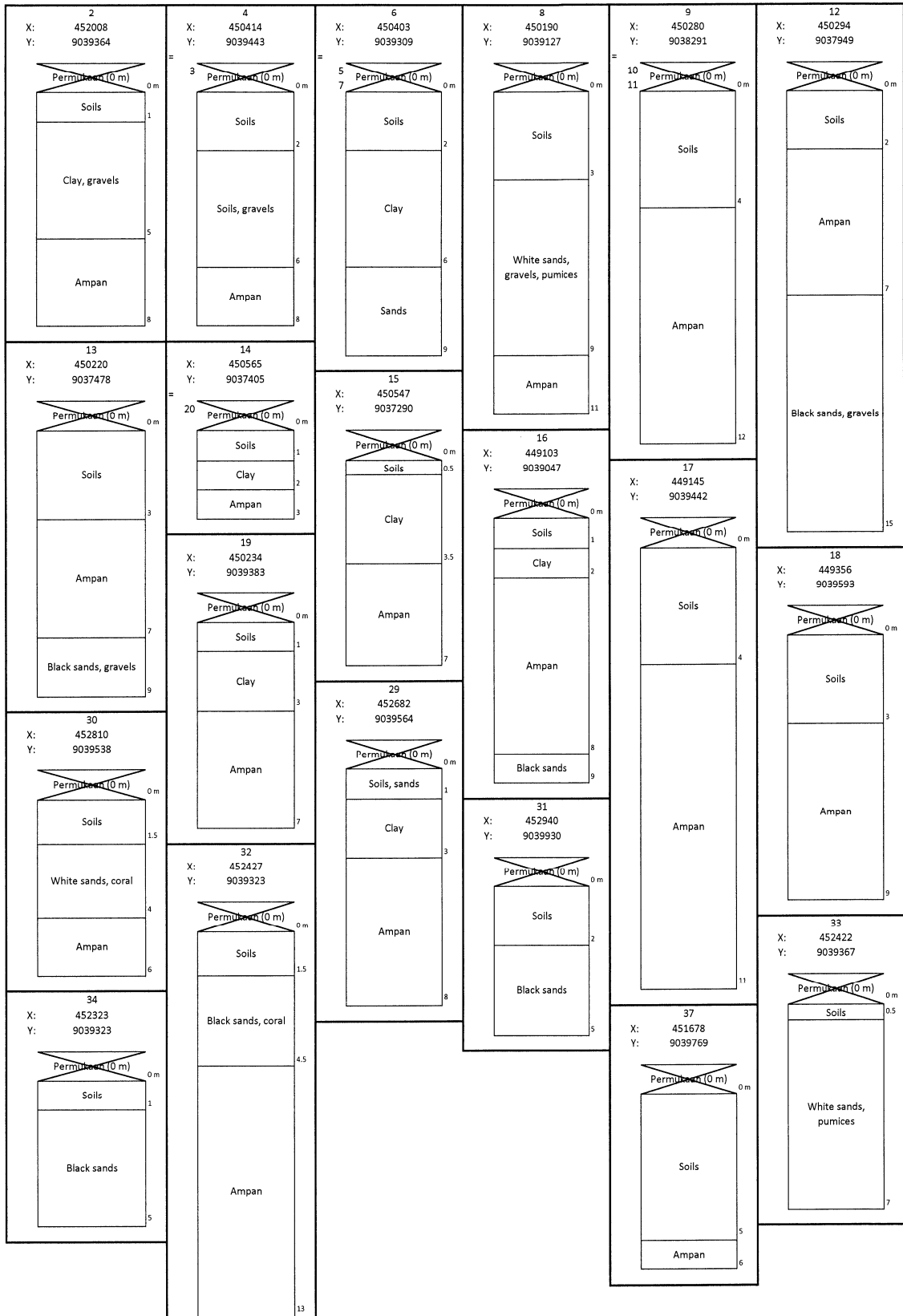


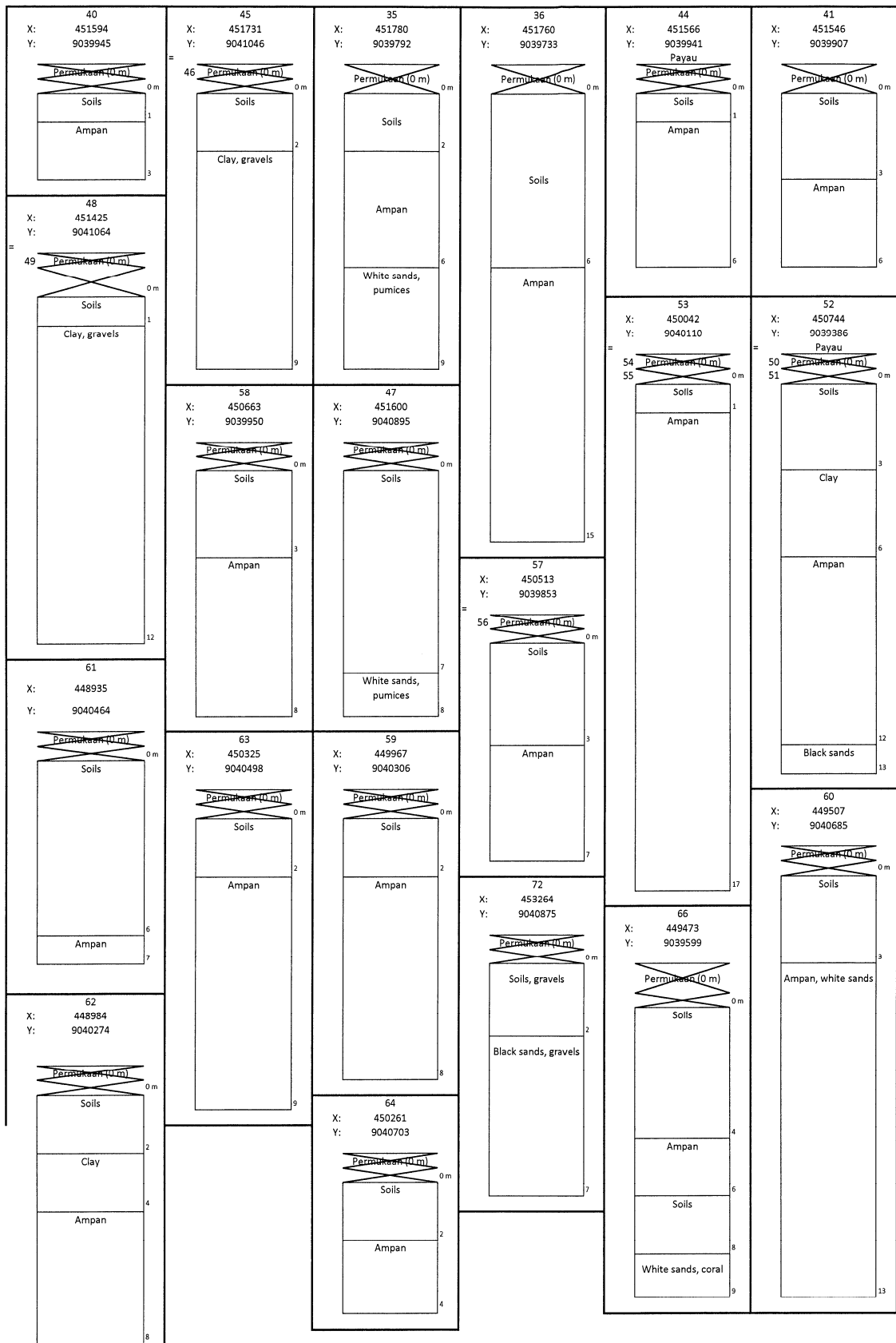


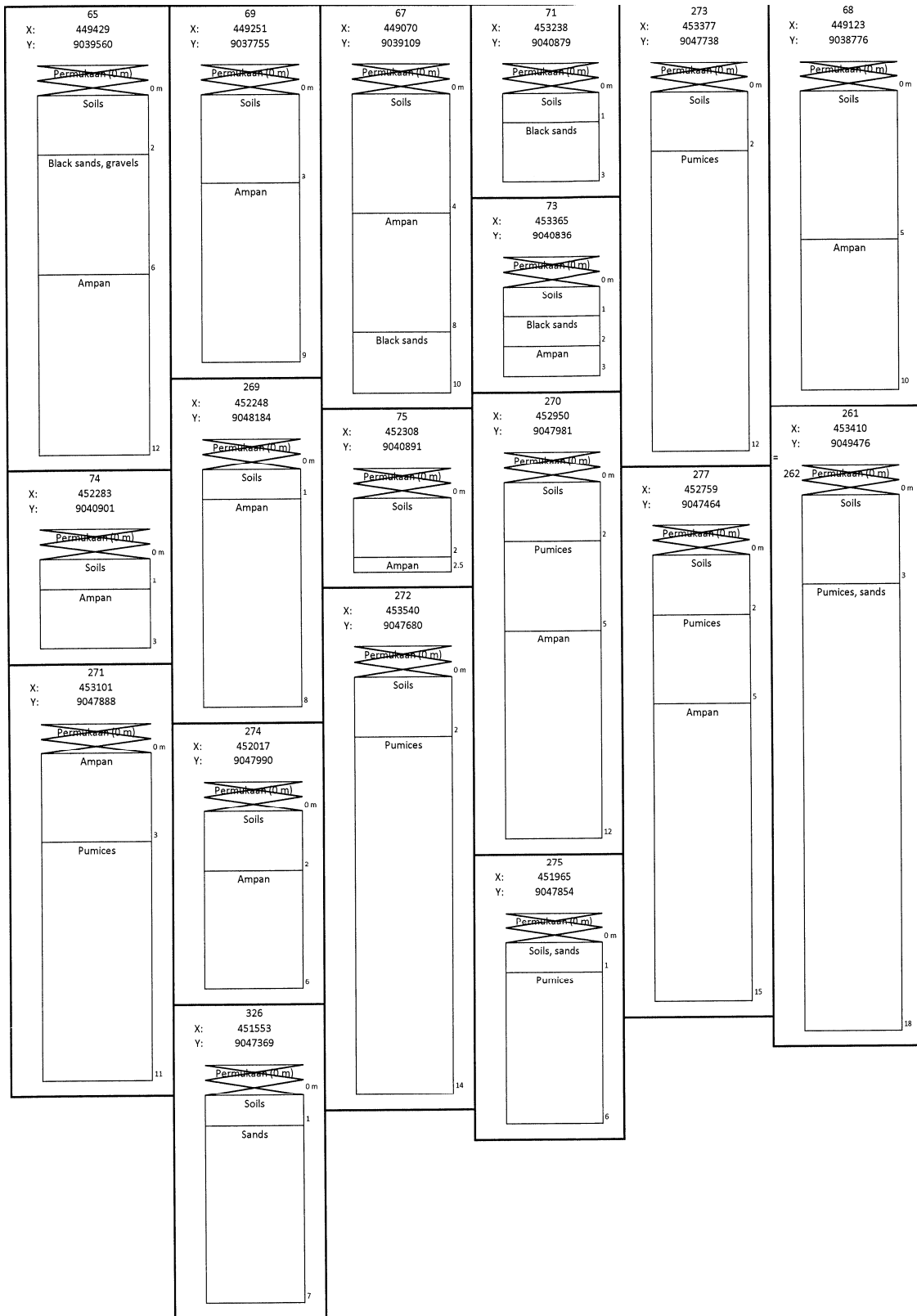


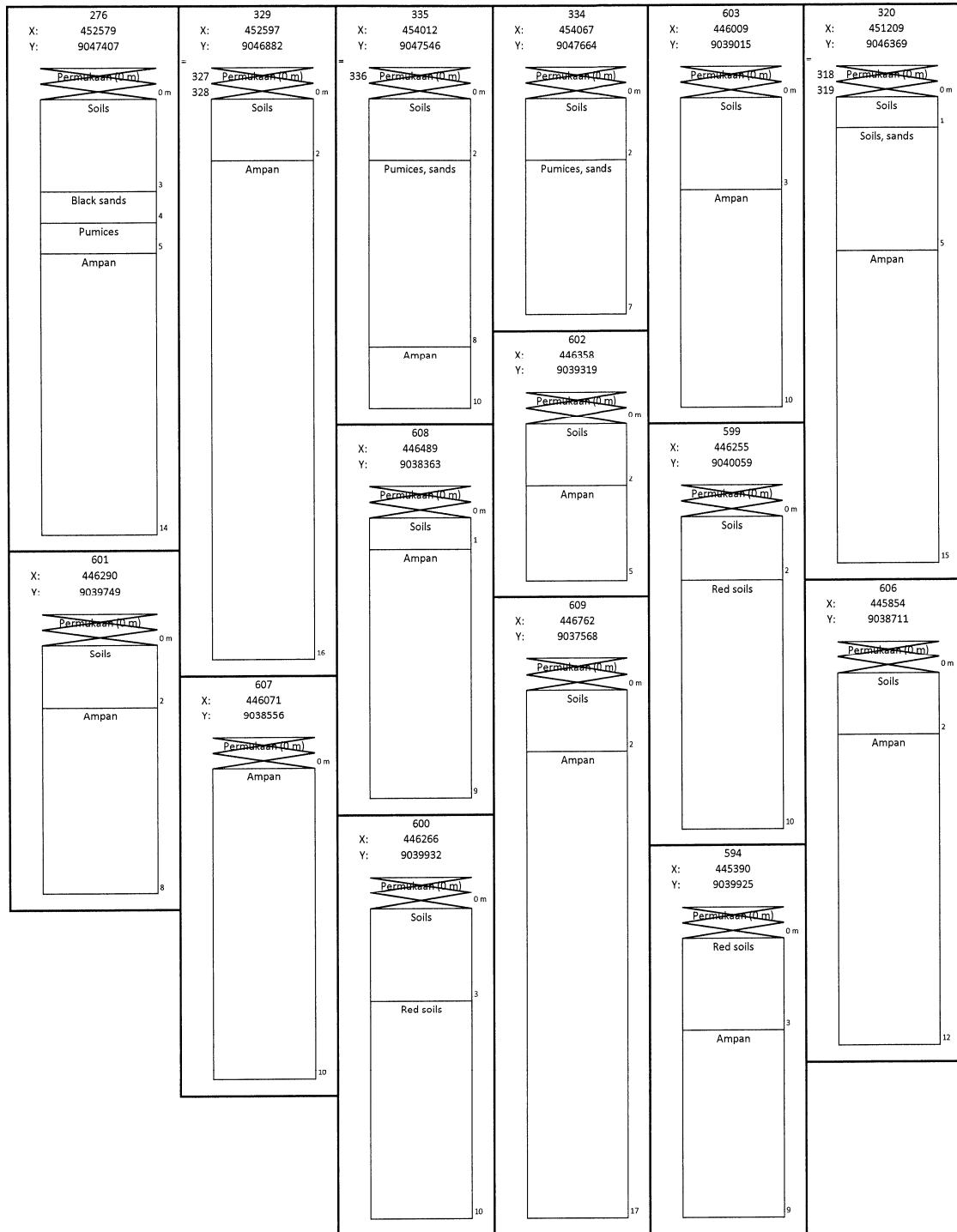


Layout Data Sumur Bor
Ket: 0,5 meter

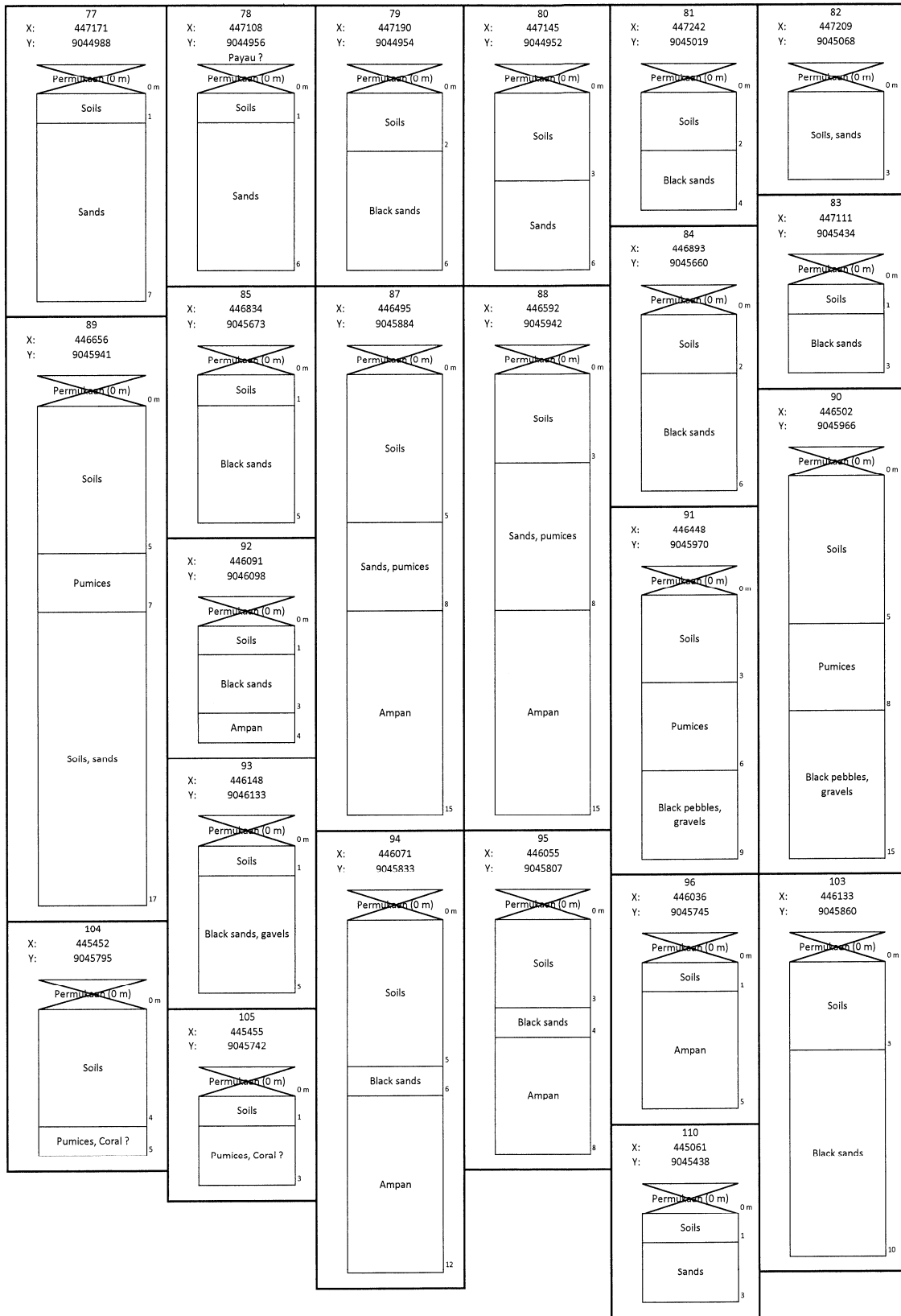


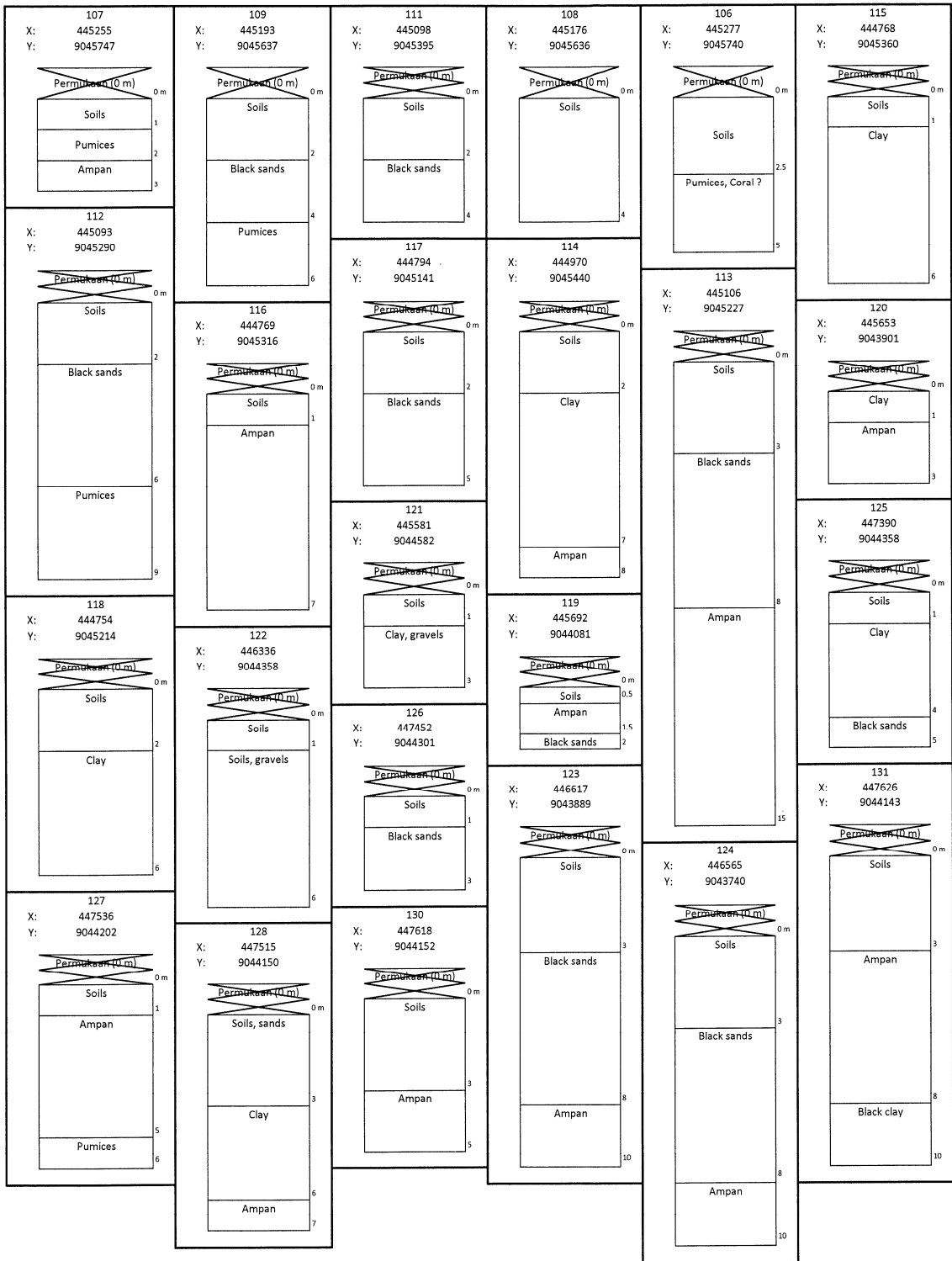


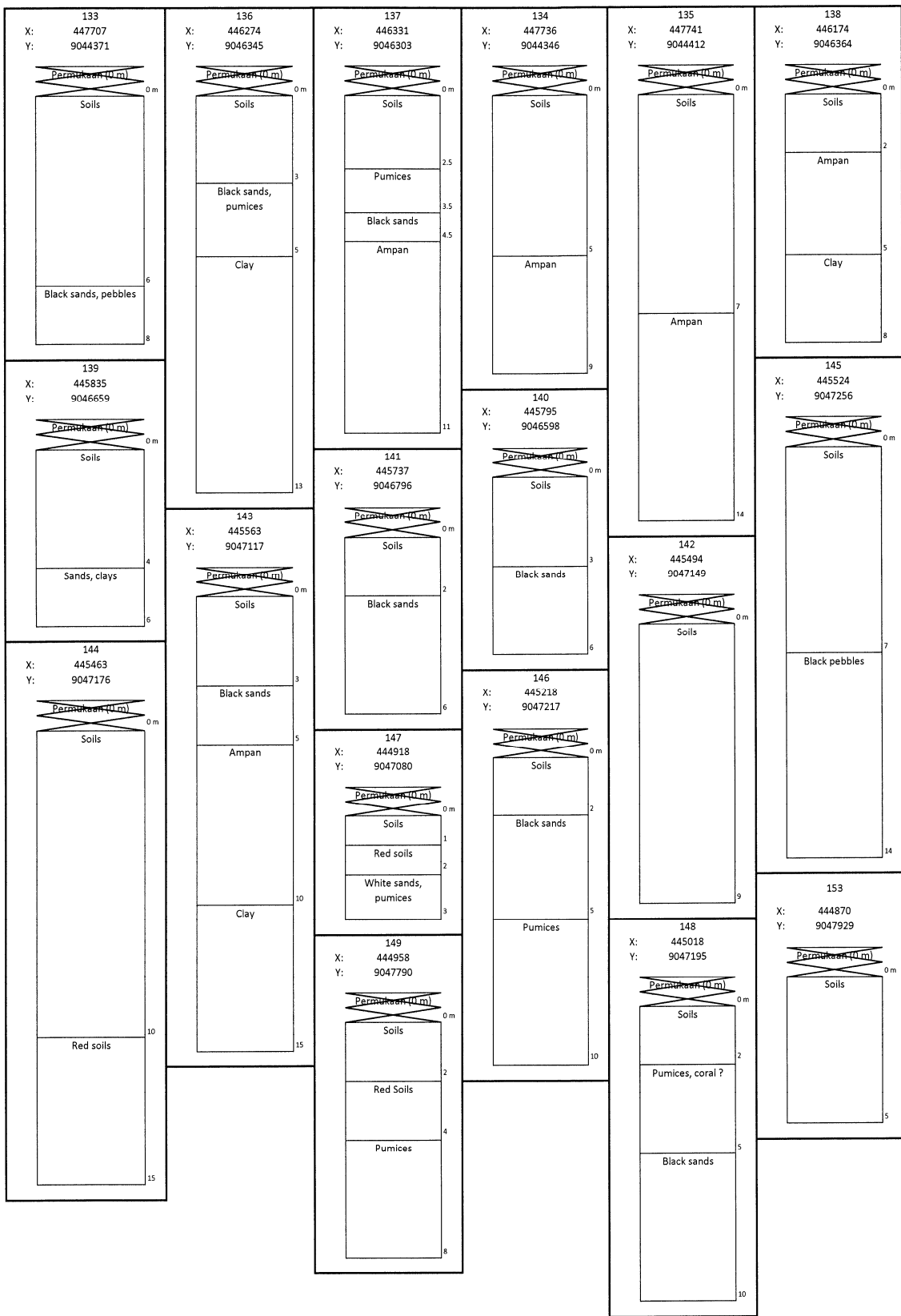


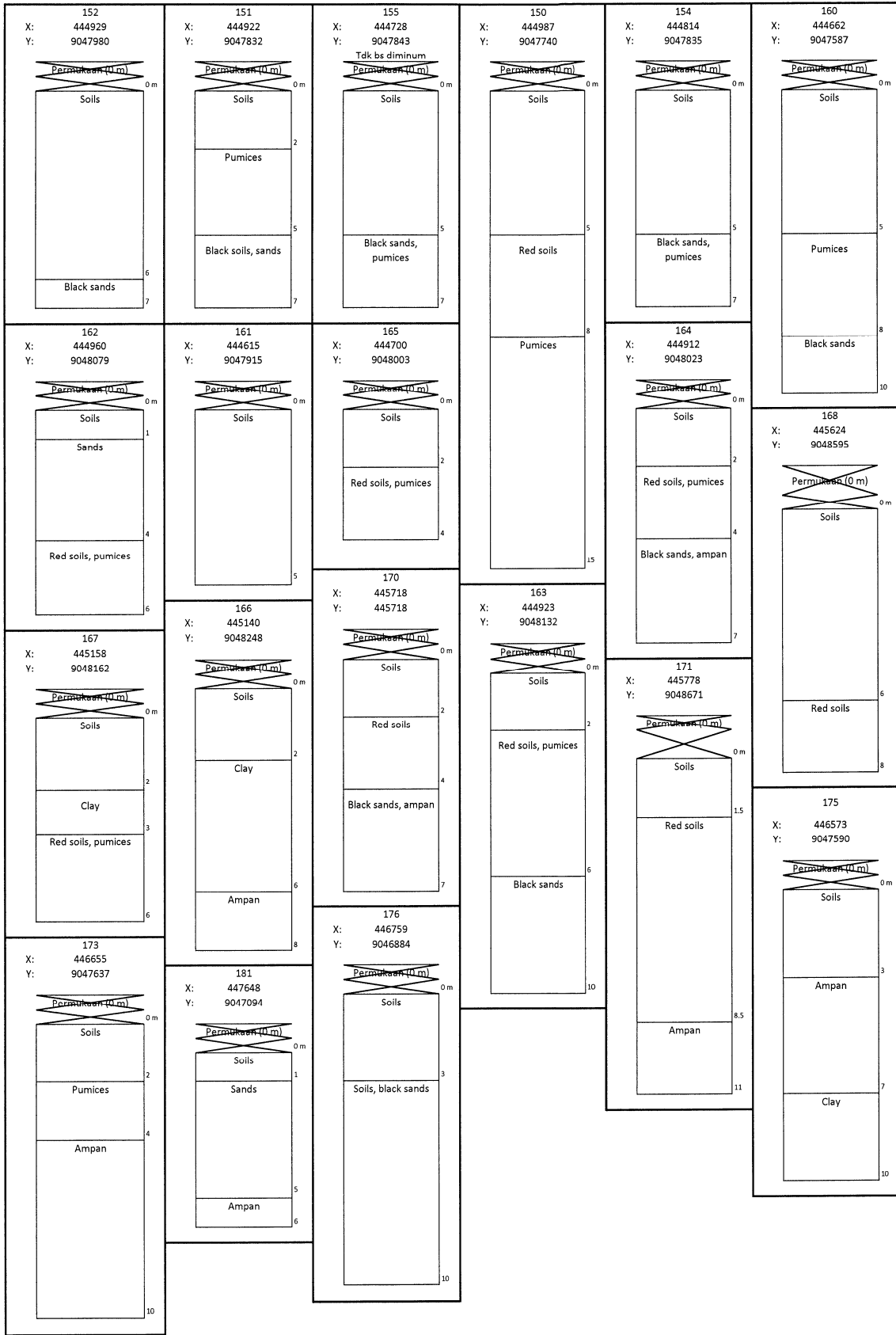


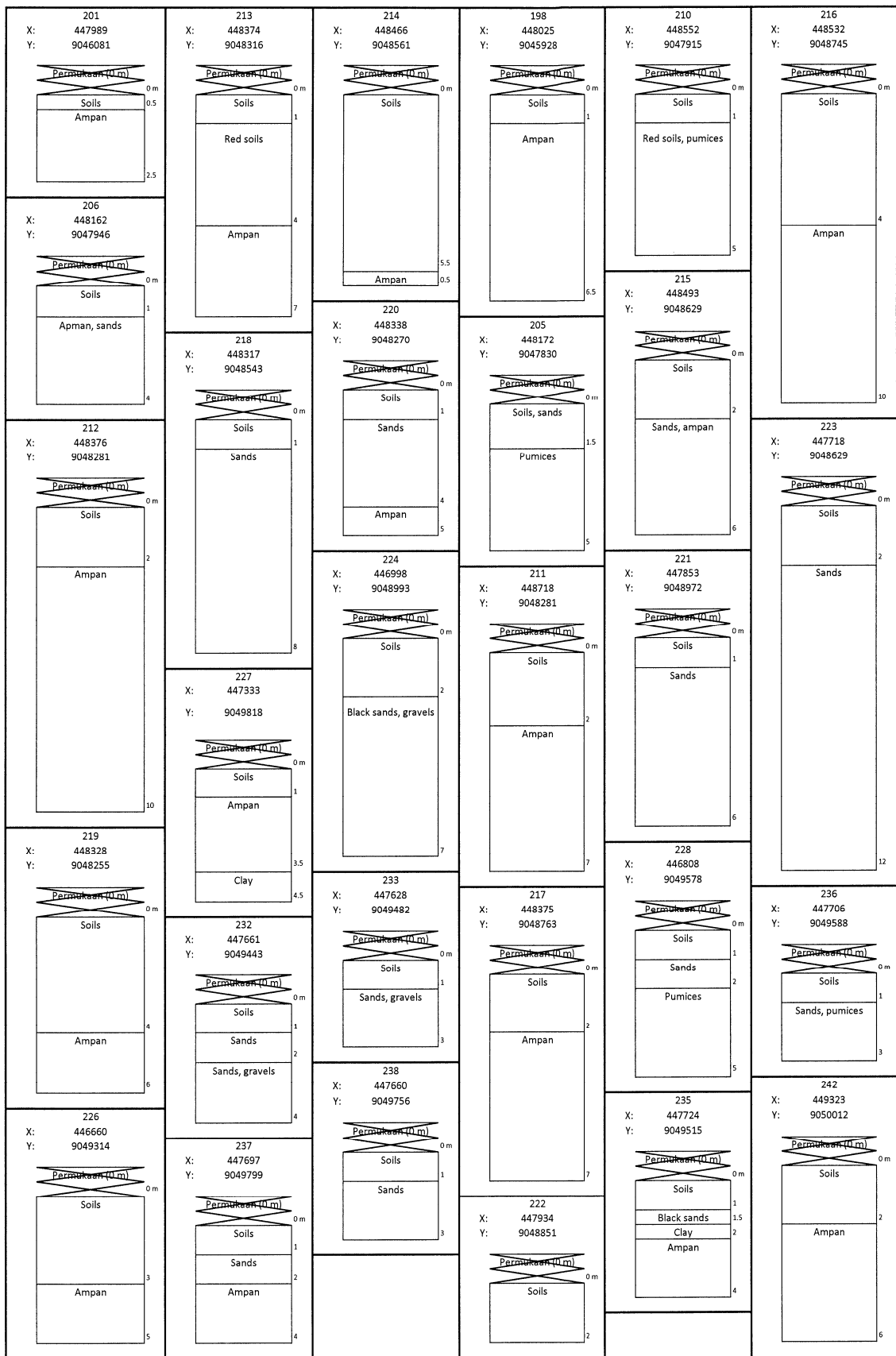
Layout Data Sumur Bor
Ket: 0,5 meter

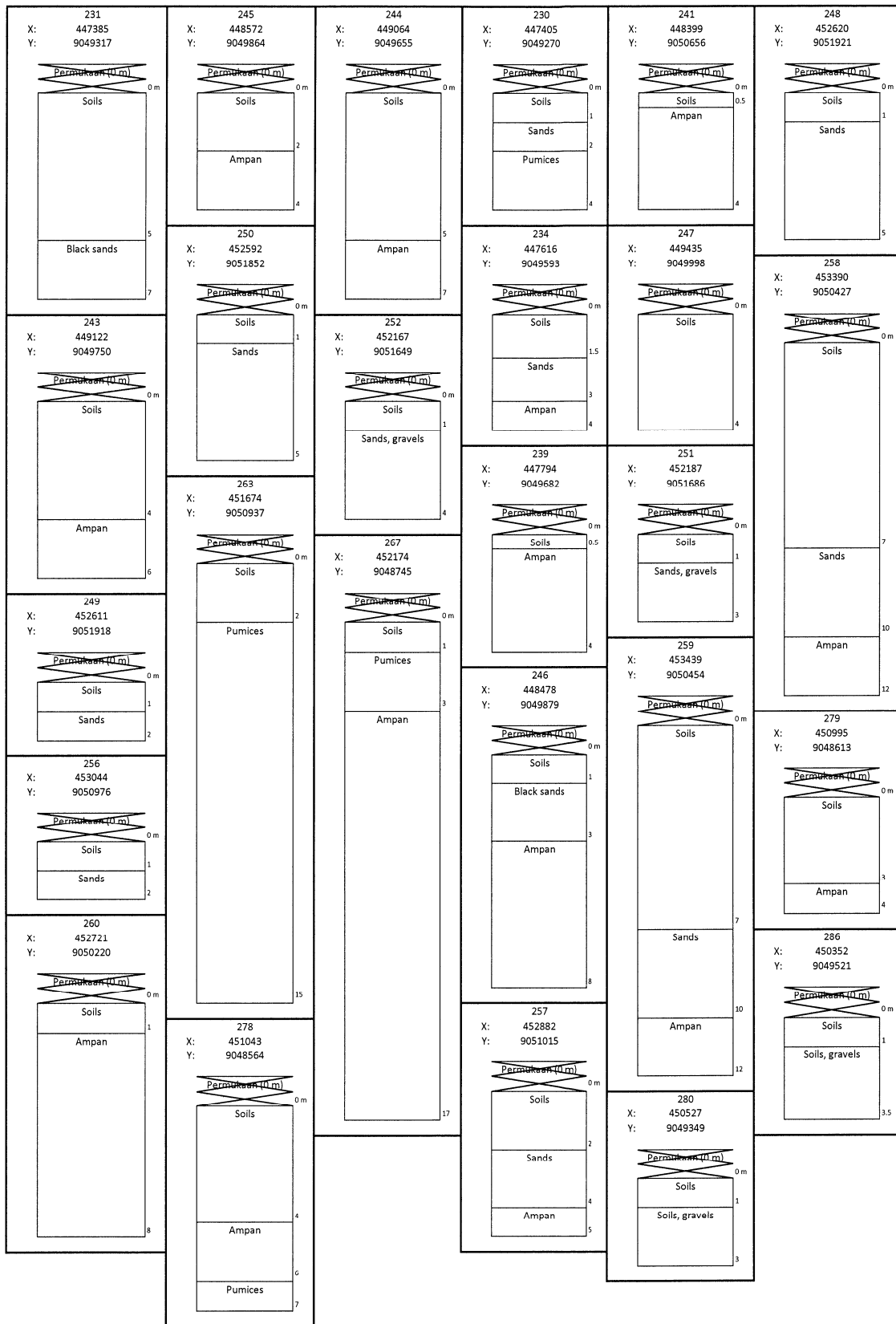


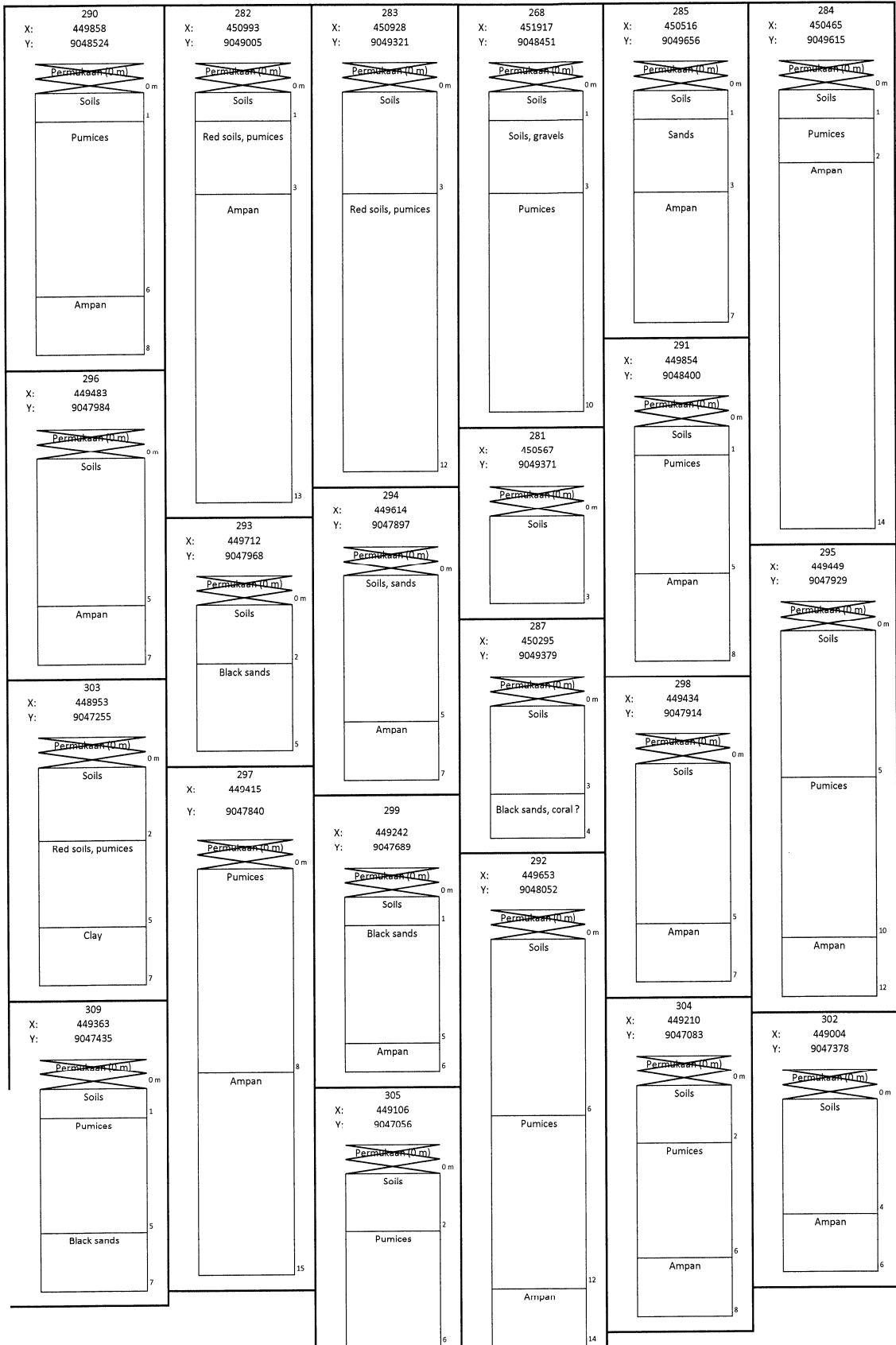


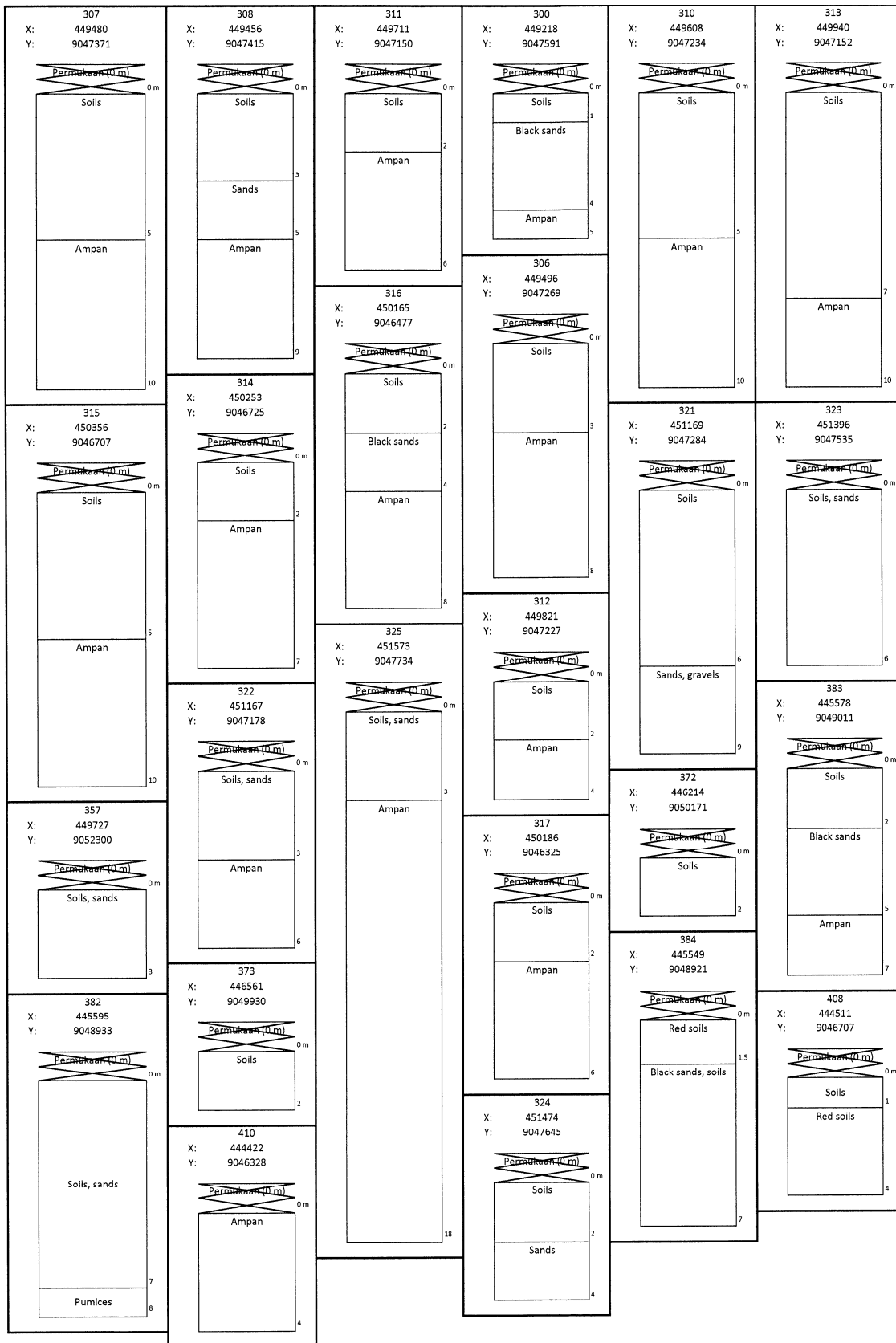


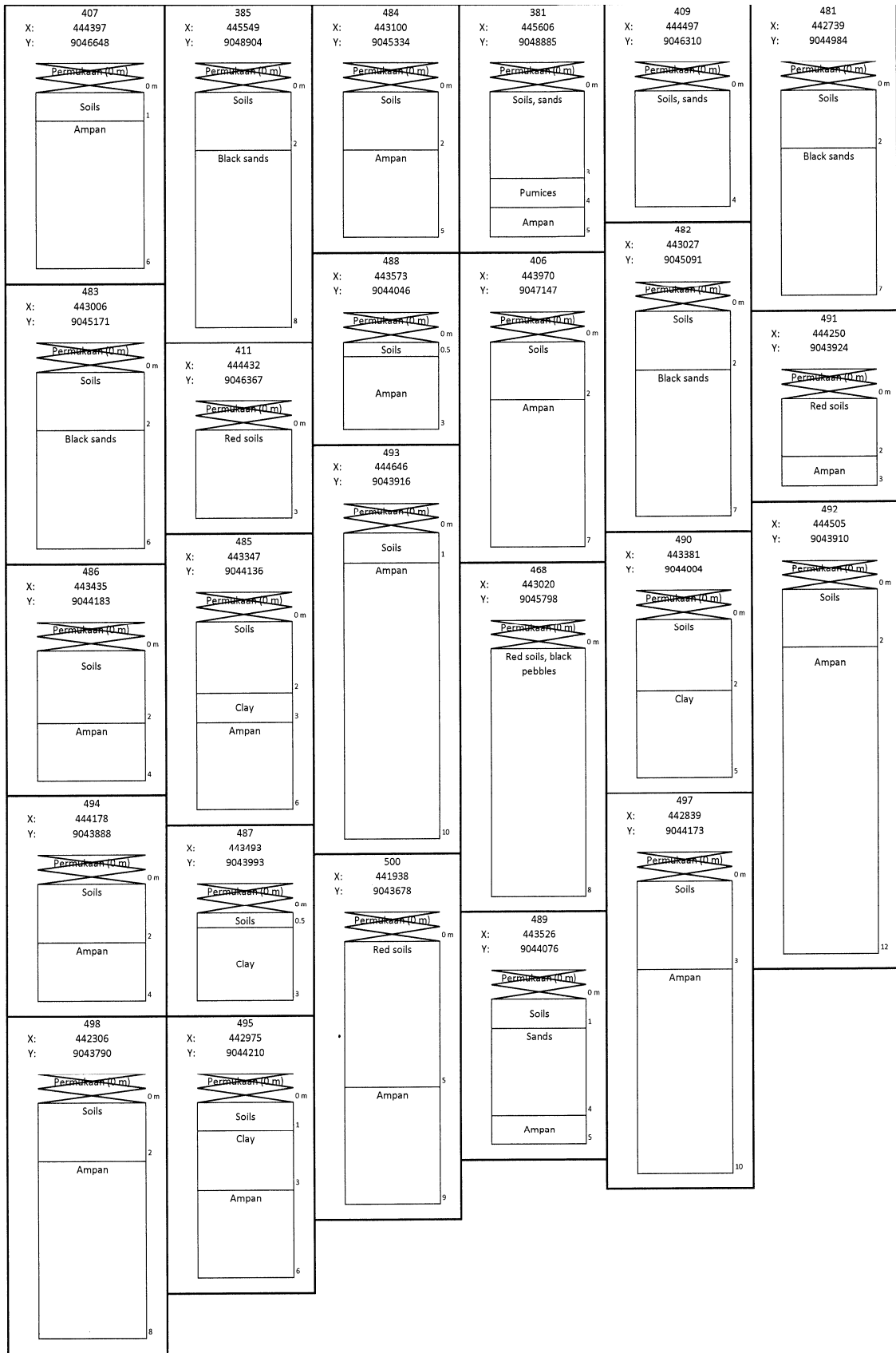


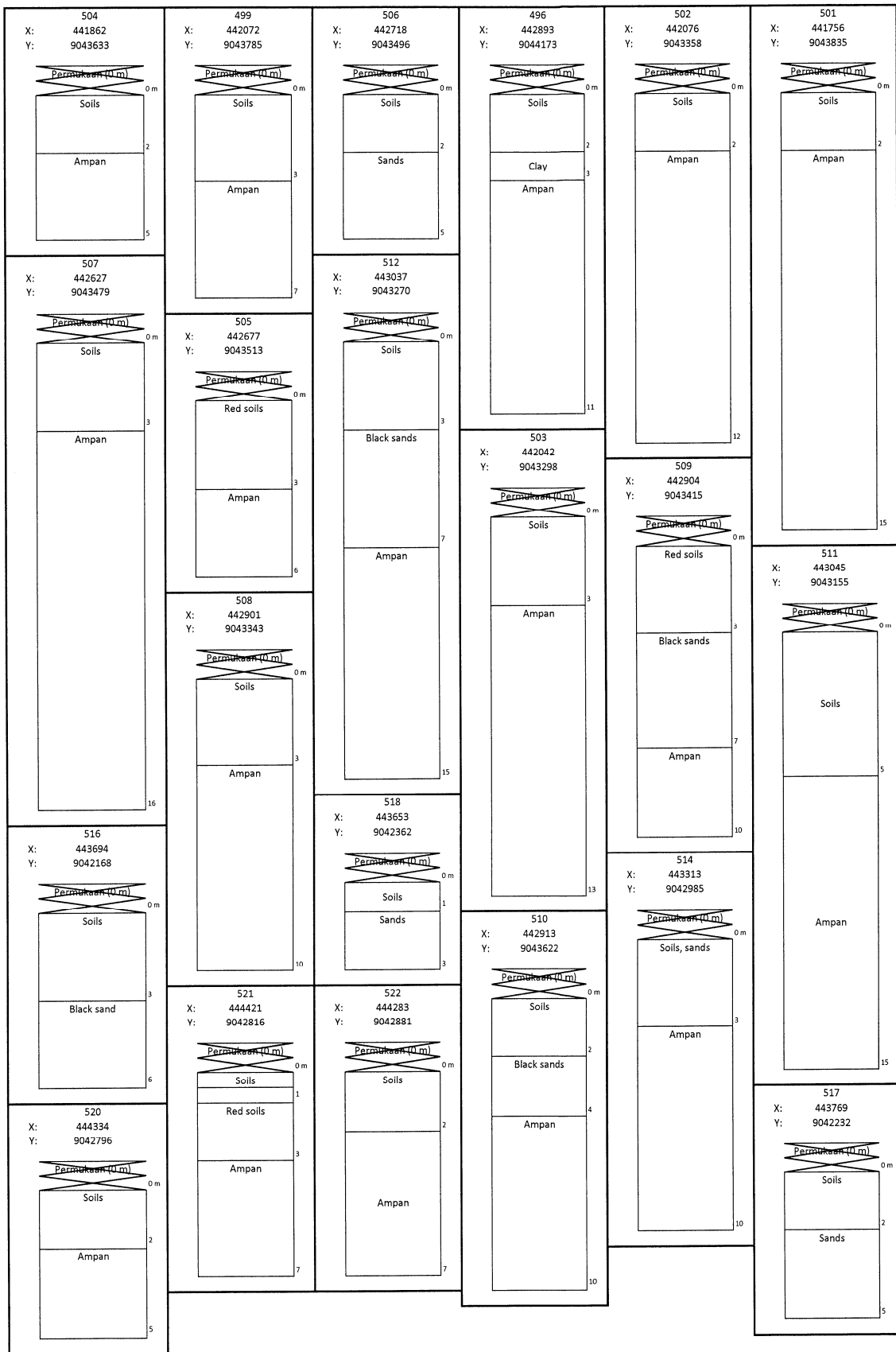


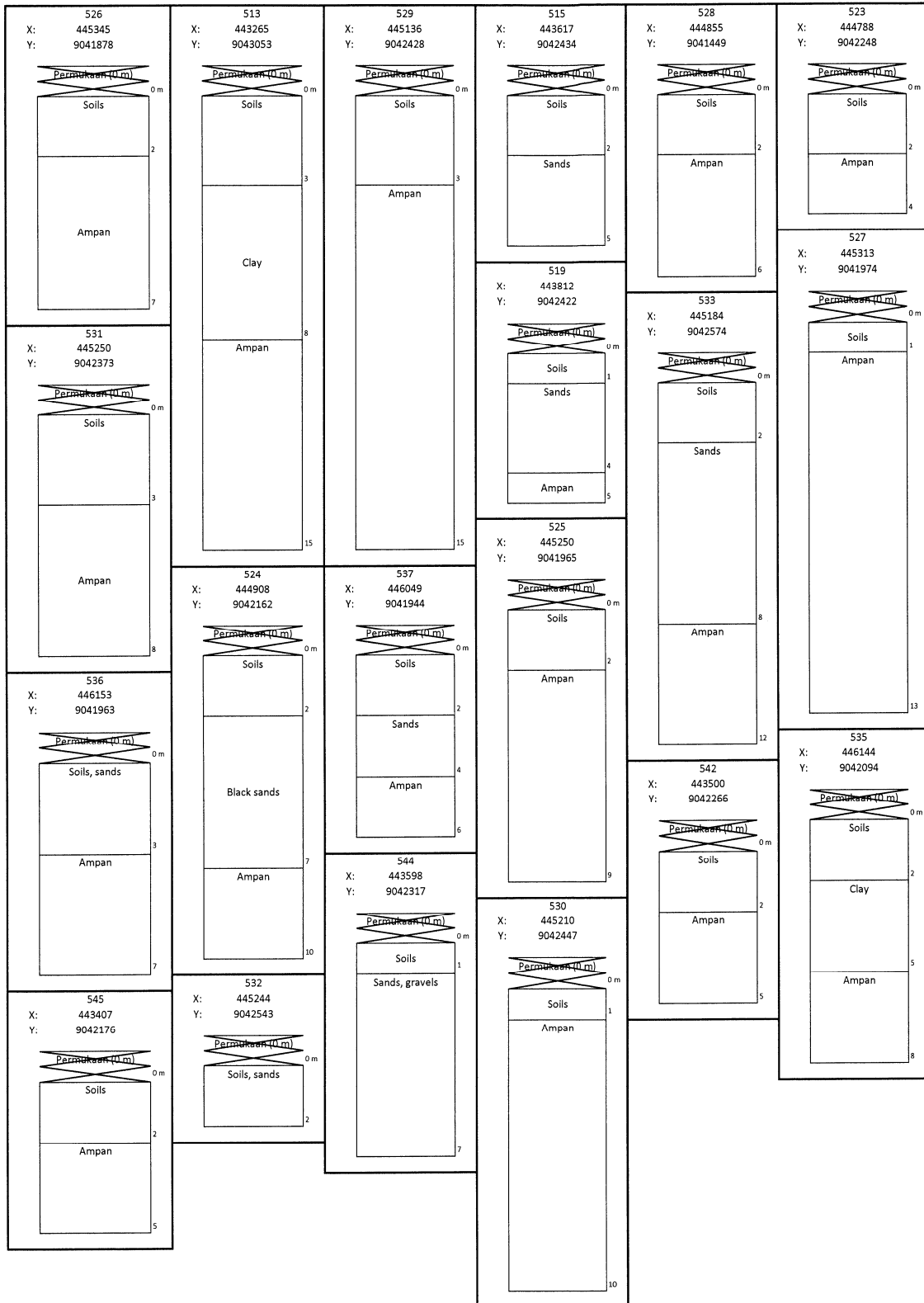


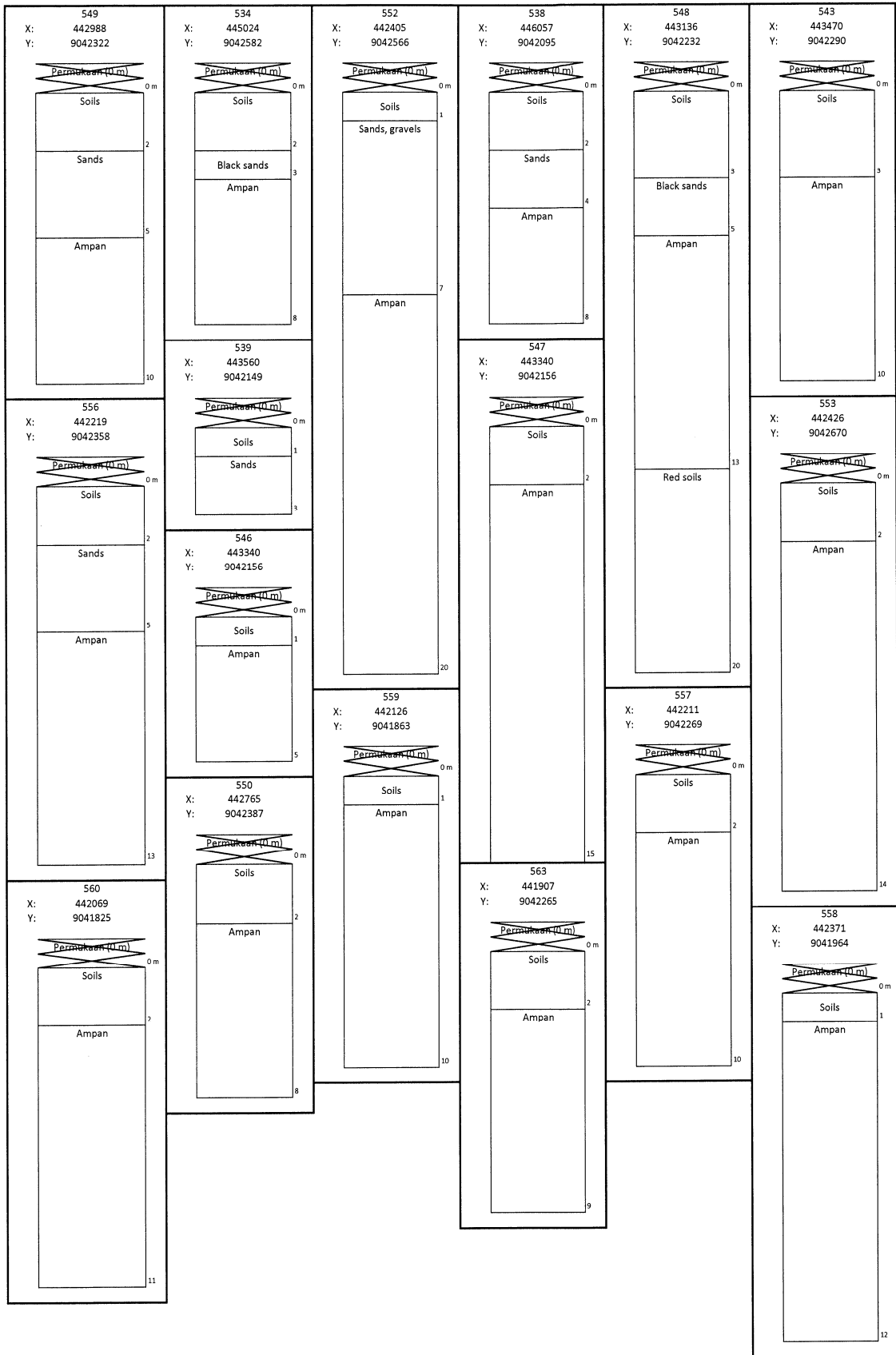


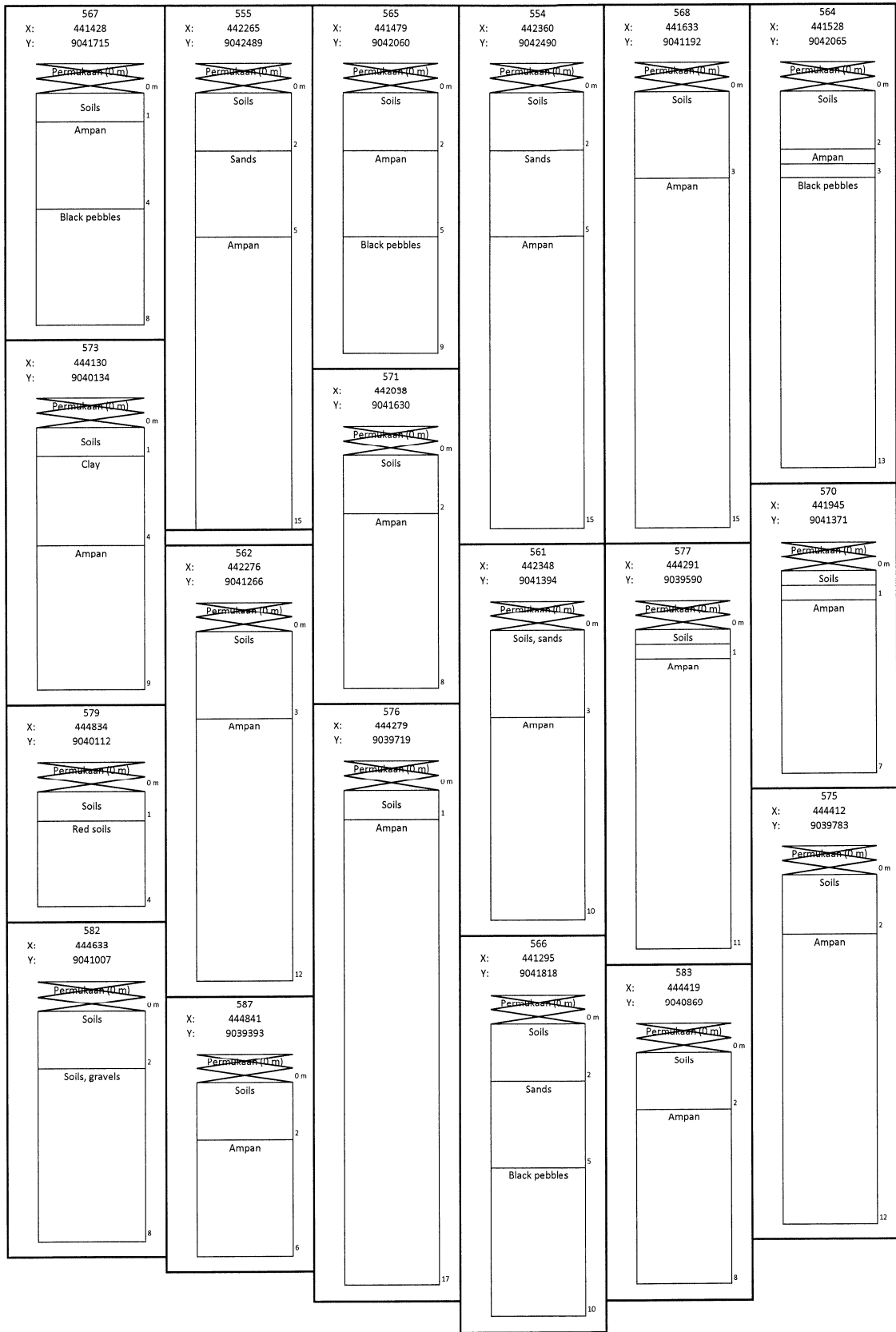


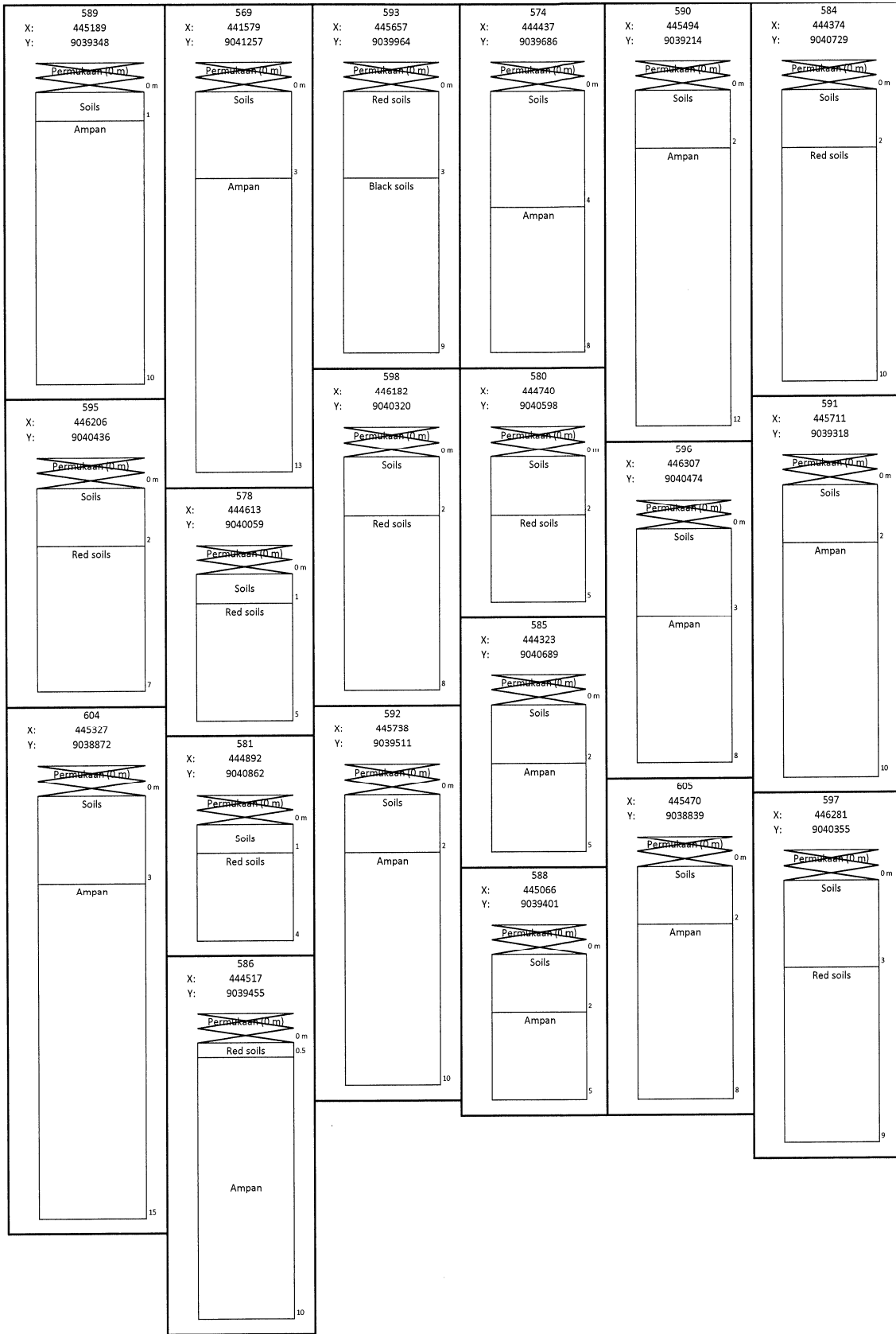




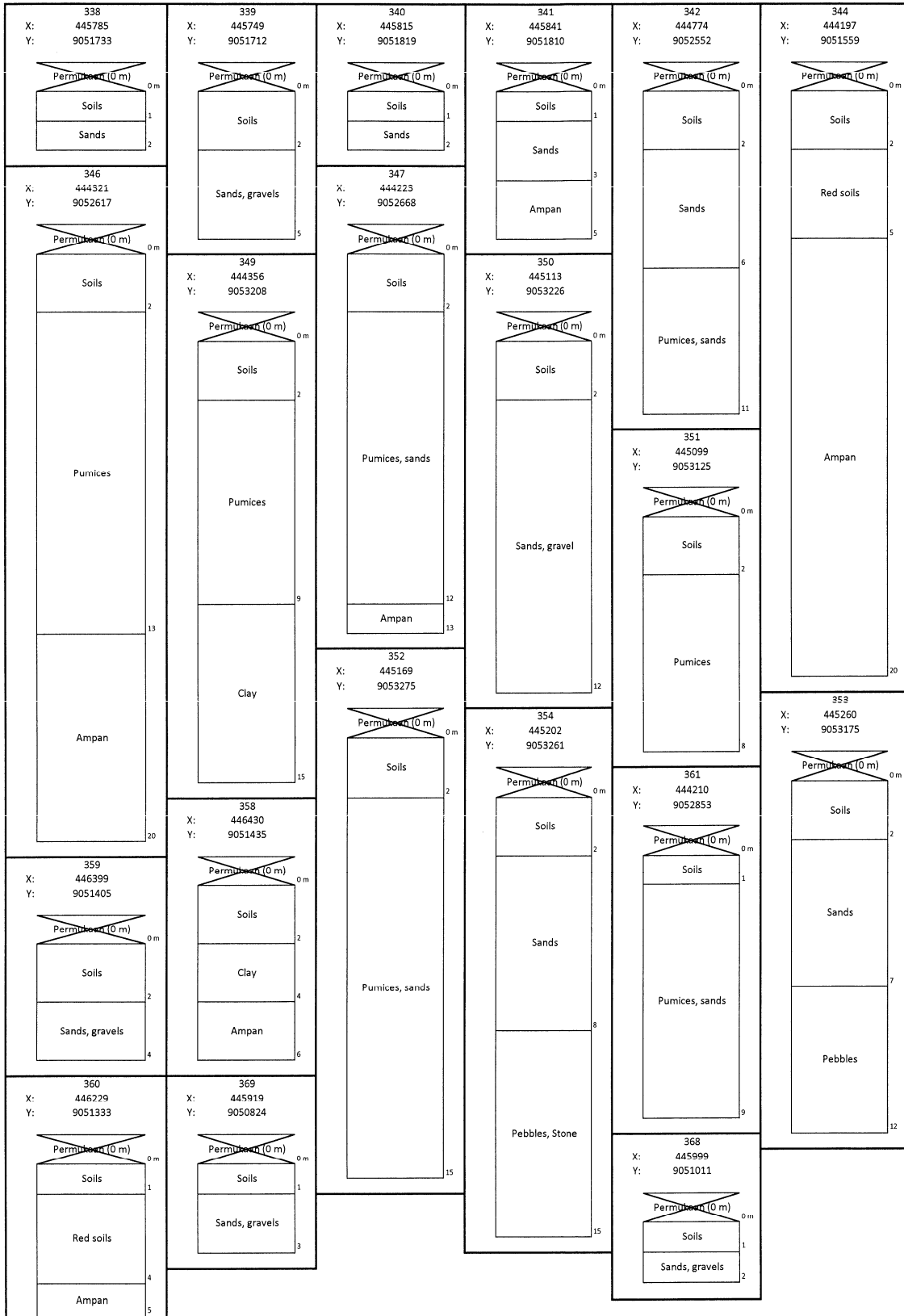


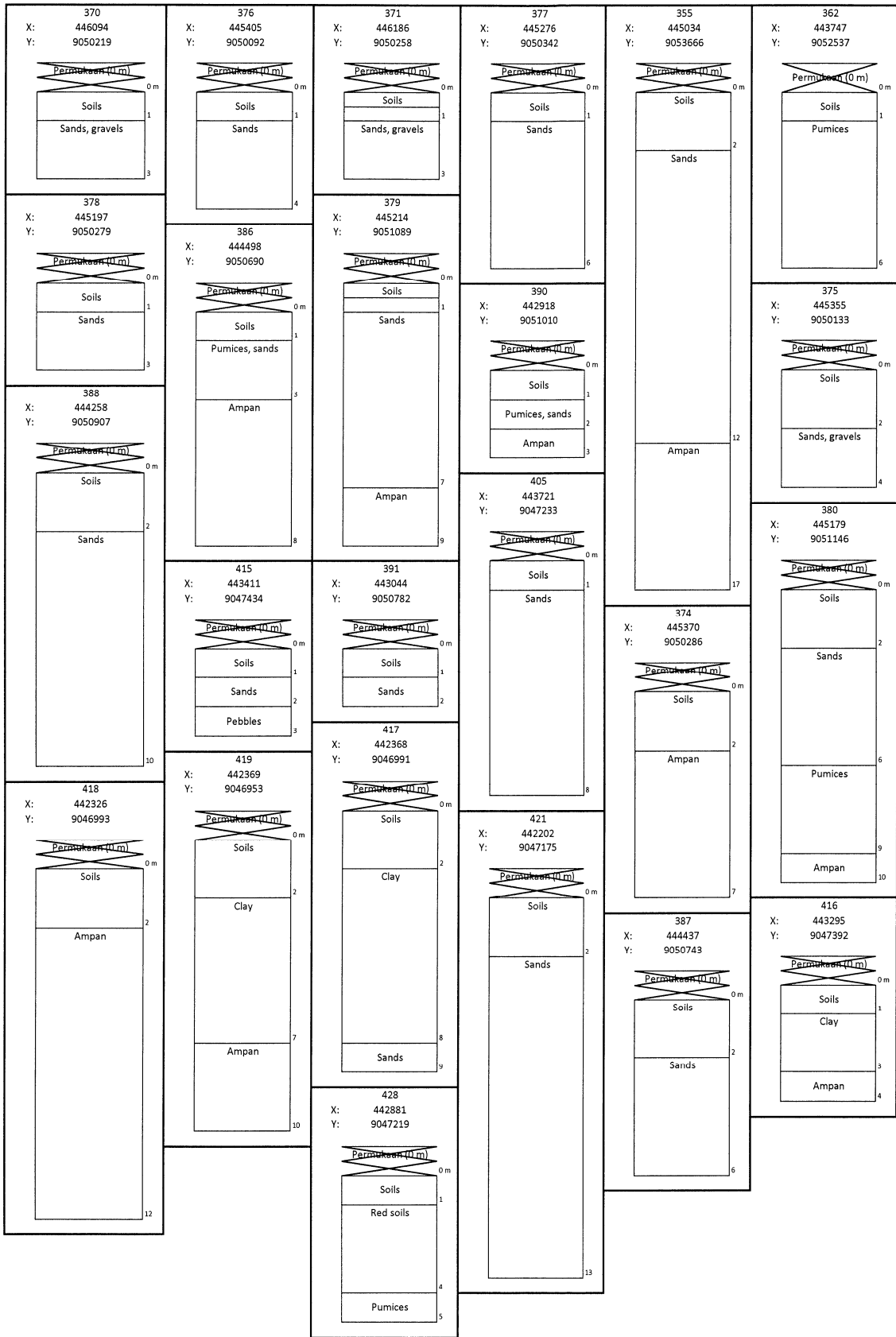


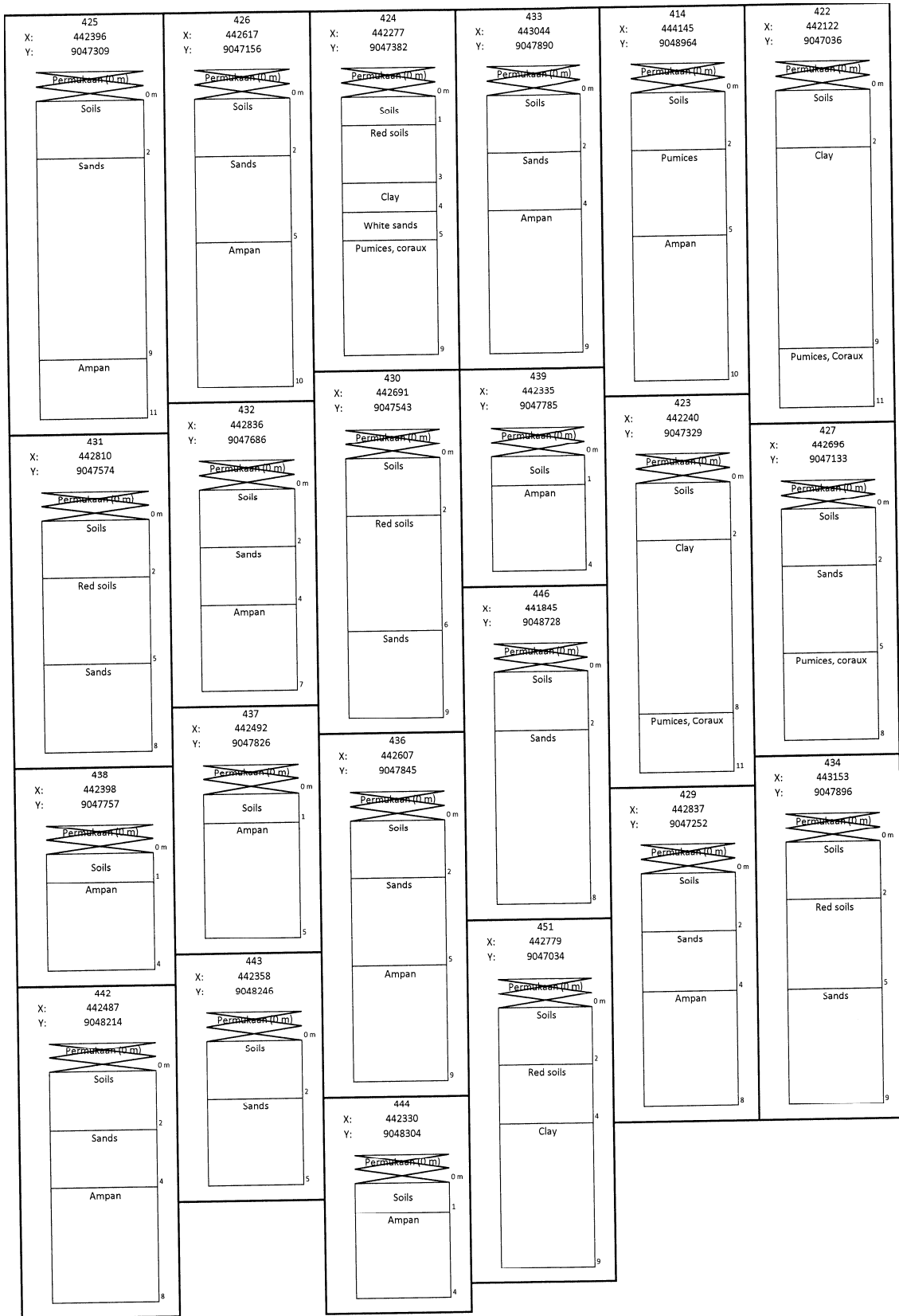


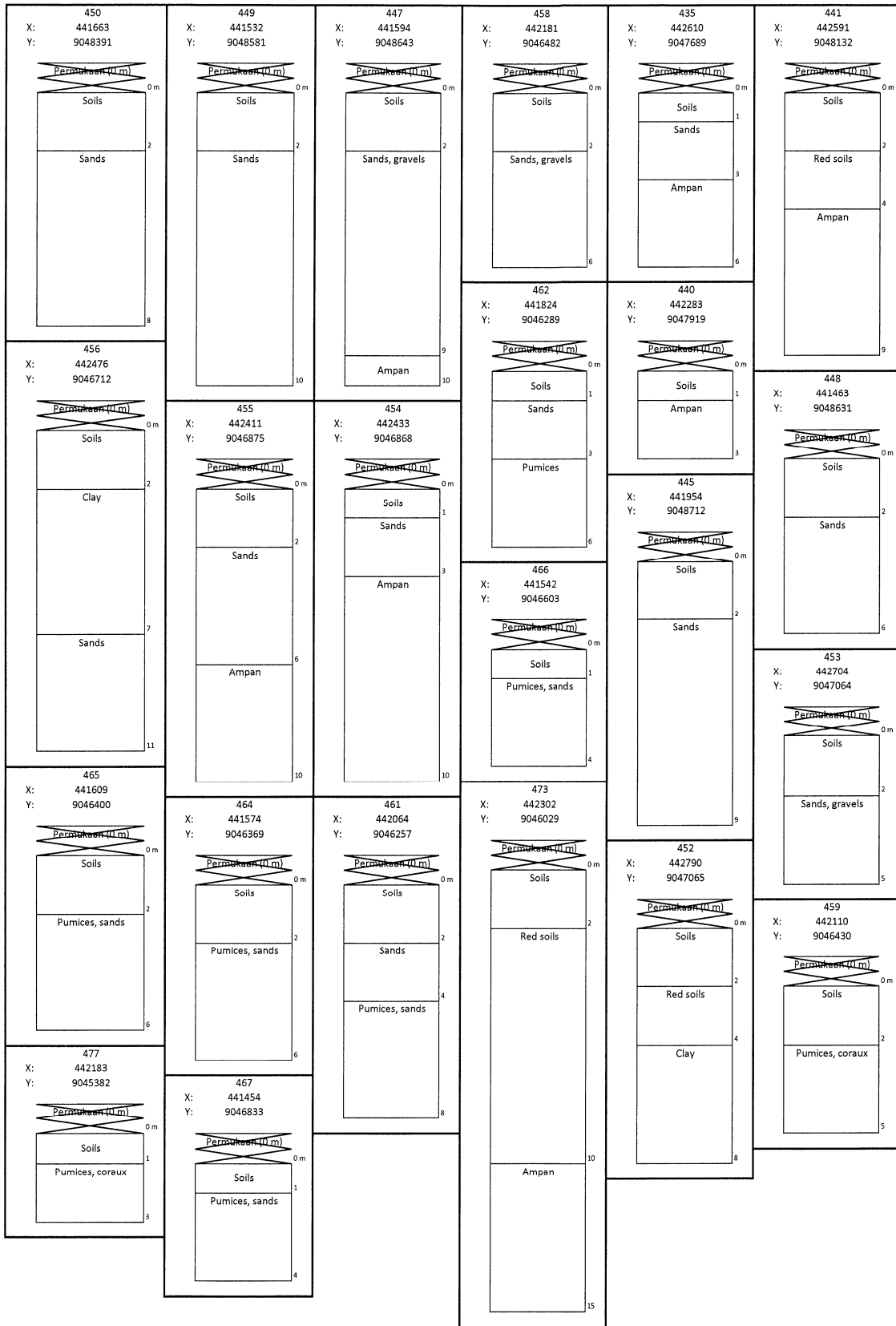


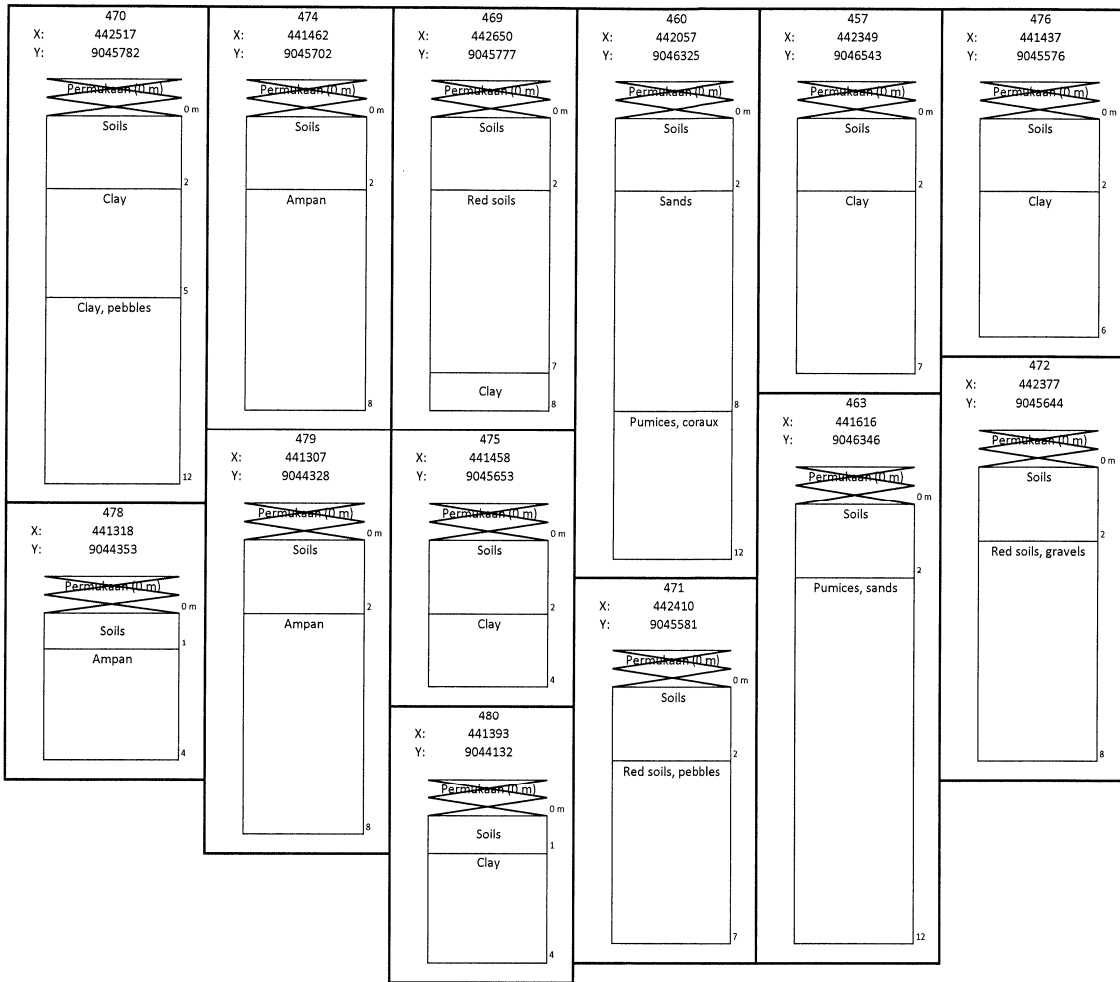
Layout Data Sumur Bor
Ket: 0,5 meter



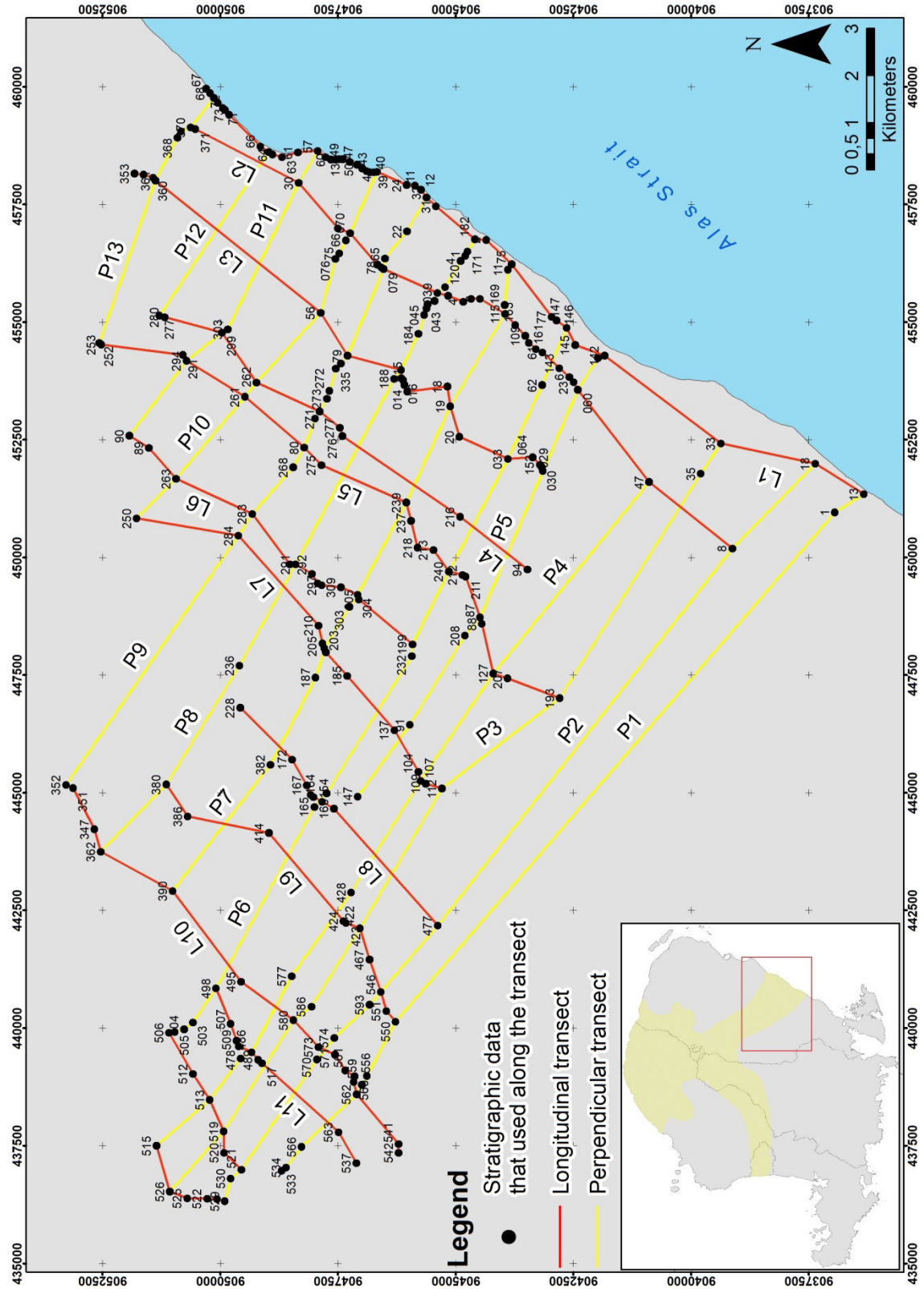








Appendix 2: Perpendicular and parallel transects



Appendix 3: Grain-size analysis

